UNIVERSITY OF SOUTHAMPTON

To: The Academic Registrar
University of Southampton.

Title of thesis . Vibrations of and sound radiation from some periodic structures under convected loadings

The requisite number of copies of the above thesis are now formally submitted for the degree of DOCTOR OF PHILOSOPHY. Should the Senate of the University award me either this degree or another higher degree in respect of this thesis I, . Kewal Krishan Pujara . . . . , hereby agree that from the date of the award the thesis may be made available for inter-library loan or for photocopying.

Signed [redacted] Date . . . . NOV. 1970 . . . . .

VIBRATIONS OF AND SOUND RADIATION FROM SOME PERIODIC STRUCTURES UNDER CONVECTED LOADINGS

by

K.K. Pujara, B.Sc. (Engg.)

Thesis submitted for the degree of

Doctor of Philosophy

in

The Faculty of Engineering and Applied Science

University of Southampton

November 1970.

ACKNOWLEDGEMENTS

Foremost thanks are due to Dr. D.J. Mead, Reader, Department of Aeronautics and Astronautics, for suggesting the project and for supervising it. His readiness to discuss at all times and his friendly encouragement throughout the duration of this work have been most valuable. Thanks are due to the British Council and The Imperial College Committee for collaboration with The Indian Institute of Technology, Delhi for making arrangements so that the author was able to persue this work at the Institute of Sound and Vibration Research. The initiative by his employers, The I.I.T., Delhi, for this arrangement is acknowledged. He wishes to thank Professor B.L. Clarkson, Director, Institute of Sound and Vibration Research, for providing the facilities necessary for this work and for many words of appreciation.

The author wishes to thank all co-workers and the Institute staff with whom many informal but useful discussions have taken place from time to time. Some 'around coffee time' meetings with Dr. F.J. Fahy provided a good deal of stimulation. Ahmed Amin, a constant office companion occasionally helped with computational difficulties. His presence in the Institute in the evenings facilitated compliance with the safety regulation regarding laboratory work outside official hours. The workshop and laboratory staff assisted generously during the experimental stage of the project. This assistance is greatly appreciated.

Thanks are due to Miss Mavis Bull for help in locating many references and to Miss Maureen Andrews for a quick and neat typing of

the thesis. The assistance of Mr. Laurie Dykes and his staff in tracing diagrams is also gratefully recorded.

Finally, the author wishes to record his heartfelt gratitude and apologies to those near and dear ones who patiently or otherwise endured unavoidable difficulties resulting from his preoccupation with this work.

C O N T E N T S

		Page
Abstract		(i)
Notations		(iii)
1.	INTRODUCTION AND REVIEW OF PREVIOUS WORK	1
1.1	The aim of the investigation	1
1.2	Nature of the structure, excitation and response	1
	1.2.1 The typical structure	1
	1.2.2 The excitation	2
	1.2.3 The nature of response	4
1.3	Previous methods of vibration analysis	5
	1.3.1 The normal mode approach	5
	1.3.1.1 Structural idealisations	7
	1.3.1.2 Modal coupling	7
	1.3.1.3 Flexibility of the supports	8
	1.3.1.4 The difficulties of the modal analysis	9
	1.3.2 Other methods and idealisations	10
	1.3.3 The direct formulation finite element method	10
1.4	Sound radiation from panels	11
	1.4.1 Sound radiation from uniform infinite plates	11
	1.4.2 Transmission of sound into an aircraft fuselage	12
	1.4.3 Sound radiated by finite panels	17
	1.4.4 Sound radiation from stiffened panels	18
1.5	Methods applicable to periodic structures	19
	1.5.1 Earlier work	19
	1.5.2 Mead's wave approach	21
	1.5.2.1 The notion of a propagation constant	21
	1.5.2.2 The free wave motion as a wave group	24
	1.5.3 The wave approach and the structural models of this thesis	25
	1.5.3.1 Loading and response of an infinite stiffened beam	26
	1.5.3.2 The structural models considered	27
	1.5.3.3 Application to the finite structures	27
1.6	Arrangement of the text	28
2.	SPACE HARMONIC ANALYSIS OF PERIODICALLY SUPPORTED BEAM; RESPONSE TO CONVECTED RANDOM LOADING	29
2.1	Introduction	29
	2.1.1 Approximation of a plate by a beam	29
	2.1.2 The excitation and the analysis of response	31
2.2	Forced waves and their series representation	32
	2.2.1 The forced waves	32
	2.2.2 The series representation of the forced flexural motion	33
2.3	Determination of the coefficients of the series	34

Page

2.3.1 Derivation of equations for the coefficients 34
2.3.2 The special case of transversely rigid supports 38
2.3.3 The special case of zero rotational stiffness of the supports 39
2.3.4 Relative magnitudes of A_m's 40
2.4 Response to harmonic plane waves 41
2.5 Response to boundary layer and random acoustic plane waves 42
2.5.1 The response to random convected pressure fields 42
2.5.2 Numerical response calculations 44
2.6 Discussion of results 45
2.6.1 Acoustic plane wave excitation 45
2.6.2 Boundary layer excitation 47
2.7 Conclusions 48

3. SOUND RADIATION FROM 'ONE DIMENSIONAL' STIFFENED PLATES UNDER RANDOM CONVECTED LOADING 50

3.1 Introduction 50
3.2 The structure and excitation 51
3.3 Acoustic effects 52
3.3.1 Inclusion of the acoustic radiation in the equation of motion 52
3.3.2 Sound pressure and sound power radiated 54
3.4 Equations for the coefficients of the series 55
3.5 Conditions for real radiation 57
3.5.1 The radiating harmonics 57
3.5.2 The frequency bands of radiation 60
3.6 Sound power radiated by random convected loadings 61
3.6.1 The sound power spectrum and mean power radiated 61
3.6.2 Computations of sound power spectra 62
3.6.3 Results for plane wave excitation 63
3.6.4 Boundary layer excitation 66
3.6.5 Comparison of sound power spectra 67
3.7 Conclusions 69

4. RESPONSE OF ORTHOGONALLY STIFFENED PLATES TO CONVECTED LOADINGS 72

4.1 Introduction 72
4.2 Representation of the two-dimensional convected pressure field 72
4.3 Representation of the structure, stiffnesses of supports and response 74
4.3.1 Representation of the structure 74
4.3.2 The rotational and translational constraints of the supports 75
4.3.3 The governing equation of the plate motion 77
4.3.4 The series representation of the response 78
4.4 The acoustic radiation 79
4.4.1 Inclusion of acoustic radiation effect in the governing equation 79
4.4.2 Expression for sound power 81

Page

4.5 The response of the plate to harmonic and random pressure fields 82
4.5.1 Equations for the coefficients of the series 82
4.5.2 The harmonic response of the plate 87
4.5.3 Response to random convected loads 87
4.6 Computation and results 91
4.6.1 Structural details 91
4.6.2 The excitation considered 93
4.6.3 The relative magnitudes of the coefficients 93
4.6.4 Influence of different variables on the response 94
4.6.4.1 Influence of the number of terms in the series 94
4.6.4.2 Influence of damping 96
4.6.4.3 Influence of the stiffness of stiffeners 97
4.6.4.4 Influence of the direction of convection 98
4.7 Conclusions 99

5. EXPERIMENTAL WORK AND COMPARISON WITH THEORY 101

5.1 Introduction 101
5.2 Quantity to be determined and the technique of measurement 102
5.2.1 Quantity to be measured 102
5.2.2 Free field versus diffuse field measurements 102
5.2.3 The range of frequency 103
5.3 The specimen and test details 104
5.3.1 The specimen and its mounting 104
5.3.2 Excitation and the measurement of pressure levels 105
5.3.2.1 Excitation of the panel 105
5.3.2.2 Measurement of the excitation pressure 106
5.3.2.3 Measurement of pressure in the reverberant chamber 106
5.3.3 The reverberant room and the reverberation time 106
5.3.4 The measurement of the panel damping and the determination of the effective stiffness 108
5.3.4.1 The panel damping 108
5.3.4.2 Determination of effective stiffness 112
5.4 Experimental determination of sound power 112
5.4.1 Ambient sound pressure level corrections 112
5.4.2 Linear versus logarithmic averaging 113
5.4.3 Determination of the sound power 114
5.5 Theoretical calculations 115
5.5.1 Considerations of the mass law 115
5.5.2 Theoretical determination of the radiated power 116
5.6 Theoretical and experimental results 116
5.6.1 Discussion of results 117
5.7 Conclusions 119

6. RESPONSE OF INFINITELY LONG RING STIFFENED CYLINDRICAL SHELLS TO CONVECTED RANDOM LOADING 121

6.1 Introduction 121
6.2 The structure considered 122
6.3 The excitation considered 122

6.4 Shell displacements and shell theories 123
6.4.1 Shell displacements and the importance of flexural vibration in sound radiation 123
6.4.2 Different shell theories 123
6.4.2.1 Consistency of shell theories 124
6.4.2.2 Novozhilov's thin shell theory 128
6.5 The series representation of response and derivation of the governing equation in terms of flexural displacement 129
6.5.1 Series representation of response 129
6.5.2 Equation in terms of one set of coefficients only 129
6.6 Effect of the acoustic medium 131
6.6.1 Inclusion of the effect of acoustic medium inside the cylinder 131
6.6.2 Sound pressure distribution inside the cylinder 134
6.6.3 Radiation outside the cylinder 135
6.7 Evaluation of the coefficients C_m 136
6.8 Computation and discussion of results 138
6.8.1 Relative magnitudes of the coefficients 139
6.8.2 Discussion of results 140
6.9 Conclusions 141

7. GENERAL CONCLUDING REMARKS 142

APPENDIX A The excitation field 145

A.1 Introduction 145
A.2 The narrow band cross correlation coefficient 145
A.2.1 The frozen turbulence 147
A.2.2 Decaying turbulence 147
A.3 The convection velocity 148
A.4 The wave number frequency spectrum 148
A.4.1 The wave number frequency spectrum by Fourier transforming the space time correlation 148
A.4.2 Wills' wave length spectrum 153

APPENDIX B Flow diagram for computation-stiffened beam excited by boundary layer 155

APPENDIX C Time average of the product of real parts of two complex functions 156

APPENDIX D Flow diagram for computation. Stiffened plate excited by boundary layer 158

APPENDIX E The radiating harmonic for the stiffened plate 159

APPENDIX F Instruments used for experimental determination of radiated power and for measurement of damping 162

APPENDIX G The determination of damping from the vector plot 163

APPENDIX H The shell ring interaction forces 165

REFERENCES 167

LIST OF TABLES

		Page
2.1	Relative values of coefficients A_m	172
2.2	Influence of including different number of terms in the series on the values of coefficients A_m (Ω = 14.8)	173
2.3	Influence of including different number of terms in the series on the values of coefficients A_m (Ω = 8.0)	174
4.1	Relative magnitudes of A_{mn}'s. Convection parallel to X-axis, ω = 640 Hz.	175
4.2	Relative magnitudes of A_{mn}'s. Convection parallel to X-axis, ω = 500 Hz	176
4.3	Relative magnitudes of A_{mn}'s. Convection 45° to X-axis. ω = 150 Hz.	177
6.1	Relative magnitudes of coefficients. η = 0.0, CV = 8.0	178
6.2	Relative magnitudes of coefficients. η = 0.25, CV = 16.0	179
6.3	Relative magnitudes of coefficients. η = 0.25, CV = 80.0	180.

LIST OF FIGURES

		Page
1.1	Skin stringer configurations	181
1.2	The infinite beam on equispaced elastic supports	182
1.3	Some typical waves of the beam of Figure 1.2	183
1.4	Variation of component wave speed with frequency; for first propagation band of beam of Figure 1.2	184
1.5	Component amplitude ratios for the free wave group at Ω =17 (for the beam of Figure 1.2)	185
2.1	Identically constructed panels extending to infinity in the two perpendicular directions	186
2.2	The curvature admittance function $\lvert Y_x(\Omega, \mu_x)\rvert^2$ for the beam of Figure 1.2 and the pressure wave number spectrum; Ω	187
2.3	Computed response at different convection velocities by including eleven terms in the series solution	188
2.4	Computed response with different number of terms in the series (CV = 4.0)	189
2.5	The effect of number of terms on peak value of response	190
2.6	Effect of the number of terms on the rms value of response	191
2.7	Response with different values of beam damping. Eleven terms are included in the series solution. CV = 4.0	192
2.8	Response to boundary layer pressure with different number of terms in the series	193
3.1	Zones of radiation	194
3.2	Frequency bands of sound radiation	195
3.3	Spectral density of sound power radiated with different number of terms in the series	196
3.4	Effect of the number of terms on the mean value of sound power radiated at different convection velocities	197
3.5	Effect of the number of terms on the peak value of the sound power radiated at different convection velocities of plane waves	198
3.6	Mean sound power radiated at different convection velocities	199
3.7	Effect of the number of terms on the peak value of power radiated by acoustic plane waves	200
3.8	Contribution of different wave length components in the boundary layer pressure field to the sound power radiated by the beam per unit length at Ω = 24.0, CV = 4	201
3.9	Effect of the number of terms on the peak spectral density of the sound power radiated when the beam is excited by boundary layer pressure field. CV = 4.0, boundary layer decay parameter = 0.1	202
3.10	Effect of the number of terms on the mean value of sound power radiated when the beam is excited by boundary layer pressure field CV = 4.0, boundary layer decay parameter = 0.1	203
3.11	Spectal density of sound power radiated per unit length of the beam for acoustic plane waves and boundary layer pressure field	204

Page

4.1 Correspondence of stringer geometry in the case of two types of stiffeners 205
4.2 Effect of the number of terms on curvature. Structure A, $\eta = 0.15$, trace velocity = 1.5 times the velocity of sound. Convection parallel to X-axis 206
4.3 Effect of the number of terms on sound power, Structure A, $\eta = 0.15$, trace velocity = 1.5 times the velocity of sound. Convection parallel to X-axis 207
4.4 Effect of the number of terms on sound radiation. Structure B, $\eta = 0.25$, $C_t = 1.5\ C$ 208
4.5 Influence of damping on the curvature. Structure A. Trace Velocity = 1.5 times the velocity of sound. Convection parallel to X-axis. Number of terms = 25. 209
4.6 Effect of damping in structure on sound power. Structure A. Trace velocity = 1.5 times the velocity of sound. Convection parallel to X-axis. 210
4.7 Effect of variation of transverse stiffness of Y-wise stiffeners on curvature. Structure B. $\eta = 0.25$. Number of terms included = 25. Trace velocity = 1.5 times the velocity of sound. Convection in the direction of X-axis 211
4.8 Effect of variation of transverse stiffness of Y-wise stiffeners on sound power. Structure B. $\eta = 0.25$. Number of terms included = 25. Trace velocity = 1.5 times the velocity of sound. Convection in the direction of X-axis. 212
4.9 Effect of transverse stiffness of X-wise stiffeners on the curvature at midspan. Structure B, $\eta = 0.25$. Trace velocity = 0.28 times the velocity of sound. Direction of convection 45° to X-axis 213
4.10 Effect of transverse stiffness of X-wise stiffeners on the sound power radiated. Structure B, $\eta = 0.25$. Direction of convection 45° to X-axis. Trace velocity = 0.28 times the velocity of sound. Number of terms included = 25 214
4.11 Effect of the angle of convection on curvature. Structure B. $\eta = 0.25$. Trace velocity = 0.28 times the velocity of sound. Number of terms included = 25. 215
4.12 Influence of angle of inclination on sound power. Structure B, $\eta = 0.25$. Convection velocity = 0.28 times the velocity of sound. Number of terms included = 25. 216

5.1 Details of panel construction 217
5.2 Mounting arrangement for the panel 218
5.3 The general test arrangement 219
5.4 Reverberation time of the small reverberant room 220
5.5 Modulus spectrum of the response of the panel to 0.5 second swept sine wave excitation. Accelerometer was on the skin 221
5.6 Modulus spectrum of the response of the panel to 0.5 second swept sine wave excitation. Accelerometer was on the stringer 222
5.7 The apparatus used for the measurement of damping 223

Page

5.8 Block diagram for the measurement of beam damping 224
5.9 Vector plot obtained by measured values of vibration 225
5.10 Values of sound power radiated. Angle of incidence $= \sin^{-1} \frac{1}{3}$ 226
5.11 Values of sound power radiated. Normal incidence 227
5.12 Values of sound power radiated. Angle of incidence $= \sin^{-1} \frac{2}{3}$ 228

6.1 A part of an infinitely long ring stiffened cylinder with the coordinate system used 229
6.2 Influence of the number of terms on the curvature. CV = 80.0 η = 0.25, n = 1 230
6.3 The spectral density of reactive sound power at different frequencies, CV = 80.0, η = 0.25, n = 1 231
6.4 Spectral density of curvature at midspan, η = 0.25, n = 1 232

A.1 Amplitudes of narrow band space time correlations of the pressure field 233
A.2 Low frequency value of narrow band pressure correlation amplitudes. Curve 1 represents the longitudinal correlation and curve 2 the lateral correlation 234
A.3 Convection velocities derived from narrow band longitudinal space time correlations of the pressure field 235
A.4 The wave number frequency spectrum 236
A.5 The wave length spectrum of boundary layer field at constant frequency ω 237
E.1 Diagram to locate the radiating harmonic in case of orthogonally stiffened plate 238
H.1 Vibrating shell with interaction forces Y_R, Z_R and interaction moments M_R 239

ABSTRACT

FACULTY OF ENGINEERING AND APPLIED SCIENCE

INSTITUTE OF SOUND AND VIBRATION RESEARCH

Doctor of Philosophy

VIBRATIONS OF AND SOUND RADIATION FROM SOME PERIODIC STRUCTURES UNDER CONVECTED LOADINGS

by Kewal Krishan Pujara

This thesis deals with the forced vibrations of infinite periodically supported beams, orthogonally stiffened plates and ring stiffened cylindrical shells excited by random convected loadings. The sound power radiated under these conditions is also dealt with. The stiffened structures are represented by uniform beams, plates or shells on periodically spaced elastic supports which represent stiffener-skin interaction forces and moments.

The available literature on the response of stiffened structures is first reviewed. A special infinite series of space harmonics is then evolved and employed to obtain the response of infinite stiffened beams, plates and cylindrical shells to spatial and temporal harmonic loadings. The coefficients of this series are determined by applying the principle of virtual work. The series is shown to be satisfactorily converging so that only a limited number of terms need be included for an actual solution of a reasonable accuracy. The method easily predicts and explains the sound radiation by structures excited by loadings convected at subsonic convection velocities. The terms in the series contributing to this radiation can be easily identified with the help of a simple diagram included in the thesis.

The response to boundary layer pressure field has been obtained by analysing this field into a wave length frequency spectrum and then

numerically integrating the response due to each wave length component. The low wave numbers in the spectrum are important for sound power radiated by the structure especially at subsonic convection velocities of loading.

An experiment has been carried out to determine the sound power radiated by an orthogonally stiffened damped panel representative of aircraft construction under excitation by acoustic plane waves. A satisfactory agreement has been obtained between experimental and theoretical results.

NOTATIONS

A	Area of cross section of stiffener
A_m, $A_{m'}$ A_{mn}, $A_{m'n'}$ C_m, D_m etc.	Coefficients of different terms in the series of space harmonics
A_{mn}^*	Complex conjugate of A_{mn}
A_x', A_y'	(EC_{ws}) of X-wise and Y-wise stiffener respectively
a	radius of cylindrical shell
B_x, B_y	(GJ) of X-wise and Y-wise stiffener respectively
b	Boundary layer decay parameter in the longitudinal direction
C	Velocity of sound in air
c	Boundary layer decay parameter in the lateral direction
CV	non-dimensional convection velocity parameter $= (mb/D')\ell_x U_c$
C_x, C_y	(ρA) for X-wise and Y-wise stiffeners respectively
C_{ws}	Warping constant with respect to S
D	Stiffness of the plate or beam (may be complex)
D'	Real part of D
D_x, D_y	Transverse stiffness of X-wise and Y-wise stiffener respectively
E	Young's modulus of elasticity
F_x, F_y	(ρI_s) for the X-wise and Y-wise stiffeners respectively
$f(Z)$	Function of Z
G	Shear modulus of elasticity
H_n	Hankel function of order n
h	thickness of beam, plate or shell
I_η	Second moment of area
I_s	Polar moment of stiffener section about S
i	$\sqrt{-1}$
J	Torsion constant of stiffener section

J_n	Bessel function of order n
J_{rst}	Joint acceptance
$\bar{K}$, K	Wave number of loading
K_1, K_3	Wave number components of loading in the direction of convection and the lateral direction respectively
$\underline{K}$	The wave number of sound $(= \omega/C)$
K_r	Rotational stiffness of the support
K_t	Transverse stiffness of the support
K_x, K_y	Wave numbers in X and Y directions respectively
K_m	Wave number component of the m^{th} harmonic in the radial direction
K_{mz}	Wave number component of the m^{th} harmonic in the Z-direction
K_{mnz}	Wave number component of the $(m,n)^{th}$ harmonic in the Z-direction
ℓ_x	Distance between two consecutive supports measured in the X-direction
ℓ_y	Distance between two consecutive supports measured in the Y-direction
m,m', n,n'	Integers
m_b	Mass of the beam per unit area
m_p	Mass of the plate per unit area
[N]	Reference no. N in the list
P	The loading parameter
P_s	Sound pressure
p	pressure intensity
p_r	Radiated pressure
p_o	Amplitude of the harmonic exciting pressure intensity
q	The aspect ratio (ℓ_y/ℓ_x)
Re( )	Real part of ( )
R_p	Cross correlation function of pressure
r	Radial coordinate for the cylindrical shell

S	Projection point of the shear centre on the 'skin'
SPL	Sound pressure Level
$S_p(\omega)$	Spectral density of pressure at frequency ω
$S_p(\mu_x, \mu_y, \Omega)$	Spectral density component corresponding to μ_x, μ_y, Ω
$S_p(\xi_1, \xi_3, \omega)$	Cross power spectral density of pressure
T	Reverberation time in seconds
t	Time variable
U_c	Convection velocity of loading
U_ω, $U_c(\omega)$	(Frequency dependent) convection velocity of loading
u	Axial displacement in case of cylindrical shell
v	Tangential displacement in case of a cylindrical shell
w	Radial displacement in case of a shell and transverse displacement in case of a beam or a plate
W(x", y)	X-wise curvature at point (x, y)
X,Y,Z	The coordinate axes
$\lvert Y_p(\Omega, \mu_x)\rvert^2$	Power admittance function corresponding to Ω and μ_x
Π	Averaged sound power per unit area
$<\Pi>$	Mean power in a frequency band
$\bar{\xi}$	Separation vector
ξ_1, ξ_3	Separation in the direction of convection and lateral direction respectively
η, η_p	Beam and plate loss factors
κ_r	Non dimensional rotational stiffness parameter
κ_t	Non dimensional translational stiffness parameter
μ	(Complex) propagation constant for free flexural wave motion
μ_i	Imaginary part of μ
μ_r	Real part of μ
ν	Poisson's ratio
ρ	Density of cylinder material

ρ_a	Density of the acoustic medium
ρ_p	Cross correlation coefficient of pressure
τ	Time delay
ω	Frequency in radians per second
ω_n	Natural frequency in radians per second
Ω	Non dimensional frequency parameter $(= m_b/D')^{\frac{1}{2}}\omega\ell_x^2$

Other notations in the text are defined where employed.

1. INTRODUCTION AND REVIEW OF PREVIOUS WORK

1.1 The Aim of the Investigation

The chief aim of the investigation reported in this thesis is to present a wave theory for the determination of response of some stiffened structures to random convected loading in a manner that facilitates the calculation of sound radiation and to evaluate this radiation. Such structures are used in the construction of aircraft fuselage and are sometimes referred to and treated as periodic structures. Since they are extensively employed in aerospace applications where jet noise and boundary layer pressure provide the exciting field, attention in this thesis has been mainly directed to obtain their forced response and radiated power resulting from these two types of excitation. Though the work applies in the first place to aeronautical structures, the results are expected to have wider applications, e.g. in the design of missiles and underwater structures. In the particular case of aircraft fuselage, the sound power radiated by the vibrating structure has obvious relevance to passenger comfort, crew efficiency and efficiency of voice communication.

1.2 Nature of the Structure, Excitation and Response

1.2.1 The typical structure

The actual construction of stiffened structures varies with application. It is generally a curved panel with stiffeners running in mutually perpendicular directions. In the case of an aircraft fuselage, one common construction involves a continuous panel rivetted or bonded to a network of relatively flexible stringers and relatively stiff frames.

Where the fatigue considerations are important, the stiffeners may be made integral with the panel. The material used for construction is usually aluminium alloy. The thickness of the panel (or the 'skin') may lie between 0.025 inch and 0.1 inch.

Figure 1.1 shows two typical structures between the frames. Figure 1.1(a) shows the conventional construction involving open section stringers rivetted to the skin. Figure 1.1(b) shows the more recent integrally stiffened structure machined out of a solid slab of metal by mechanical or chemical means.

1.2.2 The excitation

The excitation in the case of aircraft structures may be due to jet noise or boundary layer pressure field or both. Both of these excitations are broad band and random in nature. Though each of the above excitations can be idealised by a random acoustic plane wave, their exact nature is usually described by their space-time cross correlation functions.

The jet noise is caused by the hydrodynamic and acoustic pressure fluctuations associated with the turbulence in the jet as it enters and mixes with the surrounding air. It is characterised by a broad peak spectrum, the peak moving to lower frequencies as the distance from the jet increases. The total noise is quite directional, the maximum sound power levels being radiated out from the jet at approximately 35° to the jet axis.

The boundary layer pressure fluctuations or the normal pressure

fluctuations on a surface adjacent to the boundary layer of a high speed flow originate in the hydrodynamic pressure associated with the turbulent velocity fluctuations. This turbulence may be considered to be composed of pressure eddies of different sizes or wave numbers. Broadly speaking a unique value of convection velocity may be associated with each wave number. These eddies build up to a maximum and then decay as others are formed.

Precisely speaking the eddies associated with the boundary layer pressure fluctuations are convected downstream at a frequency dependent velocity (see Appendix A). The mean speed may, however, be taken as approximately 0.8 times the free stream velocity. Different flying speeds of the aircraft will therefore be associated with different convection velocities of the loading due to boundary layer.

The r.m.s. value of the normal pressure fluctuations exerted on an aeroplane surface may be expressed in terms of the free stream dynamic pressure as 0.6% of its value up to a Mach No. = 1.2. In dB's the empirical pressure level is

$$40 \log_{10} \frac{U_{EAS}}{100} + 105$$

i.e. 143 db at 600 mph and at sea level.

(U_{EAS} is the equivalent air speed, in feet per second).

The boundary layer pressure field is usually described in terms of its space-time cross correlation function. However, in this thesis, this field has been visualised as an infinite assemblage of harmonic pressure components of various amplitudes, frequencies and wave lengths.

This wave length-frequency spectrum has been obtained by the appropriate Fourier transformation of the cross-correlation function of the pressure fluctuations (Appendix A gives this transformation.) The spectrum for a convected boundary layer pressure field is continuous and peaks at a wave number approximately equal to frequency ÷ convection velocity.

In terms of the wave length-frequency spectrum referred to above, an acoustic plane wave may be considered as a special case of a boundary layer pressure fluctuation.

1.2.3 The nature of response

The word 'response' of the structure used here means quantities like stresses in the structure, displacements at different points in the structure, the sound power radiated by the structure, etc, which are induced by the excitation.

Since the excitation considered is random, the response must necessarily be random. The peaks in the response spectrum, however, do not necessarily correspond to the peaks in the excitation spectrum. They are modified by the impedance of the structure.

The stiffened structures are complex vibratory systems in which the rotational and flexural motion of the stiffeners is coupled with the flexural motion of the skin. There are a number of modes present in the frequency band of excitation and these modes tend to be bunched in bands of frequencies. Some of these modes are good acceptors of energy from the excitation and respond well while others respond poorly. It is difficult to identify 'good acceptors' from the large number of modes present. Damping in the structure can cause modal overlap and modal coupling. The available test data for the structures show a power

spectrum of response concentrated in wide frequency bands.

1.3 Previous Methods of Vibration Analysis

Many theoretical investigations have been made to obtain the response of stiffened structures. Usually they have had the assumption of negligible interaction between the plate vibration and the excitation field. This excludes the possibilities of instabilities like panel flutter. Most structures considered in the literature are of finite size. The exceptions are the infinitely large plates considered by Ribner [1] and by Corcos and Leipmann [2]. Corcos and Leipmann claimed that the infinite model is satisfactory since the mean square acceleration integrated over the panel area does not depend significantly on the boundary conditions imposed by the stiffeners.

Many investigators have concentrated on a row of aircraft fuselage panels having stringers and frames. A normal mode approach has generally been applied in which the modes had to be determined in the first place. This approach will be briefly discussed before the wave approach is introduced.

1.3.1 The normal mode approach

In a multimodal structure $W(\omega)$ the response at a given frequency may be obtained by adding the contribution of each individual mode. This method of determining the response by addition is generally known as the normal mode approach. The following equation due to Powell [3] may be written down to represent the summation referred to above.

$$W(\omega) = \sum_r \sum_s \frac{1}{|Z_r(\omega)|} \cdot \frac{1}{|Z_s(\omega)|} w_{po} A^2 J^2_{rs\tau}$$

$$= \sum_r \frac{1}{|Z_r|^2} w_{po}(\omega) A^2 J_{rr}{}^2 + \sum_{r \neq s} \sum \frac{1}{|Z_r|} \cdot \frac{1}{|Z_s|} w_{po}(\omega) A^2 J_{rs\tau}{}^2 \qquad (1.1)$$

with

$$J_{rs\tau}{}^2 = \frac{1}{A^2} \int_A \int_A R(\omega;\ r,\ r';\ \tau)\alpha_r(r)\alpha_s(r')drdr' \qquad (1.2)$$

$$J_{rr}{}^2 = \frac{1}{A^2} \int_A \int_A R(\omega;\ r,\ r';\ 0)\alpha_r(r)\alpha_r(r')\ drdr' \qquad (1.3)$$

where

A = overall area of the structure

w_{po} = pressure power spectrum at a reference point

α_r, α_s = normal modes

r = co-ordinate (co-ordinates) of a point on the structure

dr = differential area

R = pressure correlation, a function of frequency ω, locations r, r' of the two points on the structure and the time separation τ.

τ = difference in response lags for two modes r and s when excited at frequency ω.

The dimensionless quantity $J_{rs\tau}$ is called the 'joint acceptance' of the pressure field and the modes α_r and α_s.

It is clear that before Powell's equation can be used, the normal modes α_r and α_s must be determined or must be known. These modes have been determined by using different methods or different structural idealizations.

1.3.1.1 Structural idealisations

Lin [4-6] considered a row of panels between two frames assuming the panel skin to be continuous over the intermediate stringers which are considered simply supported on both sides by a rigid structure. The edges of the panels are simply supported as well. Using this model and employing the boundary conditions resulting from compatability and equilibrium considerations at the stringer locations, he discussed the determination of the natural frequencies and normal modes of vibration of the structure. As a result of extensive work on skin stringer structures by him and others, it is now known that their characteristic frequencies fall into groups. Lin gave the frequency equations and normal modes for the limiting frequencies of these modal groups. Once the natural frequencies and normal modes are known, equation (1.1) is employed to obtain response to a random input. A simplifying assumption may be made that most of the response comes from the frequencies within the modal bands. Presence of only a light damping may be assumed to minimise modal correlation which is represented by the last term in equation (1.1).

Clarkson and Ford [7] have experimentally justified the assumption of simple supports at the frames as the basis of estimating stress levels in the actual aircraft panels. The theoretical basis of this assumption must, however, be examined in terms of the effect of the modal coupling.

1.3.1.2 Modal coupling

There are two types of modal coupling. One is the modal coupling which is caused by the presence of damping in the structure. The second is the coupling as a result of the different modes of the structure being excited by the same input loading. The latter may better be called response correlation effect.

It is very difficult to account for true damping modal coupling in the normal mode method. The latter type of coupling has, however, been considered by Mercer [8]. Assuming the same structural idealisation as used by Lin, he obtained the response of a multi-supported finite beam to a random pressure field. In his expression for the response spectral density terms representing joint and cross acceptances arise, the cross terms giving the interactions of different modes. The joint and cross terms correspond respectively to the first and second terms of the last right hand side of equation (1.1). In Mercer's case showing maximum coupling the cross terms contributed 20% to the overall r.m.s. response level. In more typical cases, the contribution was of the order of 5 to 10 percent. It is argued by Clarkson [9] on this basis that only relatively small errors are likely to arise from the neglect of the cross terms. This may actually be taken as true only for light damping. However, even if the cross terms are small, a large number of direct terms will be significant if the excitation forces have a broad frequency bandwidth.

1.3.1.3 Flexibility of the supports

In the models analysed in the literature reviewed above, the bending rigidity of the stringers has been assumed to be infinite. This assumption may be examined in relation to the relative rotational and transverse stiffnesses of the stiffeners. The conventional stiffeners and the integral stiffeners have different relative bending and torsional stiffnesses. For a given material weight or stringer cross sectional area, for a built up structure the ratio of bending stiffness to torsional stiffness might be of the order of 200:1. For the integrally stiffened

structure, the figure is more likely to be 20:1.

1.3.1.4 The difficulties of the modal analysis

In employing the foregoing normal mode techniques, a number of assumptions have to be made in order to simplify the analysis. A low degree of damping is assumed so that the responses in different modes may be considered to be uncorrelated. The approach implies well separated resonant frequencies. Perhaps the most notable assumption is that the stringers are transversely rigid. Sometimes even with the above assumptions the design calculations seem difficult. Then a further assumption may be made that the major part of the response results from the contribution of one predominant mode. The assumption of simple supports, both at stringers and at frames is not realistic. The simple supports at the frames cannot be theoretically justified even in the case of conventional type of construction where the stringers may be considered with a fair degree of accuracy, to be simple supports for practical purposes. The model with simple supports both at stringers and frames is in any case a poor representation of the integrally stiffened panels which are currently being employed in aircraft construction. The stringers in the latter case are certainly more flexible than in the case of conventional construction. The assumption of low damping also becomes unrealistic in cases where a damping layer may have been added to the skin [10] in order to reduce the response. The normal mode approach is in fact least convenient in the case of a row of large number of panels having a high degree of damping. A knowledge of all the natural frequencies and normal modes is necessary and the number and complexity of possible vibration modes in such a configuration increases rapidly with the number of bays.

As a result, in spite of the assumptions made, the work required to calculate the random response of this type of structures soon becomes prohibitive. Since the modal frequencies are not widely separated but are rather grouped together into distinct bands (the number of frequencies in each band being equal to the number of panel bays), the correlation between different modes will not, in fact, be negligible, thereby increasing the complexity of the modal analysis still further. Besides it is most difficult to determine the modes of vibration exactly when the damping is high, because the mechanism of damping modal coupling is complex.

1.3.2 Other methods and idealisations

Hoppmann (II) and Magness [11] treated the orthogonally stiffened plates as orthotropic plates and used the measured values of stiffnesses in bending and twisting of the plate for the analysis to obtain the natural frequencies and the nodal patterns. Olson and Lindberg [12] in their finite element method assumed all the outer edges of their panel to be clamped.

1.3.3 The direct formulation finite element method

The Direct formulation finite element method can yield the response directly without first finding the normal modes (see for example [13]). This numerical method is in general very powerful for analysing structures. Any boundary conditions can in theory be considered. However, the number of elements into which the structure must be divided has in general to be high if a good accuracy is to be achieved. The number of elements must be increased still further if the structure is built up or

complicated in some other manner. Consequently in the development of such methods, there are always problems of computer storage adequacy and the cost of the computer time. Stiffness and mass matrices generated by the computer may be of a very high order, and may lead to associated round off errors. The problem would be aggravated if the acoustic effects of the surrounding medium were to be considered. Even if the acoustic effects are not considered in the first place, the response obtained is in a form which is not readily adaptable to the problem of calculating sound radiation.

1.4 Sound Radiation from Panels

There are difficulties in analysing exactly a finite structure for determining sound radiation. The simultaneous satisfaction of the wave equation, the equation of the structure and its boundary conditions, the compatibility conditions at the fluid structure interface together with the 'radiation extinction at infinity' principle is a tedious task.

The most well known work on sound radiation from stiffened structures is due to Maidanik [14] but before that is reviewed, attention may be drawn to the work on sound radiation from uniform panels.

1.4.1 Sound Radiation from Uniform Infinite Plates

The mechanism of sound radiation from an infinite plate which is uniform is not very difficult. The mechanical properties of the plate determine its admittance at a given frequency. If random excitation is considered, the pressure field can be resolved into wave length and frequency components. The response of the plate has the same components,

and the corresponding pressure field generated by the vibrating plate can be determined. Only the components of vibration having supersonic phase velocities give rise to true acoustic radiation.

Most of the work involved with sound radiation from panels is inspired by its application to the aircraft fuselage. Some of this work will now be described.

1.4.2 Transmission of sound into an aircraft fuselage

The estimation of sound levels inside the aircraft fuselage must involve the study of vibrations of the fuselage structure coupled with that of air inside and outside the cabin, when it is subjected to the exciting pressure field. The fuselage construction involves a finite curvature but most of the authors whose work is being reviewed here have neglected the effects of curvature. This is justifiable if the wave lengths excited are small in comparison with the fuselage diameter and this is so for most cases of interest when the excitation is by boundary layer pressure field. Another factor often ignored is the effect of the interior of the fuselage as a closed acoustic space. This is explained on the basis that the fuselage is so full of sound absorbing objects that the internal reflections are negligible.

Under the assumptions given above, Ribner [1], Corcos and Liepmann [2] and Kraichnan [15] have investigated the problem of noise due to boundary layer induced vibrations. Dyer [16] has considered in addition the effects of a closed space on the vibrations of the structures. However it is assumed by all the authors that there is no interaction between the plate vibrations and the excitation field. The work done by the above authors can be reviewed with respect to three factors:

(a) The plate model and the plate vibration.

(b) The excitation field.

(c) Method of analysing transmitted sound.

(a) The plate model and the plate vibration

Corcos and Liepmann have chosen an infinite plate as their model. They argue that the mean square acceleration of the typical aircraft structures when integrated over the surface of the plate, will not be too dependent on the plate boundary conditions in the case of boundary layer excitation. They use the space time correlation of the plate normal acceleration to find the mean square acceleration integrated over the surface of the plate which can be expressed in terms of the wave number frequency spectrum integrated over all wave numbers and frequencies. By means of Fourier transforms a relation is established between the wave number frequency spectrum of the plate response and the wave number frequency spectrum of the boundary layer. This result exhibits the coincidence effect (the concept of coincidence was first given by Cremer [17]), and would lead to infinite plate response at the coincidence frequency in the absence of damping.

Ribner's approach is the same as that of Corcos and Liepmann except that the model assumed is an infinite beam rather than an infinite plate.

Dyer employs a finite model and Kraichnan has an infinite assembly of finite independent plates. Kraichnan assumes that all parts of the infinite wall are vibrating while Dyer considers a rectangular space bounded on one side by an elastic wall (the vibrating panel) and on the remaining five sides by pressure release surfaces. In both cases the plate

is simply supported on all its edges. Both the authors employ the 'normal mode approach'.

Kraichnan obtains the joint acceptance expression in terms of the Fourier transforms of the mode shapes and pressure space time correlation and making use of the homogeneity hypothesis, the joint acceptance is expressed as a double integral involving the wave number frequency spectrum rather than a quadruple integral involving the space time correlation. Kraichnan assumes further that in the special case of low damping, the discrete set of resonant frequencies of the plate are replaced by a continuous distribution. His spectrum therefore has no peaks found in practice. Dyer uses the impulse response function expanding it as the sum of responses in the plate normal modes. The response to a given loading is obtained by integrating the effect of a large number of impulses.

(b) The excitation field

All the authors quoted have dealt with excitation due to a boundary layer. The most important properties of the assumed model for the excitation are

(i) the convection characteristics

(ii) the spatial distribution or wave length spectrum

(iii) the effects of decay of the turbulence.

Out of the above three, the first two are the most important. The models assumed in any investigation should be checked against the above.

Ribner and Kraichnan assume the field to be composed of a rigid pattern of turbulence which does not decay with time. Kraichnan assumes a two dimensional turbulence pattern, the wave lengths in the flow direction having a greater contribution to the mean square pressure

fluctuation than those at right angles to the flow direction. He also assumes a cut-off in the wave number spectrum such that the wave lengths of the turbulent pressure fluctuations are all greater than the boundary layer thickness. Ribner considers a one dimensional pattern of turbulence with a wave length spectrum concentrated about a wave length which is equal to the boundary layer thickness.

Dyer describes two representations of the space-time correlation function. The first one uses exponential functions and allows for both convection and decay of the turbulent pressure fluctuations. The second is a product of two Dirac δ-functions and an exponential function representing convection, spatial separation and time delay, respectively. This corresponds to a turbulence pattern consisting of pressure fluctuations with very small wave lengths.

Corcos and Liepmann have made an assumption that the wave number-frequency spectrum of the pressure fluctuations is symmetrical in its two wave number components and is fairly smooth. By using an extension of the first mean value theorem for integrals to obtain approximate values for their integrals, they obtain their noise intensity results in terms of a function which is the wave number-frequency spectrum of the boundary layer pressure fluctuations evaluated at those wave numbers and frequencies which satisfy the coincidence condition for the plate.

(c) Method of analysing transmitted sound

The usual acoustic theory for small pressure fluctuations is used, and a solution is attempted so that the velocity of the air particles adjacent to the walls of the structure is the same as the velocity of the wall.

Corcos and Liepmann use a solution in the form of the well known integral which relates the sound field to the normal acceleration of the plate normal displacement. The mean square pressure fluctuations are then given as a function of the space time correlation of the plate normal accelerations. Introducing the concept of correlation length, the result is obtained which involves correlation area of the plate displacement and mean square normal acceleration.

Kraichnan relates the Fourier transform of the sound pressure fluctuations to the Fourier transform of the plate normal velocity. The radiation efficiency at a given frequency is greatest when the panel wave length is the same as the acoustic wave length for the same frequency. If the panel wave length is smaller than the corresponding acoustic wave length, the sound field is a reactive one and the mean square pressure fluctuation falls rapidly away with increasing distance from the plate, with no radiation energy. The radiated sound power is obtained as an integral involving the wave number frequency spectrum of the plate normal velocity.

Ribner states that the sound is radiated by supersonic waves running along the fuselage wall. The subsonic waves will generate sound only if there are discontinuities or boundaries in the structure. Since these boundaries always exist in practice, sound is radiated and Ribner produces a result similar to the approximate one by Corcos and Liepmann except that he has included a 'universal correlation length' whereas Corcos and Liepmann have retained a general correlation length.

Dyer expresses the sound field within his enclosure as a sum of the acoustic normal modes of the space. The modal pattern on the vibrating plate of the normal modes of the room corresponds exactly to the modal pattern of the normal modes of the plate. Thus the effect of the

room is the same as that of an additional generalised mass in the equation for the response of the plate in each normal mode. By equating the velocity of the air particles adjacent to the plate with that of the plate, the plate acoustic medium coupling has been obtained.

It is seen from the above that only Dyer has allowed for coupling between sound radiated and the structural vibration. It is also clear that the analyses for the most part apply to uniform panels and not to stiffened panels. Nobody seems to have considered the effects of stiffeners on the plate vibration.

1.4.3 Sound radiated by finite panels

Apart from the problem of sound radiation into an aircraft fuselage, the problems associated with sonic boom have necessitated investigations into the sound radiated by a flexible panel. For example, Bhattachanya and Crocker [18] have considered a flexible uniform panel which separates the open space from an enclosed room, the walls of the room being considered as acoustically hard. Using the modal technique, a general analytical solution of the wave equation with inhomogeneous boundary conditions has been found. In such a finite panel, and a finite room, the critical coincidence is shown to occur when the room eigenvector grazes the flexible panel under conditions of maximum coupling and panel resonance. Subsequent coincidences occur at frequencies greater than the critical coincidence frequency when the room eigenfrequency becomes equal to the forced frequency under the conditions of maximum coupling and panel response.

1.4.4 Sound radiation from stiffened panels

One of the best known works on the response of stiffened panels is by Gideon Maidanik [14]. He analysed the response of such panels to a reverberant noise field by using a statistical method. The analysis predicted that the ribbing increases the radiation resistance of the panel and hence its coupling to the acoustic field. In the statistical method, he employed, he argued that the modal density of the ribbed panel is the sum of the modal densities of the individual panels because the modal density of the ribs is small compared with the modal density of the panel. Since we are not interested in the statistical energy method in this work, we shall not review this work in detail here. However his experimental results may be generally interesting. He found that the response of the ribbed panels is considerably higher than that of unribbed panels. The increase due to ribbing was as much as 15 to 20 dB in some frequency ranges.

A study by White and Cottis [19] may be interesting. They dealt with the pressure field in the vicinity of a rib on a homogeneous infinite plate excited by a turbulent boundary layer pressure field and surrounded by a dense fluid medium. The rib was idealised by three cases, a simply supported line, a clamped line and a line supporting two independent plates. A very important conclusion of this study is that the boundary conditions at the line are found to have a significant effect on the radiated pressure field.

A work in this field reported during the present investigation is by Konovalyuk [20] who has investigated the reflection of a plane sound wave from an elastic plate reinforced with stiffness members. Using

impedances of the rib in the longitudinal and flexural vibrations, he sought to estimate the influence of N arbitrarily situated ribs on the amplitude of the reflected wave. The resulting equation became very complicated and the attention was therefore focussed on the plate with an infinite number of ribs. The calculations show that it is not always possible to replace the ribs with perfectly rigid supports in order to assess the influence of stiffening members in the scattering of sound from an elastic plate. No torsional restraint of the supports is considered in this analysis nor is the effect of inertia of stiffeners taken into account.

This work should confirm the conclusions of White and Cottis regarding the importance of correct boundary conditions at the stiffener locations.

An attempt on the survey of the literature on sound radiation from stiffened panels leads to the conclusion that there is a need for more work on the subject - both theoretical and experimental. Whether the theoretical model should be a finite or an infinite structure, would obviously be decided by the convenience of analysis. Since, as claimed by Corcos and Liepmann, the mean square acceleration integrated over the panel area does not depend significantly on boundary conditions, treatment of a finite periodic structure as an infinite structure is expected to yield fairly accurate results.

1.5 Methods Applicable to Periodic Structures

1.5.1 Earlier Work

Brillouin [21] has made excellent studies of the spatially periodic structures. Unfortunately the structures he considered are

second order systems. These studies therefore are not directly applicable to beams and plates which follow the governing equations of the fourth order. His general approach, however, has been used by Morse [22] and Cremer and Leilich, [23]. Cremer and Leilich considered lateral and rotational velocities, bending moments and shear forces at the discontinuities. (These discontinuities between segments of uniform structure, make it spatially periodic.) Since he emphasised the quantities at the discontinuities, it was difficult to predict easily the beam behaviour between these discontinuities. Morse's work, followed by Ungar's [24] (see also [25]) treats the excitation at discontinuities. This approach is not directly amenable to utilisation for obtaining response of the beam as a whole. Ungar also studied the excitation between continuities but formulated the problem as Heckl [26] had done, in terms of transmission and reflection coefficients. He (Ungar) considered the results of injecting a flexural wave of a given amplitude at one or more locations between discontinuities. The general approach consists of tracing the entire history of a wave and of all of its transmitted and reflected portions, and of superposition of all the resulting effects. This is the approach similar to that of Heckl. Ungar, however, simplified the analysis by assuming that only the regions of the structural elements well away from the discontinuities are of interest, and that the flexural wave lengths in all cases are considerably smaller than the spacing of the discontinuities. With these assumptions, it is possible to neglect the 'near field' effects in the vicinity of the discontinuities and to considerably simplify the analysis. However, in spite of these simplifications, the analysis is too involved to be applied to the problem of response of air-

craft type structures, which may be two dimensional. Ungar's work emphasises one dimensional systems. He mentions no relation between a discontinuity impedance and the dimensions of the discontinuity.

1.5.2 Mead's Wave Approach

In dealing with a very large, highly damped structure with periodic stiffening (i.e. stiffening at regular intervals) a wave approach yields the response much more readily than the normal mode approach. This has been demonstrated by Mead and Wilby [27] who used a closed form solution to represent the random displacement generated in an infinite uniform periodically supported beam subjected to random convected pressure field. A relatively simple formula was developed for the displacement, curvature or stress at any point in the beam. The closed form solution is not convenient, however, if sound radiation and acoustic damping effects are to be included as the acoustic pressure at a point on the structure is not proportional to the local displacement (or velocity). Rather it is proportional to an integral function of the velocity all over the vibrating surface.

Sound radiation effects are easily incorporated in response calculations if the transverse displacements are expressible as a series of sinusoidal travelling waves or 'space harmonics'. This approach has been developed in this thesis, for the forced vibration due to convected loads. But before the forced problem is taken up, the free wave propagation studied by Mead [28] will be reviewed.

1.5.2.1 The notion of a propagation constant

A wave may be crudely defined as disturbance that propagates itself. The disturbance travelling may be a displacement of a structure.

A simple sinusoidal wave propagating along an infinite, damped, unsupported beam may be characterised by a wave number $K_x = 2\pi/\lambda$ where λ is the wave length. This wave number is equivalent to the difference in phase between the wave motion at any two points unit distance apart. Let the wave decay as it propagates so that the amplitude of wave motion at one of these points is e^{δ} times the amplitude at the other. The complex number $(\delta \pm iK_x)$ then may be termed as a 'propagation constant' which describes the phase change and decay rate per unit length of the wave motion.

The above motion of propagation constant may be extended to the case of the multi-supported beam. Suppose an infinite beam on equispaced supports is excited at a single point by the harmonic load $Fe^{i\omega t}$ (see Figure 1.2). A harmonic wave motion is set up in the whole beam propagating outwards from the point of application of the load. On examining the motions at corresponding points in any pair of adjacent bays (see Figure 1.3) it is found that the phase difference (μ_i) and the amplitude ratio (e^{μ_r}) are the same for all adjacent pairs of bays along the whole beam. μ_i represents the phase difference in the motion over the distance between the supports, ℓ_x, and μ_r represents the decay rate over the same distance. The characteristic propagation constant for this infinite multi-supported beam is therefore $\pm (\mu_r + i\mu_i)$

The value of the characteristic propagation constant has been found by Mead by making the free wave motion satisfy the equation of motion of the beam subject to the boundary conditions imposed by the supports. This value is independent of the imposed loading but is a function of frequency of vibration and the beam/support physical characteristics. The number of values of the propagation constant equals the number

of degrees of freedom allowed at the supports. Associated with each such value of propagation constant is a unique mode of free vibration of a bay of the beam.

The details of the method of determining the propagation constants may be seen from the original reference and will not be reproduced here. But it is interesting and important to record here that the final equation giving the value of μ (in general complex) is of the following form

$$\cosh \mu = - \frac{\beta_{BB}}{\beta_{BA}} \tag{1.4}$$

where β_{BB} and β_{BA} represent the end receptances of the repeated beam element, and obviously are frequency dependent. If $|\cosh \mu| > 1$, μ will correspond to a decaying wave with no propagation. However, if $|\cosh \mu| < 1$, μ is purely imaginary and represents a propagating wave with no decay. Equation (1.4) will then modify to

$$\cos \mu_i = - \frac{\beta_{BB}}{\beta_{BA}} \tag{1.5}$$

It has actually been found that in certain frequency bands, μ is purely imaginary, and the natural frequencies of finite stiffened beams must therefore lie in these bands of frequencies. From equation (1.5) it is clear that in these bands of frequencies (or in 'propagating bands') μ_i will be multivalued, the values differing by $2m\pi$, where m is an integer lying between $-\infty$ and $+\infty$. Also $+\mu_i$ and $-\mu_i$ both represent solutions of equation (1.5).

1.5.2.2 The free wave motion as a wave group

In the band of free propagation (i.e. without attenuation) where μ is purely imaginary, equation (1.5) gives the values as

$$\mu = \pm \mu_i + 2m\pi, \quad m = -\infty \text{ to } +\infty \tag{1.6}$$

The values of μ associated with $+\mu_i$ represent a negative going wave group and those associated with $-\mu_i$ represent a positive going wave group. Corresponding to each value of m there is a different amplitude of wave motion and a different free wave length and wave velocity. The total displacement $W(x)$ at a point x due to the positive going wave group of free waves may therefore be expressed as

$$W(x) = \sum_{m=-\infty}^{m=+\infty} A_m e^{-i(\mu_i + 2m\pi)\frac{x}{\ell_x}} e^{i\omega t} \tag{1.7}$$

and the wave velocity due to m^{th} component wave is given by

$$C_m = \frac{\omega \ell_x}{\mu_i + 2m\pi} \tag{1.8}$$

Figure (1.4) gives the phase velocities of free waves in the stiffened structure as a function of frequency. It is clear that unlike in the case of unstiffened beam, there are more than one phase velocity at a given frequency. These different velocities correspond to different integral values of m in equation (1.8). When the stiffened beam is vibrating under a convected loading, the coincidence could be caused when any one of these phase velocities equals the velocity of convection of the excitation. Thus in a stiffened beam there is a greater possibility of coincidence at a frequency under given conditions of convected loading than in the case of a uniform beam.

The wave coincidence can also be interpreted as matching of wave length of excitation with the wave length of free propagation. Since at a given frequency, there are an infinite number of free component wave lengths, any one of them could match the imposed wave length and thus cause coincidence. The value of the m^{th} component wave length is given by

$$\lambda_m = \frac{2\pi \ell_x}{\mu_i + 2m\pi} \tag{1.9}$$

The convergence of the series of equation (1.7) has been studied in Figure 1.5 which compares the amplitude ratios (A_m/A_o) of the successive components of the free wave group of the multisupported beam at $\Omega = 17.0$ for which $\mu_i = \pi/2$ (Ω is a non dimensional frequency parameter and equals $(m_b\omega^2/EI)^{\frac{1}{2}}\ell_x^2$ where m_b, EI are the mass per unit length and the stiffness of the beam respectively, and ω is the frequency in radians per second). It can be seen that as m increases, the value A_m/A_o falls rapidly, thus testifying to the satisfactory convergence of the series of equation (1.7).

If the beam were unstiffened, all A_m's would be zero except A_o.

1.5.3 The Wave Approach and the Structural Models of this Thesis

The ideas presented in section 1.5.2 can be extended to obtain the forced response of stiffened structures to convected loading [29]. This will be explained here by taking the example of a stiffened beam like the one shown in Figure 1.2.

1.5.3.1 Loading and response of an infinite stiffened beam

Consider a harmonic distributed loading $p_o \exp i(\omega t - K_x x) = p_o \exp -i(\mu_x x/\ell_x)\exp(i\omega t)$ acting on the periodically supported beam shown in Figure 1.2. The phase difference between pressures at two points distance ℓ_x apart is $K_x.\ell_x = \mu_x$. This μ_x may therefore be regarded as the propagation constant imposed by the loading on the beam. The phase characteristics of the wave motion forced in the beam must follow those of the loading. As a result the total wave motion at points separated by distance ℓ_x along the beam must have the same amplitude but must differ in phase by μ_x. This condition will be satisfied by a series of harmonic waves which have phase differences of μ_x, $\mu_x \pm 2m\pi$ over the interval ℓ_x since all these phase angles are in effect identical.

Hence we can write the transverse displacement $W(x)$ in the form

$$W(x) = \sum_{m=-\infty}^{m=+\infty} A_m e^{-i(\mu_x + 2m\pi)x/\ell_x} e^{i\omega t} \qquad (1.10)$$

The series of equation (1.10) represents a spatial counterpart of the well known temporal Fourier series. We shall refer to this series as a series of space harmonics.

The details of the application and extension of this series of space harmonics to different structures and loadings will be the subject of the following chapters. In each case the response will be determined in the first place to a spatially and temporally harmonic component pressure. The response to any general loading may then be determined by the help of the wave length-frequency spectrum into which the excitation field must be analysed. (See Appendix A.)

Some remarks which are common to all the structures considered in this thesis are included in the next subsection.

1.5.3.2 The structural models considered

All the structures analysed in this thesis viz. stiffened beams, stiffened plates and stiffened cylindrical shells are assumed to be infinite (in practice the behaviour of highly damped large structures will very closely approximate to this model [30]). All the structures considered are periodic. The 'skin' of the structure considered is of uniform thickness. The complete stiffened structure may be visualised subdivided into identical substructures of uniform thickness continuous over uniformly spaced elastic supports. These supports simulate the characteristics of the stiffeners, and therefore apply constraints to the continuous structure appropriate to the type of stiffeners employed. The stiffened structure is thus a periodically supported structure and the two terms will be interchangeably employed in the text.

1.5.3.3 Application to the finite structures

Though only infinite structures have been considered in this thesis, the general theory presented can be applied to the finite structures. Mead and Sen Gupta [30] have applied the wave approach to the determination of the response of finite stiffened beams. This has been done by adding the forced response of the infinite beam and the free wave response, and then making the total response satisfy the end conditions of the finite beam. It is shown that when a finite stiffened plate structure of at least five bays is modelled by a periodically supported beam, the space-averaged rms response to a frozen random convected pressure field can

quite adequately be computed by assuming the beam to be infinite and periodic. This is shown to be true for a wide range of damping values. The forced wave propagation in infinite stiffened structures is therefore of great practical utility. The concept of the forced wave propagation is derived from Mead's wave approach [28] which in turn has been shown by Sengupta [31] to be inter-related with transfer matrix approach adopted by Lin [32]. At any frequency the propagation constant of the free flexural waves equals the natural logarithm of the eigenvalue of the transfer matrix relating the state vectors at the two ends of the basic element constituting the periodic structure.

1.6 Arrangement of the Text

The 'space harmonics' approach will be applied in Chapter II to obtain the curvature response of a periodically supported beam when it is excited by an acoustic plane wave or by a boundary layer pressure field. It will be extended in Chapter III to obtain the radiated power of such a one dimensional model. Chapter IV will extend this method to the case of orthogonally stiffened plates, obtaining results for the sound power radiated. Chapter V will describe the experimental work undertaken to obtain the values of sound power radiated by a panel under excitation by acoustic plane waves of different angles of incidence. It will compare the results with the computed values and will discuss the extent of their agreement. Chapter VI will extend the method to the ring stiffened cylindrical shells of infinite length. This extension is intended to confirm that the general method adopted may be employed to deal with a class of elastically supported structures when they are large and highly damped.

2. SPACE HARMONIC ANALYSIS OF PERIODICALLY SUPPORTED BEAMS; RESPONSE TO CONVECTED RANDOM LOADING

2.1 Introduction

The general approach for obtaining the response of stiffened structures introduced in Chapter 1 will now be applied to such structures. One such structure viz. the orthogonally stiffened plate, is shown in Figure 2.1 along with the co-ordinate system employed. ℓ_x and ℓ_y are the regular spacings between the two consecutive stiffeners extending in the Y and X directions respectively. These stiffeners are assumed to be line supports which apply suitable constraints to the skin depending upon the properties of the stiffeners employed.

2.1.1 Approximation of a Plate by a Beam

Consider the vibrations of a plate of dimensions ℓ_x and ℓ_y, stiffness D and mass per unit area m_b at a frequency ω. It can vibrate in many modes each of which corresponds to a number of half waves in the Y direction. Consider the n^{th} Y-mode. Then $W_n(x,y)$, the displacement response at a point (x, y) of the plate, may be written as follows:

$$W_n(x, y) = W_n(x) \sin \frac{n\pi y}{\ell_y} \tag{2.1}$$

where

$$W_n(x) = A_1 e^{\lambda_1 x'} + A_2 e^{-\lambda_1 x'} + A_3 e^{i\lambda_2 x'} + A_4 e^{-i\lambda_2 x'} \tag{2.2}$$

WITH $x' = x/\ell_x$

A_1, A_2, A_3, A_4 are the constants and

$$\underline{\lambda}_1^2 = \underline{\lambda}^2 + \left(\frac{n\pi\ell_x}{\ell_y}\right)^2$$

$$\underline{\lambda}_2^2 = \underline{\lambda}^2 - \left(\frac{n\pi\ell_x}{\ell_y}\right)^2 \qquad (2.3)$$

$$\underline{\lambda}^4 = \left(\frac{m_b\omega^2}{D}\right)\ell_x^4$$

Equation (2.3) shows that when the term $\frac{n\pi\ell_x}{\ell_y}$ is small, $\underline{\lambda}_1$ and $\underline{\lambda}_2$ are approximately equal. If the aspect ratio (ℓ_y/ℓ_x) is high, this term will be small specially for low values of n or low order Y-modes. Thus for n = 1 and an aspect ratio of say 3, the difference between $\underline{\lambda}_1^2$ and $\underline{\lambda}_2^2$ will be negligible, for accepted engineering accuracy. Now n = 1 often represents the most important Y-mode that is excited. So if a plate has an aspect ratio of 3 or so, it can be adequately represented by a beam for the purposes of response calculations. In fact it has been found that for an aspect ratio of 2, the bounding frequencies of the bands of frequencies (within which the natural frequencies lie) differ from those of the plate by only $5\frac{1}{2}$ per cent, while the width of the band is almost unaffected. For an aspect ratio of 3, the difference in the frequencies is about 3 per cent. This should confirm that for at least low order Y-modes, the beam should be a reasonable approximation to a plate. Thus if in a stiffened plate, it is assumed that there is no response correlation across x-wise stiffeners, it could reasonably be considered as a beam with Y-wise stiffeners only. Such a representation has in fact been used by Lin [4-6], Mercer [8], Ford [33] and Mercer and Seavey [34] in their normal mode analysis of stiffened plate response. Mead and Sengupta [30] have discussed the response of a

multi supported finite beam in relation to that of an infinite beam. They have concluded that in the case of finite beams of more than 5 bays, the infinite model may give reasonable answers for response. Such a model is analysed in this chapter.

This infinite stiffened beam then is visualised (See Figure 1.2) as a uniform beam continuous over periodically spaced (spacing ℓ_x) elastic supports having transverse stiffness K_t per unit deflection at the support and rotational stiffness K_r per unit rotation at the support.

2.1.2 The excitation and the analysis of response

The problem is first solved for the fundamental case of a convected harmonic sinusoidally distributed pressure field and from this the solutions for the more general pressure fields are developed. Random pressures of two types are considered:

(a) Corresponding to a random acoustic plane wave field, in which the instantaneous pressure distribution is convected along the beam surface without change of wave form. Such a field can be analysed into a continuous frequency spectrum of harmonic 'components' each of which can be associated with a unique wave number.

(b) Corresponding to a boundary layer pressure field in a boundary layer of constant thickness. The instantaneous pressure distribution does change as it is convected along, so each harmonic 'component' of the continuous frequency spectrum is now associated with a continuous spectrum of wave numbers.

The curvature response at the centre of one of the beam 'bays' is analysed theoretically under each of these. The series for the response

contains an infinite number of terms and attention is given to the loss of accuracy incurred by restricting the series to as few as three terms and as many as eleven.

The basis of the response analysis stems from the fact that the structure is infinite and periodic and that the pressure field can be regarded as having harmonic, sinusoidally distributed components. Under the action of one of these components, the response in the structure at a point in any one of the periodic elements must be identical to that at the corresponding point in another periodic element, apart from a phase difference which is equal to the phase difference between the component pressures at the two points. This response can be represented by a special series of sinusoidal waves, which constitutes a wave group. The relative magnitudes of the components in the wave-group are evaluated in the analysis and it is shown that relatively few of them contribute significantly to the response at any one frequency, with pressure fields of the above types.

2.2 Forced waves and their Series Representation

2.2.1 The Forced Waves

Consider a harmonic distributed loading $p_o \exp(-iK_x x)\exp(i\omega t) = p_o \exp(-i\mu_x x/\ell_x)\exp(i\omega t)$ acting on the beam of Figure 1.2. This is being convected over the beam at the velocity ω/K_x. The phase difference between pressures at two points distance ℓ_x apart is $K_x \ell_x = \mu_x$. μ_x (with subscript x) may thus be regarded as the propagation constant of the loading. The flexural wave motion which is excited in the structure by this loading has this propagation constant μ_x imposed upon it. The forced response quantities at corresponding points in

adjacent bays then have the same amplitude but they differ in phase by μ_x. When this imposed value of μ_x is equal to the characteristic value of μ for the beam at the same frequency (see section 1.5.2), the coincidence phenomenon occurs and the response is large.

2.2.2 The Series Representation of the Forced Flexural Motion

A simple harmonic flexural wave of the form $W_o \exp(-i\mu_x x/\ell_x) \cdot \exp(i\omega t)$ cannot exist on its own in the multi supported beam. The presence of elastic constraints at the supports introduces numerous reflections and 'near field' type flexural waves into the beam motion. However, when the beam is excited by the loading $p_o \exp(-i\mu_x/\ell_x)\exp(i\omega t)$, the forced flexural motion is spatially periodic over the wave length given by $2\pi\ell_x/\mu_x$ $(= 2\pi/K_x)$ and so may be analysed into spatial harmonic wave components. The total wave motion so represented must have the same amplitude at any two points, distance ℓ_x apart, but the two total motions must differ in phase by μ_x. This will be satisfied by a series of harmonic waves which have phase differences of μ_x, $\mu_x \pm 2\pi$, $\mu_x \pm 2m\pi$ over the interval ℓ_x since all these phase angles are in effect, identical.

Hence we can write a series for the transverse displacement $W(x)$ in the form

$$W(x) = \sum_{m=-\infty}^{m=+\infty} A_m e^{-i(\mu_x + 2m\pi)\frac{x}{\ell_x}} e^{i\omega t} \qquad (2.4)$$

This series must be made to satisfy the boundary conditions at elastically restrained supports by appropriate restrictions on the coefficients A_m. We observe that if a particular value of μ_x is imposed

by the loading, wave components with smaller and greater values of μ_x are present in the response. This implies that wave components are present which are propagating at speeds greater than, and less than (respectively) the convection speed of the loading. It is possible that the faster waves may be supersonic, and so will radiate sound, even though the loading itself is being convected at subsonic velocity.

Furthermore, some of the wave components have negative values of $\mu_x + 2m\pi$, and are therefore propagating in the negative direction, opposite to the direction of the loading propagation. These are associated with the reflections which occur at the supports.

2.3 Determination of the Coefficients of the Series

2.3.1 Derivation of the equations for the coefficients

The coefficients will be obtained by the principle of virtual work. Consider, in the first place, the differential equation of motion of the beam between the supports. This has the form

$$D\, w^{IV} - m_b \omega^2 w = p_o e^{(-i\mu_x x)/\ell_x}\, e^{i\omega t} \qquad (2.5)$$

where D = beam flexural rigidity

m_b = beam mass per unit length.

When the forces on and in the beam are in equilibrium, then these forces, represented by

$$D\, w^{IV} - m_b\, \omega^2\, w - p_o e^{(-i\mu_x x)/\ell_x}\, e^{i\omega t}$$

together with the elastic constraint forces and moments of the supports, must do no virtual work when moved through any one of the virtual dis-

placements

$$\delta A_{m'} \, e^{-i(\mu_x + 2m'\pi)\frac{x}{\ell_x}} \, e^{i\omega t}$$

When W is represented by the series form of equation (2.4), this statement leads on to a set of equations for the A_m's. Since the structure is spatially periodic, the virtual work contribution from only one bay element (including supports) need be considered. As usual in complex algebra the conjugate of the virtual displacement applied is used to calculate the virtual work, i.e. $\delta A_{m'} e^{+i(\mu_x + 2m'\pi)\frac{x}{\ell_x}}$.

The contribution from the beam alone (less supports) to the virtual work is then found to be

$$\delta W_b = \delta A_m \{ \int_0^{\ell_x} D \sum_{m=-\infty}^{m=+\infty} \left(\frac{\mu_x + 2m\pi}{\ell_x}\right)^4 A_m e^{-i(\mu_x + 2m\pi)\frac{x}{\ell_x}} \, e^{i(\mu_x + 2m'\pi)\frac{x}{\ell_x}} \, dx$$

$$- \int_0^{\ell_x} \sum_{m=-\infty}^{m=+\infty} m_b \omega^2 A_m e^{-i(\mu_x + 2m\pi)x/\ell_x} \, e^{i(\mu_x + 2m'\pi)x/\ell_x} dx$$

$$- \int_0^{\ell_x} p_o \, e^{-i\mu_x x/\ell_x} \, e^{i(\mu_x + 2m'\pi)x/\ell_x} dx \} \qquad (2.6)$$

where the origin of x has been taken to be at the left hand support of the bay element under consideration.

The contribution to the virtual work from the translational stiffness of one support (at $x = 0$) is equal to

$$K_t \, W(0) . \, \delta A_{m'}$$

$$= \delta A_{m'} K_t \sum_{m=-\infty}^{+\infty} A_m = \delta W_t \qquad (2.7)$$

Likewise, the contribution from the rotational stiffness of the support at $x = 0$ is

$$K_r W'(0)\, i\delta A_{m'}\left(\frac{\mu_x + 2m'\pi}{\ell_x}\right)$$

$$= \delta A_{m'} K_r \sum_{m=-\infty}^{+\infty} A_m \left(\frac{\mu_x + 2m\pi}{\ell_x}\right)\left(\frac{\mu_x + 2m'\pi}{\ell_x}\right) = \delta W_r \qquad (2.8)$$

The virtual work principle requires that

$$\delta W_b + \delta W_t + \delta W_r = 0 \qquad (2.9)$$

Evaluating the integrals involved in δW_b, we can find from equation (2.9) that

$$\left[D\left(\frac{\mu_x + 2m'\pi}{\ell_x}\right)^4 - m_b\omega^2\right] A_{m'} + \frac{K_t}{\ell_x}\sum_{m=-\infty}^{\infty} A_m + \frac{K_r}{\ell_x}\sum_{m=-\infty}^{\infty} A_m\left(\frac{\mu_x + 2m\pi}{\ell_x}\right)\left(\frac{\mu_x + 2m'\pi}{\ell_x}\right)$$

$$= 0 \quad \text{when} \quad m' \neq 0$$

$$= p_o \quad \text{when} \quad m' = 0 \qquad (2.10)$$

This constitutes a set of simultaneous equations for the A_m's. Consideration of the virtual work in any other bay element would yield an identical set of equations.

Equation (2.10) may be written in the following non-dimensional form by dividing through by D/ℓ_x^4.

$$\left[(\mu_x + 2m'\pi)^4 - \frac{m_b\omega^2\ell_x^4}{D}\right] A_{m'} + \frac{K_t\ell_x^3}{D}\sum_{m=-\infty}^{\infty} A_m + \frac{K_r\ell_x}{D}\sum_{m=-\infty}^{m=\infty} A_m\,(\mu_x+2m\pi)(\mu_x+2m'\pi).$$

$$= 0 \quad m' \neq 0; \qquad = (p_o\ell_x^4)/D \quad m' = 0 \qquad (2.11)$$

If structural damping is to be introduced into the beam, then D may be expressed in the complex form

$$D = D'(1 + i\eta) \tag{2.12}$$

when η is the beam loss factor.

The following non-dimensional quantities may be identified in the above equation:

$$\text{Frequency parameter } \Omega = \left(\frac{m_b \omega^2 \ell_x^4}{D'}\right)^{\frac{1}{2}} \tag{2.13}$$

$$\text{Transverse stiffness parameter } \kappa_t = \frac{K_t \ell_x^3}{D'} \tag{2.14}$$

$$\text{Rotational stiffness parameter } \kappa_r = \frac{K_r \ell_x}{D'} \tag{2.15}$$

$$\text{Loading parameter } P = \frac{p_o \ell_x^4}{D'} \tag{2.16}$$

Using these non-dimensional parameters the equation (2.11) now becomes

$$\left[(\mu_x + 2m'\pi)^4(1 + i\eta) - \Omega^2\right] A_{m'} + \kappa_t \sum_{m=-\infty}^{\infty} A_m + \kappa_r \sum_{m=-\infty}^{m=\infty} A_m (\mu_x + 2m\pi).(\mu_x + 2m'\pi)$$

$$= 0 \quad \text{when} \quad m' \neq 0$$

$$= P \quad \text{when} \quad m' = 0 \tag{2.17}$$

Another non-dimensional parameter which is used in the text later is the convection velocity parameter $CV = \left(\frac{m_b}{D'}\right)^{\frac{1}{2}} U_c \ell_x$ where U_c is the convection velocity of the loading $(= \omega/K_x)$.

2.3.2 The special case of transversely rigid supports

If the supports have infinite translational stiffness ($\kappa_t \to \infty$) no beam displacement is possible at the support locations.

Hence at the support at $x = 0$

$$W(0) = \sum_{m=-\infty}^{m=\infty} A_m = 0$$

or

$$A_o = - \sum_{\substack{m=-\infty \\ m\neq 0}}^{m=\infty} A_m \qquad (2.18)$$

so that

$$W(x) = \sum_{m=-\infty}^{\infty} A_m \{ e^{-i(\mu_x + 2m\pi)\frac{x}{\ell_x}} - e^{-i\mu_x \frac{x}{\ell_x}} \} \qquad (2.19)$$

This type of series can therefore be used for a beam with rigid supports, instead of the series of equation (2.4), to allow exactly for the infinite translational stiffness.

To apply the principle of virtual work in this case, the virtual displacements considered will be of the form $\delta A_m \{ e^{-i(\mu_x + 2m'\pi)\frac{x}{\ell_x}} - e^{-i\mu_x (x/\ell_x)} \}$, since they have to be compatible with the condition of zero displacement at the supports.

Following the procedure detailed already for the case of flexible supports, the following non-dimensional system of simultaneous equations for A_m's is obtained for the rigid support case:

$$\sum_{\substack{m=-\infty \\ m\neq 0}}^{m=\infty} \{\mu_x^4 - \frac{\Omega^2}{1 + i\eta}\} A_m + \frac{\kappa_r}{1 + i\eta} \sum_{\substack{m=-\infty \\ m\neq 0}}^{m=\infty} \frac{2m\pi}{\ell_x} \frac{2m'\pi}{\ell_x} A_m + \{(\mu_x + 2m'\pi)^4 - \frac{\Omega^2}{1+i\eta}\} A_m$$

$$= \frac{-P}{1 + i\eta} \qquad (2.20)$$

Equation (2.20) has been obtained by suppressing the term A_o, using equation (2.18). Actually any one of the other coefficients could have been suppressed and the same final answer for the coefficients will emerge.

2.3.3 The special case of zero rotational stiffness of the support

When $\kappa_r = 0$, equation (2.17) modifies to

$$\left[(\mu_x + 2m'\pi)^4(1 + i\eta) - \Omega^2\right]A_{m'} + \kappa_t \sum_{m=-\infty}^{m=+\infty} A_m$$

$$= 0 \quad \text{when} \quad m' \neq 0 \quad m' = -\infty \text{ to } +\infty$$

$$= P \quad \text{when} \quad m' = 0 \qquad (2.21)$$

By successively subtracting one equation from the next in the above system of equations, it is possible to express all other coefficients in terms of any one of them. This particular coefficient can then be evaluated by using any one of the equations. This procedure leads to the following expression for the coefficients:

$$A_{\substack{m \\ m\neq 0}} = \frac{-P\,\kappa_t/\mu_x(1 + i\eta)}{\left[1 - (\frac{\phi}{\mu_x})^4\right]\left[(\mu_x + 2m\pi)^4(1 + i\eta) - \Omega^2\right]\left[1 + s\right]} \qquad (2.22)$$

$$A_o = \frac{-P\,\kappa_t/\mu_x{}^4(1 + i\eta)}{\left[1 - (\frac{\phi}{\mu_x})^4\right]\left[\mu_x{}^4(1 + i\eta) - \Omega^2\right]\left[1 + s\right]} + \frac{P}{\mu_x{}^4(1 + i\eta) - \Omega^2} \qquad (2.23)$$

where

$$s = \frac{\left[\kappa_t/(1 + i\eta)\right]\left[\cot\frac{\mu_x - \phi}{2} - \cot\frac{\mu_x + \phi}{2} + i\cot\frac{\mu_x - i\phi}{2} - i\cot(\frac{\mu_x + i\phi}{2})\right]}{8\phi^3} \qquad (2.24)$$

and $$\phi = \left(\frac{m_b \omega^2}{D}\right)^{\frac{1}{4}} \ell_x = \left(\frac{\Omega^2}{1 + i\eta}\right)^{\frac{1}{4}} \qquad (2.25)$$

2.3.4 Relative magnitudes of the A_m's

It is of considerable interest to know which of the A_m's are of greatest importance in particular cases. Some computed values of the A_m's are presented in Table2.1 which applies to a beam having $\kappa_t = 10^7$ $\kappa_r = 4.0$, $\eta = 0.25$. The pressure field is that of a plane harmonic wave with a velocity parameter 4.0. Table2.1(a) is for a non-dimensional frequency parameter 12.80 which is just above the lowest frequency for the propagation of free flexural waves in the undamped beam (see Ref. 28). The convection velocity of the pressure field is then nearly equal to the free flexural wave speed in the beam at this frequency.

Table 2.1b presents values of the A_m's for a frequency parameter 22.4 and a convection velocity parameter 4.0. This frequency is near the upper frequency bound of the same zone of free propagation which begins at about $\Omega = 12.80$.

When $\Omega = 12.80$ and CV = 4.0 (see Table 2.1a), the A_o term is dominant with A_{-1} slightly less. This is due to the fact that the free wave speed of the A_o wave is closer to the convected pressure wave speed than the free wave speeds of any of the other wave components. As m increases or decreases, the magnitudes of A_m's get progressively smaller. It is significant that both A_{-5} and A_{+4} are approximately 1/1000 times A_o, thus showing that the series of terms for (a) converges rapidly.

When $\Omega = 22.4$ and CV = 4.0 (see Table 2.1(b)), the A_{-1} term has the highest value. This is again explained by the fact that m = -1

makes this component wave length nearest the free flexural wave length in the beam. Rapid convergence of the series may again be observed from the relative magnitude of the A_m's at this frequency.

That one of the coefficients is much larger than the others is in accordance with the known theory of propagation of waves in a continuous medium with periodic perturbations. Sections 28 and 35 of reference [21] deal with free vibrations of such structures in the longitudinal direction.

Tables 2.2-2.3 show how the magnitude of each term is affected by including the higher order terms. They correspond to the beam with $\kappa_r = 4.0$, $\kappa_t \to \infty$, $\eta = 0.25$ excited by loading of convection velocity parameter (CV) = 4.0. The tables are self explanatory. In particular, the $Re(A_o)$ term in the 5 term solution at $\Omega = 14.80$ (table 2.2) is different from the same term in the 9 term solution by just over 3 percent. For $\Omega = 8.0$ (table 2.3) the corresponding difference is about 1.22 percent.

2.4 Response to Harmonic Plane Waves

By solving a suitably restricted set of the simultaneous equations (equation 2.17) the A_m's can be determined. Once the A_m's are known, we can find the response at any point on the beam. For a given beam, this response is evidently a function of μ_x and Ω, and is directly proportional to p_o. In fact we can write

$$W(x) = p_o Y_x(\Omega, \mu_x) e^{i\omega t} \qquad (2.26)$$

where Y_x may be called the 'displacement admittance function' for the point x. The curvature of beam deflection (which is proportional to

the bending stresses) may be related to a 'curvature admittance function' defined (by analogy) by

$$W''(x) = p_o Y''_x(\Omega, \mu_x) e^{i\omega t} \tag{2.27}$$

Evidently if

$$W(x) = \sum_{m=-\infty}^{m=+\infty} A_m \, e^{-i(\mu_x + 2m\pi)\frac{x}{\ell_x}} \, e^{i\omega t}$$

then :

$$W''(x) = \sum_{m=-\infty}^{m=+\infty} -A_m \left(\frac{\mu_x + 2m\pi}{\ell_x}\right)^2 e^{-i(\mu_x + 2m\pi)\frac{x}{\ell_x}} \, e^{i\omega t} \tag{2.28}$$

Since all the A_m's are proportional to p_o, then $Y_x(\Omega, \mu_x)$ and $Y''_x(\Omega, \mu_x)$ are found directly from these two series.

2.5 Response to Boundary Layer and Random Acoustic Plane Waves

2.5.1 The response to random convected pressure fields

The beam response must now be obtained in the first place in the form of a response spectral density $S_w(\Omega)$.

As shown in Appendix A, the convected boundary layer pressure field can be analysed into a wave length frequency spectrum. This essentially means that at a given frequency ω, there is a range of μ_x's present in the excitation (see Figure A.4). Hence, the spectral density of boundary layer pressure at frequency ω and wave number K_x $(= \mu_x/\ell_x)$ can be denoted in the functional form as

$$S_p(\Omega, K_x) \quad \text{or} \quad S_p(\Omega, \mu_x)$$

The power spectral density of the response is also a function of Ω and μ_x. The excitation and response are related as follows:

$$S_{w(x)}(\Omega, \mu_x) = S_p(\Omega, \mu_x)|Y_x(\Omega, \mu_x)|^2 \tag{2.29}$$

$$S''_{w(x)}(\Omega, \mu_x) = S_p(\Omega, \mu_x)\ |Y''_x(\Omega, \mu_x)|^2 \tag{2.30}$$

When these functions are integrated over the whole range of μ_x, the power spectral density is obtained as a function of frequency alone, i.e.

$$S''_{w(x)}(\Omega) = \int_0^\infty S_p(\Omega, \mu_x)\ |Y''_x(\Omega, \mu_x)|^2\, d\mu_x \tag{2.31}$$

The total mean square value of $W''_{(X)}$ in the frequency band $0 < \Omega < \Omega_1$ is found by integrating this over the band, i.e.

$$\langle W''^2(X)\rangle = \int_0^{\Omega_1} \int_0^\infty S_p(\Omega, \mu_x)\ |Y''_X(\Omega, \mu_x)|^2\, d\mu_x d\Omega \tag{2.32}$$

This is in a general form suitable for calculating the response due to a boundary layer pressure field. The form often taken for $S_p(\Omega, \mu_x)$ for a boundary layer is given in Appendix A.

A random acoustic plane wave pressure field has a Ω, μ_x spectrum of δ-function form in μ_x domain, having a non-zero value only at the value of μ_x given by $\mu_x = \Omega/CV$. The mean square curvature is then given by

$$\langle W''^2(X)\rangle = \int_0^{\Omega_1} S_p(\Omega)\ |Y''_X(\Omega, \mu_x(\Omega))|^2\, d\Omega \tag{2.33}$$

2.5.2 Numerical response calculations

The double integration required to obtain $\langle W''^2(X)\rangle$ can only be accomplished numerically. This has been done for a beam with $\eta = 0.25$, $\kappa_r = 4.0$ and $\kappa_t = 10^7$ excited by:

(a) a random acoustic plane wave field having a pressure power spectral density which is constant over the frequency range $0 < \Omega < 32.0$ and a convection velocity parameter of $CV = 4.0$. The spectral density of the pressure has been arbitrarily chosen as unity;

(b) a boundary layer pressure field having a point pressure spectrum of constant unit value over the frequency range $8 < \Omega < 24$. Outside this range, the spectrum was assumed to be zero for reasons given below. The boundary layer decay parameter* was 0.1, and the convection velocity was $CV = 4.0$.

The restricted frequency range of the pressure spectrum was sufficient to cover the whole of the first frequency band of free wave propagation in the beam (see Ref. 28) in which the beam response is high. It excluded the possibility of response in the higher propagation bands. The method of this chapter however, can be used for any range of frequency whatsoever. The above restriction was desirable in order to reduce computation time.

The double integration for the boundary layer problem was first performed in the μ_x-domain at a fixed frequency. Figure 2.2 shows a typical variation of $|Y''_X(\Omega, \mu_x)|^2$ and $S_p(\Omega, \mu_x)$ with μ_x at a given frequency. The integral of their product may, in fact,

* See Appendix A

derive principally from two narrow μ_x ranges in the vicinity of the two peaks if the peaks are very sharp. Numerical integration of the product need then only be performed over these ranges to obtain results of acceptable accuracy. On the other hand, if these peaks are not sharp (i.e. the beam is heavily damped giving relatively flat response curve and the boundary layer decay parameter b is large), then the integration must be performed over a much wider range of μ_x's. In the present calculations, the integration extended over the whole μ_x range from $\mu_x = 0$ to $\mu_x = 8.0$. Trapezoidal rule integration was used with increments of $\mu_x = 0.4$.

The integration with respect to μ_x yields the response power spectral density at the given frequency. Integration of this power spectral density over the frequency range yields the mean square value of the response. This integration was conducted numerically using the trapezoidal rule with increments of frequency (Ω) of 0.4. It was found to be sufficiently accurate to integrate only over the range $8 < \Omega < 24$ for there was no significant contribution to the mean square response outside this range.

Computations were performed on an ICL 1907 computer. The flow diagram for the whole computational process is shown in Appendix B. Curvature results were normalised by dimensional quantity $p_o \ell_x^2/D'$.

2.6 Discussion of Results

2.6.1 Acoustic plane wave excitation

Figures 2.3, 2.4, 2.5, 2.6 and 2.7 show computed results for

the beam excited by acoustic plane waves. Spectra for the beam curvature at mid-span are shown in Figures 2.3 and 2.4; peak values of power spectral density at different convection velocities are shown in Figure 2.5; r.m.s. values of the curvature are shown in Figure 2.6. Figure 2.3 shows the curvature spectra computed using eleven terms in the series for the beam response. These curves are actually quite indistinguishable from accurate calculations performed by Mead and Wilby [27] (also reported by Mead in Ref. 10) who used a closed-form solution for the response. It will be observed that the spectrum peaks move to higher frequencies as the pressure field convection velocity increases. This can be easily explained by the arguments presented in Reference 28.

It may be mentioned here that computations by the method of Section 5 ($\kappa_t \to \infty$) and those by the method of Section 4 taking $\kappa_t = 10^7$ differ only in the fourth or fifth significant decimal place. This should confirm that in the limit (very high κ_t), the general method will give results agreeing completely with those from the method for the special case of rigid supports ($\kappa_t \to \infty$).

The different curves of Fig. 2.4 show the responses calculated by taking a different number of terms. The 11-term curve can be regarded as representing the exact response, and it is clear that the 7-term curve scarcely differs from it. With only three terms, the peak power spectral density is about 2% less than the exact value, and with five terms it is about 4% greater than the exact values. Hence, a very crude approximation to the beam deflection (by using only three or five terms) yields surprisingly accurate values of the curvature spectral density.

Such high accuracy is not maintained with higher values of the convection velocity parameter (see Fig. 2.5). When CV = 16, the 3-term peak spectral response is 22% greater than the exact value, whereas the 5-term response is 9% less. The 7-term response maintains close agreement throughout.

The r.m.s. response (obtained by integrating the spectra) are in rather closer agreement over the whole CV range than the peak values (see Figures 2.5, 2.6). The peak in these curves at CV = 4 has been found before by Mead and Wilby and occurs at the lowest convection velocity at which a 'primary coincidence' effect can occur (ref. 28).

Fig. 2.7 shows the influence of beam loss factor η on the spectral density of curvature at midspan of the beam for CV = 4.0 obtained by including eleven terms in the series. It is seen that the effect of damping is most marked at frequencies where there are peaks in the response curve. The damping sensitive peak value for a very low value of $\eta = 0.01$ (not plotted) was within 1.55 percent of the accurate value of Mead and Wilby. Inclusion of only three terms in the series in this case gave a peak value which differed from the exact solution by about 4 percent only.

2.6.2 Boundary layer excitation

Response spectra for boundary layer excitation are shown in Fig. 2.8. The curves for different numbers of terms are very similar in shape, and the peak and r.m.s. values differ at most by only 5%, the 7-term curve follows the 11-term (exact) curve very closely. The r.m.s. value from the 3-term curve is only 2% higher.

For the purpose of stress-calculation, therefore, we may deduce

that approximate values of sufficient accuracy may be obtained from computations using just three terms in the response series, so long as the dominant part of the response stems from the first band of free-wave propagation.

These results were obtained from a boundary layer pressure spectrum having a constant value over the frequency range $8 < \Omega < 24$. It is generally accepted that a real boundary layer pressure spectrum has a broad, flat top (between about 200 Hz and 3000 Hz) but above a certain cut-off frequency it drops off with frequency. Such a variation of pressure spectral density could easily be included in the calculation of the response spectrum and r.m.s. values, simply by multiplying the response spectral density presented in Fig. 2.8 by the known real value of the pressure spectral density.

2.7 Conclusions

The method of space harmonics as described and illustrated in the foregoing sections offers a powerful technique for obtaining the response of periodic structures to random acoustic wave and boundary layer pressure. It has been seen that the inclusion of only three terms in the series solution yields results which agree acceptably with the closed form solution in the frequency range of the first propagation band.

From the point of view of computation, this is a relatively simple method. After the linear algebraic equations are set up, it only uses a Library subroutine for the solution of simultaneous equations with complex coefficients.

There is no restriction on the magnitude of damping allowable

in the structure for the method to succeed. Normal mode methods of analysis often assume that the damping is small enough for distinct resonant peaks to occur without 'modal overlap'. No such restriction is necessary in the method of space harmonics, and the response of a system with large damping is computed as easily and accurately as that of a system with small damping.

The method lends itself readily to the determination of the sound radiated by the structure. This is so because each term of the series solution represents a travelling wave and is spatially harmonic.

3. SOUND RADIATION FROM "ONE DIMENSIONAL" STIFFENED PLATES UNDER RANDOM CONVECTED LOADING

3.1 Introduction

In Chapter 2 it was explained how the orthogonally stiffened plate could be treated as a one dimensional structure for low order lateral modes, especially when its aspect ratio was high. It was explained that the response of such a one dimensional model to random convected loading (including that to boundary layer pressure field) could be obtained in a series of space harmonics. The coefficients of this series were shown to be satisfactorily converging so that only a limited number of terms were to be included in the series to yield a solution of reasonable accuracy.

We turn now to the problem of sound radiated by such structures. This is important, for instance, in the case of an aeroplane fuselage, the structure of which can be regarded as periodic, and which transmits undesirable sound into the interior by virtue of the surface vibration. This analysis of sound radiation is usually made by the application of the normal mode approach and working in terms of resistance ratio, i.e. the ratio of the energy dissipated to the fluid to that dissipated within the structure (for the concept of radiation resistance, see for example, reference 35). It is also sometimes assumed that the radiation does not appreciably influence the response. However, even under this assumption, the analysis can be very difficult. On the other hand if the response of the structure is known in a form which is spatially harmonic, it can be done rather easily. The response in such a form (as a series of space harmonics) was obtained in Chapter 2. Each one of the terms in this infinite series is spatially harmonic and represents a forced travelling

wave with its own velocity depending upon the frequency and convection velocity of excitation and also on its order in the series. Some of these terms will have supersonic phase velocities, even at subsonic convection velocities of loading.

In this chapter the above series of space harmonics is adapted for the problem of sound radiation. The influence of radiation damping can be easily incorporated in the analysis. The amplitude of each travelling wave is determined by the principle of virtual work as in Chapter 1. Following that an expression for the pressure radiated is derived for each harmonic and the associated power is then calculated.

3.2 The Structure and Excitation

The plate considered is assumed to be flat and infinite in both directions and has parallel, equi-spaced stiffeners in the Y-direction only. The stiffeners are assumed to be identical line supports exerting translational and rotational constraints on the plate. The plate is excited by a loading intensity $p_o \exp(-iK_x x) \exp(i\omega t)$ per unit area. K_x is the wave number of the loading in the X-direction. This loading corresponds to harmonic pressure waves traversing the plate in the X-direction only.

Since the loading is independent of Y, so also must be the response. It is therefore convenient to consider a unit width of the plate which extends infinitely in the X-direction. This makes it effectively equivalent to a periodically supported beam (see Figure 1.2) tha analysis of which (excluding the sound radiation aspects) has already been reported in Chapter 2. Following the outline of that analysis this chapter will include these aspects. The extended analysis of the plate

stiffened in both perpendicular directions will form the subject of the next chapter and will then include the Y dependence of the loading as well as that of the induced response.

3.3 Acoustic Effects

3.3.1 Inclusion of the acoustic radiation in the equation of motion

The pressure at any point in the acoustic medium adjacent to the plate must satisfy the wave equation

$$\nabla^2 p_r = \frac{1}{c^2} \frac{\partial^2 p_r}{\partial t^2} \tag{3.1}$$

subject to the boundary condition that at the surface $z = 0$, the normal particle velocity in the medium adjacent to the beam must equal the normal velocity of the plate.

From equation (2.4) the normal beam velocity is given by

$$\hat{W}(x, t) = i\omega \sum_{m=-\infty}^{m=+\infty} A_m e^{-i(\mu_x + 2m\pi)\frac{x}{\ell_x}} e^{i\omega t} \tag{3.2}$$

from which it follows that the pressure must be expressed in the form

$$p_r(x,z,t) = \sum_{m=-\infty}^{m=+\infty} e^{-i(\mu_x + 2m\pi)\frac{x}{\ell_x}} f_m(z) e^{i\omega t} \tag{3.3}$$

Each term of the series of equation (3.3) must satisfy the wave equation. Substituting the general term in the wave equation, the following ordinary differential equation for $f_m(z)$ is obtained

$$\frac{d^2 f_m(z)}{dz^2} = - K_{mz}^2 f_m(z) \tag{3.4}$$

Evidently then

$$f_m(z) = B_m e^{-iK_{mz}z} + C_m e^{iK_{mz}z} \tag{3.5}$$

where

$$K_{mz}^2 = (\frac{\omega}{C})^2 - (\frac{\mu_x + 2m\pi}{\ell_x})^2 \tag{3.6}$$

The B_m term in equation (3.5) represents the pressure being radiated away from the beam surface by virtue of its vibration. The C_m term represents the reflection of the B_m wave by another boundary. It will be assumed here that no such other boundaries exist so that the pressure will be given by only one of the terms in equation (3.5). Thus it may be written as

$$p_r(x,z;t) = \sum_{m=-\infty}^{m=+\infty} B_m e^{-i(\mu_x+2m\pi)\frac{x}{\ell_x}} e^{-iK_{mz}z} e^{i\omega t} \tag{3.7}$$

The velocity V of the particles of the acoustic medium at $z = 0$ is given by

$$V = \frac{i}{\underline{K}\rho_a C} \left|\frac{\partial p_r}{\partial z}\right|_{z=0}$$

$$= \sum_{m=-\infty}^{m=+\infty} \frac{K_{mz}}{\underline{K}\rho_a C} B_m e^{-i(\mu_x+2m\pi)\frac{x}{\ell_x}} e^{i\omega t} \tag{3.8}$$

where $\underline{K} = \frac{\omega}{C}$ is the wave number of sound

and ρ_a is the density of the acoustic medium.

After equating (3.2) and (3.8), B_m is found to be equal to $A_m i\omega\rho_a C/(K_{mz}/\underline{K})$ and the radiated pressure may then be expressed as

$$p_r = \sum_{m=-\infty}^{m=+\infty} A_m \frac{i\omega\rho_a C}{(K_{mz}/\underline{K})} e^{-i(\mu_x+2m\pi)\frac{x}{\ell_x}} e^{-iK_{mz}z} e^{i\omega t} \tag{3.9}$$

This represents the pressure radiated from one side of the beam. If the contribution of both the sides of the beam is to be considered, this expression may again be used with values of C and ρ_a applying to the other side and the two contributions added.

The radiated pressure at the surface of the beam (i.e. at $z = 0$) affects the beam vibration and must therefore be included in the equation of motion of the beam. After the assumed displacement solution has been substituted into this, it becomes

$$\sum_{m=-\infty}^{m=+\infty} \left[D\left(\frac{\mu_x + 2m\pi}{\ell_x}\right)^4 - m_b\omega^2 + \frac{i\omega\rho_a C}{(K_{mz}/K)}\right] A_m e^{-i(\mu_x+2m\pi)\frac{x}{\ell_x}} = p_o e^{-i\mu_x \frac{x}{\ell_x}} \qquad (3.10)$$

3.3.2 Sound pressure and sound power radiated

From equation (3.9)

$$p_r = \sum_{m=-\infty}^{m=+\infty} A_m \frac{i\omega K\rho_a C}{K_{mz}} e^{-i(\mu_x+2m\pi)\frac{x}{\ell_x}} e^{-iK_{mz}z} e^{i\omega t}$$

$$= \sum_{m=-\infty}^{m=+\infty} A_m \frac{i\omega^2\rho_a}{K_{mz}} e^{-i(\mu_x+2m\pi)\frac{x}{\ell_x}} e^{-iK_{mz}z} e^{i\omega t} \qquad (3.11)$$

Next we obtain $\Pi(\omega)$ the space time average of the sound power radiated per unit length of the beam at frequency ω. The contributions from all the harmonics must be added.

Instantaneous Power radiated per bay length $= \int_0^{\ell_x} p_r V dx \qquad (3.12)$

where p_r and V are the pressure and velocity for $z = 0$.

Hence, $\Pi(\omega)$ the space-time average power radiated per unit length is

given by the following relation:

$$\Pi(\omega) = \frac{1}{\ell_x} \int_0^{\ell_x} \overline{p_r V} \, dx \tag{3.13}$$

If p_r and V are complex quantities as is the case here,

$$\Pi(\omega) = \frac{1}{\ell_x} \int_0^{\ell_x} \tfrac{1}{2} \, \mathrm{Re}(p_r V^*) dx \tag{3.14}$$

where V^* is the complex conjugate of velocity.

(See Appendix C for the method to find the time average of the product of two complex functions.)

When the expressions for p_r and V^* are substituted from equations (3.11) and (3.2) respectively, equation (3.14) yields

$$\Pi(\omega) = \sum_{m=-\infty}^{m=+\infty} \tfrac{1}{2} \, \frac{\omega^2 \rho_a C}{K_{mz}/\underline{K}} \, |A_m|^2 \tag{3.15}$$

where the summation extends over all real values of K_{mz}.

3.4 Equations for the Coefficients of the Series

As in Chapter 2, we may use the principle of virtual work to derive the system of simultaneous equations for the determination of A_m's. When the acoustic loading terms are included, these equations become for $m' = -\infty$ to $+\infty$

$$\left[D\left(\frac{\mu_x + 2m'\pi}{\ell_x}\right)^4 - m_b\omega^2 + \frac{i\omega\rho_a C}{K_{m'z}/\underline{K}}\right]\ell_x A_{m'} + K_t \sum_{m=-\infty}^{m=+\infty} A_m$$

$$+ \sum_{m=-\infty}^{m=+\infty} K_r \, \frac{\mu_x + 2m\pi}{\ell_x} \, \frac{\mu_x + 2m'\pi}{\ell_x} A_m = 0 \quad \text{for } m' \neq 0$$

$$= p_o \ell_x \quad \text{for } m' = 0 \tag{3.16}$$

This equation is identical to the corresponding equation (2.10) in Chapter 2, except for the term $\left(\frac{i\omega\rho_a C}{K_{mz}/K}\right)$ which allows for the effect of radiation. When K_{mz} is real, it is equivalent to additional damping in the beam, and when K_{mz} is imaginary, it has an additional mass or stiffness effect.

As in Chapter 2 equation (3.16) may be written in the non-dimensional form, by use of the following non-dimensional parameters:

$$\text{Frequency parameter } \Omega = \left(\frac{m_b \omega^2 \ell_x^4}{D'}\right)^{\frac{1}{2}} \tag{3.17}$$

where D' is given by $D = D'(1 + i\eta)$ (3.18)

(η is the beam loss factor).

$$\text{Transverse stiffness parameter } \kappa_t = \frac{K_t \ell_x^3}{D'} \tag{3.19}$$

$$\text{Rotational stiffness parameter } \kappa_r = \frac{K_r \ell_x}{D'} \tag{3.20}$$

$$\text{Loading parameter } P = \frac{p_o \ell_x^4}{D'} \tag{3.21}$$

$$\text{Medium-beam density ratio } \rho_r = \frac{\rho_a h}{m_b} \tag{3.22}$$

$$\text{z-wise phase parameter } \mu_{mz} = K_{mz} h \tag{3.23}$$

Using these non-dimensional parameters the equation (3.16) now becomes

$$\left[(\mu_x + 2m'\pi)^4(1 + i\eta) - \Omega^2 + \frac{i\Omega^2\rho_r}{\mu_{mz}}\right] A_{m'}$$

$$+ \kappa_t \sum_{m=-\infty}^{m=+\infty} A_m + \kappa_r \sum_{m=-\infty}^{m=+\infty} (\mu_x + 2m\pi)(\mu_x + 2m'\pi) A_m$$

$$= 0 \quad \text{when} \quad m' \neq 0 \qquad m' = -\infty \text{ to } +\infty$$

$$= P \quad \text{when} \quad m' = 0 \tag{3.24}$$

Another non -dimensional parameter which is used later in the text is

the convection velocity parameter

$$CV = \left(\frac{m_b}{D'}\right)^{\frac{1}{2}} U_c \ell_x \qquad (3.25a)$$

where U_c is the convection velocity of the loading $(= \omega/K_x)$. The convection velocity parameter corresponding to the velocity of sound C $(= \frac{\omega}{K})$ is

$$SV = \left(\frac{m_b}{D'}\right)^{\frac{1}{2}} C\ell_x \qquad (3.25b)$$

By solving a suitably restricted set of the above simultaneous equations, the A_m's can be determined. Once the A_m's are known, we can find the response at any point of the beam. This response would then include the effects of radiation damping. Also we would then be able to write the radiation pressure and the radiated power as given in the preceding sections.

3.5 Conditions for Real Radiation

3.5.1 The radiating harmonics

Any one of the space-harmonic wave components will radiate real sound power provided the z-wise wave number of the corresponding sound wave component is real. Such a component will be called a 'radiating harmonic'. From section 3.3 (see equation (3.6) it is seen that the z-wise wave number K_{mz} is given by

$$K_{mz}^2 = \left(\frac{\omega}{C}\right)^2 - \left(\frac{\mu_x + 2m\pi}{\ell_x}\right)^2$$

The zeroth space harmonic (m = 0) will therefore radiate provided

$$\left(\frac{\mu_x}{\ell_x}\right)^2 < \left(\frac{\omega}{C}\right)^2$$

The critical radiating condition for the zeroth harmonic may be said to exist when

$$\left|\frac{\mu_x}{\ell_x}\right| = \frac{\omega}{C}$$

i.e.

$$\text{when} \qquad |\mu_x| = \frac{\omega \ell_x}{C} = \frac{\Omega}{SV} \tag{3.26}$$

This simple condition is equally simply represented in Figure 3.1 in which the abscissa is Ω and the ordinate is μ_x. The lines OP, OR have the slopes $\pm$ 1/SV at a given Ω. If the excitation on the beam imposes a value μ_x at a frequency Ω which lies within the triangle POR, the condition represented by equation (3.26) is satisfied and the zeroth harmonic will radiate. We shall call the triangle POR the 'primary zone of radiation' to indicate its correspondence with the zeroth space harmonic which is the dominant term in the series.

If plane-wave harmonic excitation is being convected at speed CV, then μ_x is related to Ω through

$$\mu_x = \frac{\Omega}{CV}$$

Thus a line of slope 1/CV represents all the values of μ_x imposed by this pressure field over the frequency range. If this line lies outside POR, the convection velocity of the excitation is less than the speed of sound, and the zeroth term cannot radiate. However, it is possible that one of the higher terms in the series will radiate as the following argument shows.

One of the higher terms will radiate, provided

$$\frac{\mu_x + 2m\pi}{\ell_x} < \frac{\omega}{C}$$

or if $\mu_x + 2m\pi < \frac{\Omega}{SV}$

Hence if point X on Figure 3.1 represents the imposed value of μ_x at frequency Ω, the m^{th} harmonic will radiate, if the value of $\mu_x + 2m\pi$ lies within the primary zone of radiation. For the particular value of X shown, the harmonics $m = -4, -5, -6$ and -7 all satisfy this condition, so all these will radiate. If μ_x lies within the primary zone of radiation (at Y say) several harmonics may still radiate provided $\mu_x + 2m\pi$ also lies within the zone.

Next consider the frequency zone $\Omega < \Omega_d$. The diagram here is divided into triangles the sides of which are parallel to OP and OR (slopes $\pm$ 1/SV) and the apices of which are 2π apart. If μ_x in this zone falls inside one of these hatched triangles, then subtraction (or addition) of an integral number times 2π will not bring the value into the primary radiation zone, so no wave components can radiate. These hatched triangles may therefore be termed as 'dark zones' or 'zones of no radiation'. If μ_x for $\Omega < \Omega_d$ lies outside these hatched triangles, the subtraction (or addition) of an integral number times 2π will bring the value into the primary zone and true sound radiation will then result. It is easily shown that the value of Ω_d is π.SV.

To evaluate the sound power radiated at a given frequency, the number of terms included in the series (equation 3.11) must include all the radiating harmonics otherwise the misleading conclusion may be drawn that no sound radiation is possible at that frequency. However, very high order harmonics may still be neglected because their contributions to sound power will be negligible.

3.5.2 The frequency bands of radiation

We now show that bands of frequencies exist in the range $0 < \Omega < \pi(SV)$ in which sound can or cannot be radiated. Suppose plane harmonic pressure waves of all frequencies are convected over the beam at a speed corresponding to, say, $CV = SV/7$ (see now Figure 3.2). The values of μ_x in this wave field are represented by the line OABCDEF.... Since the segments OA, BC, DE lie in the dark zones, no sound is radiated in the corresponding frequency bands by any of the space harmonics generated. These segments therefore define frequency bands of no radiation. Between these bands of real radiation exist.

It is easily shown that the frequency corresponding to point A on Figure 3.2 is given by

$$\Omega_A = \frac{2\pi}{\frac{1}{CV} + \frac{1}{SV}} \tag{3.27}$$

Similarly the upper bounding frequency of the N^{th} band of no radiation is

$$\Omega_{N+} = \frac{2N\pi}{\frac{1}{CV} + \frac{1}{SV}} \tag{3.28}$$

and the lower bounding frequency of this band is

$$\Omega_{N-} = \frac{2(N-1)\pi}{\frac{1}{CV} - \frac{1}{SV}} \tag{3.29}$$

The frequency bandwidth of the N^{th} band for radiation is

$$\begin{aligned} \Delta\Omega_{rad} &= \Omega_{(N+1)-} - \Omega_{N+} \\ &= \frac{4N\pi}{SV} \left| \frac{1}{CV^2} - \frac{1}{SV^2} \right|^{-1} \end{aligned} \tag{3.30}$$

If radiation is to occur at all frequencies, i.e. $\Delta\Omega_{rad} = \infty$, then we must have $CV = SV$ which also defines the boundaries of the primary zone of radiation.

It is evident also from Figure 3.2 that with a pressure field convected at speed CV ($< SV$) there must be $NI(\frac{SV}{2CV})$ bands of no radiation where $NI(X)$ signifies 'nearest integer to X'.

3.6 Sound Power Radiated by Random Convected Loadings

3.6.1 The sound power spectrum and mean power radiated

$S_\pi(\Omega, \mu_x)$, the spectral density of the power radiated and $S_p(\Omega, \mu_x)$ that of the exciting pressure, are functions of Ω and μ_x, and are related by

$$S_\pi(\Omega, \mu_x) = S_p(\Omega, \mu_x) \; |Y_p(\Omega, \mu_x)|^2 \qquad (3.31)$$

where $|Y_p(\Omega, \mu_x)|^2$ is the power admittance function. It equals the power radiated per unit length of the beam when excited by harmonic pressure of unit amplitude at frequency Ω and phase constant μ_x. It can be derived from equation (3.15) in the following manner (see Section 3.3.2).

Let the value of A_m per unit harmonic pressure amplitude at frequency Ω and phase constant μ_x be $\bar{A}_m(\Omega, \mu_x)$; then

$$|Y_p(\Omega, \mu_x)|^2 = \sum_{m=-\infty}^{m=+\infty} \frac{1}{2} \frac{\omega^2 \rho_a C}{K_{mz}/K} \; |\bar{A}_m(\Omega, \mu_x)|^2 \qquad (3.32)$$

where the summation extends over all real values of K_{mz}. It is convenient to represent this in a non-dimensional form for computational purposes. For this we can divide equation (3.32) by the dimensional parameter $\ell_x^2/(m_b D')^{\frac{1}{2}}$.

Thus

$$|\bar{Y}_p(\Omega, \mu_x)|^2 = \frac{|Y_p(\Omega, \mu_x)|^2}{\ell_x^2/(m_b D')^{\frac{1}{2}}} \qquad (3.33)$$

The power spectral density of the radiated power can be obtained as a function of frequency alone by integrating equation (3.31) over all μ_x, i.e.

$$S_\pi(\Omega, \mu_x) = \int_0^\infty S_p(\Omega, \mu_x)|Y_p(\Omega, \mu_x)|^2 \, d\mu_x \qquad (3.34)$$

The total time averaged power radiated $<\Pi>$ in the frequency band $0 < \Omega < \Omega_1$ can be found by integrating over this band, i.e.

$$<\Pi> = \int_0^{\Omega_1} \int_0^\infty S_p(\Omega, \mu_x)|Y_p(\Omega, \mu_x)|^2 d\mu_x d\Omega \qquad (3.35)$$

$<\Pi>$ may be referred to as the total mean power or mean power in a frequency band $0 < \Omega < \Omega_1$.
The non-dimensional form of this is

$$\frac{<\Pi>}{\ell_x^2/(m_b D')^{\frac{1}{2}}} = \int_0^{\Omega_1} \int_0^\infty S_p(\Omega, \mu_x)|\bar{Y}_p(\Omega, \mu_x)|^2 d\mu_x d\Omega \qquad (3.36)$$

This is in a general form suitable for calculating the response due to any form of convected pressure field including a boundary layer pressure field.

3.6.2 Computation of sound power spectra

Computations have been performed to determine the influence of the number of terms on the calculated power spectral density of sound power radiated at different frequencies and on the total mean values. As in Chapter 2, the computations were performed on ICL 1907 computer. The general scheme of computation is the same as given in Appendix B, except that the

sound power has been computed rather than the curvature. The computation was performed with an Ω step of 0.4.

The specific structure for which the computations were made had the following non-dimensional characteristics.

$$\kappa_r = 4.0$$

$$\kappa_t = 10^7$$

$$\eta = 0.02$$

Two specific excitation fields were considered.

(a) Random plane waves having a constant pressure spectral density over the non-dimensional frequency range $8 < \Omega < 24$. Different convection velocities from CV = 2 to CV = 70 were considered.

(b) Boundary layer pressure fluctuations having the same constant power spectral density over the non-dimensional frequency range $8 < \Omega < 24$. Only one convection velocity was considered, i.e. CV = 4.0. The boundary layer decay parameter (see Appendix A) = 0.1.

The sound velocity parameter SV = 10.

3.6.3 Results for plane wave excitation

Figure 3.3 shows the spectral density of the power radiated at different frequencies, when a different number of terms are included in the series and the beam is excited by subsonic plane waves having CV = 2.0, SV = 10.0. It is seen that when three terms are included in the series, the evaluated radiation is very different from the results when five, seven or eleven terms are included. The values given by five terms and seven terms are however quite close to each other. Seven terms give results so close to those given by eleven terms that it is very difficult to show the difference on the graph.

It is seen that there is no radiated power till a frequency $\Omega = 10.8$. Then there is a band of radiation up to $\Omega = 15.6$. Thereafter there is a dark band up to $\Omega = 21.2$ wherefrom the radiating band of frequencies again starts. In the latter radiating band, i.e. from $\Omega = 21.2$, the power radiated is of the order 10^{-2} times that in the first radiating band. In this band the three term curve does not appear at all because if only three terms are included in the series for the displacement, none of these terms yields a supersonic velocity.

Figure 3.4 shows the variation of the mean value when different number of terms is included in the series solution for the beam excited by a plane wave with CV = 4.0, SV = 10.0. It is seen that except for 3 term solution, the agreement between 5, 7 and 11 term solutions is very good. At CV = 5 the 7 term value differs from the 11 term value by only about one per cent while the 5 term value varies by about three per cent. Thus it may be seen that when mean value is to be calculated for the frequency ranges lying in the first band of free propagation, only 5 terms need be included in the series.

It may be noticed that there is a peak in the curves around CV = 3.5. It is because for all convection velocities most of the contribution to mean value is derived from values near the peak and these peak values are very high for CV = 3.5 (see Figure 3.11). This may be explained by studying Figure 1.4. In the band of free propagation, segment B'C' will cause secondary coincidences for CV $\simeq$ 3.5. Hence a large response for this convection velocity.

Figure 3.5 shows the effect of the number of terms on the peak spectral density of the power radiated in the frequency range $8 < \Omega < 24$

for a range of convection velocities. The sound velocity parameter assumed for the purpose of this computation is 10.0 so that the power radiated is plotted for subsonic convection velocities. The beam considered has $\kappa_r = 4.0$, $\kappa_t = 10^7$ and $\eta = 0.02$. For CV = 4.0 if 5 terms are included in the series, the computed value of the peak radiated power is approximately ten per cent higher than the value obtained by including eleven terms. The power computed by including seven terms in the series is approximately five per cent higher than the value obtained with eleven terms in the series. The values at other convection velocities also show agreements of about the same order. Maximum variation from the values obtained by eleven terms occurs when only three terms are included. At CV = 5.0 the 3 term value is twenty per cent higher than the 11 term value though at CV = 6.0 the agreement is considerably better.

Figure 3.6 gives the mean value of the power radiated per unit length of the beam at different convection velocities of plane waves. Eleven terms are included in the series. The full curve refers to the stiffened beam and the dotted curve is for the unstiffened beam, other particulars remaining the same. The sound velocity parameter assumed for computations is taken as 10.0 so that the convection velocities with CV < 10.0 are subsonic. It may be observed that even for subsonic convection velocities of the loading, some radiated sound is present for the stiffened beam while no such power is expected for the unstiffened beam. For super-sonic convection velocities (CV > 10) the power radiated by the stiffened beam is about 7 dB higher than for the unstiffened beam. It is well known that the radiation resistance of structures carrying supersonic flexural waves is ρc per unit area. Therefore the difference in levels of sound power radiated by stiffened and unstiffened beams for CV > 10 is explained by the difference in the corresponding response levels.

It may seem surprising that for the stiffened beam there is no sound power radiated for subsonic velocities greater than 6. This may be

explained by the fact that for CV's > 6.0, the minimum frequency to be in the radiation zone is outside the range $8 < \Omega < 24$, over which the power is being averaged in the case presented. This may be verified from Figure 3.2.

Figure 3.7 studies the effect of including different numbers of terms on the peak value of sound power radiated in the given frequency band at different convection velocities. Since the convection velocity corresponding to the velocity of sound was assumed to be 10.0, all the convection velocities plotted are supersonic. As a result of this situation the zeroth term in all cases is radiating. This explains why even the three term solution peak is quite near the 11 term solution peak for the cases plotted.

3.6.4 Boundary Layer Excitation

Figure 3.8 shows the wave number spectrum of the radiated power or the contribution to the sound power from different wave lengths present in the boundary layer pressure field. This corresponds to different μ_x's where $\mu_x = K_x \ell_x$. It may be noted that for the case plotted ($\Omega = 24.0$, CV = 4.0, $\kappa_r = 4.0$, $\kappa_t = 10^7$ and $\eta = 0.02$) the sound power radiated at $\mu_x = 8.0$ is of the order of 10^{-3} times that at $\mu_x = 2.0$. This variation enables us to obtain the sound power radiated in the case of excitation by boundary layer pressure field by integration over a limited range of μ_x's, though theoretically speaking, all wave lengths must be considered for the exact analysis. The diagram also illustrates that at a given frequency, it is possible to have a range of wave lengths which will not radiate (see range of μ_x's between

2.0 and 4.0). This is consistent with the principles illustrated by Figures 3.1 and 3.2.

Figure 3.9 shows the effect of the number of terms on the peak value of the sound power radiated for the same beam under excitation by boundary layer pressure field of convection velocity CV = 4.0 and boundary layer decay parameter 0.1. The results by including only three terms are very different from 5, 7, or 11 term values. The 5-term value is approximately 11 percent higher than the 11-term value, whereas the 7-term value is approximately 4 percent higher.

Figure 3.10 shows how the computed mean power varies with the number of terms used in the series for the same data as applies to Figure 3.9. Except the 3-term value, all values have a very much closer agreement than they have in the case of the peak response which is shown in Figure 3.9. The maximum variation then is between the 5 term and the 11 term value, and is of the order of 6 percent.

3.6.5 Comparisons of Sound Power Spectra

Figure 3.11 shows the spectral density of sound power radiated when excitation is by subsonic plane waves with CV = 2, 3.5, 4.0 and 5.5. Also drawn on the same figure for comparison is the spectral density of sound power radiated when the excitation is by boundary layer pressure field having CV = 4.0. It is seen that in the case of excitation by plane waves, there are bands of real sound radiation. As the convection velocity increases, these bands start at higher frequencies. Such bands of radiation have been predicted in Section 3.5.2. It is also seen that the sound radiated by plane wave with CV = 3.5 (also see Figure 3.4) is higher than for any other plane wave. This is explained

in Section 3.6.3 with the help of Figure 1.4.

In the case of boundary layer excitation, there is sound radiation at all frequencies (see the chain dotted curve). This is explained by the fact that at a given frequency (for boundary layer excitation), there is a continuous spectrum of wave lengths, some of which must radiate. The presence of peaks in the sound power curve may also be explained by this spectrum of wave lengths. However, the maximum contribution to sound power for boundary layer excitation is in the frequency band where the plane wave of the same convection velocity (CV = 4.0) radiates, though the corresponding levels are on the whole higher in this case. This difference in levels may be explained by the fact that at a given frequency the boundary layer pressure field contains all wave length components including the one corresponding to the plane wave at that convection velocity. The difference in the sound power in the two cases then will be the contribution by these additional wave length components not present in the plane wave. (The exact comparison between powers radiated in the two cases must, however, take account of the corresponding spectral densities.) At subsonic velocities of loading, the contribution by low wave numbers can be considerable because the corresponding component phase velocities are supersonic. This enables the zeroth order space harmonic to radiate, though the falling spectrum at these wave numbers makes its contribution smaller. But it could still be comparable with the contribution by the wave number $K_x = (\Omega/CV)/\ell_x$, corresponding to which only one of the higher terms may radiate, and for which the spectrum peaks.

At supersonic convection velocities of the boundary layer, the zeroth term can radiate. Also, the pressure power spectral density peaks

at the wave number of the zeroth term. The sound radiation contribution from this wave number in the case of boundary layer is, therefore, large compared to the contribution from other wave numbers. Thus the sound power radiated by plane wave loading and that by boundary layer pressure field will be of similar magnitudes when convection velocities are supersonic. For such convection velocities the modelling of the boundary layer pressure field by a plane wave of the same convection velocity is therefore a more reasonable approximation than for subsonic convection velocities, where the contributions from small wave number components of the boundary layer may be significant. However, this could also be a reasonable approximation for subsonic velocities if the frequencies of interest are high enough to ensure sound radiation by the zeroth order term in the series.

3.7 Conclusions

In this chapter the series solution proposed in Chapter 1 has been applied to obtain the sound power radiated by the stiffened beam. It was seen that sound radiation was possible even at a subsonic velocity of loading and this was seen to be due to the presence of periodically spaced stiffeners. A simple diagram was developed to identify the terms in the series which would lead to true sound radiation. At supersonic velocities the zeroth term is able to radiate, and since this term is a dominant term of the series, the minimum number of terms necessary to be included in the series for reasonable accuracy is smaller than for the case of subsonic convection velocities where only the higher order terms may radiate.

It is seen that the series representing the sound power radiated converges satisfactorily. All available evidence suggests that if eleven terms are included in the series, the sound power evaluated would be very accurate. Inclusion of only five terms gives reasonable results. The convergence is better for the mean value than for the peak value in the frequency range discussed.

It has been shown that for a plane wave loading convected at subsonic velocities, there are bands of radiating frequencies when the frequencies of excitation are below a certain value. This value depends for a given velocity of sound, on the characteristics of the vibrating structure.

The comparison of the sound power radiated by stiffened and unstiffened beams has shown that at supersonic convection velocities of loading, the stiffened beam radiates much more power than the unstiffened beam. (There can be no sound power for unstiffened infinite beams at subsonic velocities of loading.)

This chapter deals with the sound radiation when the excitation frequency range is in the first band of free propagation [28]. However, it is expected that in the higher bands of propagation, the number of terms required to be included in the series solution for a given accuracy will be smaller. This is because at higher frequencies, the zeroth harmonic is more likely to be a radiating harmonic. Since this is a dominating term, only a small number of terms will then be necessary to be included in the series for obtaining a result with a reasonable accuracy.

In the case of excitation by boundary layer pressure, there is a range of wave numbers K_x present at a given frequency. It is possible that low values may radiate. If the radiated sound power is to be calcu-

lated accurately, the wave number spectrum must be known accurately in the region of these low wave numbers. It would thus be of practical interest to investigate the effect of taking different expressions for the wave length spectrum on the sound power radiated by the structure. This aspect is outside the scope of the present study. However, the method presented in this chapter can be used to calculate the sound power radiated by ideal, infinite, periodic structures subjected to any general excitation if the wave length-frequency spectrum of that excitation is known.

4. RESPONSE OF ORTHOGONALLY STIFFENED PLATES TO CONVECTED LOADINGS

4.1 Introduction

Chapters 2 and 3 dealt with the response of a stiffened beam to random convected loading obtained in a series of space harmonics. Stiffeners were assumed to be line supports exerting rotational and translational constraints on the beam. Such an elastically supported beam can be considered as a good representation of many stiffened aerospace structures if it is assumed that their response is uncorrelated across one set of stiffeners, usually the frames. However, such a situation does not exist in practice when the excitation is a boundary layer pressure field. Proper correlation between responses across the frames must then be taken into account. This requirement calls for a more realistic model. One such model is provided by a plate on line supports which extend in the two perpendicular directions. This chapter deals with the analysis of such a model.

As in the previous chapter, stiffened plate will be treated as a uniform plate subject to the forces and moments applied by the supports which simulate the stiffeners.

4.2 Representation of the Two-Dimensional Convected Pressure Field

The periodically supported plate is excited by a loading intensity

$$p = p_o e^{-i\mu_x \frac{x}{\ell}} e^{-i\mu_y \frac{y}{\ell_y}} e^{i\omega t} \qquad (4.1)$$

This general form is considered because most actual pressure fields can be analysed into components of this form. The random acoustic plane waves

and the boundary layer pressure field considered in the last two chapters were analysed into components of its one-dimensional version obtained by putting $\mu_y = 0$ in equation (4.1).

One of the usual cases in actual practice is the excitation by plane sound waves incident on the structure at an angle ϕ to the normal to the plate. If the velocity of sound is C the velocity with which the loading is convected across the structure is then given by trace velocity

$$C_t = C/\sin \phi \tag{4.2}$$

If ℓ_x is the distance between stiffeners measured along X direction, then

$$\mu_x = \frac{\omega \ell_x}{C_t} \tag{4.3}$$

If there is no convection in the Y direction, then $\mu_y = 0$.

It is possible to visualise an acoustic wave which moves across the plate at an angle inclined to both sets of stiffeners. This situation is also allowed for by the assumed loading intensity given by equation (4.1), which includes a Y-dependent term. The wave number K of this loading can then be resolved into two components K_x and K_y for the X and Y directions respectively, as follows:

$$K_x = K \cos \theta \tag{4.4}$$

$$K_y = K \sin \theta \tag{4.5}$$

where θ is the angle between the direction of convection and the X-axis.

It can be seen from equations (4.4) and (4.5) that

$$K^2 = K_x^2 + K_y^2 \tag{4.6}$$

Now μ_x and μ_y are the phase differences in the exciting pressures at two points ℓ_x apart in the X-direction and ℓ_y apart in the Y-direction. They are related to K_x and K_y through:

$$\mu_x = K_x \ell_x \tag{4.7}$$

$$\mu_y = K_y \ell_y \tag{4.8}$$

The boundary layer pressure field exciting the stiffened plate may also be analysed into component pressures of the form given by equation (4.1). This is done in terms of a wave length-frequency spectrum obtained by a triple Fourier transform of the space-time cross-correlation function of the boundary layer. This takes care of both longitudinal and lateral correlations of the excitation. Appendix A gives details of this transformation and obtains the (Ω, μ_x, μ_y) or (Ω, K_1, K_3) spectrum of the excitation where K_1 and K_3 are the wave numbers in the direction of convection and the lateral direction respectively.

4.3 Representation of the Structure and Stiffnesses of Supports and response

4.3.1 Representation of the structure

The structure considered may be visualised as a flat infinite uniform thin plate with two sets of equi-spaced stiffeners (see Figure 2.1).

The X and Y axes are in the mid-plane of the plate and the Z axis is normal to this plane. The origin is taken at the point of intersection of two perpendicular stiffeners. The plate is thus divided into an infinite number of elementary sub-panels formed by the intersecting stiffeners. Let ℓ_x be the spacing measured in the X direction between the Y-wise stiffeners and let ℓ_y be the spacing between the X-wise stiffeners. ℓ_x and ℓ_y are not necessarily equal to each other but are constant. The properties of all the X-wise stiffeners are identical. This also applies to Y-wise stiffeners. However, the properties of one set may be different from the properties of the other set.

In an actual structure of the aircraft fuselage type, the X-wise set could refer to the frames and the Y-wise set to the stringers.

4.3.2 The rotational and translational constraints of the supports

Though the method employed in this chapter to analyse the response of the multi-supported plate can allow for any type of constraints applied by the supports, expressions in terms of the actual physical properties of the stiffeners will be used so that a comparison can be made between theoretical and experimental results in an actual case.

Lin [4] has derived these expressions for forces and moments applied by the stringers to the skin of a skin-stringer array. His expressions will be used here for both sets of stiffeners, viz the stringers and frames. In these expressions the inertia effects of both the sets of stiffeners will be allowed for. In the following parameters of the stiffeners the subscript x refers to the X-wise stiffeners and y refers to the Y-wise stiffeners.

Thus,

$$A'_x = (EC_{ws})_x \qquad A'_y = (EC_{ws})_y$$

$$B_x = (GJ)_x \qquad B_y = (GJ)_y$$

$$C_x = (\rho A)_x \qquad C_y = (\rho A)_y \tag{4.9}$$

$$D_x = (EI_\eta)_x \qquad D_y = (EI_\eta)_y$$

$$F_x = (\rho I_s)_x \qquad F_y = (\rho I_s)_y$$

where

C_{ws} is the warping constant of the stiffener cross section about the point S, i.e. the point which is the projection of the shear centre on the 'skin' (see Figure 4.1)

E is the Young's modulus of elasticity of the stiffener material

I_η is the moment of inertia of the stiffener cross section

G is the shear modulus of the stiffener material

J is the torsion constant of the stiffener cross section

ρ is the density of the stiffener material

A is the area of cross section of the stiffener

I_s is the polar moment of inertia of the stiffener about S

The following expressions for the transverse and rotational constraints applied by the stiffeners to the skin may then be written down after Lin [4].

Rotational moment of the Y-wise stiffener

$$= (EC_{ws})_y \frac{\partial^5 w}{\partial y^4 \partial x} - (GJ)_y \frac{\partial^3 w}{\partial y^2 \partial x} + (\rho I_s)_y \frac{\partial \ddot{w}}{\partial x} \tag{4.10}$$

Rotational moment of the X-wise stiffener

$$= (EC_{ws})_x \frac{\partial^5 w}{\partial x^4 \partial y} - (GJ)_x \frac{\partial^3 w}{\partial x^2 \partial y} + (\rho I_s)_x \frac{\partial \ddot{w}}{\partial y} \qquad (4.11)$$

Transverse force applied by the Y-wise stiffener

$$= (EI_\eta)_y \frac{\partial^4 w}{\partial y^4} + (\rho A)_y \ddot{w} \qquad (4.12)$$

Transverse force applied by the X-wise stiffener

$$= (EI_\eta)_x \frac{\partial^4 w}{\partial x^4} + (\rho A)_x \ddot{w} \qquad (4.13)$$

The above expressions for the restraints of the stiffeners rivetted to the skin may be used for the integral stiffeners as well. Figure 4.1 gives the correspondence between the rivetted stiffeners and the integral stiffeners for this purpose.

4.3.3 The governing equation for the plate motion

The equation of motion of the plate reinforced by the two sets of stiffeners and excited by the loading intensity $p_o e^{-i\mu_x(x/\ell_x)} \cdot e^{-i\mu_y(x/\ell_y)} e^{i\omega t}$ is

$$D\left[\frac{\partial^4 w}{\partial x^4} + 2\frac{\partial^2 w}{\partial x^2 \partial y^2} + \frac{\partial^4 w}{\partial y^4}\right] - m_p \omega^2 w = p_o e^{-i\mu_x(x/\ell_x)} e^{-i\mu_y(x/\ell_y)} e^{i\omega t} \qquad (4.14)$$

where D is the flexural stiffness of the plate

and m_p is the plate meass per unit area.

Hysteretic damping present in the structure may easily be allowed for by making the stiffness D in the above equation complex,

i.e., by substituting $D = D'(1 + i\eta_p)$ where η_p is the plate loss factor.

4.3.4 The series representation of the response

As observed in the work reported in the previous chapters, under a steady state forced vibration of the infinite stiffened structure, the phase characteristics of the response must follow the phase characteristics of the loading. On this basis, the displacement $W(x, y)$ of a point (x, y) on the stiffened plate under excitation by a loading intensity $p_o \exp(-i\mu_x x/\ell_x) \exp(-i\mu_y y/\ell_y)\exp(i\omega t)$ may be expressed as follows

$$W(x,y) = \sum_{m,n=-\infty}^{m,n=+\infty} A_{mn}\, e^{-i(\mu_x+2m\pi)\frac{x}{\ell_x}}\, e^{-i(\mu_y + 2n\pi)\frac{y}{\ell_y}}\, e^{i\omega t} \qquad (4.15)$$

Equation (4.15) satisfies the condition that the phase difference between the displacements at any two points in different elementary subpanels is the same as that between the excitation pressures at these points.

If the plate has only X-wise stiffeners, m in equation (4.15) is put equal to zero. If it has only Y-wise stiffeners, n is put equal to zero. In either of these special cases the series is summed over only one integral variable, n in the former case and m in the latter.

In the particular case when the supports have infinite translational stiffness ($EI \to \infty$) and infinite mass ($\rho A \to \infty$), no plate displacement is possible at support locations.

Hence at the support $x = 0$, $W = 0$,

or

$$W(0,y) = \sum_{m,n=-\infty}^{m,n=+\infty} A_{mn}\, e^{-i(\mu_y+2n\pi)\frac{y}{\ell_y}}\, e^{i\omega t} = 0 \qquad (4.16)$$

Equation (4.16) must be true for all values of y. This is possible if

$$\sum_{m,n=-\infty}^{m,n=+\infty} A_{mn} = 0 \qquad (4.17)$$

Condition (4.17) must therefore be fulfilled by coefficients of the series in the case of the plate with transversely rigid supports.

4.4 The Acoustic Radiation

4.4.1 Inclusion of acoustic radiation effect in the governing equation

When the plate is vibrating in an acoustic medium the effect of the acoustic radiation on the vibration must be considered.

The pressure p_r at any point in the acoustic medium adjacent to the plate must satisfy the three dimensional wave equation

$$\nabla^2 p_r = \frac{1}{c^2} \frac{\partial^2 p_r}{\partial t^2} \qquad (4.18)$$

Subject to the boundary condition that at the surface $z = 0$ (i.e., at the plate surface) the normal particle velocity in the medium adjacent to the plate must be equal to the normal velocity of the plate.

From equation (4.15) the normal plate velocity is given by

$$\dot{W}(x,y,t) = i\omega \sum_{m,n=-\infty}^{m,n=+\infty} A_{mn}\, e^{-i(\mu_x + 2m\pi)\frac{x}{\ell_x}}\, e^{-i(\mu_y + 2n\pi)\frac{y}{\ell_y}}\, e^{i\omega t} \qquad (4.19)$$

From where it follows that the pressure must be expressed in the form

$$p_r(x,y,z,t) = \sum_{m,n=-\infty}^{m,n=+\infty} e^{-i(\mu_x + 2m\pi)\frac{x}{\ell_x}}\, e^{-i(\mu_y + 2n\pi)\frac{y}{\ell_y}}\, f_{mn}(z) e^{i\omega t} \qquad (4.20)$$

Each term of the series of equation (4.20) must satisfy the wave equation.

Substituting the general term in the wave equation, we obtain the following ordinary differential equation for $f_{mn}(z)$

$$\frac{d^2 f_{mn}(z)}{dz^2} = -K_{mnz}^2 f_{mn}(z) \tag{4.21}$$

Evidently then,

$$f_{mn}(z) = B_{mn} e^{-iK_{mnz}z} + C_{mn} e^{iK_{mnz}z} \tag{4.22}$$

where

$$K_{mnz}^2 = (\frac{\omega}{C})^2 - (\frac{\mu_x + 2m\pi}{\ell_x})^2 - (\frac{\mu_y + 2n\pi}{\ell_y})^2 \tag{4.23}$$

The B_{mn} term in equation (4.23) represents the pressure being radiated away from the plate top surface by virtue of the plate motion. The C_{mn} term can only derive from the reflection of the B_{mn} wave from another boundary. We shall assume that such other boundaries do not exist. This makes $C_{mn} = 0$. Thus

$$p_r(x,y,z,t) = \sum_{m,n=-\infty}^{m,n=+\infty} B_{mn} e^{-i(\mu_x+2m\pi)\frac{x}{\ell_x}} e^{-i(\mu_y+2n\pi)\frac{y}{\ell_y}} e^{-iK_{mnz}z} e^{i\omega t} \tag{4.24}$$

The velocity V of the particles of the acoustic medium at $z = 0$ is given by

$$V = \frac{i}{\underline{K}\rho_a C} \left|\frac{\partial p_r}{\partial z}\right|_{z=0}$$

$$= \sum_{m,n=-\infty}^{m,n=+\infty} \frac{K_{mnz}}{\underline{K}\rho_a C} B_{mn} e^{-i(\mu_x+2m\pi)\frac{x}{\ell_x}} e^{-i(\mu_y+2n\pi)\frac{y}{\ell_y}} e^{i\omega t} \tag{4.25}$$

where $\underline{K} = \frac{\omega}{C}$

ρ_a = the density of the acoustic medium

Equating (4.19) and (4.25), B_{mn} can be expressed in terms of A_{mn}. The radiated pressure may then be expressed as

$$p_r = \sum_{m,n=-\infty}^{m,n=+\infty} A_{mn} \frac{i\omega\rho_a C}{(K_{mnz}/\underline{K})} e^{-i(\mu_x+2m\pi)\frac{x}{\ell_x}} e^{-i(\mu_y+2n\pi)\frac{y}{\ell_{ye}}} e^{-iK_{mnz}z} e^{i\omega t} \tag{4.27}$$

Equation (4.27) expresses the pressure radiated from one side of the plate. If the contribution of the other side of the plate is to be considered, this expression could again be used but the velocity of sound C and density ρ_a of the medium must then correspond to the acoustic medium on the other side.

The radiation pressure expressed above can now be included in the governing equation of the plate motion which modifies to

$$D\left[\frac{\partial^4 w}{\partial x^4} + 2\frac{\partial^2 w}{\partial x^2 \partial y^2} + \frac{\partial^4 w}{\partial y^4}\right] - m_p\omega^2 w + p_r = p_o e^{-i\mu_x(x/\ell_x)} e^{-i\mu_y(y/\ell_y)} e^{i\omega t} \tag{4.28}$$

It is clear from the expression for p_r (see equation (4.27) that when K_{mnz} is real, it results in additional damping of the plate, and when K_{mnz} is imaginary, additional mass effect results. Only in the former case is there a true sound radiation.

4.4.2 Expression for sound power

Following the procedure of Chapter 3, the following expression for $\Pi(\omega)$, the space time average sound power radiated by a unit area of the structure at a frequency ω, is obtained

$$\Pi(\omega) = \sum_{m,n=-\infty}^{m,n=+\infty} \frac{1}{2} \frac{\omega^2\rho_a C}{K_{mnz}/\underline{K}} A_{mn}A^*_{mn} \tag{4.29}$$

where A^*_{mn} is the complex conjugate of A_{mn}.

For the determination of the power radiated only those values of m, n need be considered which lead to real values of K_{mnz}. Imaginary values of K_{mnz} would lead to a pressure field which decays exponentially with distance z and is responsible only for the near field pressure. It therefore radiates no sound power. The values of m and n for which K_{mnz} is real may be determined by using equation (4.23). Then the terms in series corresponding to these values are called radiating harmonics. A graphical method of identifying radiating harmonics is given in Appendix E.

4.5 The Response of the Plate to Harmonic and Random Pressure Fields

4.5.1 Equation for the coefficients of the series

When the forces on and in the plate are in equilibrium, then these forces represented by

$$D\left(\frac{\partial^4 w}{\partial x^4} + 2\ \frac{\partial^4 w}{\partial x^2 \partial y^2} + \frac{\partial^4 w}{\partial y^4}\right) - m_p \omega^2 w + p_r - p_o e^{-i\mu_x \frac{x}{\ell_x}} e^{-i\mu_y \frac{y}{\ell_y}} e^{i\omega t}$$

together with the elastic constraint forces and moments of the supports must do no net virtual work when moved through any one of the virtual displacements

$$\delta A_{m'n'} e^{-i(\mu_x + 2m'\pi)\frac{x}{\ell_x}} e^{-i(\mu_y + 2n'\pi)\frac{y}{\ell_y}} e^{i\omega t}$$

When W is represented by the series form of equation (4.15) this equation leads to a set of equations for the A_{mn}'s. Since the structure is periodic, the virtual work contribution from only one elementary subpanel (including its supports) need be considered. As done in Chapters 2 and 3, the conjugate of the virtual displacement applied is used to calculate the virtual work, i.e. $\delta A_{m'n'} e^{i(\mu_x + 2m'\pi)x/\ell_x} e^{i(\mu_y + 2n'\pi)y/\ell_y}$

Taking the origin at the left bottom corner of the sub-panel, the contribution of the plate alone (less supports but including acoustic effects) to the virtual work is then found to be

$$\delta W_p = \int_0^{\ell_x}\int_0^{\ell_y} \delta A_{m'n'}\{D[(\frac{\mu_x + 2m\pi}{\ell_x})^4 + 2(\frac{\mu_x + 2m\pi}{\ell_x})^2(\frac{\mu_y + 2n\pi}{\ell_y})^2 + (\frac{\mu_y + 2n\pi}{\ell_y})^4] - m_p\omega^2 + \frac{i\omega\rho_a C}{(K_{mnz}/\underline{K})}\}$$
$$e^{-i(\mu_x+2m\pi)\frac{x}{\ell_x}} e^{-i(\mu_y+2n\pi)\frac{y}{\ell_y}} e^{+i(\mu_x+2m'\pi)\frac{x}{\ell_x}}$$
$$e^{i(\mu_y+2n'\pi)\frac{y}{\ell_y}} e^{i\omega t}\, dxdy \qquad (4.30)$$

The above expression has a non zero value only when $m = m'$ and $n = n'$. It takes care of the effect of acoustic radiation since the term allowing for it has been included.

The contribution to the virtual work from the transverse stiffness and transverse inertia of the Y-wise stiffeners ($x = 0$) from equation (4.12) is equal to

$$\int_0^{\ell_y} \delta A_{m'n'} \sum_{m,n=-\infty}^{m,n=+\infty} \{D_y(\frac{\mu_y + 2n\pi}{\ell_y})^4 - C_y\omega^2\} A_{mn} e^{-i(\mu_y+2n\pi)\frac{y}{\ell_y}} .e^{i(\mu_y+2n'\pi)\frac{y}{\ell_y}} dy$$

$$= \delta A_{m'n'} \sum_{m,n=-\infty}^{m,n=+\infty} A_{mn} [D_y(\frac{\mu_y+2n\pi}{\ell_y})^4 - C_y\omega^2]\ell_y \qquad n = n'$$

$$= \delta W_{ty} \qquad (4.31)$$

Similarly δW_{tx} the contribution to the virtual work by transverse stiffness and transverse inertia of the X-wise stiffeners may be evaluated

as

$$\delta W_{tx} = \delta A_{m'n'} \sum_{m,n=-\infty}^{m,n=+\infty} A_{mn} \left[D_x \left(\frac{\mu_x + 2m\pi}{\ell_y} \right)^4 - C_x \omega^2 \right] \ell_x \qquad (4.32)$$

δW_{ry}, the contribution by the rotational stiffness and rotational inertia of the Y-wise stiffeners to the virtual work may be written as

$$\delta W_{ry} = \delta A_{m'n'} \int_0^{\ell_y} \left\{ \sum_{m,n=-\infty}^{m,n=+\infty} \left[A'_y \left(\frac{\mu_y + 2n\pi}{\ell_y} \right)^4 + B_y \left(\frac{\mu_y + 2n\pi}{\ell_y} \right)^2 - F_y \omega^2 \right] \right.$$

$$\left(\frac{\mu_x + 2m\pi}{\ell_x} \right) \left(\frac{\mu_x + 2m'\pi}{\ell_x} \right) e^{-i((\mu_y + 2n\pi)/\ell_y)}$$

$$\left. e^{i(\mu_y + 2n'\pi)(y/\ell_y)} \right\} dy \qquad (4.33)$$

The above expression has a non zero value only for $n = n'$.

Similarly δW_{rx}, the contribution to the virtual work from rotational stiffness and rotational inertia of the X-wise stiffener is written as

$$\delta W_{rx} = \delta A_{m'n'} \int_0^{\ell_x} \left\{ \sum_{m,n=-\infty}^{m,n=+\infty} A_{mn} \left[A'_x \left(\frac{\mu_x + 2m\pi}{\ell_x} \right)^4 + B_x \left(\frac{\mu_x + 2m\pi}{\ell_x} \right)^2 - F_x \omega^2 \right] \right.$$

$$\left(\frac{\mu_y + 2n\pi}{\ell_y} \right) \left(\frac{\mu_y + 2n'\pi}{\ell_y} \right) e^{-i((\mu_x + 2m\pi)/\ell_x)}$$

$$\left. e^{i((\mu_x + 2m'\pi)/\ell_x)} \right\} dx \qquad (4.34)$$

The above expression has a non zero value only for $m = m'$.

Now the virtual work principle requires that

$$\delta W_p + \delta W_{tx} + \delta W_{ty} + \delta W_{rx} + \delta W_{ry} = 0 \qquad (4.35)$$

Evaluating the integrals involved in the various terms of equation (4.35)

and re-arranging, this equation leads to the following set of equations in the non dimensional form:

$$A_{m'n'}\left\{\left[(\mu_x + 2m'\pi)^4 + \frac{2}{q^2}\left(\frac{\mu_x + 2m'\pi}{}\right)(\mu_y + 2n'\pi) + \frac{(\mu_y + 2n'\pi)^4}{q^4}\right](1 + i\eta) - \Omega^2 + \frac{i\Omega^2\rho_{ra}}{\mu_{mnz}}\right\} + \sum_{m,n=-\infty}^{m,n=+\infty} A_{m'n}\,\kappa_{ry}\,(\mu_x + 2m\pi)(\mu_x + 2m'\pi)$$

$$+ \sum_{m,n=-\infty}^{m,n=+\infty} A_{mn'}\,\kappa_{rx}\,(\mu_y + 2n\pi)(\mu_y + 2n'\pi) + \sum_{m,n=-\infty}^{m,n=+\infty} A_{m'n}\,\kappa_{ty}$$

$$+ \sum_{m,n=-\infty}^{m,n=+\infty} A_{mn'}\,\kappa_{tx} = 0 \text{ when } m' \neq 0,\ n' \neq 0 \quad m', n' = -\infty \text{ to } +\infty$$

$$= P \text{ when } m' = n' = 0 \qquad (4.36)$$

where

$$\text{Frequency parameter } \Omega = \omega\,\ell_x^2\sqrt{\frac{m_p}{D'}} \qquad (4.37)$$

Rotational stiffness and inertia parameter of Y-wise stiffener

$$\kappa_{ry} = \frac{\ell_x}{D'}\left[A'_y\left(\frac{\mu_y + 2n\pi}{\ell_y}\right)^4 + B_y\left(\frac{\mu_y + 2n\pi}{\ell_y}\right)^2 - E_y\omega^2\right] \qquad (4.38)$$

Rotational stiffness and inertia parameter of X-wise stiffener

$$\kappa_{rx} = \frac{\ell_x}{D'}\left[\frac{A'_x}{q^3}\left(\frac{\mu_x + 2m\pi}{\ell_x}\right)^4 + \frac{B_x}{q^3}\left(\frac{\mu_x + 2m\pi}{\ell_y}\right)^2 - \frac{E_x\omega^2}{q^3}\right] \qquad (4.39)$$

Translational stiffness and inertia parameter of Y-wise stiffener

$$\kappa_{ty} = \frac{\ell_x^3}{D'}\left[D_y\left(\frac{\mu_y + 2n\pi}{\ell_y}\right)^4 - C_y\omega^2\right] \qquad (4.40)$$

Translational stiffness and inertia parameter of X-wise stiffener

$$\kappa_{tx} = \frac{\ell_x^3}{D'}\left[\frac{D_x}{q}\left(\frac{\mu_x + 2m\pi}{\ell_y}\right)^4 - \frac{C_x\omega^2}{q}\right] \qquad (4.41)$$

Aspect ratio $q = \frac{\ell_y}{\ell_x}$ (4.42)

Loading parameter $P = p_o \frac{\ell_x^4}{D'}$ (4.43)

The density ratio $\rho_{ra} = \frac{\rho_a h}{m_p}$ (4.44)

Phase parameter in the z direction $\mu_{mnz} = K_{mnz} h$ (4.45)

The non dimensional convection velocity parameter CV used elsewhere is defined as follows:

$$CV = \left(\frac{m_p}{D'}\right)^{\frac{1}{2}} U_c \ell_x \tag{4.46}$$

The convection velocity parameter corresponding to the velocity of sound is designated as SV $\left(= \left(\frac{m_p}{D'}\right)^{\frac{1}{2}} C\ell_x\right)$.

The different non dimensional stiffness parameters above involve μ_x and μ_y terms and are therefore wave length dependent. Each space harmonic associated with a particular m and n has a different wave length in the X and Y direction, thus meeting, in effect, a different rotational or translational constraint. This wave length dependence of the constraints could not arise in the cases of the beam considered in Chapters 2 and 3 but has been allowed here.

Equation (4.36) constitutes a set of simultaneous equations from which the A_{mn}'s may be determined. Since all the elementary sub-panels are identical in every respect, considerations of virtual work contribution of any other elementary sub-panel would yield an identical set of equations. By solving a suitably restricted set of the above equations, the A_{mn}'s can be determined. Once the A_{mn}'s are known we can find the response at any point on the plate.

4.5.2 The harmonic response of the plate

For a given plate, the response is a function of Ω, μ_x and μ_y, and is proportional to the excitation pressure amplitude p_o. The displacement $W(x, y)$, the X-wise curvature $W(x'', y)$, the Y-wise curvature $W(x, y'')$ and the sound power Π per unit area of the plate may then be written down in the following formal manner:

$$W(x, y) = p_o Y_{xy}(\Omega, \mu_x, \mu_y) e^{i\omega t} \tag{4.47}$$

$$W(x'', y) = p_o Y_{x''y}(\Omega, \mu_x, \mu_y) e^{i\omega t} \tag{4.48}$$

$$W(x, y'') = p_o Y_{xy''}(\Omega, \mu_x, \mu_y) e^{i\omega t} \tag{4.49}$$

$$\Pi = |p_o^2| Y_p(\Omega, \mu_x, \mu_y)|^2 \tag{4.50}$$

where Y_{xy}, $Y_{x''y}$, $Y_{xy''}$ and $|Y_p|^2$ are the 'admittance functions' of the appropriate response, and can be defined in each case as the appropriate response due to harmonic excitation intensity of unit amplitude under conditions specified in the parenthesis. For example, the $Y_{x''y}(\Omega, \mu_x, \mu_y)$ may be derived from equation (4.15) leading to

$$Y_{W(x'',y)}(\Omega,\mu_x,\mu_y) = \sum_{m,n=-\infty}^{m,n=+\infty} -A_{mn} e^{-i(\mu_x+2m\pi)\frac{x}{\ell_x}} \cdot \left(\frac{\mu_x + 2m\pi}{\ell_x}\right)^2 e^{-i(\mu_y+2n\pi)\frac{y}{\ell_y}} e^{i\omega t} \tag{4.51}$$

where $A_{m,n}$ have been determined for a unit amplitude of harmonic excitation intensity. Since all A_{mn}'s are proportional to p_o, the admittance functions referred to above can be found directly.

4.5.3 Response to random convected loads

For any random excitation of the plate, the power spectral

densities of both excitation and response being functions of Ω, μ_x and μ_y are related as follows:

$$S_{W(x,y)}(\Omega, \mu_x, \mu_y) = S_p(\Omega, \mu_x, \mu_y)|Y_{xy}(\Omega, \mu_x, \mu_y)|^2 \tag{4.52}$$

$$S_{W(x'',y)}(\Omega, \mu_x, \mu_y) = S_p(\Omega, \mu_x, \mu_y)|Y_{x'',y}(\Omega, \mu_x, \mu_y)|^2 \tag{4.53}$$

$$S_{W(x,y'')}(\Omega, \mu_x, \mu_y) = S_p(\Omega, \mu_x, \mu_y)|Y_{xy''}(\Omega, \mu_x, \mu_y)|^2 \tag{4.54}$$

$$S_{\pi}(\Omega, \mu_x, \mu_y) = S_p(\Omega, \mu_x, \mu_y)\,|Y_p(\Omega, \mu_x, \mu_y)|^2 \tag{4.55}$$

When these functions are integrated over the whole ranges of μ_x and μ_y, the power spectral density is obtained as a function of frequency alone. For example,

$$S_{W(x'',y)}(\Omega) = \int_0^\infty \int_0^\infty S_p(\Omega, \mu_x, \mu_y)|Y_{(x'',y)}(\Omega, \mu_x, \mu_y)|^2 \, d\mu_x d\mu_y \tag{4.56}$$

$$S_{\pi}(\Omega) = \int_0^\infty \int_0^\infty S_p(\Omega, \mu_x, \mu_y)|\,Y_p(\Omega, \mu_x, \mu_y)|^2 \, d\mu_x d\mu_y \tag{4.57}$$

The total mean square value of the response quantities in the frequency band $0 < \Omega < \Omega_1$ is found by integrating this over this band.

When the response quantity involved is Π, the sound power radiated per unit area, the total mean value is given by

$$\langle \Pi \rangle = \int_0^{\Omega_1} \int_0^\infty \int_0^\infty S_p(\Omega, \mu_x, \mu_y)|Y_p(\Omega, \mu_x, \mu_y)|^2 \, d\mu_x d\mu_y d\Omega \tag{4.58}$$

Appendix A shows how the two dimensional boundary layer pressure field may be analysed into a (μ_x, μ_y, Ω) spectrum. Theoretically speaking, the response to the boundary layer pressure field then can be obtained only by integrating the response over all μ_x's and μ_y's (see

equations (4.56) and (4.57)). However, the knowledge of the wave length frequency spectrum can enable us to cut down considerably the summation required for a reasonable accuracy. It is shown in equation (A.24) that most of the contribution to the pressure spectrum will derive from low values of μ_y (low order y-modes) and from μ_x's near the value given by $\mu_x = \Omega/CV$, approximately. If while selecting the values of μ_x and μ_y over which the response is integrated, these facts are taken into consideration, the results obtained will be reasonably accurate for curvature response. (For sound power contribution other wave numbers may be significant, see section 3.6.5.)

When the boundary layer convection is inclined to the X-axis, the value of the spectral density of excitation is best obtained in terms of K_1 and K_3, which are the wave numbers of the excitation in the direction of convection and the lateral direction respectively. (See Appendix A). A set of K_1 and K_3 has a corresponding unique set of μ_x and μ_y imposed on the structure.

The procedure for determining the response of the plate due to a boundary layer pressure field convected in a direction inclined at θ to the X-axis may be set out in the following steps:

1. Select the range of K_1's and K_3's over which the integration of the response is to be obtained. This is decided by the accuracy desired in the light of the fact that the spectrum of the boundary layer falls rapidly at high values of lateral wave numbers and that the spectrum tends to peak at a wave number $K_1 = \frac{\omega}{U_c}$. (See Appendix A for details.)
2. Take one set of values of K_1 and K_3 in the above range. Calculate

the corresponding μ_x and μ_y imposed on the structure as follows:

$$\mu_x = K_1 \cos\theta - K_3 \sin\theta$$
$$\mu_y = K_1 \sin\theta + K_3 \cos\theta \qquad (4.59)$$

3. Compute the admittance $Y(\Omega, \mu_x, \mu_y)$ of the response under these conditions.
4. Multiply $|Y(\Omega, \mu_x, \mu_y)|^2$ found in step 3 by the spectral density of excitation for K_1 and K_3 taken in step 2. The result is the spectral density corresponding to the actual excitation for K_1 and K_3.
5. Repeat steps 2-4 with a new value of K_1 for the same K_3, and add the response to that found in step 4.
6. Continue steps 2-5 till all values of K_1 are exhausted.
7. Repeat steps 2-6 with a new value of K_3.
8. Repeat step 7 till all values of K_3 are exhausted.

The result then would yield the spectral density of response contributed by one frequency component. This may be integrated over all frequencies to obtain the r.m.s. value. The flow diagram corresponding to the procedure outlined above is shown in Appendix D.

When the excitation is a random acoustic plane wave of a given convection velocity CV inclined at angle θ to the X-axis, (Ω, μ_x, μ_y) spectrum is non zero only for unique values of μ_x and μ_y which are then functions of Ω, CV and θ (see equations (4.4)-(4.5)). The mean square response to such an excitation is then given by

$$< W^2_{(x'',y)} > = \int_0^{\Omega_1} S_p(\Omega) |Y_{x''y}(\Omega, \mu_x(\Omega), \mu_y(\Omega))|^2 d\Omega \qquad (4.60)$$

By analogy similar expressions could then be written down for the mean square of other response quantities.

4.6 Computation and Results

Computations have been performed to determine the influence on the response of the following factors:

(a) the number of terms included in the series,

(b) the damping in the structure,

(c) different stiffnesses of stiffeners and of the direction of convection.

As in earlier chapters, these computations were performed using an ICL 1907 computer, the system of simultaneous equations for the coefficients being solved by using a standard ICL Fortran subroutine F4CXACSL. This subroutine allows for complex coefficients in the system of simultaneous equations which is the case when there is damping in the structure or when acoustic radiation effects are included.

Since some of the broad features of the solution of one dimensional version of the stiffened plate problem have already been illustrated in Chapters 2 and 3, computation for this chapter was kept to the minimum to minimize computation cost. No actual computation has therefore been made for the boundary layer excitation. However, a computational procedure for this case has been included in Section 4.5.3 and the flow diagram for this procedure has been given in Appendix D. Curvature and sound power results presented were normalised as in Chap. 2 and

4.6.1 Structural details

The structures computed for have the following properties and dimensions.

(a) Structure A

$h = 0.028$ inch

$\ell_x = 4.5$ inches

$\ell_y = 9.0$ inches

$(C_{ws})_x = 0.002666$ in^4

$(C_{ws})_y = 0.0000099$ in^4

$J_x = 0.000003414$ in^4

$J_y = 0.0000034$ in^4

$(I_s)_x = 0.32808$ in^4

$A_x = 0.1176$ square inch

$A_y = 0.0585$ square inch

$(I_\eta)_x = 0.01037$ in^4

$(I_\eta)_y = 0.002499$ in^4

$\rho = 0.101/386$ lb.sec^2/in^4

$\nu = 0.3$

$E = 10.5\ (10^6)$ lbs/sq.inch.

$(I_s)_y = 0.022756$ in^4

(b) Structure B

$h = 0.028$ inch

$\ell_x = 4.5$ inches

$\ell_y = 9.0$ inches

$(C_{ws})_x = 0.023996$ in^4

$(C_{ws})_y = 0.0000444$ in^4

$J_x = 0.000030732$ in^4

$J_y = 0.0000153$ in^4

$(I_s)_x = 0.32808$ in^4

$A_x = 0.1176$ square inch

$A_y = 0.0585$ square inch

$(I_\eta)_x = 0.09335$ in^4

$(I_\eta)_y = 0.011245$ in^4

$\rho = 0.101/386$ lb.sec^2/in^4

$\nu = 0.3$

$E = 10.5\ (10^6)$ lb/sq.inch.

$(I_s)_y = 0.022756$ in^4

(The above values correspond to the type of structure used for experimental work described in the next chapter.)

The above structures were considered with $\eta_p = 0.05$, $\eta_p = 0.15$ and $\eta_p = 0.25$. Also considered was the effect of varying the stiffness of stiffeners (relative to those of structure B) with other characteristics being constant.

The curvature results refer to x-wise curvature computed for $x/\ell_x = 0.5$, $y/\ell_y = 0.5$.

4.6.2 The excitation considered

The following specific types of excitation were considered.

(a) A random acoustic plane wave at an oblique angle of incidence. This effectively means a random plane wave of supersonic trace velocity convected in the direction of the X-axis. The angle of incidence considered gave the trace velocity as 1.5 times the velocity of sound.

(b) A random plane wave convected across the plate in a direction inclined to the X-axis. A subsonic velocity of 0.28 times the velocity of sound inclined to the X-axis at 80°, 40°, 20° and 10° was considered. Also considered was a subsonic velocity = $1/9$ times the velocity of sound convected in a direction at 45° to the X-axis.

The frequency ranges considered extend from 100 Hz to 1,200 Hz. Over this range the spectral density of excitation has been assumed to be unity. The response was computed at a frequency interval of 10 Hz.

4.6.3 The relative magnitudes of the coefficients

Table 4.1 shows the relative magnitudes of different A_{mn}'s. 49 terms were included in the series. This may be interpreted as 7 terms for the longitudinal direction and 7 in the lateral direction for each of the above 7. The convection velocity of the loading was 1.5 times the velocity of sound and the direction of convection was parallel to the X-axis so that $\mu_y = 0$. The results are for the structure A with $\eta = 0.15$.

The relative magnitudes of the coefficients tabulated show that the A_{oo} term is dominant and that as m,n increase, the magnitudes of the corresponding coefficients fall. This is in line with the observation

made in Chapter 2 regarding the convergence of the coefficients of series of displacement for the stiffened beam.

From the table it may be noticed that $A_{m,n} = A_{m,-n}$ for all values of m. This is explained by the fact that there is no convection in the Y-direction in the pressure field, so $\mu_y = 0$. The two components $A_{m,n} e^{-i(\mu_x+2m\pi)(x/\ell_x)} e^{-i(\mu_y+2n\pi)(y/\ell_y)} e^{i\omega t}$ and $A_{m,-n} e^{-i(\mu_x+2m\pi)(x/\ell_x)} e^{-i(\mu_y-2n\pi)(y/\ell_y)} e^{i\omega t}$ with $\mu_y = 0$ and with $A_{m,n} = A_{m,-n}$ combine to yield no resultant wave motion in the structure in the Y-direction.

Table 4.2 shows the relative magnitudes for the above structure and excitation at a frequency of 500 Hz. The symmetry of the coefficients with respect to n may again be observed and can again be explained by the reasons applicable to Table 4.1.

Table 4.3 lists the relative magnitudes of A_{mn}'s when Structure B with $\eta_p = 0.25$ is excited by a plane wave of a convection velocity 1/9 times the velocity of sound convected at 45° to the X-axis at a frequency of 150 Hz. A satisfactory convergence is again observed but the symmetry with respect to n which was observed in the earlier two tables has now disappeared. This is explained by the fact that 45° convection amounts effectively to a convection in both the perpendicular directions.

4.6.4 Influence of different variables on the response

The influence on response of including a different number of terms in the series, of damping in the structure, of stiffnesses of stiffeners and of the direction of convection of loading were studied. The response in each case has been plotted against frequency in Hz. The rms values of curvature and mean values of sound power tabulated on the figures are only relative.

4.6.4.1 Influence of the number of terms in the series

Figure 4.2 shows the effect of including a different number of terms on X-wise curvature response of the stiffened plate at midpoint of a sub-panel (Structure A with $\eta_p = 0.15$). The acoustic plane waves

were convected in the X-direction with the trace velocity which equalled 1.5 times the velocity of sound. It can be seen that the 9 term solution gives an r.m.s. value which is different from the 49 term solution by about 85 percent while the 25 term solution yields a value which differs from the 49 term solution by only 5 percent.

The effect of the number of terms on the sound power radiated under the above conditions is shown by Figure 4.3. The curves corresponding to the 25 term solution and the 49 term solution agree so well that it is convenient to represent both solutions by a single curve. The total mean values corresponding to different number of terms are shown in the table given in this figure. The solutions by including 25 terms and 49 terms differ only by about 1.5 percent.

Figure 4.4 gives the comparison of results of sound power by including 25 terms and 49 terms for structure B, $\eta = 0.25$, when $C_t = 1.5C$. Again the two curves are quite close for most of the frequency range covered. The peaks are within 5 percent of each other. Another calculation (not plotted) for the same structure for a subsonic velocity of loading ($C_t = 0.5C$) showed that mean power by including 25 terms was only 2.5 percent different from that obtained by including 49 terms.

That 25 terms would yield a quite accurate result in the case of the stiffened plate could be guessed from the fact that 5 terms yielded accurate results in the corresponding one-dimensional case of the stiffened beam. This could also be expected from the relative magnitudes of the coefficients for the two-dimensional structure presented already. This has now been confirmed by the computation presented above. It is therefore felt that no further computation need be done to prove that 25 terms are sufficient for a reasonable answer. This number of terms will be included

in the series for obtaining other results presented in this chapter.

4.6.4.2 Influence of damping

Figures 4.5 and 4.6 show the effect of damping on the X-wise curvature response of the plate (Structure A, $\eta_p = 0.15$) and the sound power radiated per unit area from it respectively. The particulars of the loading are the same as correspond to Figures 4.2 and 4.3. It is clear from Figure 4.5 that the damping considerably reduces the curvature response. Increasing the damping three fold from $\eta_p = 0.05$ to $\eta_p = 0.15$ reduces the r.m.s. response in proportion to $1 : \sqrt{3}$ approximately. However the effect on the value of the sound power (Figure 4.6) is not marked except near the peak values. The difference between the mean values for $\eta_p = 0.05$ and $\eta_p = 0.15$ is only 3 percent, though the corresponding peak values are in the ratio 5 to 2 approximately.

The comparison of Figures 4.2 and 4.3 would indicate that the peaks for sound radiation occur at about the same frequencies at which the peaks for the curvature response occur. This is due to the fact that the convection velocity is supersonic so that the zeroth order term is a radiating harmonic. Since this term has a dominant contribution in the determination of both responses, the correspondence between the peaks of the two responses is achieved.

4.6.4.3 Influence of the stiffnesses of stiffeners

Figures 4.7 and 4.8 show the effect of the transverse stiffness of the Y-wise stiffness D_y of Structure B on the spectral density of X-wise curvature and on the spectral density of sound power radiated in a frequency range 400 - 1,000 Hz, $\eta_p = 0.25$. The loading is convected in the direction of the X-axis at a speed 1.5 times the speed of sound. 25 terms were included in the series solution. It is difficult to conclude any straightforward law between the transverse stiffness and the response. It is, however, possible to say from the results presented that at fairly high values of D_y, any further increase in stiffness will not result in any appreciable change in the response. At the lower end, however, the effect of varying D_y suggests that there may be an optimum stiffness for minimizing both curvature and sound levels. 0.01 value of D_y yields the minimum response in the results presented for the case considered. (See tables in Figures 4.7 and 4.8)

Figures 4.9 and 4.10 show the effect of varying the transverse stiffness of the X-wise stiffeners of Structure B ($\eta_p = 0.25$) at one of the higher bands of sound radiation, on curvature and sound power. The convection velocity is 0.28 times the velocity of sound and the direction of convection is 45° to the X-axis. The variations observed again do not follow any straightforward law and point to the necessity of the structure being studied from the point of view of optimisation. Also it is seen that sound radiation is not affected by these variations in stiffness in the same pattern as is followed by curvature response.

The influence of rotational stiffness of the stiffeners on the response is more difficult to determine because it has two components depending on warping constant and torsion constant respectively. They are both wave length dependent but their dependence is of a different order. A computation was made to study the response by varying warping constant while keeping constant the torsion constant for Structure B, $\eta_p = 0.25$, $C_t = 1.5C$ with convection parallel to the X-axis. 25 terms were included in the series. The reduction of the warping constant to one tenth its value reduced the mean sound power by only 3.3 percent. Further ten fold reduction in the constant reduced it by 2.5 percent while a third ten fold reduction reduced it by only 0.4 percent. The corresponding reductions in r.m.s. curvature were 18 percent, 0.6 percent and -2.5 percent respectively. From these computations again no straightforward law can be deduced about the variation of response with A'_y.

4.6.4.4 Influence of the direction of convection

Figures 4.11 and 4.12 present results which study the influence of varying the angle of inclination of the acoustic plane wave with a subsonic velocity equal to 0.28 times the velocity of sound. Structure considered is B with $\eta_p = 0.25$.

Figure 4.11 shows the effect of the inclination on the X-wise curvature (values for all inclinations are not actually plotted to avoid crowding of the diagram). As the angle decreases, the main peak of the response becomes higher and moves to a smaller frequency. The r.m.s. value also increases. Decrease in the angle progressively reduces the convection velocity in the X-direction so that μ_x gets larger and μ_y smaller. Prediction of the effect of the angle of convection on the response can only be made in exact terms by studying the free wave values

of μ_x and μ_y which would in turn depend upon the various stiffnesses of the stiffeners involved.

Figure 4.12 studies the effect of inclination on the sound power. It is seen that there are bands of frequencies which do not radiate any sound. The location of these bands is affected by the inclination because it affects the values of μ_x and μ_y. The mean value decreases with the decrease in inclination with the X-axis down to 20°, then increases and decreases without any simple order. The study of the effect of inclination and in fact of other parameters as well shows that the behaviour of sound radiation is more complex than the behaviour of curvature response.

4.7 Conclusions

It has been shown that the method of space harmonics used to obtain the curvature response and sound power radiated in earlier chapters can be successfully extended to the case of the doubly stiffened plate to obtain its response. Only 25 terms need be included in the series to obtain the solution with a reasonable accuracy. This would correspond to

5 terms in the X-direction and 5 terms corresponding to each such term in the Y-direction. It is possible to deal with the excitation by random acoustic plane waves and by boundary layer pressure convected in a direction inclined to the X-axis. In the case of boundary layer pressure, it is possible to allow for the lateral correlation of the field.

The effect of damping on the curvature response has been seen to be marked. Damping is, however, relatively ineffective in reducing the sound radiation except near the peak values. These peaks can be due to one of the space harmonics matching with the free wave length and thus causing coincidence. A number of such coincidences may be present in the case of a stiffened structure in a given frequency range (see Chapter 1) as opposed to only one coincidence present in an infinite uniform structure. Thus damping is seen to be more effective in the case of the stiffened structure than in the case of uniform structure for reducing sound radiation. But this is so only in relative terms, and damping as a means of reducing noise cannot be recommended on the basis of the studies made.

The study of the variation of response with the variation in stiffnesses of stiffeners does not allow any generalisations to be made. The variations do not necessarily affect the sound power in the same pattern as they affect the curvature response. There are indications, however, that the type of structure considered may be optimised with respect to the stiffener parameters.

5. EXPERIMENTAL WORK AND COMPARISON WITH THEORY

5.1 Introduction

The theoretical work reported in the foregoing chapters applies strictly to infinite periodically supported structures. It is expected that the behaviour of finite heavily damped panels would approximate to that of the infinite panel (Section 1.5.3.3). Though the theoretical approach presented could be adapted for the case of finite structures (see [30]) it was decided to check experimentally the 'infinite' theory. If the agreement was reasonable, it would be confirmed as a quick method of evaluation of sound power radiated. So the experimental work described in this chapter was undertaken before the attempt was made to extend the theoretical work to the case of the reinforced cylindrical shells described in the next chapter.

An aircraft type of panel was excited by acoustic plane waves with oblique incidence and the acoustic measurements made for comparison with values predicted by the theory presented in the previous chapters. The measurements were made by making use of the ISVR anechoic and reverberant rooms. These rooms are adjoining and there is an opening between the two in the common wall. This opening was used for mounting the specimen. The anechoic room could house the loudspeaker for exciting the panel while the absence of reflections in this room ensured unidirectional sound waves. There was proper space for test equipment outside these rooms but near enough to be convenient for the necessary control on the experimental conditions.

5.2 Quantity to be Measured and the Technique of Measurement

5.2.1 Quantity to be determined

The aim of acoustic measurements in engineering is sound control. Such measurements are therefore followed by sound control calculations which are usually based on statistical concepts of acoustic energy and acoustic power. It was therefore decided to determine the acoustic power transmitted at different frequencies in the experimental work reported in this chapter. These have then been compared with those obtained by the theory advocated in the previous chapters.

For theoretical calculations, the actual value of damping in the experimental panel and its stiffness were required. The damping was directly measured and stiffness was calculated from the natural frequency of a test specimen having the same properties as the panel. Mass per unit area was determined by actual weighing of a test specimen.

5.2.2 Free field versus diffuse field measurements

The acoustic power is calculated from sound pressure measurements. This is accurately determined in a simple manner in two limiting cases:

(a) In the region of a free field beyond the near radiation field.

(b) In a diffuse sound field.

Measurement in the free field provide not only acoustic power spectra but also directivity information. The facility and test effort however are relatively costly. There is another method of measurement in the free field, i.e. that of near field measurements. This method

does not require any special facilities and is thus ideal for on site tests. The test effort is, however, very high due to the large number of measurement points and corresponding data processing required. On the other hand, measurements in the reverberant field require only moderate facilities and amount of effort. This method therefore was attractive.

The purpose of the experiment was to study the behaviour of the stiffened panel under excitation by acoustic plane waves. The best available method to create an acoustic plane wave (at least approximately) was to place a loudspeaker at a large distance from the panel in the anechoic room. The sound pressure level measurements were then made in the reverberant room in order to determine the radiated power.

5.2.3 The range of frequency

It was considered that for a built up structure of the aircraft fuselage type, the frequency range 100 Hz-1000 Hz was most difficult to analyse for response. The stiffeners are likely to influence the result most in this range. At higher frequencies the influence of the boundaries is expected to become less important, thus making the agreement between the 'infinite' and the 'finite' theory much closer. Besides, at higher frequencies the zeroth term in the series of space harmonics is more likely to be a radiating harmonic. This would therefore enhance the accuracy of prediction of sound power with a given number of terms in the series. Thus if the agreement between the experimental and theoretical results in the range 100-1000 Hz is proved to be acceptable, the theory could be considered acceptable.

5.3 The Specimen and Test Details

5.3.1 The specimen and its mounting

The specimen is constructed completely from 22 s.w.g. L73 alloy. The main 4' by 6' panel is sub-divided into smaller panels, each 9" by 4.5" by six channel type frames and sixteen z-section stringers, all of which are rivetted to the skin. Figure 5.1 shows the details of the construction. The stringer constants are as follows:

$$A = 0.0585 \text{ in}^2$$

$$I_\eta = 0.011245 \text{ in}^4$$

$$I_s = 0.022756 \text{ in}^4$$

$$C_{ws} = 0.000444 \text{ in}^4$$

$$J = 0.0000153 \text{ in}^4$$

Similarly the constants of the frames are as follows:

$$A = 0.1176 \text{ in}^2$$

$$I_\eta = 0.09335 \text{ in}^4$$

$$I_s = 0.32808 \text{ in}^4$$

$$C_{ws} = 0.023996 \text{ in}^4$$

$$J = 0.000030732 \text{ in}^4$$

The above constants have been obtained from [33] and the Royal Aeronautical Society data sheets. The panel so constructed represents aircraft type of construction.

The specimen was mounted with the longer side horizontal, in a wooden frame, which was surrounded by a brickwork partition between the anechoic chamber and the reverberation chamber (see Figure 5.2). The wooden frame work had recesses in it to contain the stringers and

frames of the panel. The side of the panel having stringers and frames faced the reverberation room and the flat side looked into the anechoic room. The joint between the panel and the wooden frame was sealed by using two layers of draft excluder and screwing a wooden strip from the anechoic room side so that the panel and the draft excluder packing was contained between the wooden strips and the wooden frame in the brick-work surround. Care was taken to ensure that there were no cracks in the masonry work or at other points and the rivet holes in the panel were filled up by squeezing silicone rubber into them. To obtain the damped panel, sheets of aquaplas (D8/SA sheets manufactured by Revertex Ltd) were pressed on to the flat surface of the panel.

5.3.2 Excitation and the measurement of pressure levels

5.3.2.1 Excitation of the panel

The panel was excited by a 15 watt loudspeaker placed in the anechoic room at a distance of 21 ft. from the panel so that the sound waves falling on the panel could be reasonably considered to be plane waves. The angle of incidence was varied by changing the location of the loudspeaker in the anechoic room while keeping its vertical position at mid height of the panel, at a constant distance of 21 ft.

The panel is thus seen to be excited under conditions similar to those in actual practice, where the flat side is exposed to excitation and the stiffener side looks into the cabin.

Figure 5.3 gives a general arrangement for the test and Appendix F gives a list of instruments used for experimental determination of sound power radiated and for determining the damping of the panel.

5.3.2.2 Measurement of the excitation pressure

Before the actual panel was excited, the loudspeaker was made to face a wall of the anechoic room. Pressures at a distance of 6' and 21' from the loudspeaker were measured at different frequencies in the range 100 Hz to 1000 Hz by sweeping through this range using a B. & K. level recorder and a B. & K. beat frequency oscillator. This gave a measure of the loss of pressure over a distance of 15' of travel of sound waves at different frequencies without involving errors due to reflection at the panel. During the actual experiment, pressure was measured only at a distance of 6 ft from the loudspeaker, and the pressure at the panel deduced by the assumption that the same dB loss will occur at a given frequency for the same distance of travel of the sound wave.

5.3.2.3 Measurement of pressure in the reverberant chamber

The power radiated by the panel vibrating under given conditions was determined from the average sound pressure in the reverberant room. This was done by keeping a microphone at a position in the reverberant room and sweeping the excitation of the panel through 100-1000 Hz frequency range while recording the pressure picked up by this microphone. This was repeated for a number of microphone positions in the reverberant room under one set of conditions of excitation which was also recorded. A mean was then taken of all the recorded pressures under one set of conditions at one frequency of excitation.

5.3.3 The reverberant room and the reverberation time

The details of the reverberant room used are given in reference 36. Some relevant details will, however, be included here. The room has

plane, non-parallel walls and an inclined ceiling. The mean edge lengths are 6.4 metres and 4.6 metres and the mean height is 4.3 metres. The volume enclosed is 131 cubic metres. The walls and the ceiling are finished with a hard gloss paint. Three sets of doors in this room connect it to a larger reverberation room, a large anechoic room (used in these experiments) and the common control area. The average transmission loss of these doors of sandwich construction is 50 dB. In the wall of the room dividing it from the control area, there are four cable ports and a double glazed observation window.

During the experiment, the panel was mounted in the position of the door between the anechoic room and the reverberation room. The second door leading to the larger reverberant room was kept shut all the time and the door leading to the control area was shut at the time of taking observations.

The empty room is claimed to have the following 1/3 octave reverberation times [36]

Centre frequency	100	125	160	200	250	315	400	500	630
R.T. seconds	7.4	7.6	8.7	9.9	10.8	9.2	6.8	5.2	4.7

In spite of the above information being available, it was considered desirable to record the reverberation time at discrete frequencies for the conditions under which the experiment was being performed.

For this purpose, the loudspeaker was placed in the reverberant room. It was excited by the beat frequency oscillator at a discrete frequency. The power was then cut off to the loudspeaker and the decay of the pressure recorded by the help of the level recorder. The

reverberation time was then found by the slope of the decay curve as the time for the level of sound to decay 60 dB. The procedure was repeated at a number of frequencies, yielding the reverberation time at these frequencies. The following reverberation time was obtained at these discrete frequencies.

Frequency	100	150	200	260	300	400	500	600	700	800	900	1000
Reverberation Time, Secs.	4.9	5.1	5.3	5.3	4.7	4.5	4.7	4.7	4.4	4.7	4.6	4.6

The reverberation time has been plotted against frequency in Figure 5.4. It is seen that the above reverberation times are different from those recorded for the empty room in reference 36. The general level is lower. This is expected since the room at the time of use had plaster boards and some other miscellaneous items in it which would absorb sound. Also the variation with frequency is different. It was not considered necessary to remove the miscellaneous items from the room at the time of experiment, since their presence would not affect the results as long as the reverberation time was known and was constant at a given frequency.

5.3.4 The measurement of the panel damping and determination of effective stiffness

5.3.4.1 The panel damping

In order to compute the theoretical response of the panel tested, the damping present must be known. This was therefore experimentally measured.

Two methods were attempted to measure the damping present.

(a) A special transient test method developed at the Institute of Sound and Vibration Research, in which a sine wave excitation is swept

through the frequency range of interest, in a relatively short time with the help of a special ISVR sweep oscillator, and the tape recorded data is analysed by an analog-digital computer.

(b) By testing separately a specimen built up of the same material as the actual panel in a device (originally used by Mead [37]) where the desired modes can be excited, and by measuring by a vibration meter the induced response and its phase around the resonant frequency. A Kennedy-Pancu diagram can again be obtained by this method.

(a) The method of transient excitation by the ISVR sweep oscillator

The details of this method may be seen in reference |38|, but for the sake of completeness, the following brief remarks are made:

The method consists in exciting the structure by a sine wave loading swept through a frequency range of interest in a short time, say 0.5 seconds. The (accelerometer) response of the structure to this type of excitation is recorded on a magnetic tape. The data is then converted into the digital form by the help of an A to D converter. A Fourier transform of this response is obtained digitally to obtain the frequency spectrum of the response. The peaks in this spectrum may then be identified as resonant frequencies of the structure. Since both the amplitude and phase of response in the frequency range of interest are available, Kennedy-Pancu phase plots may be obtained. From these plots the resonant frequencies may be identified more accurately and the loss factor measured. It is claimed that this method preserves the accuracy of the steady state methods (and considerably reduces the test time).

The above method was tried. The loading was acoustic, obtained by feeding the ISVR sweep oscillator signal to the loudspeaker which excited the panel at normal incidence. The signal was swept through 100-1000 Hz in 0.5 seconds. Figure 5.5 gives the response spectrum when the accelerometer was on the skin, and Figure 5.6 gives the spectrum when it was on the stringer. The peaks correspond to different modal frequencies. The resulting phase plots were, however, not such as could be interpreted conveniently. Since the structure is built up, very many modes are present and interlinked. As a result the vector plot contained so many loops that it was very difficult to pass a reasonable circle through the points. This method of transient testing was therefore dropped as unsuitable for this type of built up structure and use was made of a rig originally developed by Mead for the measurement of damping. The method of this rig also employs Kennedy Pancu vector plots to determine the damping in the specimen.

Before the work using Mead's rig is described, it may be mentioned that White [39] has dealt with the problem of resolution of close natural frequencies of the structure in relation to the method of transient testing. But before the applicability of this method is established in the case of a complicated structure with a high damping, it is best to depend upon a simpler method of determination of damping.

(b) Measurement of damping using Mead's rig

In this method the specimen is made to vibrate in a single mode by an appropriate excitation. The phase plot is then obtained by plotting the actual measured values of the in-phase and quadrature components of response at different frequencies. Figure 5.7 shows the rig

employed. The specimen tested consisted of a strip of the same metal as formed the panel with a layer of aquaplas damping, which was actually used for the panel tested. The specimen, 0.3 inch wide and 11 inches long, was held in brass supports (see Figure 5.7) in a clamped clamped condition.

The general arrangement of the test is outlined in Figure 5.8. An audio oscillator was used to generate the exciting frequency signal. It was input to a power amplifier whose output was passed through a step down transformer and measured before being fed to the specimen (up to 7 amperes could be passed through the specimen). This oscillating current passing through the metal part of the test specimen together with the steady transverse magnetic flux provided by the permanent magnets (see Figure 5.7) results in an oscillating load on the specimen. By suitable arrangement of the polarity of the magnets, up to the first four modes of the strip could in theory be excited.

The vibration of the strip was measured by employing Wayne-Kerr proximity probes and the Wayne Kerr vibration meter, together with the resolved component indicator. Thus the method of excitation as well as the method of measurement of vibration, did not change the impedance of the structure under test. The resonant frequency was first detected approximately by using the Wayne-Kerr meter alone and then the in phase and quadrature components were measured around this frequency in order to obtain the vector plot.

Figure 5.9 shows the phase plot obtained for the fundamental mode of the beam specimen. The modal frequency is 125.5 Hz and the corresponding damping is $\eta = 0.25$.

The basis of the method employed to determine damping from the phase plot is outlined in Appendix G.

5.3.4.2 Determination of effective stiffness

Figure 5.9 shows the vector plot obtained by testing the damped specimen in the fundamental mode of vibration. The natural frequency was found to be 125.5 Hz. The mass per unit length of this beam was then measured by actual weighing and the stiffness EI determined from the following relationship:

$$\left(\frac{m_b \omega^2}{EI}\right)^{\frac{1}{4}} \ell = \underline{\lambda}\ell \qquad (5.1)$$

with ℓ as the length of the beam between supports (= 8.5 inches) where the value of $\underline{\lambda}\ell$ for the fundamental mode of the clamped clamped beam (= 4.730) was taken from the standard tables (see for example 'Mechanics of Vibration' by Bishop and Johnson). The value EI calculated for a beam of unit width works out to be 104.3 lb.in units.

The damping was found to be 0.25. These two values are used for the determination of computed sound power throughout the frequency range of interest.

5.4 Experimental Determination of Sound Power

The experimental value of the power radiated is determined from the corrected average values of the pressure levels measured in the reverberant room.

5.4.1 Ambient sound pressure level corrections

We wish to measure the sound pressure radiated by the panel. However, the microphone will also pick up the background noise or the ambient sound pressure for which a correction must be made. It is known that if the sound pressure level with the source operating compared to

the ambient sound pressure level alone is 10 decibels or more, the sound pressure level due to both the sound source and the ambient sound is only 0.4 dB more than the sound pressure level due to the sound source. If the increase is 3 dB or less, the sound pressure level contributions of the source and the ambient level cannot be separated with the conventional measuring techniques. For other increases over the ambient levels the following corrections are suggested by USA standard [40]

Increase in dB	4	5	6	7	8	9	10
Correction (to be subtracted from the reading)	2.2	1.7	1.3	1.0	0.8	0.6	0.4

To keep the pressure levels as high as possible compared to the background levels, the experiments were conducted during quiet evenings. The difference between the two was always greater than 10 dB and the corresponding correction in the observations being very small was not therefore considered necessary.

5.4.2 Linear versus logarithmic averaging

As expected, there was a spread in the values of pressure levels recorded by placing the microphone at different positions in the reverberant room. For the purpose of computing the sound power, the spatial averages of these values was to be taken. It could be a linear average or a logarithmic average. Cox [41] and Mitchel [42] have discussed this point in the light of the fact that both these methods are used in acoustic practice. Cox has investigated the lower bound on the ratio of geometric mean to the arithmetic mean of a set of data. He has noted that for a data having a spread of 10 dB, the geometric mean is less

than 1.5 dB below the arithmetic mean. For a spread of 6 dB, the geometric mean is less than 0.52 dB below the arithmetic mean. Mitchel has introduced further refinements in the averaging process by including the influence of statistical distribution of data. In view of the bounds of error given above, and for the obvious reasons of convenience, the arithmetic average was taken of the values of recorded pressure levels in the reverberant room. The data averaged in this chapter had a spread of around 9 dB. Thus a maximum error of 1.5 dB is likely in the averaged result. The true average will be lower by this level.

5.4.3 Determination of the sound power

Sound power radiated by the panel was determined indirectly from the average sound pressure level in the reverberation room obtained by measuring at a number of points, and then taking their spatial average. This pressure is in terms of dB. The actual pressure, P_s, may be calculated by the relation

$$SPL_{Total} = 20 \log \frac{P_s}{P_o} \qquad (5.2)$$

where SPL_{Total} is the averaged sound pressure level with all corrections

and $$P_o = 2 \times 10^{-4} \quad \mu bars \qquad (5.3)$$

After the pressure, P_s, is known in μbars, the following relation [43] is used to obtain the sound power Π_{tot}

$$\Pi_{tot} = 2.8 \times 10^{-8} \times (P_s^2 V/T) \qquad (5.4)$$

where Π_{tot} is the sound power in Watts

V is the volume of the reverberant room in cubic feet

P_s is the sound pressure in microbars

T is the reverberation time of the room in seconds.

5.5 Theoretical Calculations

5.5.1 Considerations of the mass law

For the purpose of comparison, it is useful to know how much transmission loss would be there if the panel and the added damping sheet were acting as a massive partition. This transmission loss may then be estimated from the following equation, usually called the mass law [44]:

$$D_o = 10 \log \left[1 + \left(\frac{\omega m_s \cos\phi}{2\rho C}\right)^2\right]$$

$$\text{or } D_o \simeq 20 \log \frac{\omega m_s \cos \phi}{2\rho C} \qquad (5.5)$$

where D_o is the transmission loss

m_s is the mass per unit area of the partition

ω is the frequency of the sound wave impinging on the partition normally

ρC is the characteristic impedance of air

ϕ is the angle of incidence

The above equation is based on the assumption that the wall acts as a mass and that the wave length at all frequencies in the wall is very large in comparison with the wall thickness, and that the characteristic impedance of the wall material is very large in comparison with that of the air (a condition fulfilled at all frequencies).

It may be seen from the equation for the mass law that D_o would increase 6 dB for every doubling of m_s. The same applies to the dependence upon frequency, i.e. for every octave increase in frequency D_o should increase by 6 dB.

The transmission loss according to the mass law has been calculated and incorporated into the curves presented. For these calculations

it is assumed that the mass of the stiffeners is uniformly distributed over the area of the panel. The total mass taking into account the skin, the stiffeners and the damping material works out to be 1.090 lb. per sq. ft.

5.5.2 Theoretical determination of radiated power

For the purpose of computing radiated power, the method presented in Chapter 4 was employed. The parameter of the actual structure was used. The stiffness and damping were as follows (see section 5.3.4.2)

$$D' = 104.2 \text{ lb.in. units}$$

$$\eta = 0.25.$$

Properties of the stiffeners and skin have already been listed in section 5.5.1. Mass of the damped panel was found to be 0.006040 lb per square inch. This was determined by actually weighing the specimen which was later tested to determine the value of damping (see section 5.3.4.1b). This mass does not include the contribution of the stiffeners which was considered concentrated at the boundary of two sub-panels.

5.6 Theoretical and Experimental Results

For the sake of convenience of comparison between theoretical and experimental results, both sets of results for a given set of conditions have been included in the same diagram. The curve corresponding to the mass law with the correct angle has also been plotted. The sound power radiated has been plotted in decibels in accordance with the usual practice in acoustics work, and is referred to as 10^{-12} watts. The

results correspond to an incident pressure of 80 db constant over the frequency range of interest.

Figures 5.10, 5.11 and 5.12 give the values of radiated sound power against frequency when the panel vibrated under the action of acoustic plane waves incident at the panel at different angles. The full line in each case gives the values determined by computation on the basis of the theory presented in the previous chaphers. These were computed for a unit value of the exciting pressure and then brought down to correspond to the actual exciting pressure on the basis that the radiated power is proportional to the square of the exciting pressure. The broken line in each case represents the experimental values determined from the actual pressure levels measured in the reverberant room by using relation given by equation (5.4). The chain dotted line in each figure gives the value of the sound power radiated based on the Mass Law.

5.6.1 Discussion of Results

Figures 5.10-5.12, showing theoretical and experimental values of the sound power radiated by the panel under excitation by acoustic plane waves with different angles of incidence, have some common features. In each case the experimental curves have some peaks. It intersects the theoretical curve at many points, and is on the whole lower than the Mass Law curve. This is, of course, subject to the averaging errors. If a true logarithmic averaging were done, the experimental curve will move down (see section 5.4.2). The peaks in the experimental curve, e.g. around 120 Hz, 185 Hz and those around 600 Hz, suggest a broad

correspondence with the modal frequencies (see Figures 5.5-5.6).

The total value of sound power radiated at a given frequency may be visualised as the sum of two components: (a) the forced response, or the contribution by the forced waves in the infinite stiffened panel excited by the convected loading; (b) the resonant response or the contribution from the free waves reflected at the boundaries. Subject to the experimental and averaging errors, the difference between the experimental and theoretical values may be attributed to the resonant response.

In Figure 5.12 representing results for acoustic plane waves incident on the panel at an angle = Sin^{-1} 2/3, the difference between the theoretical and experimental curves varies at different frequencies, the maximum being 5 db and the minimum being 0 db. The two curves intersect at nine different points. In the complete frequency range considered, the agreement between the computed results is within 3 db except near the peaks of the experimental curve.

In Figure 5.10 (for angle of incidence = Sin^{-1} 1/3), the difference between the non peak parts of the experimental curve and the computed curve is small - less than 2.5 dB over most of the frequency range. The two curves intersect at nine different points. The agreement between the two sets of results has broadly the same features for normal incidence of acoustic plane waves (Figure 5.11).

Over most the frequency range of the experiment, for the panel tested, the sound power radiated falls linearly with frequency in the computed

curve. This behaviour is similar to that of the uniform panel where the Mass Law would then give a fairly exact answer to the sound power radiated. The Mass Law applied to the panel tested (the stiffened panel) gives results which are higher than the experimental and theoretical values. The maximum difference between the Mass Law results and the theoretical calculations (see Figure 5.12) is about 5 dB.

It is relevant to emphasis again that the experimental curves plotted have been obtained by linear averaging of different observations of pressure levels. This was done for the sake of convenience. However, if the logarithmic averaging were performed, the curve will be expected to be about 1.5 dB lower, thus making the computed values higher than the experimental values over most of the frequency range.

It is difficult to evaluate the influence of the assumption that the loudspeaker sound impinging on the panel 21 feet away from it in the anechoic room is an acoustic plane wave. Perhaps this assumption will lead to no appreciable error in the analysis.

5.7 Conclusions

The experimental results for sound power presented in this chapter have been seen to agree with the theoretical calculations within an average of 3 dB (except near the peaks of the experimental curve). The agreement at higher frequencies (i.e. over 1000 Hz) is expected to be better because of reduced influence of finiteness on the response. It may

therefore be stated on the basis of the work reported in this chapter that for obtaining the sound power radiated by an orthogonally stiffened panel with heavy damping, the stiffened panel may be treated as infinite. The method of space harmonics presented in this thesis may then be employed to compute the results.

6. RESPONSE OF INFINITELY LONG RING STIFFENED CYLINDRICAL SHELLS TO CONVECTED RANDOM LOADING

6.1 Introduction

In previous chapters the method of space harmonics was developed and then applied to obtain the response of periodically supported beams and plates. The method was found to yield results which agreed reasonably with experiment. To confirm that the general theory presented can be applied to all periodically supported structures, it was decided to preliminarily test the method for yet another case. This is to determine the response of periodically supported cylinder which is infinite in the axial direction. This is a simple representation of an aeroplane fuselage structure.

The actual stiffened cylinder will be treated as a uniform cylinder subject to the constraints applied by the stiffeners. The response will be obtained in a series of space harmonics, and the coefficients of this series will be determined. Once these coefficients are known the sound radiation characteristics may be determined from methods in analogy with the treatment in the previous chapters. The purpose here is not to go into details of determining the sound field after the response has been obtained in a series form. (Such associated problems are dealt with in references 45-49) This chapter will, therefore, restrict itself mainly to obtaining the expression for the coefficients of the series of response and to examining the convergence of response, apart from including a few comments about the pressure field inside and outside the cylinder which will clarify the application of this approach to the actual problem.

6.2 The Structure Considered

The structure considered is diagrammatically shown in Figure 6.1. The cylinder is infinite in the axial direction and has ring stiffeners at uniform intervals ℓ_x along the axial direction. The rings shown are external but they could as well be inside the cylinder skin and then could in a practical case represent frames in the fuselage construction.

The ring stiffness will be considered as line supports applying constraints to the cylinder skin which are given by Lin's expressions (see Chapter 4) applicable to the flat panel. For a rigorous analysis, however, the more exact shell-ring interaction forces and moments should be considered. These are not actually used but are given in Appendix H.

6.3 The Excitation Considered

In the previous chapters, the response of the structure considered is in the first place determined for a harmonic loading. The response to a general random loading could then be determined by analysing the excitation field into a wave length frequency spectrum. Following the same procedure, the response in this chapter will be determined to the basic loading excitation

$$P = P_o e^{-i\mu_x \frac{x}{\ell_x}} \cos n\theta \; e^{i\omega t} \qquad (6.1)$$

acting on the cylinder. This pressure field represents n standing waves around the circumference of the cylinder and is convected along the cylinder at a velocity $U_c = \omega \ell_x / \mu_x$.

Any general excitation may theoretically be analysed into

components of the form of equation (6.1). The response to a general excitation may therefore be determined from the method of this chapter.

6.4 Shell Displacements and Shell Theories

6.4.1 Shell displacements and the importance of flexural vibration in sound radiation

When the cylinder is excited, the vibrational displacement of any point on the surface of the cylinder has three components, viz, radial, axial and tangential. These different displacements are actually coupled but the radial vibrations can be said to be analagous to the transverse vibrations of the beam or a plate and correspond to the bending action. The axial and tangential vibrations on the other hand are chiefly due to extensional deformation and in-plane shear deformation. All these components of displacement have corresponding components of the velocity of the surface which are capable of transmitting energy to the surrounding fluid. The axial and tangential velocity components radiate this energy by a shearing action as opposed to compression and rarefaction as in the case of flexural or radial components. In actual situation, in the case when the acoustic medium is air, the amount of energy radiated by shear waves is very small and is therefore neglected here. For the purpose of this chapter, it will be assumed that the acoustic medium is a perfect gas having zero viscosity. Under these circumstances, the flexural vibrations are the most important from the point of view of sound radiation.

6.4.2 Different shell theories

Before the cylinder can be analysed for displacement response to the applied loading, its equations of motion must be known in terms

of its displacements. These are given by a number of shell theories in the literature. The most general analysis is obviously by three-dimensional theory of elasticity. If small deformations are assumed, linear theory of elasticity may be employed. Compared to this general treatment, the following approximations are made by some of the different shell theories (see reference 50 for more complete treatment).

(a) Normals to the reference surface remain straight during deformation.

(b) Normals to the reference surface do not extend during deformation.

(c) Normals to the reference surface remain normal during deformation.

(d) Rotary inertia is neglected.

(e) Tangential translatory inertia is neglected.

(f) Bending stiffness of the shells is neglected.

(g) Extensional stiffness of the shells is infinite.

Approximation (a) distinguishes a shell theory from the exact theory of elasticity. Assumptions (a) and (b) affect thickness stretch and thickness shear modes. Assumptions (a) to (d) lead to the classical theory dealt with by Love. Love's theory would therefore correspond to small deformations of thin shells.

Assumption (e) is justified if the vibrational motion is transverse. Assumption (f) leads to the membrane theory of shells. This theory will not predict the flexural modes correctly, and is therefore limited in scope. Assumption (g) leads to the inextensional theory of shells.

6.4.2.1 Consistency of the shell theories

One of the requirements of a reliable shell theory is that it should be consistent. This means that it must predict strain free modes for rigid body motions. To be able to compare the behaviour of

different theories in this respect, one must know the strain displacement relationships corresponding to different theories [51]. These will now be examined after the constitutive laws of the thin shell theory are given.

After using the Maxwell's principle for a linear structure, the constitutive laws of the thin shell linear theory are written as follows:

$$\begin{Bmatrix} N_x \\ N_y \\ N_{xy} \\ M_x \\ M_y \\ M_{xy} \end{Bmatrix} = \begin{bmatrix} k_1 & k_2 & 0 & 0 & 0 & 0 \\ k_2 & k_1 & 0 & 0 & 0 & 0 \\ 0 & 0 & k_3 & 0 & 0 & 0 \\ 0 & 0 & 0 & D_1 & D_2 & 0 \\ 0 & 0 & 0 & D_2 & D_1 & 0 \\ 0 & 0 & 0 & 0 & 0 & D_3 \end{bmatrix} \begin{Bmatrix} \epsilon_x \\ \epsilon_y \\ \epsilon_{xy} \\ \kappa_x \\ \kappa_y \\ \kappa_{xy} \end{Bmatrix} \tag{6.2}$$

$$\text{or} \quad \{\bar{N}\} = |\bar{E}|\{\bar{\epsilon}\} \tag{6.3}$$

where $\{\bar{N}\}$ vector of shell forces and moments

$|\bar{E}|$ matrix of elastic constants

$\{\bar{\epsilon}\}$ vector of strains and curvatures

For the isotropic material for the cylindrical shell, the values of the elastic constants may be calculated as follows:

$$k_1 = \frac{Eh}{1 - \nu^2} \tag{6.4}$$

$$k_2 = \nu k_1 \tag{6.5}$$

$$k_3 = 0.5(1 - \nu)k_1 \tag{6.6}$$

$$D_1 = \frac{Eh}{12(1 - \nu^2)} \tag{6.7}$$

$$D_2 = \nu D_1 \tag{6.8}$$

$$D_3 = 0.5(1 - \nu)D_1 \tag{6.9}$$

Also strain displacement relationships can be expressed as follows

$$\{\bar{\varepsilon}\} = [D]\{\bar{u}\} \tag{6.10}$$

where $[D]$ is the matrix of operators

$\{\bar{u}\}$ is the vector of displacements.

Thus different theories have some variations in $[D]$. These matrices according to different theories may be written as follows:

(a) According to Donnel and Flügge

$$[D] = \begin{bmatrix} \partial/\partial x & 0 & 0 \\ 0 & \partial/\partial y & 1/r \\ \partial/\partial_y & \partial/\partial x & 0 \\ 0 & 0 & -\partial^2/\partial x^2 \\ 0 & 0 & -\partial^2/\partial y^2 \\ 0 & 0 & -2\partial^2/\partial x \partial y \end{bmatrix} \tag{6.11}$$

(b) According to Reissner and Wang

$$[D] = \begin{bmatrix} \partial/\partial x & 0 & 0 \\ 0 & \partial/\partial y & 1/r \\ \partial/\partial y & \partial/\partial x & 0 \\ 0 & 0 & -\partial^2/\partial x^2 \\ 0 & \partial/r\partial y & -\partial^2/\partial y^2 \\ 0 & \partial/r\partial x & -2\partial^2/\partial x \partial y \end{bmatrix} \tag{6.12}$$

(c) According to Novozhilov

$$[D] = \begin{bmatrix} \partial/\partial x & 0 & 0 \\ 0 & \partial/\partial y & 1/r \\ \partial/\partial y & \partial/\partial x & 0 \\ 0 & 0 & -\partial^2/\partial x^2 \\ 0 & \partial/r\partial y & -\partial^2/\partial y^2 \\ 0 & 2\partial/r\partial x & -2\partial^2/\partial x\partial y \end{bmatrix} \qquad (6.13)$$

(d) According to Naghdi

$$[D] = \begin{bmatrix} \partial/\partial x & 0 & 0 \\ 0 & \partial/\partial y & 1/r \\ \partial/\partial y & \partial/\partial x & 0 \\ 0 & 0 & -\partial^2/\partial x^2 \\ 0 & 2\partial/r\partial y & -\partial^2/\partial y^2 + \frac{1}{r^2} \\ 0 & 2\partial/r\partial x & -2\partial^2/\partial x\partial y \end{bmatrix} \qquad (6.14)$$

[51]

Cantin has shown that theory (a) introduces artificial constraints under two components of rigid translation and all the three components of rigid rotation. Theory (b) introduces two artificial constraints for two rigid rotations about the Y and Z axes. Theories (c) and (d) are completely strain free for all rigid motion. It is also shown by the converse process that if the theories are employed with the assumption $\{\bar{\varepsilon}\} = \{0\}$, theory (a) gives five erroneous strain free modes that should be really straining. Theory (b) yields two erroneous strain free modes. However, theories (c) and (d) lead to strain free modes for, and only for, rigid body motions.

Theory (c) due to Novozhilov is thus shown to be consistent. It is also simple to use. Also, Warburton [52] reviewing the current state of knowledge relating to shell dynamics has indicated Novozhilov's theory to be reasonable. In the sections to follow therefore, this theory will be employed.

6.4.2.2 Novozhilov's thin shell theory

For uniform thin cylindrical shells, Novozhilov's theory leads to the following three equations in terms of axial displacement u, tangential displacement v and radial displacement w, when the vibration is due to an excitation intensity $p_o e^{-i\mu_x(x/\ell_x)} \cos n\theta\, e^{i\omega t}$.

$$\frac{\partial^2 u}{\partial x^2} + \frac{1-\nu}{2a^2}\frac{\partial^2 u}{\partial \theta^2} + \frac{1+\nu}{2a}\frac{\partial^2 v}{\partial x \partial \theta} + \frac{\nu}{a}\frac{\partial w}{\partial x} = \frac{\rho(1-\nu^2)}{E}\frac{\partial^2 u}{\partial t^2} \tag{6.15a}$$

$$\frac{1+\nu}{2a}\frac{\partial^2 u}{\partial x \partial \theta} + \frac{1-\nu}{2}\frac{\partial^2 v}{\partial x^2} + \frac{1}{a^2}\frac{\partial^2 v}{\partial \theta^2} + \beta\left[\frac{1}{a^2}\frac{\partial^2 v}{\partial \theta^2} + 2(1-\nu)\frac{\partial^2 v}{\partial x^2}\right]$$

$$+ \frac{1}{a^2}\frac{\partial w}{\partial \theta} - \beta\left[(2-\nu)\frac{\partial^3 w}{\partial x^2 \partial \theta} + \frac{1}{a^2}\frac{\partial^3 w}{\partial \theta^3}\right] = \frac{\rho(1-\nu^2)}{E}\frac{\partial^2 v}{\partial t^2} \tag{6.15b}$$

$$\frac{\nu}{a}\frac{\partial u}{\partial x} + \frac{1}{a^2}\frac{\partial v}{\partial \theta} - \beta\left[(2-\nu)\frac{\partial^3 v}{\partial x^2 \partial \theta} + \frac{1}{a^2}\frac{\partial^3 v}{\partial \theta^3}\right] + \frac{w}{a^2}$$

$$+ \beta\left[a^2\frac{\partial^4 w}{\partial x^4} + 2\frac{\partial^4 w}{\partial x^2 \partial \theta^2} + \frac{1}{a^2}\frac{\partial^4 w}{\partial \theta^4}\right]$$

$$= -\frac{\rho(1-\nu^2)}{E}\frac{\partial^2 w}{\partial t^2} + \frac{(1-\nu^2)}{Eh} p_o e^{-i\mu_x(x/\ell_x)} \cos n\theta\, e^{i\omega t} \tag{6.15c}$$

where

$$\begin{aligned} a &= \text{mean radius of the shell} \\ \beta &= \frac{h^2}{12a^2}, \quad h \text{ being the thickness of the shell.} \end{aligned} \tag{6.16}$$

ρ is the density of the cylinder material.

6.5 The Series Representation of Response and Derivation of the Governing Equation in Terms of Flexural Displacement

6.5.1 Series representation of response

The infinitely long cylinder being considered has ring stiffeners at regular distance ℓ_x along the axis. It is therefore a periodic structure with the periodicity in the axial direction. The response will follow the excitation and will therefore be constituted by the displacements of the following form

$$u = \sum_{m=-\infty}^{m=+\infty} A_m e^{-i(\mu_x + 2m\pi)\frac{x}{\ell_x}} \cos n\theta \; e^{i\omega t} \tag{6.18}$$

$$v = \sum_{m=-\infty}^{m=+\infty} B_m e^{-i(\mu_x + 2m\pi)\frac{x}{\ell_x}} \sin n\theta \; e^{i\omega t} \tag{6.19}$$

$$w = \sum_{m=-\infty}^{m=+\infty} C_m e^{-i(\mu_x + 2m\pi)\frac{x}{\ell_x}} \cos n\theta \; e^{i\omega t} \tag{6.20}$$

The above forms of displacements represent a standing wave along the circumference and a travelling wave along the axis of the cylinder. Thus they follow the condition that the forced response must follow the excitation.

6.5.2 Equation in terms of one set of coefficients only (viz. in terms of C_m)

For simplifying the involved algebra it will be necessary to express the other two coefficients in terms of the third. Here A's and B's will be expressed in terms of C's. For this purpose it is assumed that each term of the series of displacements u, v and w satisfies the equations of motion (6.15a and 6.15b) for the shell. The m^{th} term of

each displacement is substituted in these equations of motion and then A_m and B_m are found in terms of C_m. A_m and B_m can then be eliminated from equation (6.15c), which then becomes

$$\sum_{m=-\infty}^{m=+\infty} C_m \{ \frac{\nu}{a} \frac{\mu_x + 2m\pi}{\ell_x} f_a + \frac{n}{a^2} f_b + \beta\left[(2-\nu)\left(\frac{\mu_x + 2m\pi}{\ell_x}\right)^2 n f_b + \frac{n^3}{a^2} f_b\right]$$

$$+ \frac{1}{a^2} + \beta\left[a^2\left(\frac{\mu_x + 2m\pi}{\ell_x}\right)^4 + 2\left(\frac{\mu_x + 2m\pi}{\ell_x}\right)^2 n^2 + \frac{n^4}{a^2}\right] - \frac{\rho(1-\nu^2)}{E}\omega^2\}$$

$$e^{-i(\mu_x + 2m\pi)(x/\ell_x)} \cos n\theta$$

$$= p_o e^{-i\mu_x \frac{x}{\ell_x}} \cos n\theta \frac{(1-\nu^2)}{Eh} \tag{6.21}$$

where

$$f_a = \frac{n_4 d_1 - n_2 d_2}{n_3 d_1 - n_1 d_2} \tag{6.22}$$

$$f_b = \frac{n_1}{d_1}\left(\frac{n_4 d_1 - n_2 d_2}{n_3 d_1 + n_1 d_2}\right) + \frac{n_2}{d_1} \tag{6.22}$$

with

$$n_1 = \frac{-\rho(1-\nu^2)}{E} + \left(\frac{\mu_x + 2m\pi}{\ell_x}\right)^2 + \left(\frac{1-\nu}{2a^2}\right)n^2 \tag{6.23}$$

$$n_2 = \nu/a \tag{6.24}$$

$$n_3 = -\frac{1+\nu}{2a}\left(\frac{\mu_x + 2m\pi}{\ell_x}\right)n \tag{6.25}$$

$$n_4 = \frac{n}{a^2} + \beta\left[(2-\nu)\left(\frac{\mu_x + 2m\pi}{\ell_x}\right)^2 n + \frac{n^3}{a^2}\right] \tag{6.26}$$

$$d_1 = -\left(\frac{1+\nu}{2a}\right)\left(\frac{\mu_x + 2m\pi}{\ell_x}\right)n \tag{6.27}$$

$$d_2 = \frac{1-\nu}{2}\left(\frac{\mu_x + 2m\pi}{\ell_x}\right)^2 - \left(\frac{\mu_x + 2m\pi}{\ell_x}\right)^2 \frac{n^2}{a^2} + \beta\left[\frac{-n^2}{a^2} - 2(1-\nu)\left(\frac{\mu_x + 2m\pi}{\ell_x}\right)^2\right]$$

$$+ \frac{\rho(1-\nu^2)\omega^2}{E} \tag{6.28}$$

Equation (6.21) applies to the cylinder between stiffeners.

6.6 Effect of the Acoustic Medium

6.6.1 Inclusion of the effect of acoustic medium inside the cylinder

The pressure at any point in the acoustic medium adjacent to the plate must satisfy the wave equation

$$\nabla^2 p_r = \frac{1}{c^2} \frac{\partial^2 p_r}{\partial t^2} \tag{6.29}$$

subject to the boundary condition that at the cylinder surface $r = a$, the radial cylinder velocity must be equal to the radial velocity of the particles of the acoustic medium adjacent to the cylinder.

From equation (6.20) the radial velocity of the cylinder is given by

$$\dot{W}(r,x,t) = \sum_{m=-\infty}^{m=+\infty} i\omega C_m \cos n\theta \; e^{-i(\mu_x + 2m\pi)\frac{x}{\ell_x}} e^{i\omega t} \tag{6.30}$$

from where it follows that the pressure must be expressed in the form

$$p_r(r,x,t) = \sum_{m=-\infty}^{m=+\infty} \cos n\theta \; e^{-i(\mu_x + 2m\pi)\frac{x}{\ell_x}} f_{mn}(r) e^{i\omega t} \tag{6.31}$$

Each term of the series of equation (6.31) must satisfy the wave equation. Substituting the general term in the wave equation in cylindrical coordinates ($\nabla^2 = \frac{1}{r} \frac{\partial}{\partial r} (\frac{r\partial}{\partial r}) + \frac{1}{r^2} \frac{\partial^2}{\partial \theta^2} + \frac{\partial^2}{\partial x^2}$), and separating different variables, we are led to the following ordinary differential equation

$$f_{mn}'' + \frac{1}{r} f_{mn}' + K_m^2 f_{mn} = 0 \tag{6.32}$$

$$\text{with} \quad K_m^2 = (\frac{\omega}{c})^2 - (\frac{\mu_x + 2m\pi}{\ell_x})^2 \tag{6.33}$$

which can be recognised as a Bessel differential equation. This has a

solution in the form

$$f_{mn}(r) = D_m J_n(K_m r) + E_m N_n(K_m r) \tag{6.34}$$

$J_n(K_m r)$ is the Bessel function of order n and $N_n(K_m r)$ is the Neumann's function of order n. It is known that the latter function has a singularity at $r = 0$. For the pressure field inside the cylinder, this function cannot therefore be included, so that

$$E_{mn} = 0.$$

Thus

$$p_r(r,x,t) = \cos n\theta \sum_{m=-\infty}^{m=+\infty} D_m J_n(K_m r) e^{-i(\mu_x + 2m\pi)\frac{x}{\ell_x}} e^{i\omega t} \tag{6.35}$$

from where the radial velocity v of the particles of the acoustic medium is given by

$$v = \frac{i}{\omega\rho}\left(\frac{\partial p_r}{\partial r}\right)_{r=a} = \sum_{m=-\infty}^{m=+\infty} \frac{iD_m \cos n\theta}{2\omega\rho_a}\left[J_{n-1}(K_m r) - J_{n+1}(K_m r)\right](K_m)$$

$$e^{-i(\mu_x + 2m\pi)\frac{x}{\ell_x}} e^{i\omega t}$$

$$= \sum_{m=-\infty}^{m=+\infty} \frac{iD_m \cos n\theta}{2\omega\rho_a}\left[J_{n-1}(K_m a) - J_{n+1}(K_m a)\right]K_m e^{-i(\mu_x + 2m\pi)\frac{x}{\ell_x}} e^{i\omega t} \tag{6.36}$$

Equating (6.30) and (6.36), D_m can be expressed in terms of C_m as follows:

$$D_m = \frac{2\omega^2\rho_a C_m}{(K_m)\left[J_{n-1}(K_m a) - J_{n+1}(K_m a)\right]} \tag{6.37}$$

The pressure then may be expressed as follows:

$$p_r = \cos n\theta \sum_{m=-\infty}^{m=+\infty} \frac{2\omega^2\rho_a C_m J_n(K_m r) e^{-i(\mu_x + 2m\pi)(x/\ell_x)} e^{i\omega t}}{(K_m)\left[J_{n-1}(K_m a) - J_{n+1}(K_m a)\right]} \tag{6.38}$$

The pressure at the cylinder surface $r = a$ affects its vibration and should therefore be included in the governing equation, which will then modify to

$$\sum_{m=-\infty}^{m=+\infty} C_m \{ \frac{\nu}{a} \frac{\mu_x + 2m\pi}{\ell_x} f_a + \frac{n}{a^2} f_b + \beta\left[(2-\nu)\left(\frac{\mu_x + 2m\pi}{\ell_x}\right)^2 n f_b + \frac{n^3}{a^2} f_b\right]$$

$$+ \frac{1}{a^2} + \beta\left[a^2\left(\frac{\mu_x + 2m\pi}{\ell_x}\right)^4 + 2\left(\frac{\mu_x + 2m\pi}{\ell_x}\right)^2 n^2 + \frac{n^4}{a^2}\right]$$

$$- \frac{\rho(1-\nu^2)}{E}\omega^2 \} e^{-i(\mu_x + 2m\pi)\frac{x}{\ell_x}} \cos n\theta + p_a$$

$$= \frac{(1-\nu^2)}{Eh} p_o e^{-i\mu_x \frac{x}{\ell_x}} \cos n\theta \qquad (6.39)$$

where p_a is given by equation (6.38) with $r = a$.

The pressure inside the cylinder given by equation (6.38) does not result in any dissipation of energy for real values of K_m. This may be seen from the expression for the time average sound power per unit length of the cylinder obtained as follows by the method adopted in Chapters 2 and 3.

$$\langle \Pi \rangle = \int_0^{2\pi} d\theta \, \tfrac{1}{2} \mathrm{Re}(pv^*)$$

$$= \int_0^{2\pi} \sum_{m=-\infty}^{m=+\infty} \tfrac{1}{2} \mathrm{Re}\left[\frac{\cos n\theta \; 2\omega^2 \rho_a J_n(K_m a) e^{-i(\mu_x + 2m\pi)\frac{x}{\ell_x}}}{(K_m a)\left| J_{n-1}(K_m a) - J_{n+1}(K_m a)\right|} C_m \right.$$

$$\left. \times \; -i\omega \cos n\theta \; e^{i(\mu_x + 2m\pi)\frac{x}{\ell_x}} C_m^* d\theta \right]$$

$$= \sum_{m=-\infty}^{m=+\infty} -i\{ \frac{\pi \omega^2 \rho_a C J_n(K_m a) \; C_m C_m^*}{(K_m/K)\left[J_{n-1}(K_m a) - J_{n+1}(K_m a)\right]} \} \qquad (6.40)$$

Equation (6.40) shows that the power radiated is reactive for real values of K_m. This is expected because in a closed space, there is no possibility of energy dissipation unless the acoustic medium contains sound absorbing materials. In this case, D_{mn} and E_{mn} in equation (6.34) will become complex.

6.6.2 Sound pressure distribution inside the cylinder

In the absence of any material inside the cylinder except the acoustic medium, the distribution of pressure inside will be determined by n and $J_n(K_m r)$. Since the Bessel Function is an oscillatory function with r, it will result in nodal circles. The nodal diameters will be given by n. The sound field inside the shell will thus contain n nodal diameters and nodal circles whose number will depend upon the value of $(K_m a)$.

The pressure at the centre $(r = 0)$ is very much dependent on n, since $J_n(0) \simeq 0$ for $n \geq 1$. Hence when the pressure at the centre is of the greatest interest, $n = 0$ is the most important mode.

The actual sound field inside the cylinder will in practice be greatly modified by the presence of various sound absorbing and reflecting materials as in an actual aircraft fuselage. The actual distribution of these materials is very difficult to deal with in a theoretical model. However, the problem could be tackled by assuming that the sound absorbing material is spread as a 'blanket' around the inside of the cylinder. The pressure could then be treated as propagating through the blanket with attenuation. In other words it would correspond to a 'damped' Bessel function, damping depending upon the attenuation provided by the absorbing material. The approach then is

similar to that used by Beranek [53] for sound propagation through multiple (flat) structures.

Alternatively the sound absorbing material could be assumed to be concentrated in an annulus concentric with the cylindrical shell. The proper matching at the annulus boundaries could also be accounted for. In such a situation the pressure field between the annulus and the cylinder will have an expression of the form

$$p_r = \sum_{m=-\infty}^{m=+\infty} \left[F_m J_n(K_m r) + G_m Y_n(K_m r)\right] e^{-i(\mu_x + 2m\pi)\frac{x}{\ell_x}} e^{i\omega t} \qquad (6.41)$$

F_m and G_m could be determined by the boundary conditions at the annulus and the cylinder. A somewhat similar treatment is being employed by Hine [49] for dealing with vibrations of a cluster of rods inside a cylindrical duct.

6.6.3 Radiation outside the cylinder

If the sound field outside the cylinder is considered, the expression for the pressure will contain the Hankel Function, since the field does not cover the point $r = 0$ where the Neumann function becomes infinite. Also it represents an outgoing wave. Thus

$$p_{\substack{r \\ r>a}} = \sum_{m=-\infty}^{m=+\infty} E_m H_n(K_m r) \cos n\theta \; e^{-i(\mu_x + 2m\pi)\frac{x}{\ell_x}} e^{i\omega t} \qquad (6.42)$$

The constant E_m can be determined by the condition that at $r = a$, i.e. at the cylinder surface, the radial velocity of the cylinder must be the same as that of the medium adjoining it.

$$\text{Thus velocity of the medium} = \frac{i}{\omega \rho_a} \left(\frac{\partial p_r}{\partial r}\right)$$

$$= \frac{i}{\omega \rho_a} \sum_{m=-\infty}^{m=+\infty} E_m H'_n(K_m a) \operatorname{Cos} n\theta \; e^{-i(\mu_x + 2m\pi)\frac{x}{\ell_x}} e^{i\omega t} \qquad (6.43)$$

Equating this to the velocity of the structure given by equation (6.30), we obtain

$$E_m = \frac{\omega^2 \rho_a C_m}{\frac{\partial}{\partial r} H(K_m r)_{r=a}} \tag{6.44}$$

The pressure may then be written as

$$p_{r \atop r>a} = \sum_{m=-\infty}^{m=+\infty} \frac{\omega^2 \rho\, C_m\, H_n(K_m r) \cos n\theta}{\frac{\partial}{\partial r} H(K_m r)_{r=a}} e^{-i(\mu_x + 2m\pi)\frac{x}{\ell_x}} e^{i\omega t} \tag{6.45}$$

Since the derivative of the Hankel function in the above expression involves i, it can be seen then that this pressure would amount to an effective damping of the structure for real values of K_m. This is different from the sound pressure field inside the cylinder which does not result in any energy dissipation, the sound power being reactive.

6.7 Evaluation of the Coefficients C_m

C_m's will be evaluated as in earlier chapters by applying the principle of virtual work. Since all the bays in the axial direction are identical, only one bay need be considered. This will involve the virtual work of the cylinder between one set of supports and the work of one of the supports. The virtual displacement assumed will be of the form

$$e^{i(\mu_x + 2m'\pi)\frac{x}{\ell_x}} \cos n'\theta \; e^{i\omega t}$$

Virtual work of the cylinder between supports

$$= \sum_{m=-\infty}^{m=+\infty} C_m \int_0^{2\pi} \int_0^{\ell_x} \left[R_m e^{-i(\mu_x + 2m\pi)\frac{x}{\ell_x}} - p_o \frac{(1-\nu^2)}{Eh}\right] \cos n\theta \; e^{i(\mu_x + 2m'\pi)\frac{x}{\ell_x}} \cos n'\theta \, d\theta \, dx$$

$$= \delta W_c \tag{6.46}$$

where

$$R_m = \{ \frac{\nu}{a} \frac{\mu_x + 2m\pi}{\ell_x} f_a + \frac{n}{a^2} f_b + \beta \left[(2-\nu) \left(\frac{\mu_x + 2m\pi}{\ell_x} \right)^2 n f_b + \frac{n^3}{a^2} f_b \right]$$

$$+ \frac{1}{a^2} + \beta \left[a^2 \left(\frac{\mu_x + 2m\pi}{\ell_x} \right)^4 + 2 \left(\frac{\mu_x + 2m\pi}{\ell_x} \right)^2 n^2 + \frac{n^4}{a^2} \right] - \frac{\rho(1 - \nu^2)}{E} \omega^2 \} \qquad (6.47)$$

It may be noted that in the above expression, the two integrations are independent of each other.

For evaluating the virtual work done by the support stiffnesses, the values of the radial stiffness and rotational stiffness of the ring stiffeners are required. For this purpose it is assumed that the stiffeners act as though they are straight and not curved. With this assumption and following the procedure given in Chapter 4, the virtual work of the rotational stiffness is

$$\int_0^{2\pi} \sum_{m=-\infty}^{m=+\infty} C_m E C_{ws} \left(\frac{n}{a} \right)^4 \left(\frac{\mu_x + 2m\pi}{\ell_x} \right) \left(\frac{\mu_x + 2m'\pi}{\ell_x} \right) \cos n\theta \cos n'\theta \, d\theta$$

$$+ \int_0^{2\pi} \sum_{m=-\infty}^{m=+\infty} C_m GJ \left(\frac{n}{a} \right)^2 \left(\frac{\mu_x + 2m\pi}{\ell_x} \right) \left(\frac{\mu_x + 2m'\pi}{\ell_x} \right) \cos n\theta \cos n'\theta \, d\theta$$

$$= \delta W_r \qquad (6.48)$$

Similarly the virtual work of the radial stiffness is

$$\int_0^{2\pi} \sum_{m=-\infty}^{m=+\infty} C_m EI \left(\frac{n}{a} \right)^4 \cos n\theta \cos n'\theta \, d\theta = \delta W_t \qquad (6.49)$$

Now the principle of virtual work states that

$$\delta W_c + \delta W_r + \delta W_t = 0 \qquad (6.50)$$

Substituting the values of δW_c, δW_r and δW_t, cancelling the common integral over θ and rearranging, the following system of

equations is obtained for evaluating C_m's.

$$C_{m'}R_{m'} + \sum_{m=-\infty}^{m=+\infty} C_m \Big[E\, C_{ws} \left(\frac{n}{a}\right)^4 \left(\frac{\mu_x + 2m\pi}{\ell_x}\right)\left(\frac{\mu_x + 2m'\pi}{\ell_x}\right) + GJ\left(\frac{n}{a}\right)^2 \left(\frac{\mu_x + 2m\pi}{\ell_x}\right)\left(\frac{\mu_x + 2m'\pi}{\ell_x}\right)$$

$$+ EI_\eta \left(\frac{n}{a}\right)^4 \Big] \frac{1}{\ell_x} = 0 \quad \text{when} \quad m' \neq 0 \quad m' = -\infty \quad \text{to} \quad +\infty$$

$$= p_o \quad \text{when} \quad m' = 0. \qquad (6.51)$$

When the influence of the acoustic medium inside the cylinder is included, the above equation would modify to:

$$C_{m'}\Big[R_{m'} + \frac{2\omega^2 \rho \; J_n(K_m a)}{(K_m)\left[J_{n-1}(K_m a) - J_{n+1}(K_m a)\right]}\Big]$$

$$+ \sum_{m=-\infty}^{m=+\infty} C_m \Big[E\, C_{ws} \left(\frac{n}{a}\right)^4 \left(\frac{\mu_x + 2m\pi}{\ell_x}\right)\left(\frac{\mu_x + 2m'\pi}{\ell_x}\right) + GJ\left(\frac{n}{a}\right)^2 \left(\frac{\mu_x + 2m\pi}{\ell_x}\right)\left(\frac{\mu_x + 2m'\pi}{\ell_x}\right)$$

$$+ EI_\eta \left(\frac{n}{a}\right)^4 \Big] \frac{1}{\ell_x} = 0 \quad \text{when} \quad m' \neq 0, \; m' = -\infty \quad \text{to} \quad \infty$$

$$= p_o \quad \text{when} \quad m' = 0. \qquad (6.52)$$

6.8 Computation and Discussion of Results

Computations were performed to obtain the relative magnitude of coefficients C_m, and to study the effect of the number of terms included in the series on the response. The excitation considered was by random 'plane' waves of CV = 8.0, 16.0, 80.0 and 160.0 with n = 1, 3 convected in a direction parallel to the axis of the cylinder. The frequency range of excitation was $0 < \Omega < 32$. The spectral density of excitation over this range of frequency was assumed to be constant and equal to unity.

The values of the parameters for the structure considered are

given below: C_{ws}, the warping constant = 0.000444

a, the radius of the cylinder = 40 inches

the thickness, h, = 0.04 inch

spacing ℓ_x = 4.5 inches

I, the moment of inertia of the stiffening ring = 0.011245 in^4

J the torsion constant of the stiffening ring = 0.0000153 in^4

The above structure was considered with η = 0.0 and η = 0.25. The X-wise curvature at x/ℓ_x = 0.5 and the reactive power due to acoustic medium inside the cylinder are presented. These results are presented in terms of the non-dimensional frequency parameter Ω, and convection velocity parameter, CV, which are defined as follows:

$$\Omega = \omega \ell_x^2 \sqrt{\frac{m_c}{D'}}$$

$$CV = U_c \ell_x \sqrt{\frac{m_c}{D'}}$$

where m_c is the mass of the cylinder per unit surface area and D' = $Eh^3/12(1 - \nu^2)$. Curvature results were normalised as in Chapter 2.

6.8.1 Relative magnitudes of the coefficients C_m

The convergence of the series of space harmonics has already been demonstrated in the cases of stiffened beams and plates. In Table 6.1 the values of the different coefficients are given for the case of the ring stiffened cylinder. CV = 8.0, η = 0.0, n = 2, for Ω = 0.4, 5.6 and 22.4. It is clear from the table that the higher order terms are small compared to the zeroth order term except for Ω = 22.4.

Table 6.2 shows relative magnitudes of the coefficients for CV = 16.0, η = 0.25, n = 2 for Ω = 1.6 and 16.0. Table 6.3

gives the values for CV = 80.0, η = 0.25, n = 1 for Ω = 19.6. The satisfactory convergence of the coefficients may again be clearly seen from their relative values given in these tables.

6.8.2 Discussion of results

Figure 6.2 shows the effect of the number of terms on the curvature at midspan of the cylinder for $\theta = \pi/4$, η = 0.25, CV = 80.0, n = 1. The maximum response is given by the 3 term solution and the results corresponding to 7 and 9 terms lie between those obtained by including 3 and 5 terms. The curves for 7 terms and 9 terms are so close to each other that only one curve has been drawn for them. The 3 term solution which reflects maximum variation from the 9 term solution is out by less than 5%, for the peak value, and by about 2.6% in the r.m.s. value. These features are very similar to the case of the stiffened beam in Chapter 2.

Figure 6.3 presents results for the reactive sound power. The structure and loading is the same as corresponds to Figure 6.2. Difference in response by including different numbers of terms was not appreciable so that only one curve has been drawn for all of them. This close agreement between results obtained by including a different number of terms may be explained by the fact that the convection velocity is supersonic so that the zeroth term is associated with a contributing K_m. This term being very large compared to others dominates the result.

The peaks across the frequency scale are explained by $K_m^2 \left[= \left(\frac{\omega}{c}\right)^2 - \left(\frac{\mu_x + 2m\pi}{\ell_x}\right)^2\right]$ becoming small for different values of m. This should be clear from almost equal frequency intervals between the first and second peak on one hand and between the second and third on

the other. The decreasing magnitude of the peaks is due to the fact that as m increases C_m decreases.

Figure 6.4 shows the spectral density of curvature at the midspan for $\theta = \pi/4$ for different values of n and CV, $\eta = 0.25$. It is seen that for the same convection velocity, the response for $n = 3$ is much smaller than the one for $n = 1$. $n = 3$ corresponds to a higher mode and therefore this sort of behaviour is expected.

6.9 Conclusions

The purpose of this chapter was to provide another check on the applicability of the method of space harmonics to periodic structures. As in other periodic structures, the response of the stiffened cylindrical shells dealt with in this chapter was expressed in the series of space harmonics and the coefficients of different terms in the series were determined. The series has been seen to converge satisfactorily. A relatively small number of terms has been seen to be necessary to be included for the response to be determined with a reasonable accuracy compared with that which can be achieved by including a large number of terms.

The general equations developed in this chapter are similar to those in the case of stiffened beams and plates. The general characteristics regarding convergence of the series of space harmonics and the influence of including different numbers of terms are similar. It can therefore be stated that the series method will be equally successful for the stiffened cylinder.

7. GENERAL CONCLUDING REMARKS

The theoretical work presented in this thesis leads to the conclusion that for obtaining the response of an infinite periodic structure, the method of space harmonics may be successfully employed. Because of the satisfactory convergence of the series of such harmonics, only a limited number of such terms need be included to obtain the response with acceptable accuracy. For obtaining the sound power radiated at subsonic convection velocities of loading, the number of terms in the series must include the lowest radiating harmonic. (The method of identifying the radiating harmonics has been included in the thesis.) In general, 5 term series is sufficient for obtaining the response of stiffened beams and ring stiffened cylindrical shells, and 25 terms are sufficient for the response of an orthogonally stiffened plate. For supersonic velocities of loading, smaller number of terms is necessary because the zeroth order term in the series is then a radiating harmonic. For a given convection velocity of loading, this term is more likely to be radiating harmonic, at higher frequencies so that the accuracy of the calculated response will be better at these frequencies than at lower frequencies.

The results for sound power radiated by the orthogonally stiffened plate predicted by this theory agree reasonably well with the experimental results for the frequency range covered by the experiment. At higher frequencies the agreement is expected to be closer, since at higher frequencies the influence of the finiteness of the structure will be smaller.

The method adopted is obviously simpler than the normal mode

approach where all the modes would have to be determined first, and then the response integrated taking proper account of modal coupling. While the greater degree of damping in the structure makes the exact normal mode analysis very difficult (and the approximate normal mode analysis less accurate) it enhances the validity of the method of space harmonics because the higher degree of damping in the structure brings its behaviour closer to that of the infinite structure.

The theory presented can be applied to any infinite periodic structure, that is to any infinite multi-supported structure irrespective of the characteristics of the supports. This is because any displacement, wave length or frequency dependence of the support stiffness can be readily taken into account while formulating the set of simultaneous equations for the coefficients of space harmonics employed.

The theory explains sound radiation by stiffened structures even when excited by subsonic convection velocities of loading. It has been found that for subsonic velocities of loading, below a certain frequency determined by the structural parameters, there are bands of frequencies where real sound power is radiated. These bands may be easily determined from a simple diagram included in the thesis.

For the purpose of applying the method of space harmonics to obtain the response of a structure to boundary layer, this excitation is analysed to obtain wave length frequency spectrum. This enables the visualisation of the boundary layer field as an assemblage of plane waves of different convection velocities at a given frequency. The wave length components leading to a large response can then be identified. The method employed therefore reduces the computation necessary to analyse a particular problem by identifying the most significant wave numbers. It must be emphasised that the low wave numbers of the boundary

layer can be important especially at subsonic convection velocities of loading. Therefore the importance of the correctness of the wave length spectrum for the excitation field for low wave numbers is clearly seen.

The study brings out some differences between the uniform structures and the stiffened structures. For example, unlike the uniform infinite structure which radiates for only supersonic velocities of loading, the infinite stiffened structure can radiate sound power at subsonic velocities of loading as well. For supersonic convection velocities of loading, the power radiated by infinite stiffened beam has been seen to be much higher than that by the uniform infinite beam.

It has been seen that introduction of damping in the structure cannot be recommended as an effective means for reducing sound power radiated over a band of frequencies. Carefully designing the dimensions of the stiffeners with this end in view may offer a better alternative.

Future work should be done to optimise the structural parameters to minimise the sound power radiated by the structure. The influence on sound power radiated of various wave length spectra or cross correlation functions to represent a boundary layer pressure field also offers a useful area for future work.

APPENDIX A

THE EXCITATION FIELD

A.1 Introduction

The excitation field considered in this thesis may generally be described as a boundary layer pressure field. Such a field in practice is a broad frequency phenomenon, the frequency range in the case of a subsonic aircraft being from approximately 100 Hz to 3000 Hz. As will be shown in this appendix, the acoustic plane wave may be considered as a special case of this general field.

For obtaining the response of the structures to boundary layer pressure, the excitation has been analysed into a wave length frequency spectrum. This spectrum is obtained by the Fourier transform of the spatial cross correlation coefficient of the excitation. The actual expression used for this coefficient is based on the laboratory measurements by Bull et al [54]. The frequency wave length spectrum has been earlier discussed by Wills [55]. Though the expressions given by him have not been actually used for the computations reported, these expressions have been included in this appendix for completeness and comparison.

A.2 The Narrow Band Cross Correlation Coefficient

The narrow band cross correlation coefficient of a pressure field is one of its most important properties and contains a lot of statistical information about it. The field considered here is a homogeneous and stationary boundary layer pressure. The space-time

correlation of the field with these properties will be independent of the instant at which the measurements are made and of the spatial locations of the points where the measurements are made. Thus it will be a function of the time delay τ and spatial separation $\bar{\xi}$ only. Spatial separation is a vector $\bar{\xi}$ having two components, viz ξ_1 in the longitudinal direction (or in the direction of convection) and ξ_3 in the lateral direction.

Under the above assumptions of homogeneity and stationarity, the narrow band cross correlation coefficient at frequency ω may be defined as follows:

$$\rho_p(\xi_1, \xi_3, \tau; \omega) = \frac{R_{p',\Delta\omega}(\xi_1, \xi_3, \tau; \omega)}{R_{p',\Delta\omega}(0, 0, 0; \omega)} \qquad (A.1)$$

where $\rho_p(\xi_1, \xi_3, \tau; \omega)$ is the narrow band cross correlation coefficient at frequency ω and corresponding to spatial separation components ξ_1, ξ_3 and to time delay τ.

and $R_{p',\Delta\omega}(\xi_1, \xi_3, \tau; \omega)$ is the corresponding narrow band space-time cross correlation function.

The narrow band cross correlation function may be actually determined by measuring pressures at two points separated by ξ_1 in the longitudinal direction and ξ_3 in the lateral direction, with a time delay τ, and then passing the signal through a filter centred at frequency ω and having a bandwidth $\Delta\omega$. The function can then be determined by the following relationship

$$R_{p',\Delta\omega}(\xi_1, \xi_3, \tau; \omega) = \underset{T\to\infty}{\text{Limit}} \frac{1}{2T} \int_{-T}^{+T} p_{\Delta\omega}(\bar{x}, t; \omega) p_{\Delta\omega}(\bar{x} + \bar{\xi}, t+T; \omega) dt \qquad (A.2)$$

where $\bar{x}$ is the vector locating one of the measurement points and $p_{\Delta\omega}(\bar{x}, t; \omega)$ is the filter output when the pressure signal is passed through a filter of bandwidth $\Delta\omega$ and centre frequency ω.

A2.1 The frozen turbulence

In the case of frozen turbulence convected with velocity U_c in the longitudinal direction

$$R_p(\xi_1, \xi_3, \tau) = R_p(0, \xi_3, \tau - \tau_o) \quad \text{where} \quad \tau_o = \frac{\xi_1}{U_c}$$

$$= R_p(\xi_1 - U_c\tau, \xi_3, 0) \tag{A.3}$$

and

$$\rho_p(\xi_1, \xi_3, \tau; \omega) = \frac{|S_p(\xi_1, \xi_3, \omega)|}{S_p(\omega)} \cos \omega(\tau - \frac{\xi_1}{U_c}) \tag{A.4}$$

where $S_p(\xi_1, \xi_3, \omega)$ is the pressure cross power spectral density and $S_p(\omega) = S_p(0, 0, \omega)$ is the pressure power spectral density.

A.2.2 Decaying turbulence

For decaying turbulence, Bull has shown that

$$\rho_p(\xi_1, \xi_3, \tau; \omega) = F(\frac{\xi_1}{U_c}, \frac{\xi_3}{U_c}) \cos \omega(\tau - \frac{\xi_1}{U_c}) \tag{A.5}$$

except at small values of $\frac{\omega\xi_1}{U_c}$ and $\frac{\omega\xi_3}{U_c}$.

Bull's measurements also show that except at small values of $\frac{\omega\xi_1}{U_c}$,

$$|\rho_p(\xi, \xi_3, \tau; \omega)| = |\rho_p(\xi_1, 0, \tau; \omega)| \; |\rho_p(0, \xi_3, \tau; \omega)| \tag{A.6}$$

Also that

$$|\rho_p(\xi_1, 0, \tau; \omega)| = e^{-\frac{b\omega|\xi_1|}{U_c}} \tag{A.7}$$

and $$|\rho_p(0, \xi_3, \tau; \omega)| = e^{-\frac{c\omega|\xi_3|}{U_c}} \qquad (A.8)$$

where b and c are called the boundary layer decay parameters in the longitudinal and lateral directions respectively.

Figures A.1-A.2 show respectively the longitudinal correlation coefficient as given by equation (A.7) and lateral coefficient as given by equation (A.8). Combining equations (A.6-8), the complete coefficient may be expressed (except for low values of $\frac{\omega \xi_1}{U_c}$) as

$$\rho_p(\xi_1, \xi_3, \tau; \omega) = e^{-\frac{b\omega|\xi_1|}{U_c}} e^{-\frac{c\omega|\xi_3|}{U_c}} \cos \omega(\tau - \frac{\xi_1}{U_c}) \qquad (A.9)$$

For $\tau = 0$

$$\rho_p(\xi_1, \xi_3, 0; \omega) = e^{-\frac{b\omega|\xi_1|}{U_c}} e^{-\frac{c\omega|\xi_3|}{U_c}} \cos \frac{\omega\xi_1}{U_c} \qquad (A.10)$$

A.3 The Convection Velocity

Bull's measurements lead to the following expressions for the convection velocity in terms of free stream velocity U_o and boundary layer displacement thickness δ^*.

$$U_c = U_c(\omega) = \left[0.59 + 0.30\, e^{\frac{-0.89\omega\delta^*}{U_o}} \right] \qquad (A.11)$$

Figure A.3 shows the relationship given by equation (A.11).

A.4 The Wave Number Frequency Spectrum

A.4.1 The wave number frequency spectrum by Fourier transforming the space-time correlation

The wave number frequency spectrum is the double Fourier transform of the space time correlation function $R_p(\bar{\xi}, \tau)$ of the pressures at two points separated by $\bar{\xi}$. Thus the wave number frequency

spectrum of the pressure field is

$$S_p(\bar{K}, \omega) = \frac{1}{(2\pi)^2} \int_{-\infty}^{+\infty} e^{-i\bar{K}\bar{\xi}} \int_{-\infty}^{+\infty} R_p(\bar{\xi}, \tau) e^{-i\omega\tau} d\tau d\bar{\xi} \qquad (A.12)$$

Now the cross power spectral density of the pressures at points separated by $\bar{\xi}$ is

$$S_p(\bar{\xi}, \omega) = \frac{1}{2\pi} \int_{-\infty}^{+\infty} R_p(\bar{\xi}, \tau)\, e^{-i\omega\tau} d\tau \qquad (A.13)$$

and for a homogeneous pressure field with respect to the direction of convection is commonly expressed in the form

$$S_p(\bar{\xi}, \omega) = S_p(\omega) \rho_p(\bar{\xi}, \omega) \qquad (A.14)$$

where $S_p(\omega)$ is the power spectral density of the pressure at any point in the field and $\rho_p(\bar{\xi}, \omega)$ is in general a complex function. From equations (A.12-14) we see

$$S_p(\bar{K}, \omega) = S_p(\omega) \frac{1}{2\pi} \int_{-\infty}^{+\infty} \rho_p(\bar{\xi}, \omega) e^{-i\bar{K}\bar{\xi}} d\bar{\xi} \qquad (A.15)$$

where K can take any value between $+\infty$ and $-\infty$ for the most general pressure fields. It is reasonable however to suppose that a boundary layer pressure field has positive values of $\bar{K}$ only since all component pressure waves are convected in the direction of flow (see reference [55] for some relevant discussion).

Now express the complex $\rho_p(\bar{\xi}, \omega)$ in the form

$$\rho_p(\bar{\xi}, \omega) = \rho_{pr}(\bar{\xi}, \omega) + i\rho_{pi}(\bar{\xi}, \omega) \qquad (A.16)$$

and substitute in equation (A.15). Since $S_p(\bar{K}, \omega)$ is an entirely real function and must have zero value for negative K, we find

$$S_p(\bar{K}, \omega) = S_p(\omega)\frac{1}{2\pi}\int_{-\infty}^{+\infty} \rho_{pr}(\bar{\xi}, \omega)\cos \bar{K}\bar{\xi}\, d\bar{\xi} \qquad (A.17)$$

Thus the form of $\rho_{pr}(\bar{\xi}, \omega)$ only is required and not of $\rho_{pi}(\bar{\xi}, \omega)$. The value of $\rho_{pr}(\bar{\xi}, \omega)$ is given by equation (A.10) as

$$\rho_p(\xi_1,\xi_3, 0, \omega) = e^{-\frac{b\omega|\xi_1|}{U_c}} e^{-\frac{c\omega|\xi_3|}{U_c}} \cos\frac{\omega\xi_1}{U_c} \qquad (A.18)$$

where b is the boundary layer decay parameter in the longitudinal direction and c in the corresponding parameter for the lateral direction. When $b = c = 0$, ρ_p corresponds to the acoustic plane wave. The wave number frequency spectrum then has zero value for all $\bar{K}$ except for $\bar{K} = \frac{\omega}{\bar{U}_c}$ at which it takes the form of a δ function, such that

$$\int_c^\infty S_p(\bar{K}, \omega)d\bar{K} = S_p(\omega) \qquad (A.19)$$

or

$$\int_0^\infty \frac{1}{2\pi}\int_0^\infty \rho_p(\bar{\xi}, \omega)e^{-i\bar{K}\bar{\xi}}d\bar{\xi}\,d\bar{K} = 1 \qquad (A.20)$$

When b and c are non zero, the $S_p(\bar{K}, \omega)$ has non zero values for all $\bar{K}$ but has a maximum value at $\bar{K} = \frac{\omega}{\bar{U}_c}$.

$\bar{K}$ has two components, K_1 in the direction of convection and K_3 laterally. We may therefore speak of K_1, K_3,ω spectrum or of $S_p(K_1, K_3, \omega)$. When this is integrated over all $\bar{K}$ (or over all K_1 and K_3) it yields power spectral density, or

$$\int_0^\infty\int_0^\infty S_p(K_1, K_3, \omega)dK_1dK_3 = S_p(\omega) \qquad (A.21)$$

Evidently then

$$S_p(K_1,K_3,\omega) = \frac{1}{(2\pi)^2}\int_{-\infty}^{+\infty} e^{-iK_1\xi_1}d\xi_1 \int_{-\infty}^{+\infty} e^{-iK_3\xi_3}\rho_p(\xi_1, \xi_3, \omega, 0)d\xi_3 \qquad (A.22)$$

Substituting for $\rho_p(\xi_1, \xi_3, \omega, 0)$ from equation (A.18) and evaluating the integrals yields after some arrangement

$$S_p(K_1,K_3, \omega) = \frac{S_p(\omega)}{2\pi^2} \left\{ \frac{1}{\frac{c\omega}{U_c}\left[\left(\frac{K_3}{\frac{c\omega}{U_c}}\right)^2 + 1\right]} \right\}$$

$$\times \left\{ \frac{\frac{b\omega}{U_c}}{\left(\frac{b\omega}{U_c}\right)^2 + \left(\frac{\omega}{U_c} - K_1\right)^2} + \frac{\frac{b\omega}{U_c}}{\left(\frac{b\omega}{U_c}\right)^2 + \left(\frac{\omega}{U_c} + K_1\right)^2} \right\} \qquad (A.23)$$

The first term on the right hand side represents the contribution of K_3, the lateral wave number. At high K_3, this contribution can be seen to be small. The second term represents the contribution of K_1 components and peaks at $K_1 \doteq \frac{\omega}{U_c}$.

If the direction of convection of the boundary layer is parallel to the X-axis

$$\mu_x = K_1 \ell_x$$

$$\mu_y = K_3 \ell_y$$

Therefore, from equation (A.23) $S_p(\mu_x, \mu_y, \Omega)$ may be obtained as

$$S_p(\mu_x, \mu_y, \omega) = \frac{S_p(\omega)}{\pi^2} \left\{ \frac{1}{cq\frac{\Omega}{CV}\left[\left(\frac{\mu_y}{cq\Omega/CV}\right)^2 + 1\right]} \right\}$$

$$\times \left\{ \frac{b\frac{\Omega}{CV}\left|(1+b^2) + \left(\mu_x \frac{CV}{\Omega}\right)^2\right|}{\left[b^2 + \left(1 - \frac{\mu_x CV}{\Omega}\right)^2\right]\left[b^2 + \left(1 + \frac{\mu_x CV}{\Omega}\right)^2\right]} \right.$$

$$= S_p(\omega)\, S_p(\mu_y, \Omega).S_p(\mu_x, \Omega) \qquad (A.24)$$

where

$$S_p(\mu_x, \Omega) = \frac{b\frac{\Omega}{CV}\left[(1+b^2)+(\mu_x\frac{CV}{\Omega})^2\right]}{\pi\left[b^2+(1-\frac{\mu_x CV}{\Omega})^2\right]\left[b^2+(1+\frac{\mu_x CV}{\Omega})^2\right]} \qquad (A.25)$$

and

$$S_p(\mu_y, \Omega) = \frac{1}{\pi cq\frac{\Omega}{CV}\left[(\frac{\mu_y}{cq\ \Omega/CV})^2+1\right]} \qquad (A.26)$$

The first term in equation (A.24) given by equation (A.25), is almost inversely proportional to μ_y^2 for large values of μ_y. It will then become very small at fairly high frequencies. The contribution to the overall spectrum will then be only from μ_x or convection in the longitudinal direction.

For a large value of q $(\frac{1}{q^2} \to 0)$, the first term is inversely proportional to q. Hence for a beam (a large q), the contribution of the first term may be considered constant in the calculation of the wave-length frequency spectrum. In that case the wave length frequency spectrum is given by equation (A.25) as

$$S_p(\mu_x,\mu_y, \omega) = S_p(\mu_x,\omega) = \frac{b\frac{\Omega}{CV}\left[(1+b^2)+(\frac{\mu_x CV}{\Omega})^2\right]}{\pi\left[b^2+(1-\frac{\mu_x CV}{\Omega})^2\right]\left[b^2+(1+\frac{\mu_x CV}{\Omega})^2\right]} \qquad (A.27)$$

Clearly then, for small values of b, the spectrum of (A.27) would peak at a value when $\frac{\mu_x(CV)}{\Omega} \doteq 1$. This expression for the spectrum has been used in computation of response due to the boundary layer pressure field described in Chapter 2.

The usual values taken for b and c are:

$b = 0.1$ $\qquad\qquad$ $c = 0.715$

The one dimensional spectrum corresponding to equation (A2 7) has been shown in Figure A.4. It has been plotted in Figure A.5 again to compare with the spectrum presented by Wills.

An acoustic plane wave has a δ-function form of wavelength-frequency spectrum at $\bar{K} = \frac{\omega}{\bar{U}_c}$. If the acoustic plane wave is inclined at θ to the x axis, the non zero values are for

$$\begin{aligned} \mu_x &= K\ell_x \cos\theta \\ \mu_y &= K\ell_y \sin\theta \end{aligned} \tag{A.28}$$

When the boundary layer is inclined at θ to the X-axis

$$\begin{aligned} \mu_x &= K_1 \cos\theta - K_3 \sin\theta \\ \mu_y &= K_1 \sin\theta + K_3 \cos\theta \end{aligned} \tag{A.29}$$

The wavelength-frequency spectrum in that case is most conveniently found in terms of K_1 and K_3. This is given by equation (A.23). The response, however, may be more conveniently calculated in terms of μ_x and μ_y given by equation (A.29).

A.4.2 Wills' wavelength spectrum

Wills has presented the values of wave number-frequency and wave number phase velocity spectrum of the wall pressure for a two dimensional turbulent boundary layer in zero pressure gradient obtained from a Fourier transform of experimental filtered spatial correlations. He found that in the region of significant energy the wave number spectra are similar at all frequencies measured within experimental accuracy. This means that the height of the main peak of the wave

number spectrum is proportional to the integrated spectral density at each frequency. Thus the complete (K_1, ω) spectrum can be approximated by

$$\phi_1(K_1, \omega) = \phi(\omega)F\left(\frac{\omega}{K_1 U_\omega}\right) \tag{A.30}$$

where $\phi(\omega)$ is the frequency spectrum and U_ω is the convection velocity. The subscript ω is there to emphasise that it is frequency dependent.

Figure A.5 shows the function F under the relation shown by equation (A.30). This has been seen to fit a normal distribution curve $e^{-(\omega/K_1 U_\omega - 1)^2/0.2^2}$ very closely, except at very small values of the argument. Figure A.5 also shows (chain double dotted line) the spectrum obtained from equation (A.27) for $b = 0.1$ and for $b = 0.2$ (chain dotted line). It is interesting to observe that Wills has proposed that the more general spectrum $\phi(K, \omega)$ may be given by

$$\phi(K, \omega) = \phi_3(K_3, \omega)F\left(\frac{\omega}{K_1 U_\omega}\right) \tag{A.31}$$

This form may be seen to be similar to the form presented in this thesis (see equations (A.23-24)).

APPENDIX B

FLOW DIAGRAM FOR COMPUTATION

Stiffened Beam Excited by Boundary Layer

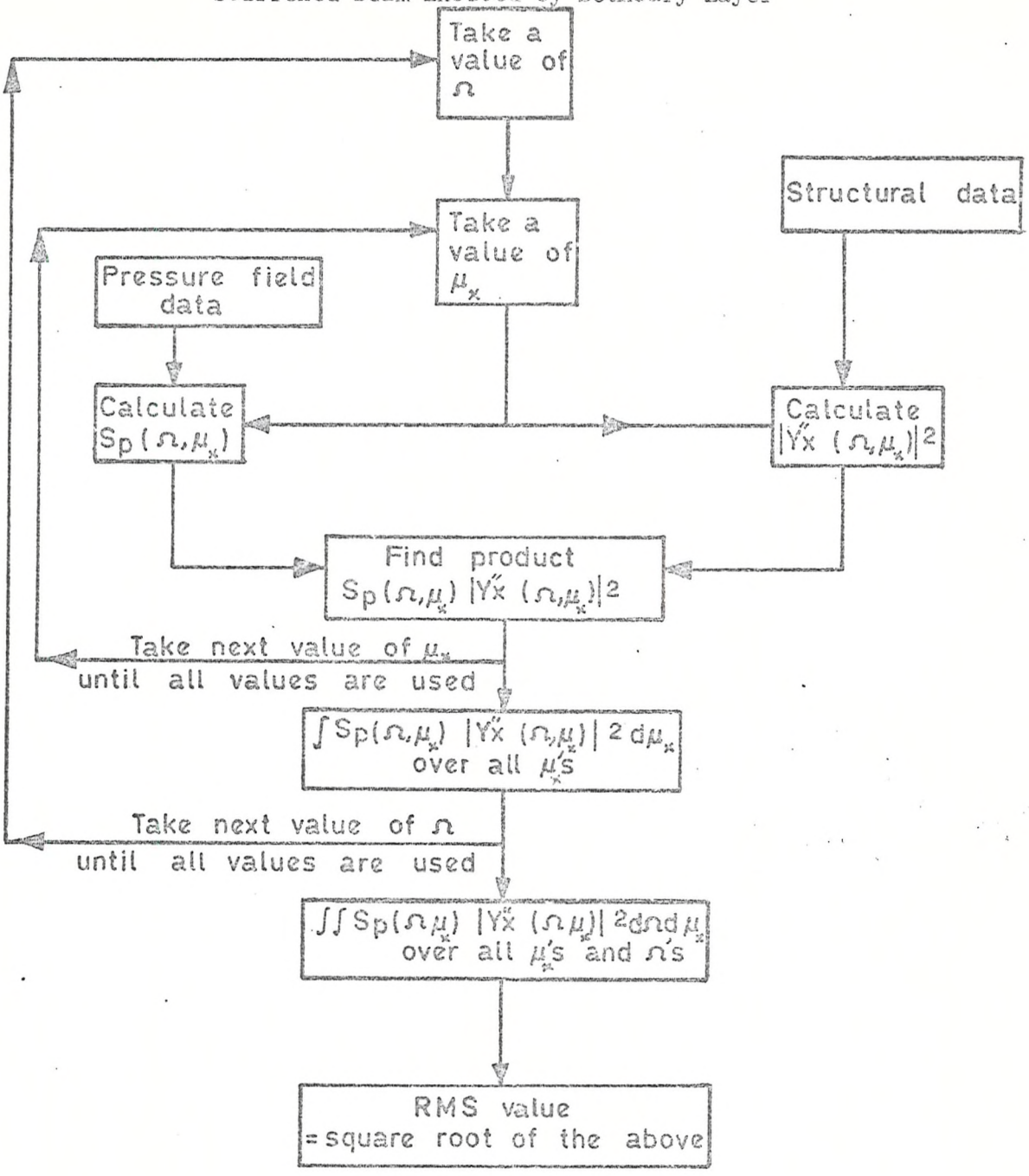

APPENDIX C

TIME AVERAGE OF THE PRODUCT OF REAL PARTS OF TWO COMPLEX FUNCTIONS

Let the product of real parts of two complex functions f and F be required.

Let $$f = f_o e^{i(\omega t - \psi)} \tag{C.1}$$

and $$F = F_o e^{i(\omega t - \phi)} \tag{C.2}$$

Now,

$$\begin{aligned} \langle \mathrm{Re}(f) \times \mathrm{Re}(F) \rangle &= f_o F_o \langle \cos(\omega t - \psi) \cos(\omega t - \phi) \rangle \\ &= f_o F_o \frac{1}{T} \int_o^T \cos(\omega t - \psi) \cos(\omega t - \phi) dt \end{aligned} \tag{C.3}$$

where T is the period of f and F and equals $\frac{2\pi}{\omega}$

Expanding the integrand of (C.3)

$$\begin{aligned} \langle \mathrm{Re}(f) \times \mathrm{Re}(F) \rangle &= \frac{f_o F_o}{T} \int_o^T \cos(\omega t - \psi)\cos(\omega t - \psi + \psi - \phi) dt \\ &= \frac{f_o F_o}{T} \int_o^T \cos(\omega t - \psi)\big[\cos(\omega t - \psi)\cos(\psi - \phi) \\ &\qquad - \sin(\omega t - \psi)\sin(\psi - \phi)\big] dt \end{aligned} \tag{C.4}$$

Let $$(\psi - \phi) = \theta \tag{C.5}$$

Then

$$\begin{aligned} \langle \mathrm{Re}(f) \times \mathrm{Re}(F) \rangle = \frac{f_o F_o}{T} \int_o^T \big[&\cos\theta \cos^2(\omega t - \psi) - \sin\theta \sin(\omega t - \psi) \\ &\cdot \cos(\omega t - \psi)\big] dt \end{aligned} \tag{C.6}$$

The second term in the integrand of equation (C.6) becomes zero on integration while the first term yields $\frac{T}{2} \cos \psi$.

Therefore

$$\langle \mathrm{Re}(f) \times \mathrm{Re}(F) \rangle = \frac{1}{T} f_o F_o \frac{T}{2} \cos\theta = \tfrac{1}{2} f_o F_o \cos\theta \qquad (C.7)$$

Now

$$\begin{aligned} \tfrac{1}{2} f_o F_o \cos &= \tfrac{1}{2}\mathrm{Re}(f_o F_o e^{-i\theta}) \\ &= \tfrac{1}{2}\mathrm{Re}\left[f_o e^{-(\omega t-\psi)} . F_o e^{-i(\omega t-\phi)}\right] \\ &= \tfrac{1}{2}\mathrm{Re}(fF^*) \end{aligned} \qquad (C.8)$$

where F^* is the complex conjugate of F.

From equations (C.7) and (C.8)

$$\langle \mathrm{Re}(f) \times \mathrm{Re}(F) \rangle = \tfrac{1}{2}\mathrm{Re}(fF^*) \qquad (C.9)$$

or the time average of the product of real parts of two complex functions is given by half the real part of the product of one and the complex conjugate of the other.

APPENDIX D

FLOW DIAGRAM FOR COMPUTATION

Stiffened plate excited by boundary layer

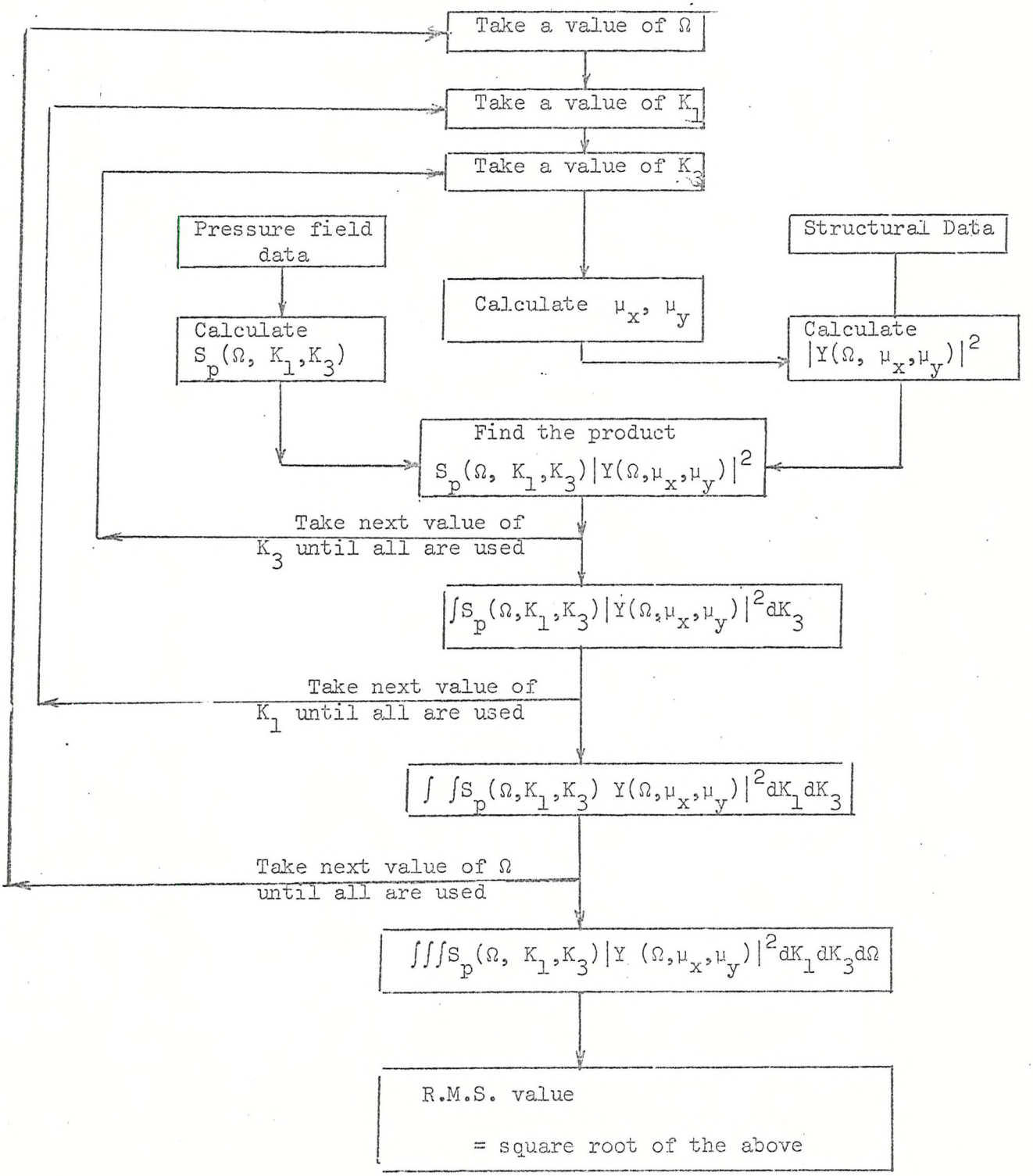

APPENDIX E

THE RADIATING HARMONIC FOR THE STIFFENED PLATE

An $(m,n)^{th}$ term in the series of space harmonics given by equation (4.27) will result in true sound radiation if the corresponding K_{mnz} is real, i.e. if

$$(\frac{\omega}{C})^2 - (\frac{\mu_x + 2m\pi}{\ell_x})^2 - (\frac{\mu_y + 2n\pi}{\ell_y})^2 > 0$$

The above relation is similar to that for the case of the beam (see section 3.5.1) except for the additional term involving μ_y (and n). For a given μ_y, it should therefore be possible to draw a diagram like Figure 3.1 for each value of n. However if only one diagram is desired for all values of m and n, it will have to be three dimensional. The straight lines parallel to the sides of the primary radiation triangle POR in Figure 3.1 will now be surfaces parallel to the surface of the primary radiating cone. An $(m,n)^{th}$ term will now radiate if it is possible to bring the value of μ_x and μ_y within the primary radiating cone by adding $2m\pi$ to μ_x and $2n\pi$ to μ_y.

A more general case of the plane wave loading inclined at an angle θ to the X-axis will introduce still further complication in the diagram. The mechanism by which the $(m, n)^{th}$ term radiates, may therefore be better illustrated by looking at a given frequency as the following analysis indicates.

The harmonics (m,n) will radiate if

K_{mnz} is real

or if $(\frac{\omega}{C})^2 - [(\frac{\mu_x + 2m\pi}{\ell_x})^2 + (\frac{\mu_y + 2n\pi}{\ell_y})^2]$ is positive.

In the critical case

$$(\frac{\omega}{C})^2 = (\frac{\mu_x + 2m\pi}{\ell_x})^2 + (\frac{\mu_y + 2n\pi}{\ell_y})^2 \qquad (E.1)$$

or

$$(\frac{\omega \ell_x}{C})^2 = (\mu_x + 2m\pi)^2 + (\frac{\mu_y + 2n\pi}{q})^2 \qquad (E.2)$$

or

$$(\frac{\Omega}{SV})^2 = (\frac{\Omega \cos\theta}{CV} + 2m\pi)^2 + (\frac{\frac{q\Omega}{CV}\sin\theta + 2n\pi}{q})^2 \qquad (E.3)$$

equation (E.2) may also be rewritten as

$$(\frac{\mu_x + 2m\pi}{R_x})^2 + (\frac{\mu_y + 2n\pi}{R_y})^2 = 1 \qquad (E.4)$$

where $$R_x = \frac{\omega \ell_x}{C} = \frac{\Omega}{SV} \qquad (E.5)$$

and $$R_y = q\frac{\omega \ell_x}{C} = \frac{\omega \ell_y}{C} = \frac{q\Omega}{SV} \qquad (E.6)$$

Equation (E.4) represents an ellipse where R_y and R_x give the major and minor axes respectively. Substituting $m = n = 0$ in this equation would yield equation of the primary radiating ellipse. If particular values of (m,n) satisfy equation (E.4), the $(m, n)^{th}$ harmonic will be a radiating one.

The above statements are illustrated by Figure E.1. Ellipses have not been drawn because only their major and minor axes are of importance. These are along the Y and X axes of the figure respectively. μ_x is drawn on the X-axis and μ_y on the Y-axis. Concentric circles with O as centre and radial lines at different angles to the X-axis have been drawn to facilitate locating points on the diagrams. The numbers 1, 2, 3,... on the X-axis on the left of the origin represent the aspect

ratio q. Any value OE on the Y-axis may be multiplied by q by drawing a line through E parallel to one of the lines joining P to these numbers. For multiplying OE by q = 2, draw EF' parallel to P2. Then OF' = q.OE. Evidently OE' = OF' = q OE.

Let us consider a case where $\frac{\Omega}{SV}$ = OA, q = 2, $\frac{\Omega}{CV}$ = OB and $\theta = 30^{\circ}$.

Let A'A" = q.OA' = OA"'

The primary radiating ellipse for these conditions is given by major diameter OA"' and minor diameter OA. Thus if the value of μ_x can be brought within OA by adding $2m\pi$ to it, and the value of μ_y can be brought within OA"' by adding $2n\pi$ to it, the $(m, n)^{th}$ harmonic will radiate.

For $\frac{\Omega}{CV}$ = OB and q = 2, μ_x = OD and μ_y = OE'. By adding -2π to μ_x it can be brought within OA. Also μ_y is within OA"'. So the radiation will take place for m = -1 and n= 0. It will radiate for all values of m, n for which μ_x is brought within OA, and μ_y within OA"'.

Other conditions of excitation may similarly be tested for true radiation.

APPENDIX F

INSTRUMENTS USED FOR EXPERIMENTAL DETERMINATION OF RADIATED POWER AND FOR MEASUREMENT OF DAMPING

B. & K. beat frequency oscillator Type 1014.

15 Watt loudspeaker.

B. & K. ½" condenser microphone S.N. 164197.

B. & K. ½" condenser microphone S.No. 218312.

B. & K. audiofrequency spectrometer type 2111.

B. & K. audiofrequency spectrometer type 2112.

E.M. Ltd. Accelerometer S.N. 299 (sensitivity 11.8 mv/g).

Tape recorder T.3000

B. & K. level recorder type 2305.

Power amplifier Cape 25. Serial No. VLI MK2.

Cathode ray oscilloscope. Type 502 (Tektronix Inc.)

Universal avometer no. 13754 - 3A.

6 Watt audio oscillator (Dawe) type 44.B, serial no. 685.

Step down transformer Inst. No. 13088.

Wayne-Kerr probes.

Wayne-Kerr vibration meter. type B731A, serial no. 85.

Solartron resolved component indicator, model VP. Serial no. 39736.

APPENDIX G

THE DETERMINATION OF DAMPING FROM THE VECTOR PLOT

The method applied to a continuous system vibrating in a single mode has been derived from the analysis of a single degree of freedom system. The equation of motion of a single degree of freedom system with mass M, stiffness K_s and hysteretic damping η under a constant harmonic excitation $P_o e^{i\omega t}$ is

$$M\ddot{w} + K_s(1 + i\eta)w = P_o e^{i\omega t} \tag{G.1}$$

Assume a solution $w = \bar{w}\, e^{i\omega t}$ (G.2)

Substituting (G.2) into (G.1) yields

$$\bar{w} = \frac{P_o}{(K_s - Mw^2) + i\eta K_s} \tag{G.3}$$

Let static deflection $\bar{w}_s = P_o/K_s$ (G.4)

the resonant frequency of the system $\omega_n = \sqrt{\frac{K_s}{M}}$ (G.5)

and non dimensional frequency ratio $\Omega_r = \frac{\omega}{\omega_n}$ (G.6)

Now

$$\mathrm{Re}(\bar{w}) = \frac{\bar{w}_s(1 - \Omega_r{}^2)}{(1 - \Omega_r{}^2) + \eta^2} \tag{G.7}$$

where Re represents the real part of

Differentiating (G.7) with respect to Ω_r

$$\frac{d}{d\Omega_r}\mathrm{Re}(\bar{w}) = \frac{\bar{w}_s 2\Omega_r\left[(1 - \Omega_r{}^2)^2 - \eta^2\right]}{(1 - \Omega_r{}^2)^2 + \eta^2} \tag{G.8}$$

$\frac{d}{d\Omega_r}\mathrm{Re}(\bar{w})$ therefore has a maximum at $\Omega_r = 1$ and has then a value

$$\left| \frac{d}{d\Omega_r} \mathrm{Re}(\bar{w}) \right|_{\Omega_r=1} = \frac{-2\Omega_r \bar{w}_s}{\eta^2} \qquad (G.9)$$

The response vector $\bar{w}$ is entirely imaginary at $\Omega = 1$ and therefore the resonant frequency is given by the point on the circle through which a tangent drawn at the point is parallel to the reference axis. The diameter of this circle D can be found from equation (G.3) and is given by

$$D = \frac{\bar{w}_s}{\eta} \qquad (G.10)$$

From equations (G.9) and (G.10)

$$\eta = \frac{2D}{\left| \frac{d\ \mathrm{Re}(\bar{w})}{d\Omega_r} \right|_{\Omega=1}} \qquad (G.11)$$

The diameter of the circle D can be actually measured from the vector plot obtained and the denominator of the above equation can be determined as the rate of change of the real part of the response vector with respect to the non dimensional frequency, Ω_r, in the region of the resonant frequency. Then equation (G.11) will readily yield the value of damping η.

APPENDIX H

THE SHELL RING INTERACTION FORCES

(See also reference [56])

The ring displacements v_R, w_R at the median axis of the ring are related to the shell displacements v_s, w_s at the median surface by

$$v_R = (1 - \frac{e}{a})v_s + \frac{e}{a} \frac{\partial w_s}{\partial \theta} \tag{H.1}$$

and

$$w_R = w_s \tag{H.2}$$

where e is the distance between the median surface of the shell and the median axis of the ring. These displacement relations are a consequence of the classical thin shell theory assumptions. According to this analysis the ring shell interaction forces Y_R and Z_R in the tangential and radial directions resulting from inplane deformation of the stiffening ring, and M_R the circumferentially distributed moment necessary to keep the out of plane rotation of the ring compatible with the slope of the shell in the axial direction, are given by the following expressions (see Figure H.1).

$$Y_R(\theta) = K_{\theta\theta}\left[(1 - \frac{e}{a})v_s + \frac{e}{a} \frac{\partial w_s}{\partial \theta}\right] + K_{\theta r} w_s \tan n\theta \tag{H.3}$$

$$Z_R(\theta) = K_{r\theta}\left[(1 - \frac{e}{a})v_s + \frac{e}{a} \frac{\partial w_s}{\partial \theta}\right] \cot n\theta + K_{rr} w_s \tag{H.4}$$

$$M_R(\theta) = K_T \frac{\partial w}{\partial x} \tag{H.5}$$

where $K_{\theta\theta}$, $K_{\theta r}$, K_{rr} and K_T are the stiffness coefficients in the n^{th} circumferential mode, and e is the distance between the median

surfaces of the shell and the ring. The stiffness coefficients may be expressed as follows:

$$K_{\theta\theta} = \frac{EA}{R^2} n^2 \left(1 - \frac{I}{R^2 A}\right) \quad \{\text{Except for } n = 0 \text{ when } K_{\theta\theta} = \frac{2}{R^2/EA} \tag{H.6}$$

$$K_{\theta r} = \frac{EA}{R^2} n \left(1 - \frac{I}{R^2 A}\right) \tag{H.7}$$

$$K_{rr} = \frac{EA}{R^2} \left\{1 - \frac{I}{R^2 A} + \frac{C_1 (n^2 - 1)^2 \, I/R^2 A}{n^2 \, I/R^2 A + C_1}\right\} \tag{H.8}$$

$$K_T \text{ (for a thin ring)} = \frac{a^2}{(n^2-1)^2} \left[\frac{1}{EI} + \frac{n^2}{GJ}\right] \tag{H.9}$$

where A is the area of cross section of the ring

I is the moment of inertia of the ring cross section

R is the mean radius of the ring

C_1 is the shear coefficient (may be taken as $\frac{5}{6}$ after [57])

EI is the bending stiffness of the ring

GJ is the torsional stiffness of the cross section

e is usually small compared to a. Assuming it to be negligible equations (H.3-5) simplify to

$$Y_R(\theta) = K_{\theta\theta} v_s + K_{\theta r} w_s \tan\theta \tag{H.10}$$

$$Z_R(\theta) = K_{r\theta} v_s \cot n\theta + K_{rr} w_s \tag{H.11}$$

$$M_R(\theta) = K_T \frac{\partial w}{\partial x} \tag{H.12}$$

REFERENCES

1. H.S. Ribner (1956) — Boundary Layer Induced Noise in the Interior of Aircraft. University of Toronto, U.T.I.A. Report 37.

2. G.M. Corcos (1956) H.W. Liepmann — On the contribution of turbulent boundary layers to the noise inside a fuselage. NACA TM 1420 (September 1956).

3. Powel, A. (1958) — On the fatigue failure of structures due to vibrations excited by random pressure fields. Journal of Acoustical Society of America, Vol. 30 (December 1958).

4. Y.K. Lin (1960) — Free vibrations of continuous skin stringer panels. Journal of Applied Mechanics, Dec. 1960. p.669-676.

5. Y.K. Lin (1962) — Stresses in continuous skin-stiffener panels under random loading. Journal of Aerospace Sciences, Vol. 29, No. 1.

6. Y.K. Lin (1964) I.D. Brown P.C. Deutschle — Free vibrations of a finite row of continuous skin stringer panels. Journal of Sound and Vibration (1964) 1, 14-27.

7. B.L. Clarkson (1962) R.D. Ford — The response of a typical aircraft structure to jet noise. J. R. Aero. Soc. 66, 31.

8. C.A. Mercer (1965) — Response of a multi-supported beam to a random pressure field. Journal of Sound and Vibration (1965), 2, 3, 293-306.

9. B.L. Clarkson (1968) — Stresses in skin panels subjected to random acoustic loading. The Aeronautical Journal, Vol. 72, No. 695, November 1968.

10. D.J. Mead (1967) — The use of stiffened sandwich plates on aircraft. International symposium on "The damping of the vibrations of plates by means of a layer", Leuven 1967.

11. W.H. Hoppmann II L.S. Magness (1957) — Nodal patterns of the free flexural vibrations of stiffened plates. Journal of Applied Mechanics, 24, 526-530.

12. Garry M. Lindberg (1967) Mervyn D. Olson — Vibration modes and random response of a multi-bay panel system using finite elements. Aeronautical report LR-492, National Research Council of Canada, December 1967.

13. Mervyn D. Olson (1970) Garry M. Lindberg — Free vibrations and random response of an integrally stiffened panel. Conference on 'Current Developments in sonic fatigue'. Univ. of Southampton, July 1970.

14. G. Maidanik (1962) — Response of ribbed panels to reverberant acoustic fields. Journal of the Acoustical Society of America, 34, 6 (1962), 809.

15. R.H. Kraichnan (1957) — Noise transmission from boundary layer pressure fluctuations Journal of the Acoustical Society of America, 29, 1, pp.65-80 (January 1957).

16. I. Dyer (1958) — Sound radiation into a closed space from boundary layer turbulence. Bolt, Beranek and Newman Inc. Report 602. December 1958.

17. L. Cremer (1942) — Theorie der Schalldammung dunner Wande bei Schra Einfall. Akust. Z, 7, 81 (1942).

18. M.C. Bhattacharya M.J. Crocker (1969) — Forced vibration of a panel and radiation of sound into a room. Report BS/A/61/1. Dept. of Building Science, Univ. of Liverpool (February 1969).

19. Pritchard H. White Milt. G. Cottis (1968) — Acoustic radiation from a plate rib system excited by boundary layer turbulence. Report MAC 702-06, January 1968.

20. I.P. Konovalyuk (1969) — Diffraction of a plane sound wave by a plate reinforced with stiffness members. Soviet Physics. Acoustics 14,4,465(1969).

21. Leon Brillouin (1946) — Wave propagation in periodic structures. McGraw Hill Book Co. Inc.

22. P.M. Morse (1955) — Bolt, Beranek and Newman Inc. Report 302. (April 1955).

23. L. Cremer (1953) H.O. Leilich — Arch. elek. Vebertrag. 7, 261 (1953).

24. Eric E. Ungar (1966) — Steady-state responses of one dimensional periodic flexural systems. Journal of the Acoustical Society of America, 39, 887- 1966.

25. E.E. Ungar (1961) — Transmission of plate flexural waves through reinforcing beams: dynamic stress concentrations. Journal of the Acoustical Society of America, 33, pp. 633-639.

26. M. Heckl (1964) — Investigations on the vibrations of grillages and other beam structures. Journal of the Acoustical Society of America, 36 (7), 1335-1343.

27. D.J. Mead, E.M. Wilby (Mrs.) — Forced vibrations of periodically supported beams subjected to convected homogeneous pressure fields. Univ. of Southampton Report (under preparation).

28. D.J. Mead (1970) — Free wave propagation in periodically supported infinite beams. Journal of Sound and Vibration, Feb. 1970.

29. D.J. Mead (1971), K.K. Pujara — Space-harmonic analysis of periodically supported beams; response to convected random loading. (Accepted for publication in the) Journal of Sound and Vibration, vol. 14 (Feb. 1971).

30. D.J. Mead (1970), G. Sengupta — Wave group theory applied to the response of finite structures. Paper presented at conference on 'Current developments in sonic fatigue', held at the Univ. of Southampton, (July 1970).

31. G. Sengupta (1970) — On the relation between the propagation constant and the transfer matrix used in the analysis of periodically stiffened structures. Journal of Sound and Vibration, vol. 11, No. 4. (April 1970).

32. Y.K. Lin (1969), T.J. McDaniel — Dynamics of beam-type periodic structures. Paper no. 69-Vibr-17, presented at the Vibrations Conference at the American Society of Mechanical Engineers (March 30-April 2, 1969).

33. R.D. Ford (1962) — The response of structures to jet noise. Ph.D. Thesis, Univ. of Southampton.

34. C.A. Mercer (1967), Miss C.A. Seavey — Prediction of natural frequencies and normal modes of skin stringer panel rows. Journal of Sound and Vibration (1967) 6(1), 149-162.

35. Charles J. Runkle, Franklin D. Hart — The radiation resistance of cylindrical shells. NASA CR-1437, (1969).

36. George Dodd (1968), A. Garcia, P.E. Doak — The Rayleigh Building anechoic and reverberation chambers. ISVR Memorandum No. 267.

37. D.J. Mead (1963) — The effect of certain damping treatments on the response of idealized aeroplane structures excited by noise. Ph.D. Thesis, Univ. of Southampton, April 1963.

38. R.G. White (1969) — Measurement of structural frequency response by transient excitation. ISVR Technical Report 12 (January 1969).

39. R.G. White (1969) — The resolution of close natural frequencies in the impulse response and severe truncation effects. ISVR Technical Report No. 17 (June 1969).

40. U.S.A.S. (1967) — USA standard method for the physical measurement of sound. U.S.A.S. S1.2 - 1962 (Revision of Z24.7-1950) Corrected copy Dec. 18 (1967).

41. Henry Cox (1966) — Linear versus logarithmic averaging. Journal of the Acoustical Society of America, Vol. 39, p.688-69.

42. S.K. Mitchell (1967) — Comments on linear vs. logarithmic averaging. Journal of the Acoustical Society of America, Vol. 41, p. 863-864.

43. Lawrence E. Kinsler, Austin R. Frey (1962) — Fundamentals of Acoustics. John Wiley & Sons, Inc. New York, London.

44. L.L. Beranek (Ed.) (1960) — Noise reduction. McGraw Hill Book Co. Inc.

45. Jerome E. Manning, Gideon Maidanik (1964) — Radiation properties of cylindrical shells. Journal of Acoustical Society of America, Vol. 36.

46. Charles J. Runkle, Franklin D. Hart (1969) — The radiation resistance of cylindrical shells. NASA CR-1437, October 1969.

47. J.H. Foxwell (1959), R.E. Franklin — The vibrations of a thin walled stiffened cylinder in an acoustic field. The Aeronautical Quarterly (Feb. 1959).

48. J.R. Bailey (1969) — Response and radiation of cylinders excited by sound. ISVR Memorandum No. 328.

49. M.J. Hine (1969 & 70), F.J. Fahy — The vibrations of a cluster of slender rods in parallel flow with an acoustic field. ISVR Memoranda 296, 322, 351, 378, 379.

50. A. Kalnins (1965) — Dynamic problems of elastic shells. Applied Mechanics Reviews Vol.18, no. 11, Nov. 1965.

51. Gilles Cantin (1968) — Strain displacement relationships for cylindrical shells. A.I.A.A. Journal, vol. 6, no. 9 (Sept. 1968).

52. G.B. Warburton (1970) Dynamics of shells.
Paper No. A.1. Symposium on structural dynamics, 23-26 March 1970.

53. L.L. Beranek (1949)
G.A. Work
Sound transmission through multiple structures containing flexible blankets.
Journal of the Acoustical Society of America, 21, 419.

54. M.K. Bull (1963)
J.F. Wilby
D.R. Blackman
Wall pressure fluctuations in boundary layer flow and response of simple structures to random pressure fields.
AASU Report No. 243, July 1963.

55. J.A.B. Wills (1967)
Measurements of the wave number/phase velocity spectrum of wall pressure beneath a turbulent boundary layer.
NPL Aero. Report 1224 (3rd February 1967).

56. Hyman Garnet (1969)
Alvin Levy
Free vibrations of reinforced elastic shells.
Journal of Applied Mechanics (December 1969)

57. P.M. Naghdi (1956-57)
On the theory of thin elastic shells.
Quarterly of Applied Mathematics, April 1956-January 1957.

Relative Values of Coefficients A_m

CV = 4.0; $\kappa_r = 4.0$; $\kappa_t = 10^7$, $\eta = 0.25$.

(a) Frequency parameter = 12.8

m	$Re(A_m)$	$Im(A_m)$
-5	-0.0002098	-0.001420
-4	-0.0004833	-0.003027
-3	-0.001515	-0.008362
-2	-0.009358	-0.03979
-1	-0.1542	+1.496
0	+0.1657	-1.496
+1	-0.0004751	+0.03768
+2	+0.0002659	+0.008091
+3	+0.0001586	+0.002957
+4	+0.00009114	+0.001394
+5	+0.00005571	+0.0007649

(b) Frequency parameter = 22.4

m	$Re(A_m)$	$Im(A_m)$
-5	-0.0002961	-0.0003890
-4	-0.0008553	-0.001069
-3	-0.003859	-0.004527
-2	-0.06167	-0.06005
-1	+0.1519	0.2569
0	-0.0797	-0.1868
+1	-0.004502	-0.003490
+2	-0.0007367	-0.0004701
+3	-0.000203	-0.00009428
+4	-0.00007298	-0.00001824
+5	-0.00003073	0.0000005922

TABLE 2.1

Influence of including different number of terms in the series on the values of coefficients A_m

$CV = 4.0 \quad \kappa_r = 4.0 \quad \kappa_t \to \infty \quad \eta = 0.25 \quad \Omega = 14.8$

(a) Real Parts of A_m's

m	3 terms	5 terms	7 terms	9 terms
-4				-0.00201
-3			-0.00638	-0.00625
-2		-0.0409	-0.0394	-0.03876
-1	0.674	0.6639	0.655	0.6504
0	-0.685	-0.632	-0.619	-0.6135
+1	0.0109	0.00746	-0.00664	0.00628
+2		0.00254	0.00235	0.00226
+3			0.00102	0.000988
+4				0.000510

(b) Imaginary Parts of A_m's

m	3 terms	5 terms	7 terms	9 terms
-4				-0.00103
-3			-0.00327	-0.00313
-2		-0.0208	-0.0189	-0.0181
-1	0.791	0.612	0.575	0.558
0	-0.800	-0.599	-0.560	-0.544
+1	0.00920	0.00611	0.00553	0.00529
+2		0.00174	0.00158	0.00151
+3			0.000647	0.000619
+4				0.000310

TABLE 2.2

Influence of including different number of terms in the series on the values of coefficients

$CV = 4.0 \quad \kappa_r = 4.0 \quad \kappa_t \to \infty \quad \eta = 0.25 \quad \Omega = 8.0$

(a) Real Parts of A_m's

m	3 terms	5 terms	7 terms	9 terms
-4				-0.00006170
-3			-0.00009606	-0.0001013
-2		-0.00268	-0.002715	-0.002739
-1	-0.2110	-0.2117	-0.2126	-0.21317
0	0.2350	0.2415	0.2433	0.2441
+1	-0.0239	-0.0240	-0.02399	-0.02397
+2		-0.00306	-0.003059	-0.003054
+3			-0.000865	-0.0008637
+4				-0.0003487

(b) Imaginary Parts of A_m's

m	3 terms	5 terms	7 terms	9 terms
-4				-0.00009531
-3			-0.0001787	-0.0001747
-2		-0.0001146	-0.00008504	-0.0000668
-1	0.05341	0.0548	0.05567	0.05617
0	-0.0618	-0.0643	-0.06535	-0.06590
+1	0.008441	0.00844	0.00843	0.008420
+2		0.001165	0.001160	0.001157
+3			0.000346	0.0003451
+4				0.0001446

Table 2.3

Relative Magnitudes of A_{mn}'s

Stiffened plate, structure A, $\eta = 0.15$, trace velocity = 1.5 times the velocity of sound. Frequency 640 Hz.

(a) Real Parts of A_{mn}

n \ m	-3	-2	-1	0	+1	+2	+3
-3	5.97	13.29	-358.8	612.8	250.2	-18.45	-3.92
-2	17.93	-28.73	-3342.06	6066.0	-2320.4	-297.04	-88.79
-1	-16.03	12.43	1874.7	-3529.0	1381.9	228.2	67.29
0	-15.75	5.981	3652.3	-10753.1	2377.1	174.3	50.83
+1	-16.03	12.43	1874.7	-3529.0	1381.9	228.2	67.29
+2	17.93	-28.73	-3342.06	6066.0	-2320.4	-297.04	-88.79
+3	5.97	13.29	-358.8	612.8	250.2	-18.45	-3.92

(b) Imaginary Parts of A_{mn}

n \ m	-3	-2	-1	0	+1	+2	+3
-3	-10.5	-45.08	5.33	163.1	-87.8	-18.01	-5.34
-2	-20.86	-80.25	708.2	-885.9	232.3	39.76	14.45
-1	-41.22	-211.48	2301.8	1022.35	-914.6	5.241	7.28
0	145.2	673.4	-6034.8	-3712.4	1539.7	-53.9	-32.78
+1	-41.22	-211.48	2301.8	1022.35	-914.6	5.241	7.28
+2	-20.86	-80.25	708.2	-885.9	232.3	39.76	14.45
+3	-10.5	-45.08	5.33	163.1	-87.8	-18.01	-5.34

TABLE 4.1

Relative Magnitudes of A_{mn}'s

Stiffened plate, structure A, $\eta = 0.15$, trace velocity = 1.5 times the velocity ofsound. Frequency 500 Hz.

(a) Real Parts of A_{mn}

		m				
		-2	-1	0	+1	+2
	-2	21.7	332.0	-673.0	323.0	41.3
	-1	-16.1	-645.0	1370.0	33.8	-14.1
n	0	-11.9	509.0	-131000.0	-722.0	-55.0
	+1	-16.1	-645.0	1370.0	33.8	-14.1
	+2	21.7	332.0	-673.0	323.0	41.3

(b) Imaginary Parts of A_{mn}

		m				
		-2	-1	0	+1	+2
	-2	-0.454	-39.1	87.1	-53.2	-3.23
	-1	-1.91	-108.0	210.0	-91.0	-9.72
n	0	4.74	295.0	-1001.0	288.0	12.99
	+1	-1.91	-108.0	210.0	-91.0	-9.72
	+2	-0.454	-39.1	87.1	-53.2	-3.23

TABLE 4.2

Relative Magnitudes of A_{mn}'s

Stiffened plate, structure B, $\eta = 0.25$, trace velocity 1/9 times the velocity of sound convected at 45° to the X-axis. Frequency 150 Hz.

(a) Real Parts of A_{mn}

n \ m	-2	-1	0	+1	+2
-2	-3.79	7.81	-4.20	0.239	-0.0673
-1	-131.5	904.0	-1204.6	356.1	108.44
0	164.2	-1142.5	1666.9	-489.5	-162.9
+1	29.3	147.5	-837.5	114.5	46.0
+2	7.89	18.9	-53.3	17.9	8.43

(b) Imaginary Parts of A_{mn}

n \ m	-2	-1	0	+1	+2
-2	-0.063	4.69	-8.46	3.07	0.763
-1	45.5	-231.7	299.6	-86.1	-27.1
0	-40.3	295.7	-424.3	126.4	42.7
+1	-3.61	-57.7	112.4	-37.2	-13.8
+2	-1.44	-8.21	18.3	-6.15	-2.48

TABLE 4.3

Relative Magnitudes of Coefficients

Ring stiffened cylinder. CV = 8.0; η = 0.0; n = 2.

(a) For Ω = 0.4

m	A_m
-5	-2.997
-4	-7.736
-3	-26.06
-2	-143.9
-1	-2775.0
0	1,688,000.0
+1	-1676.0
+2	-124.1
+3	-26.53
+4	-8.864
+5	-3.794

(b) For Ω = 5.6

m	A_m
-5	25.25
-4	59.84
-3	201.7
-2	1608.0
-1	-26,240,000.0
0	26,400,000.0
+1	-202.7
+2	-60.02
+3	-25.31
+4	-12.95
+5	-7.498

(c) For Ω = 22.4

m	A_m
-5	2615.0
-4	-10,350,000.0
-3	-2445.0
-2	-311.1
-1	-92.72
0	10,320,000.0
+1	-20.12
+2	-11.65
+3	-7.346
+4	-4.924
+5	-3.460

TABLE 6.1

Relative Magnitudes of Coefficients

Ring stiffened cylinder. CV = 16.0; η = 0.25; n = 2.

(a) For Ω = 1.6

m	Real Part of A_m	Imaginary part of A_m
-5	-7.10	-2.10
-4	-19.7	-5.26
-3	-71.6	-17.3
-2	-435.0	-96.9
-1	-10300.0	-2120.0
0	46,300,000.0	-2,550,000.0
+1	-3740.0	-663.0
+2	-322.0	-53.4
+3	-73.9	-11.5
+4	-25.8	-3.78
+5	-11.4	-1.58

(b) For Ω = 16.0

m	Real Part of A_m	Imaginary Part of A_m
-5	7.329	-0.74
-4	14.51	-3.26
-3	12.3	-27.1
-2	-4620.0	-1780.0
-1	-29400.0	-5900.0
0	634,000,000.0	-54,600,000.0
+1	-61.44	-7.192
+2	-19.5	-1.97
+3	-8.45	-0.760
+4	-4.38	-0.366
+5	-2.55	-0.198

TABLE 6.2

Relative Magnitudes of the Coefficients

Ring Stiffened Cylinder. CV = 80.0 η = 0.25 n = 1

(a) For Ω = 19.6

m	Real Part of A_m	Imaginary Part of A_m
-4	1.59	-2.24
-3	-4.36	-7.64
-2	-81.2	-44.5
-1	-3320.0	109.0
0	255,000,000.0	-48,900.0
+1	-1420.0	-262.0
+2	-149.0	-22.74
+3	-38.90	-5.07
+4	-15.00	-1.71

TABLE 6.3

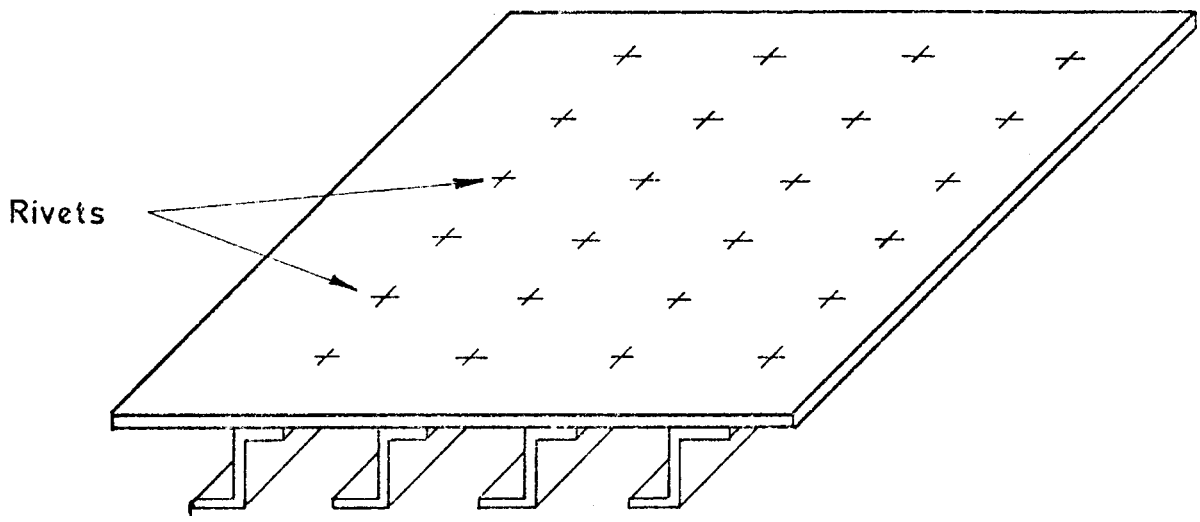

(a). Conventional skin stringer structure

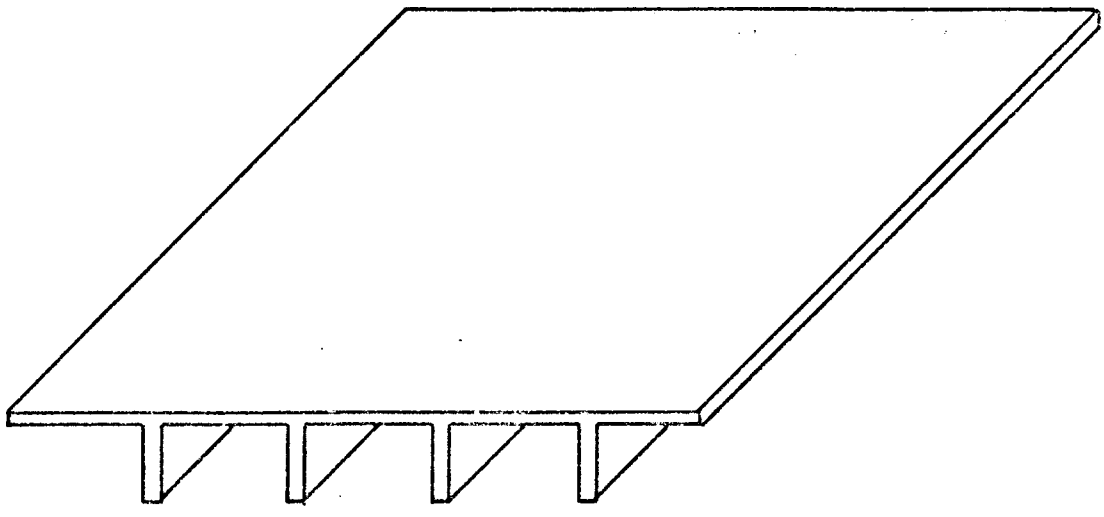

(b). Integrally stiffened structure machined from a solid slab .

Fig. 1.1 Skin stringer configurations

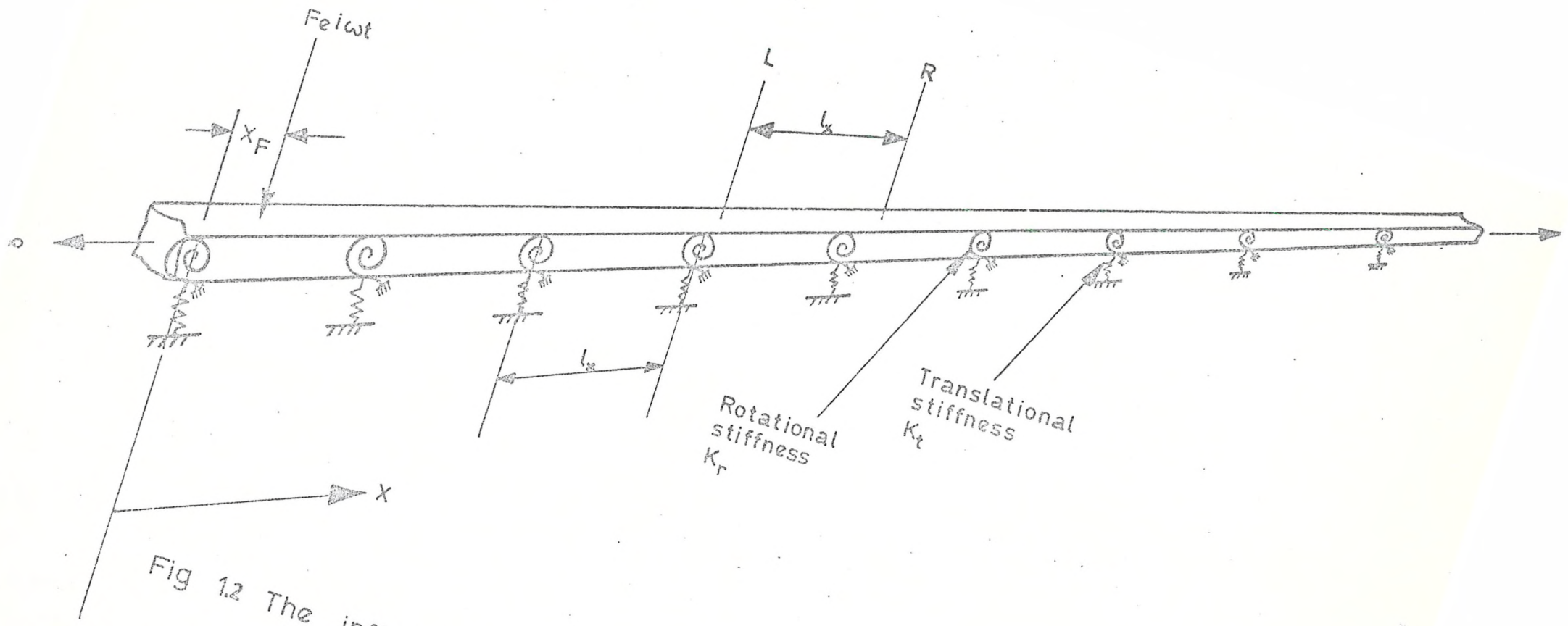

Fig 1.2 The infinite beam on equispaced elastic supports

1.3a

1.3b

1.3c

Fig.1.3 Some typical waves of the beam of Fig.1.2
(a) at a very low frequency ($\Omega < 12.8$)
(b) at the lower bounding frequency, $\Omega = 12.8$
(c) at the upper bounding frequency, $\Omega = 22.4$

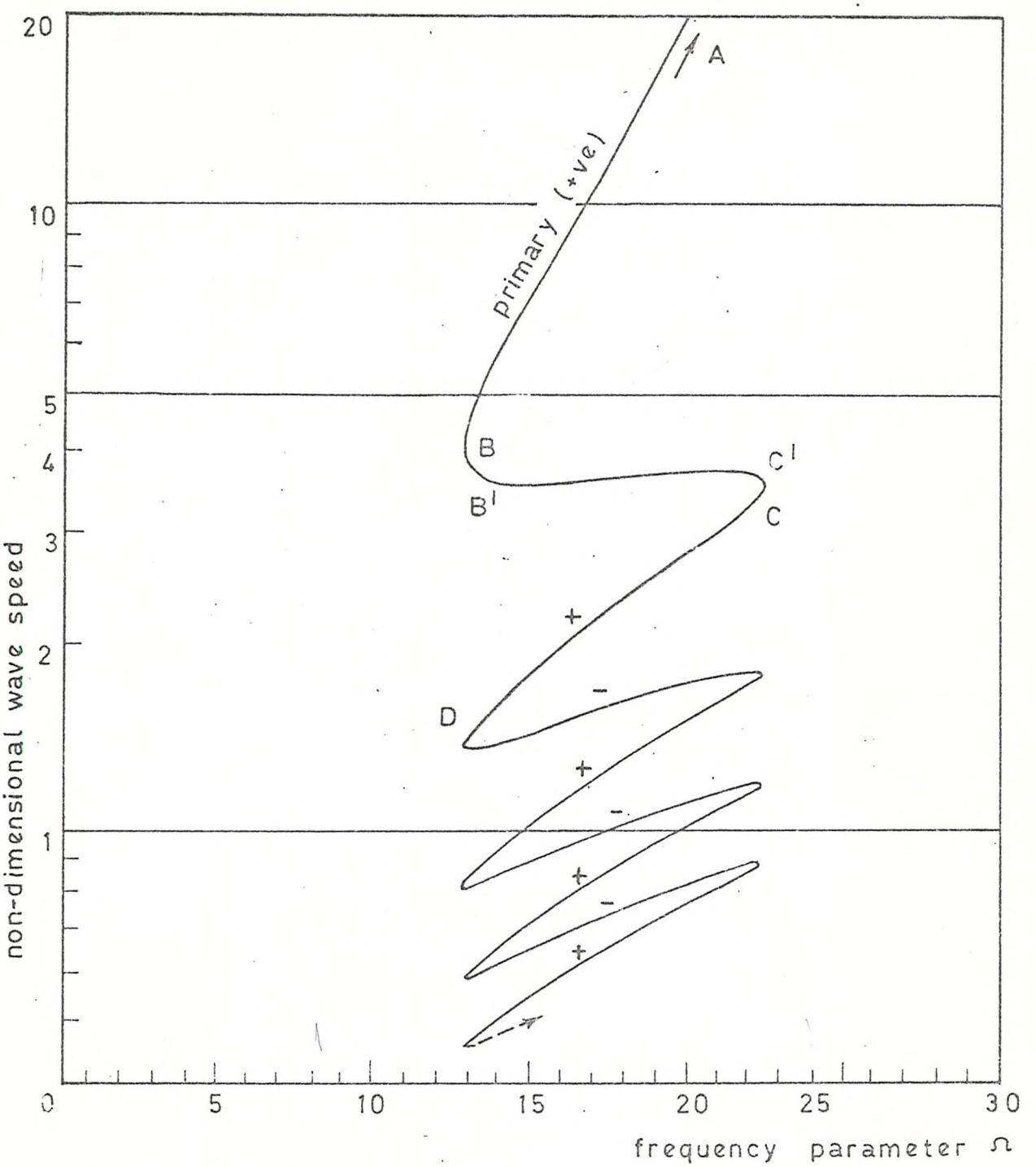

Fig.1.4 Variation of component wave speed with frequency; for first propagation band of beam of Fig.1.2.

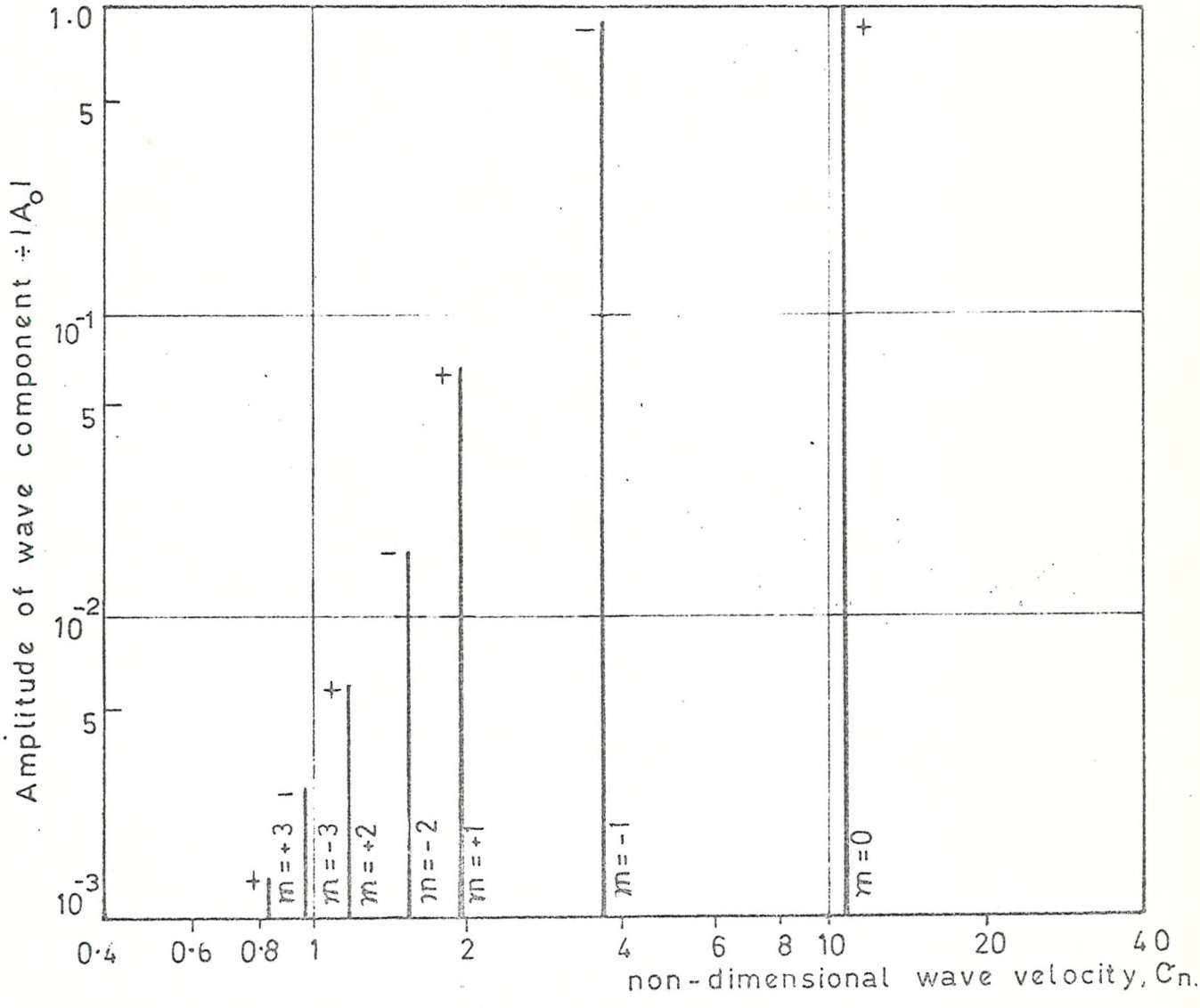

Fig.1.5. Component amplitude ratios for the free wave group at $\Omega = 17$. (for the beam of Fig.1.2.)

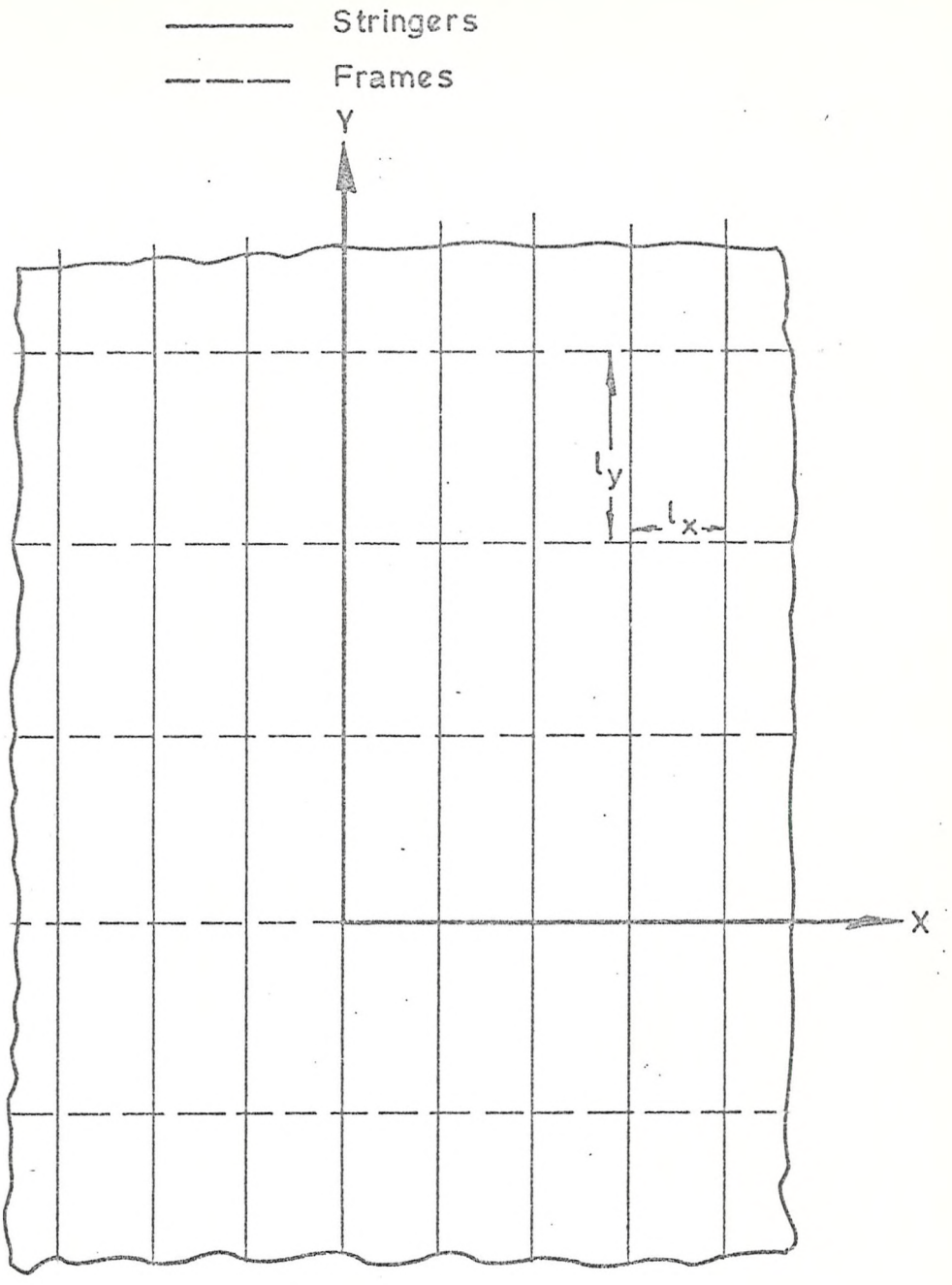

Fig. 2.1 Identically constructed panels extending to infinity in the two perpendicular directions.

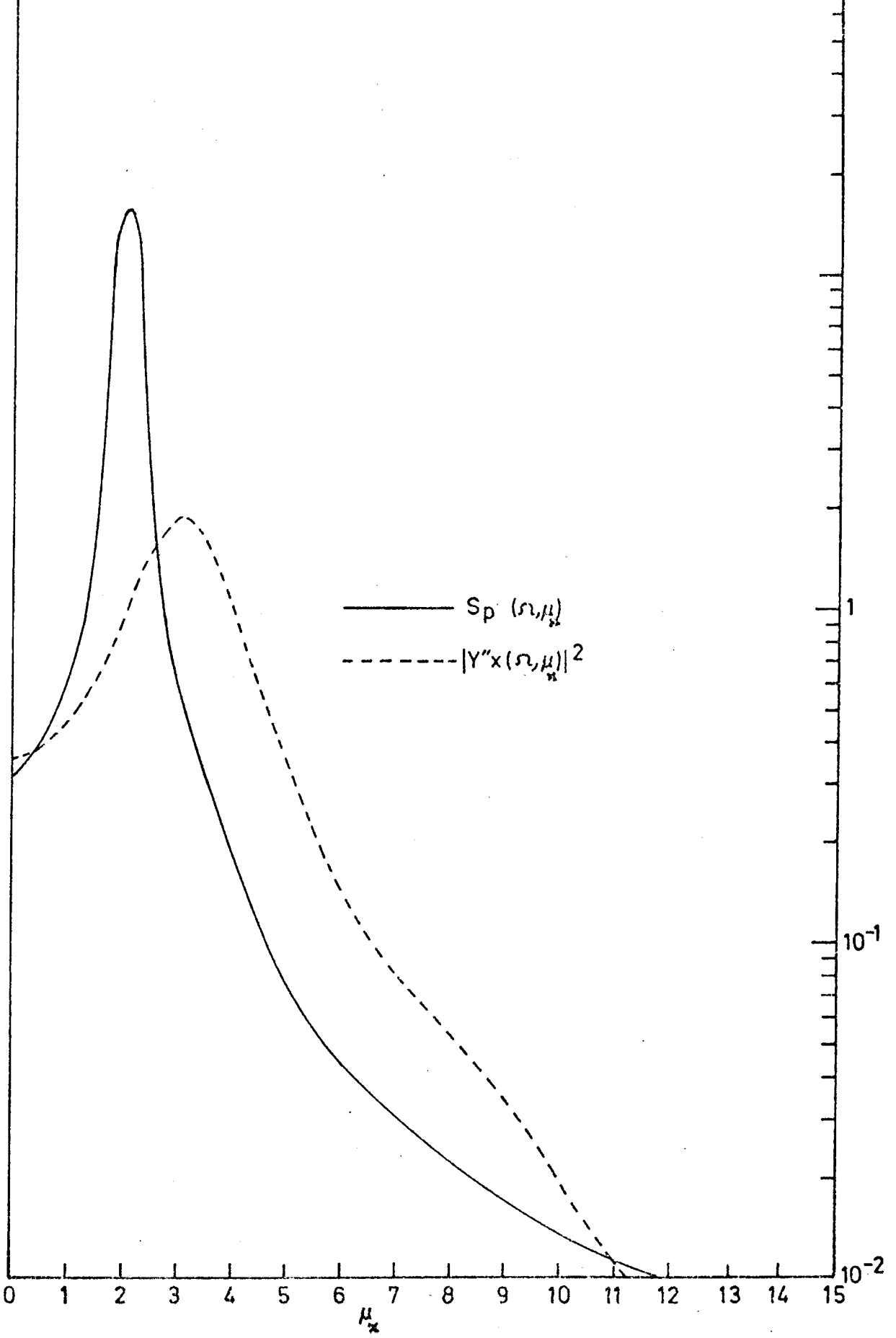

Fig 2.2 The curvature admittance function $|Y''x(\Omega, \mu_x)|^2$ for the beam of Figure 1.2. and the pressure wave-number spectrum; $\Omega = 8.0$, CV = 6.0

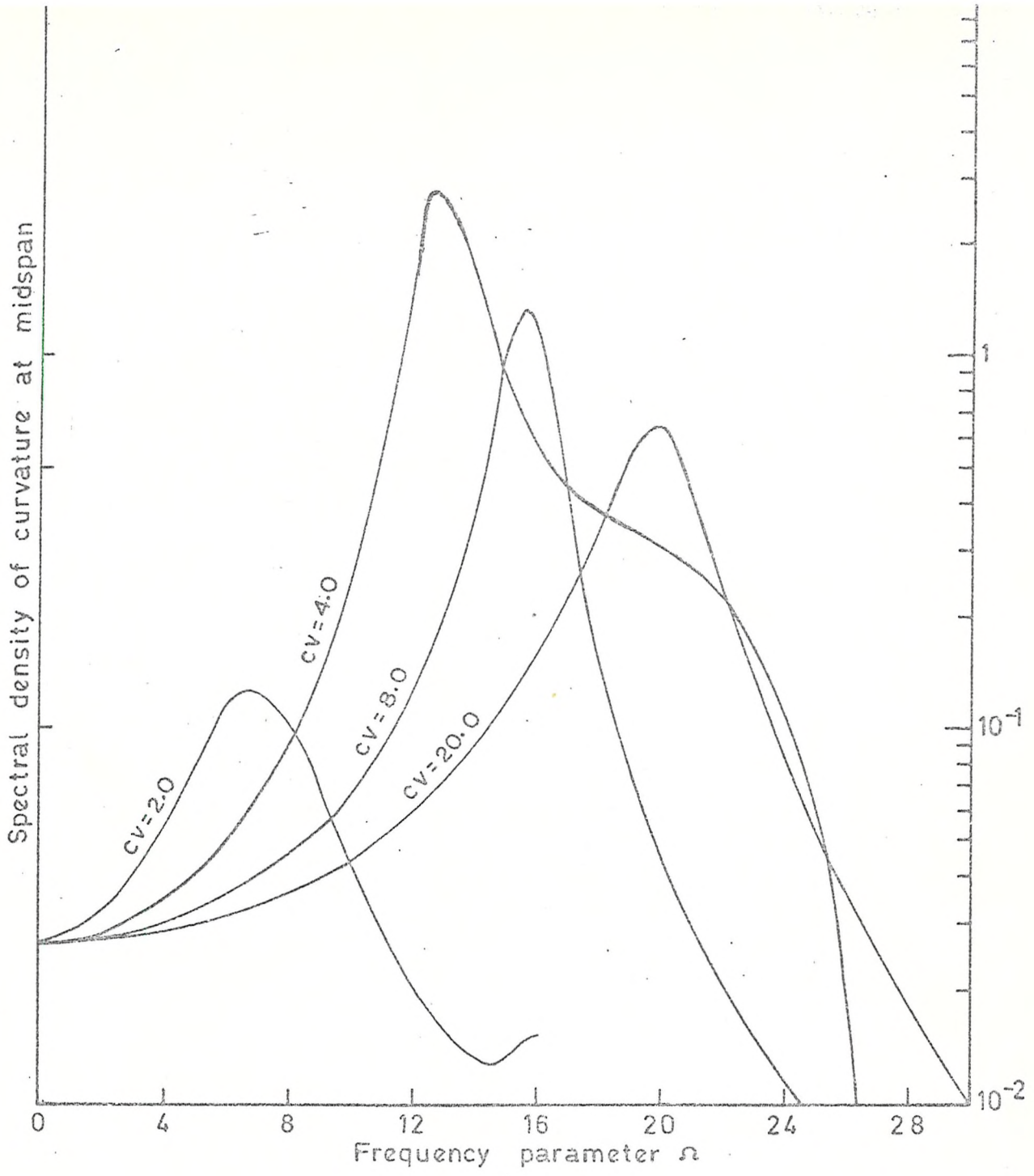

Fig2.3 Computed response at different convection velocities by including eleven terms in the series solution

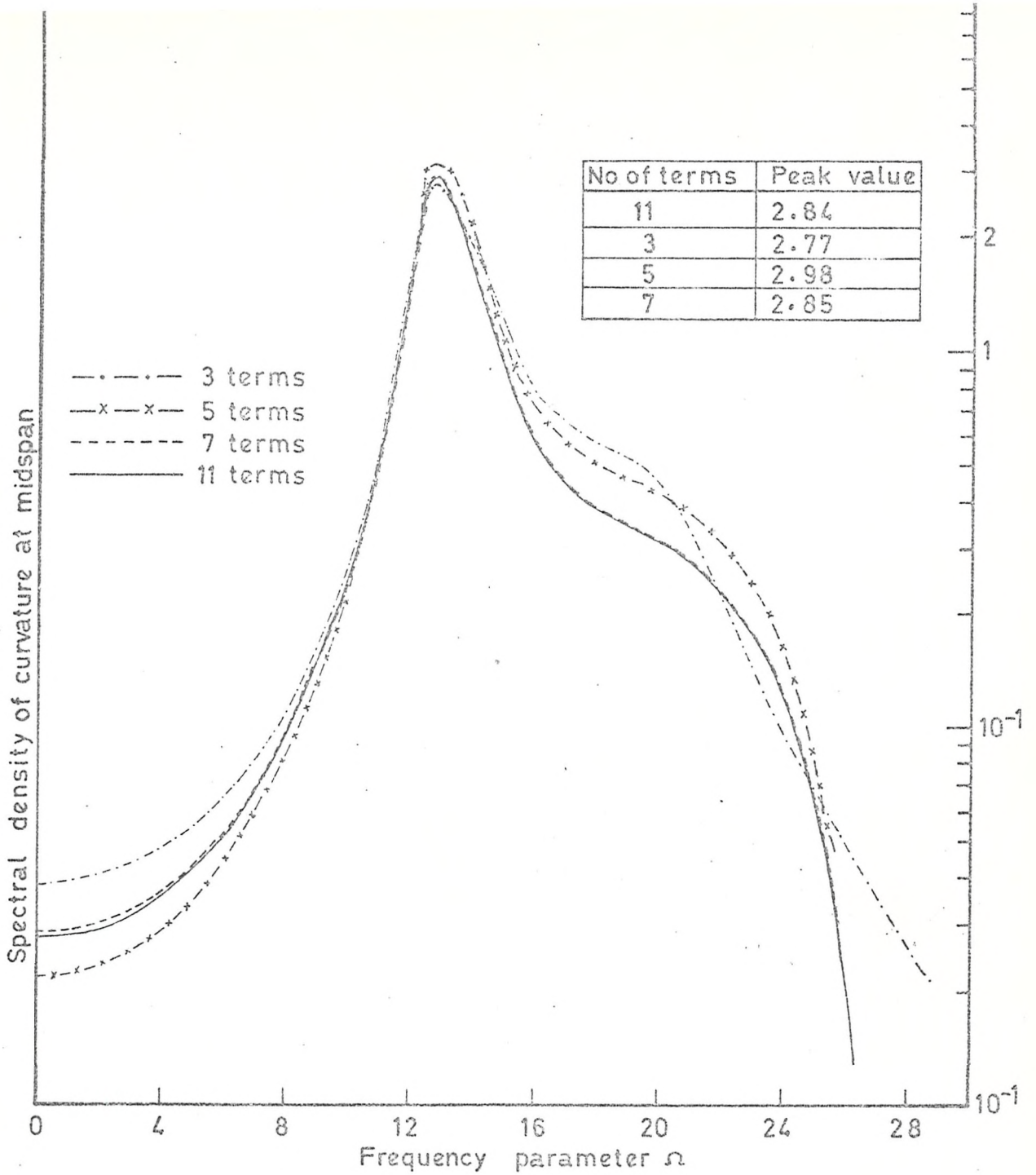

Fig 2.4 Computed response with different number of terms in the series (CV = 4·0)

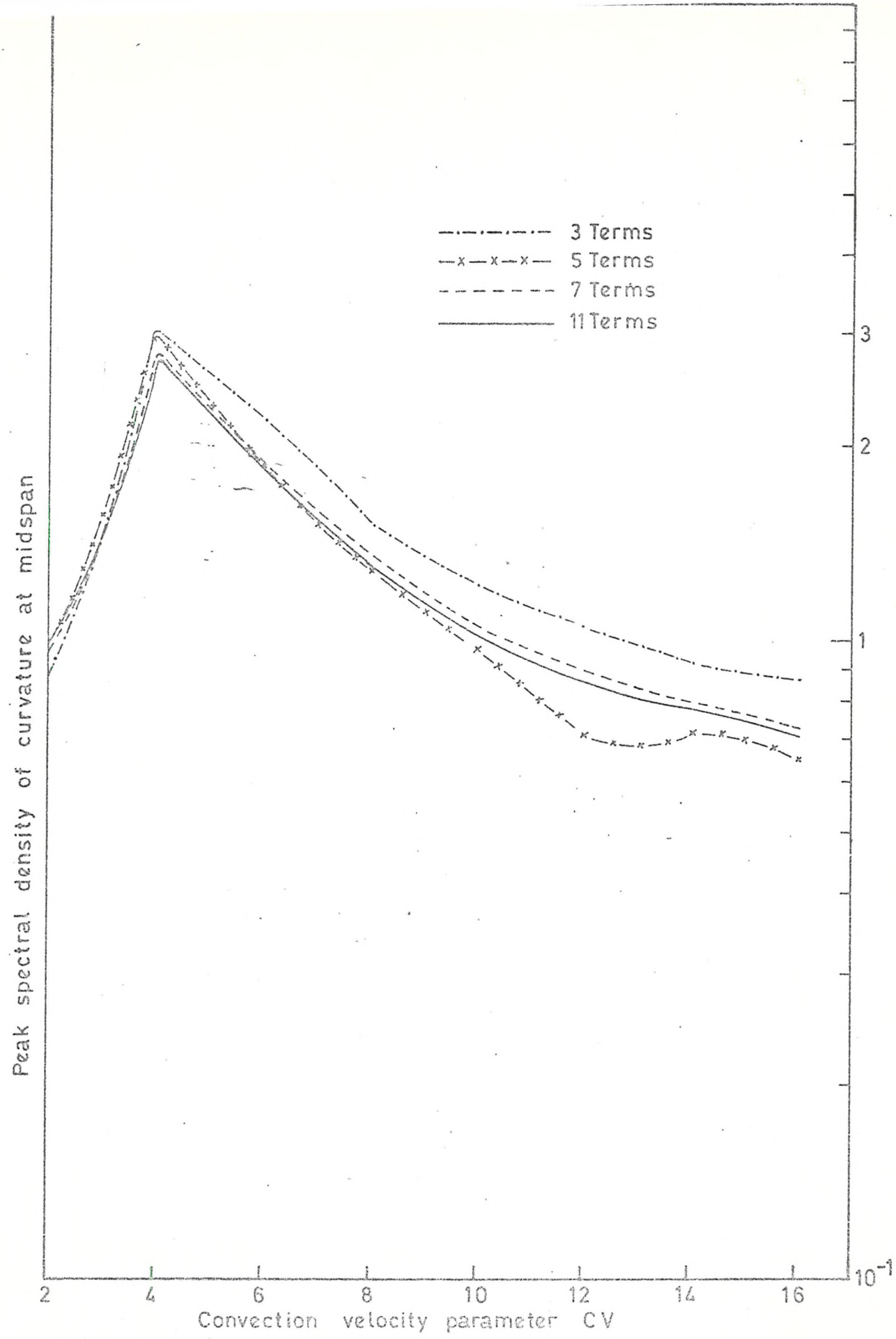

Fig 2.5 The effect of number of terms on peak value of response

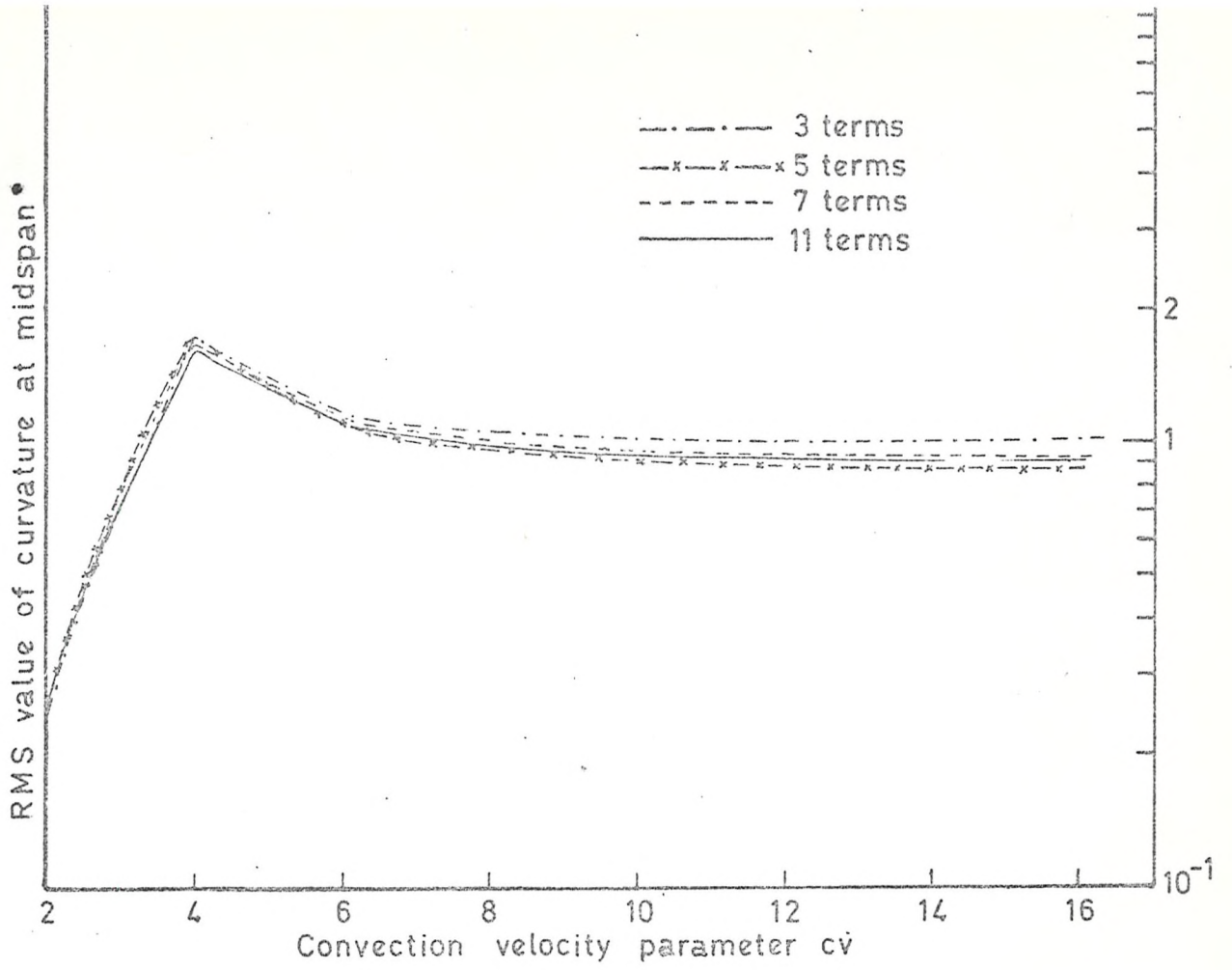

Fig 2.6 Effect of the number of terms on the RMS value of response

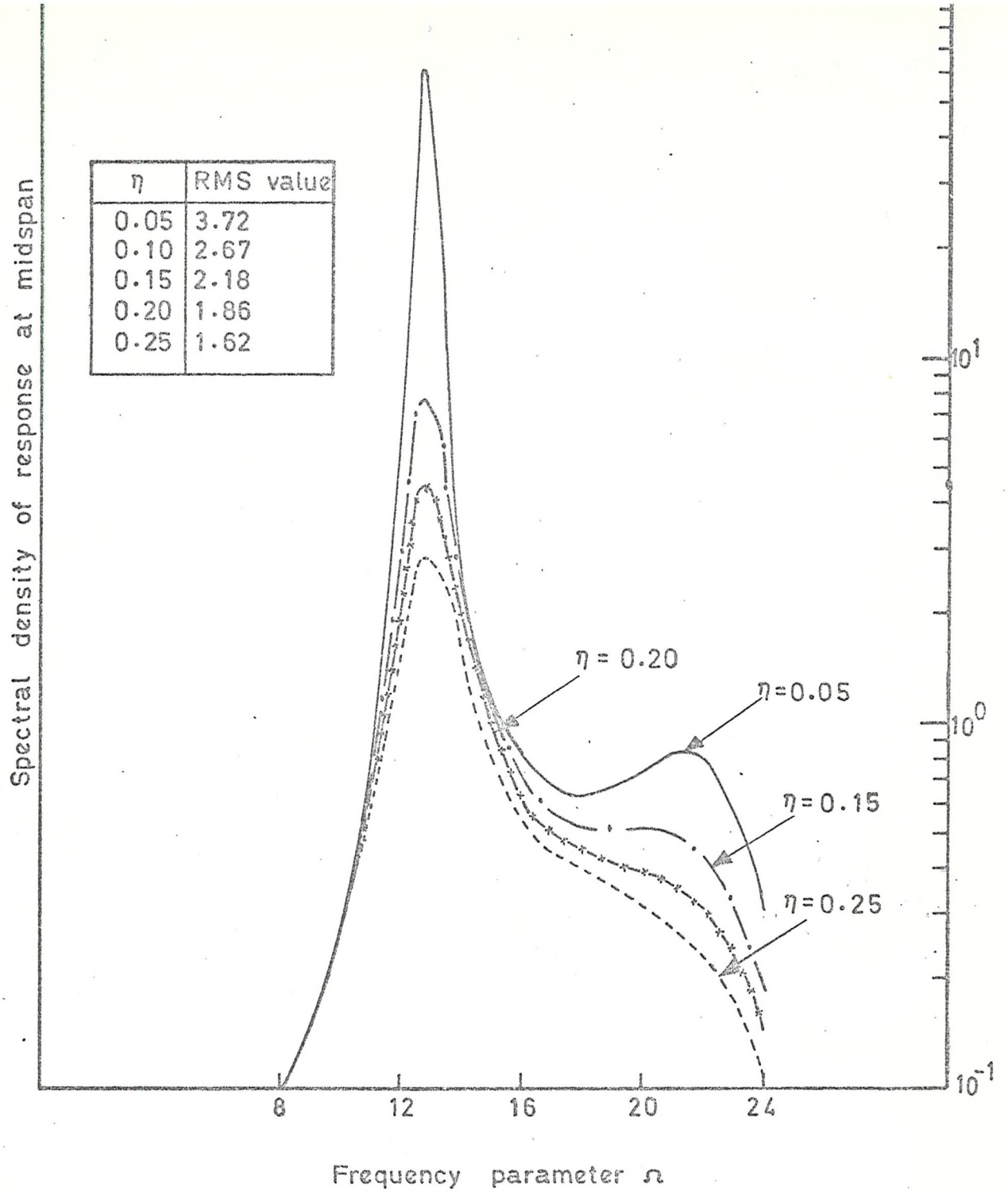

Fig 2.7 Response with different values of beam damping Eleven terms are included in the series solution

ÇV=4

No of terms	Peak spectral density	RMS value
3	2·05	1·43
5	2·09	1·47
7	1·95	1·40
9	1·94	1·40

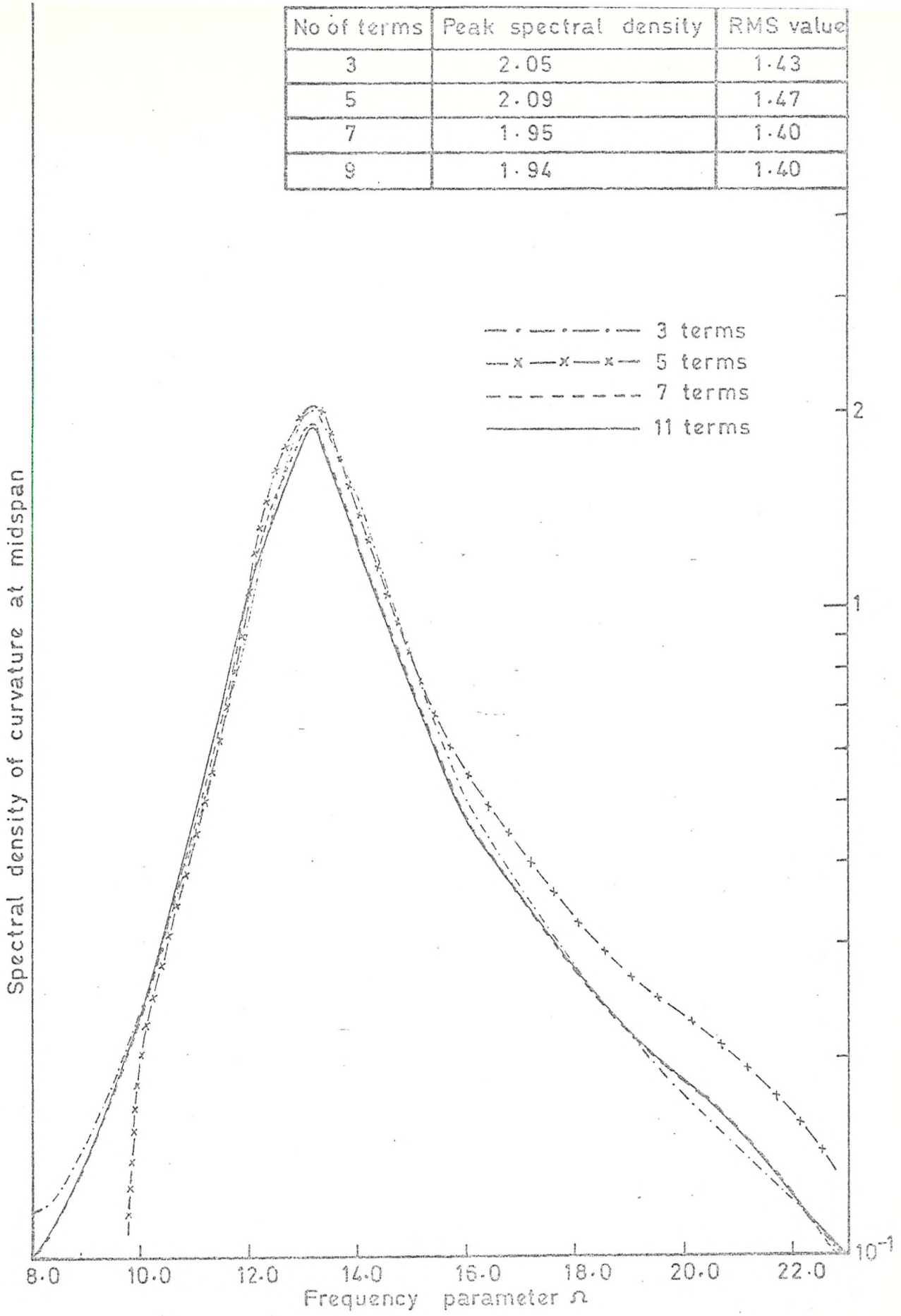

Fig 2.8 Response to boundary layer Pressure with different number of terms in the series

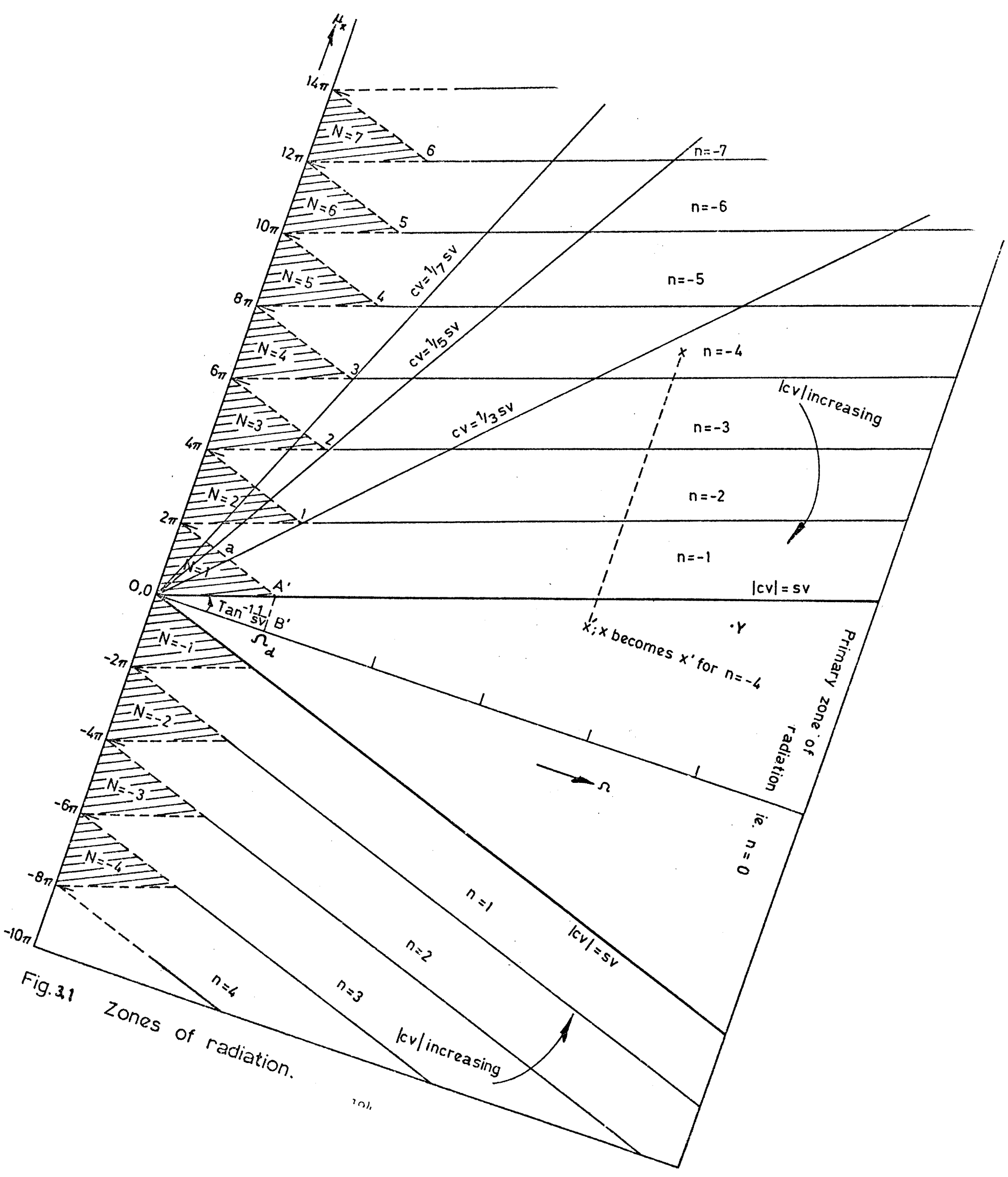

Fig. 3.1 Zones of radiation.

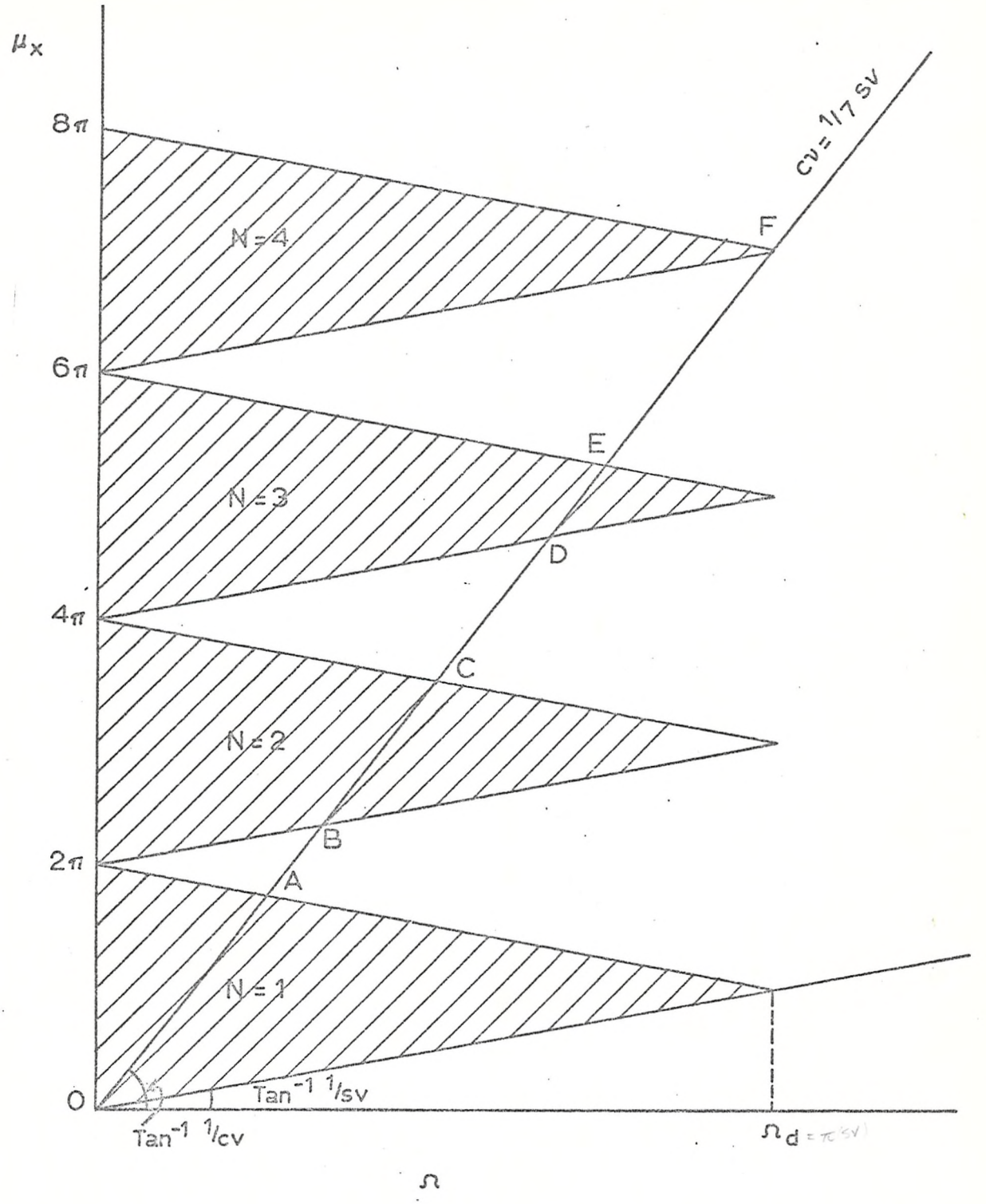

Fig. 3.2 Frequency bands of sound radiation.

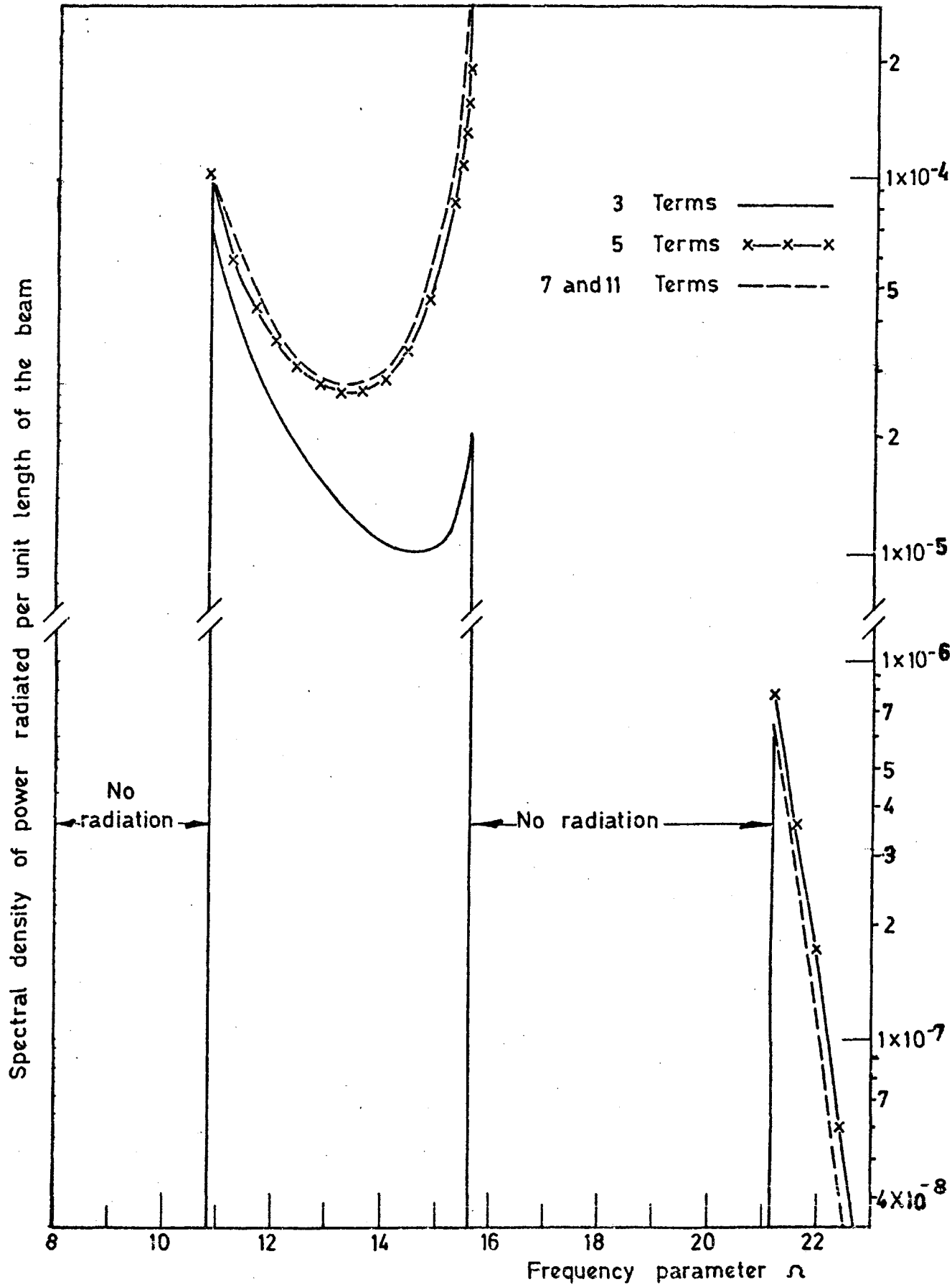

Fig. 3.3 Spectral density of the sound power radiated with different terms in the series. Plane wave convection velocity $cv = 2.0$, $K_r = 4.0$, $\eta = 0.02$.

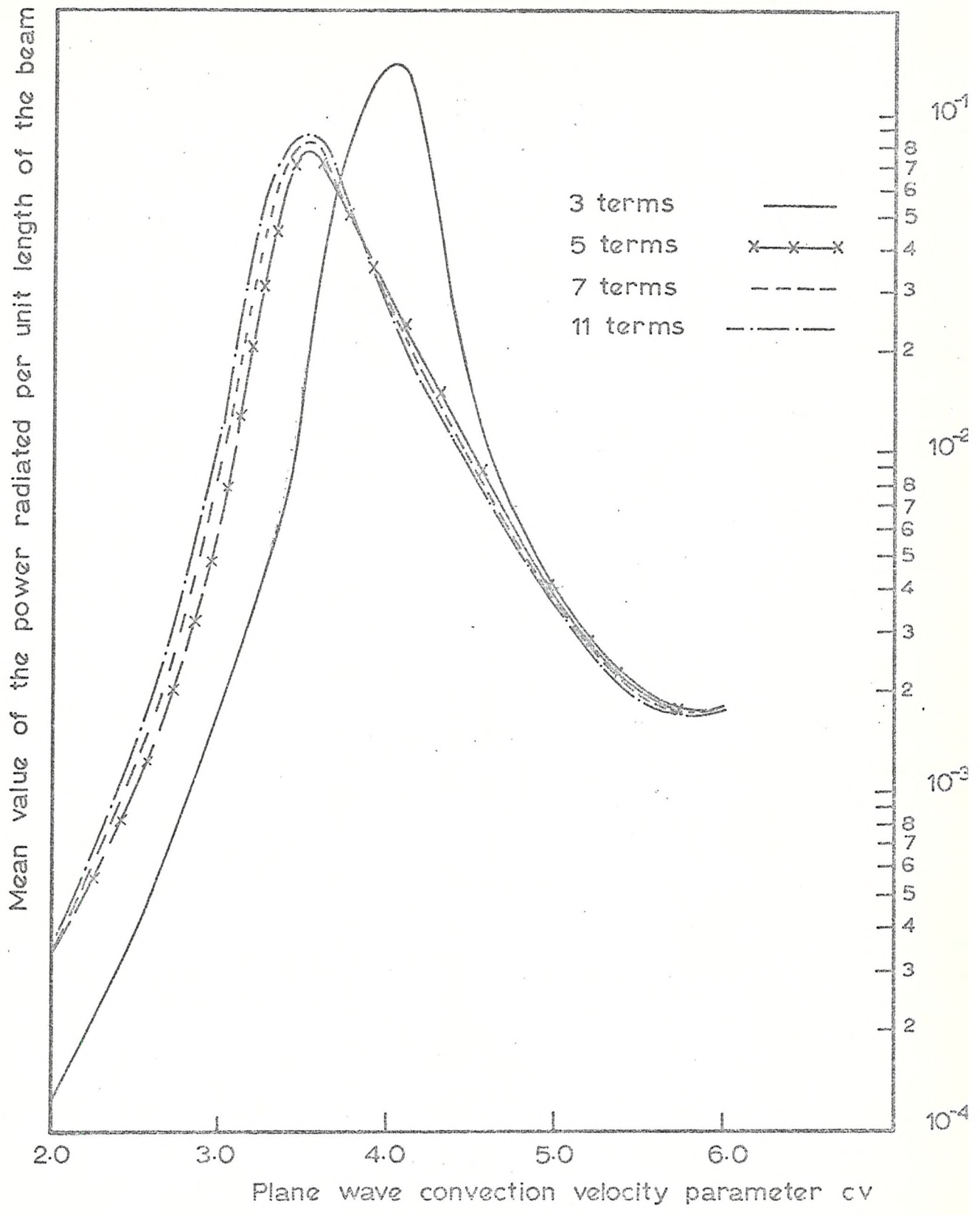

Fig. 3.4 Effect of the number of terms on the mean value of sound power radiated at different convection velocities. sv = 10.0.

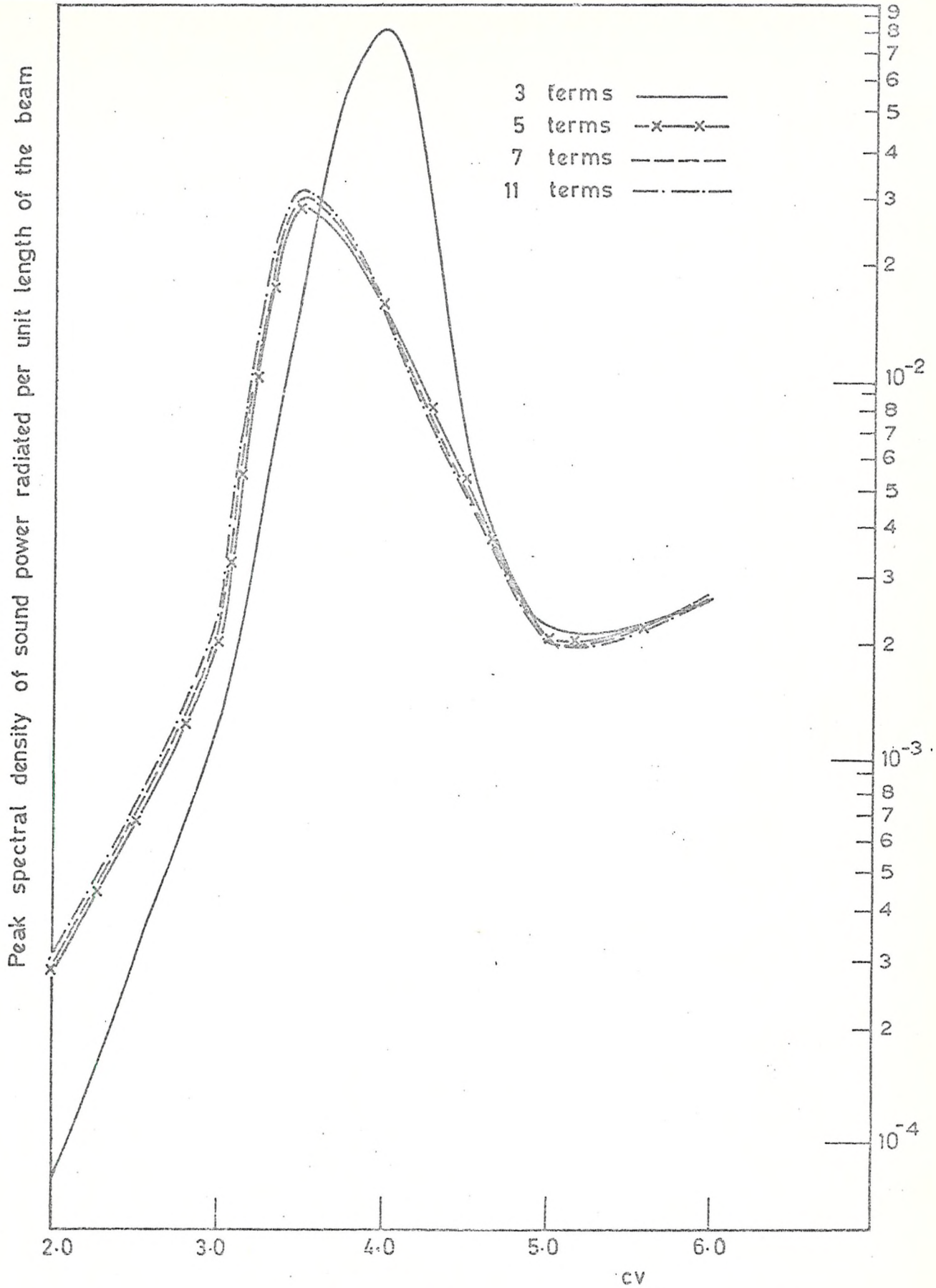

Fig. 3.5 Effect of the number of terms on the peak value of the sound power radiated at different convection velocities of plane waves. sv = 10.0.

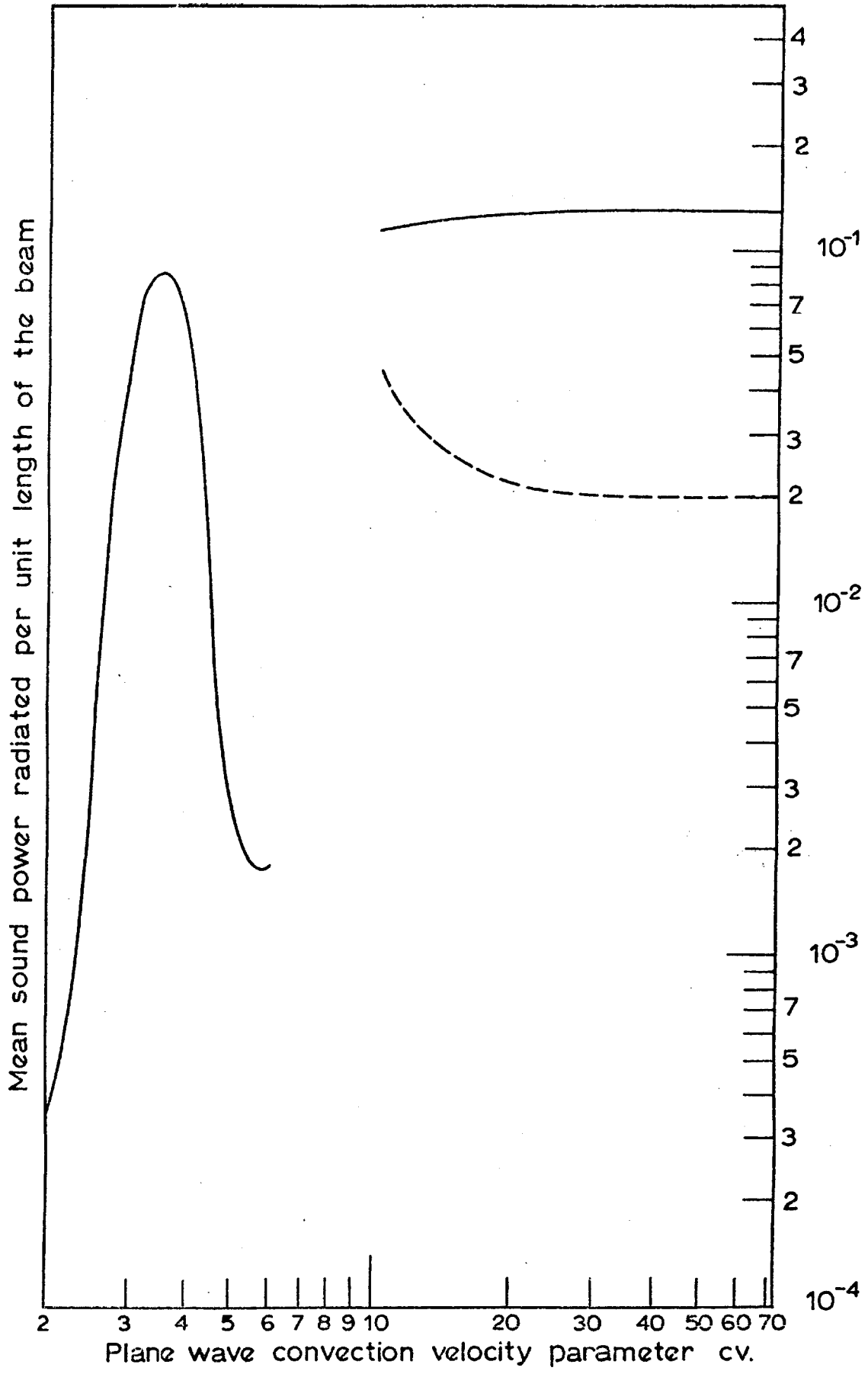

Fig. 3.6 Mean sound power radiated at different convection velocities. sv = 10·0. The broken line corresponds to the power radiated by the unstiffened beam under similar conditions.

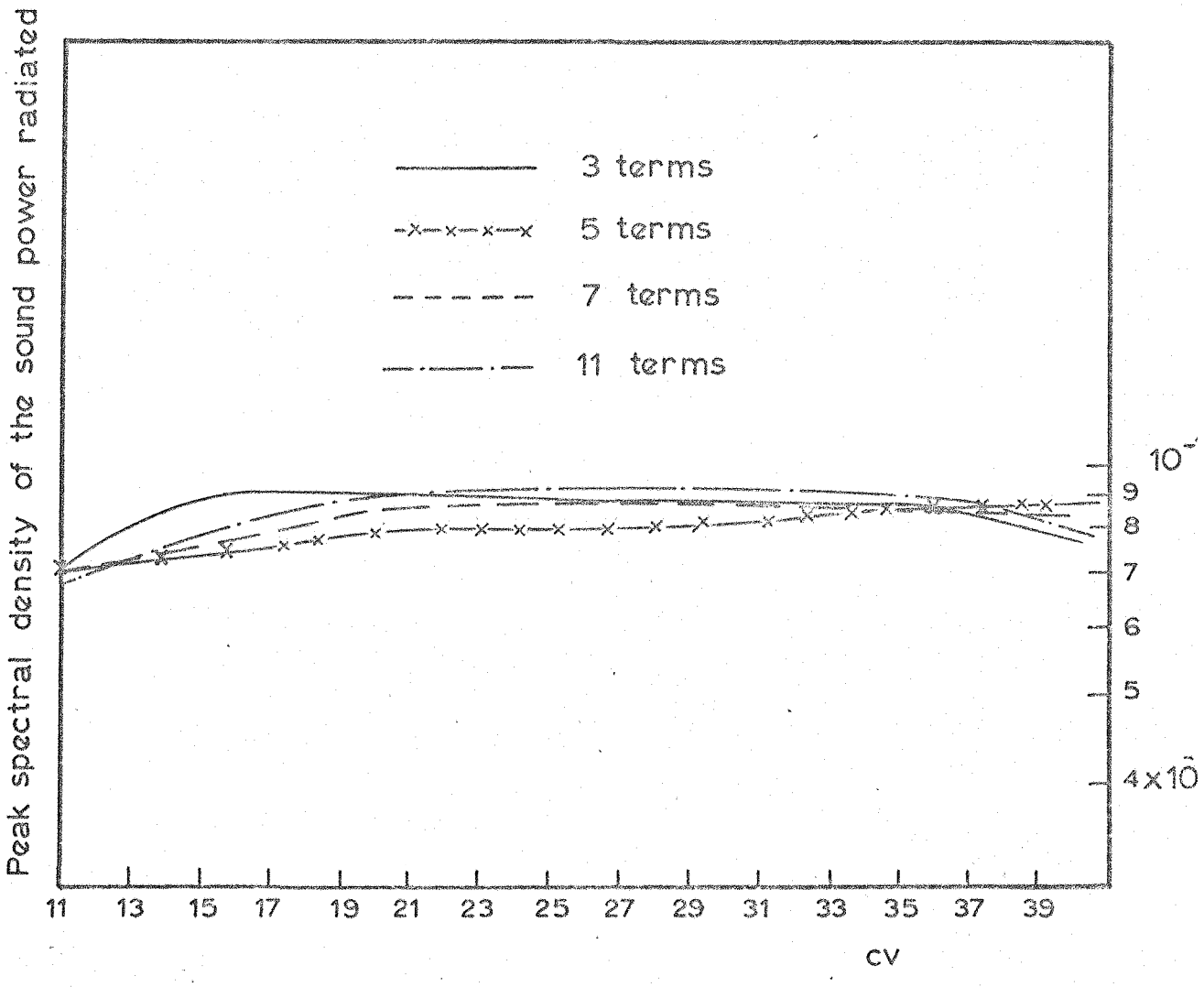

Fig. 3.7 Effect of the number of terms on the peak value of power radiated by acoustic plane waves. sv = 10.0.

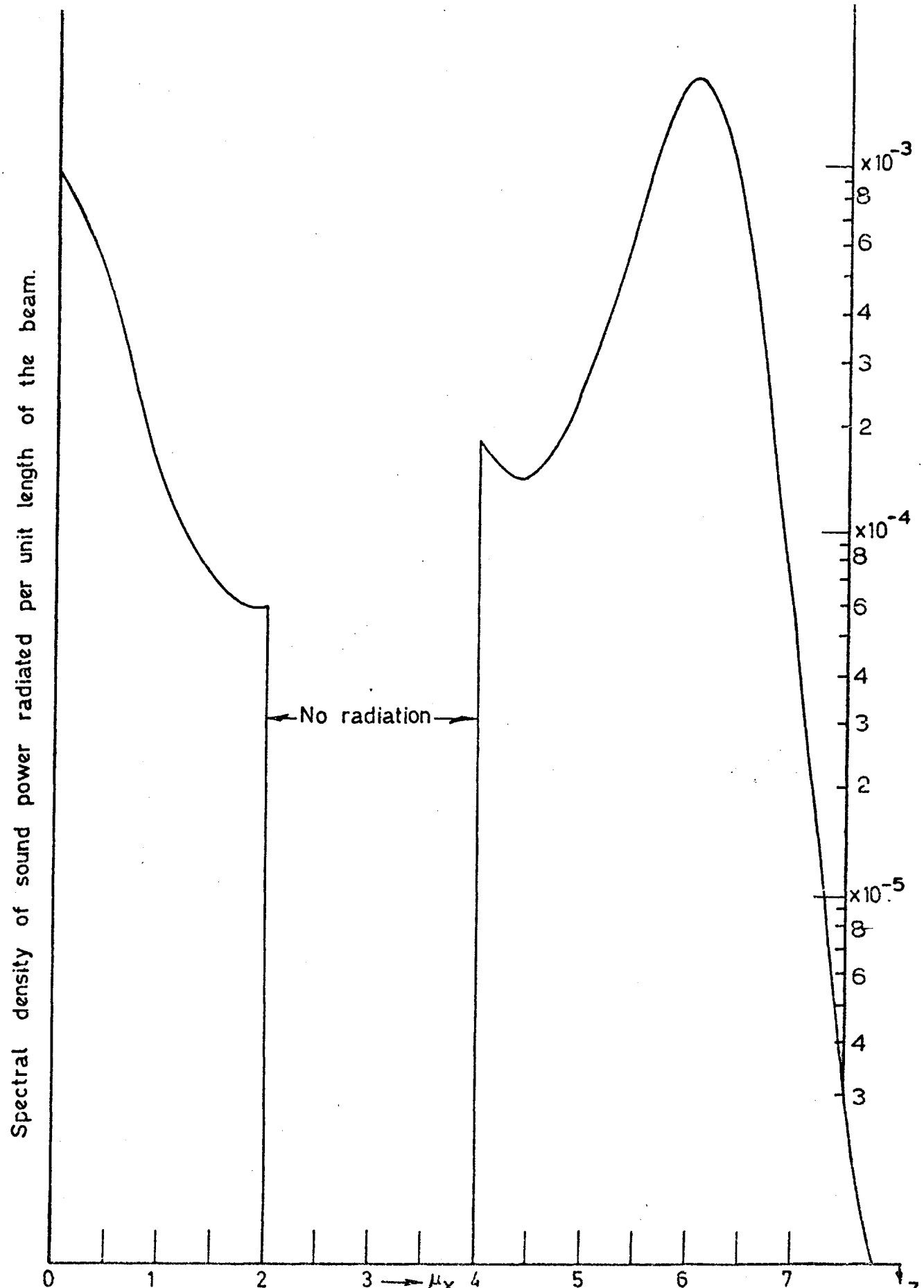

Fig.3.8 Contribution of different wave lengths in the boundary layer pressure field to the sound power radiated by the beam per unit length at Ω =24.0, cv=4.0, sound velocity parameter = 10.0

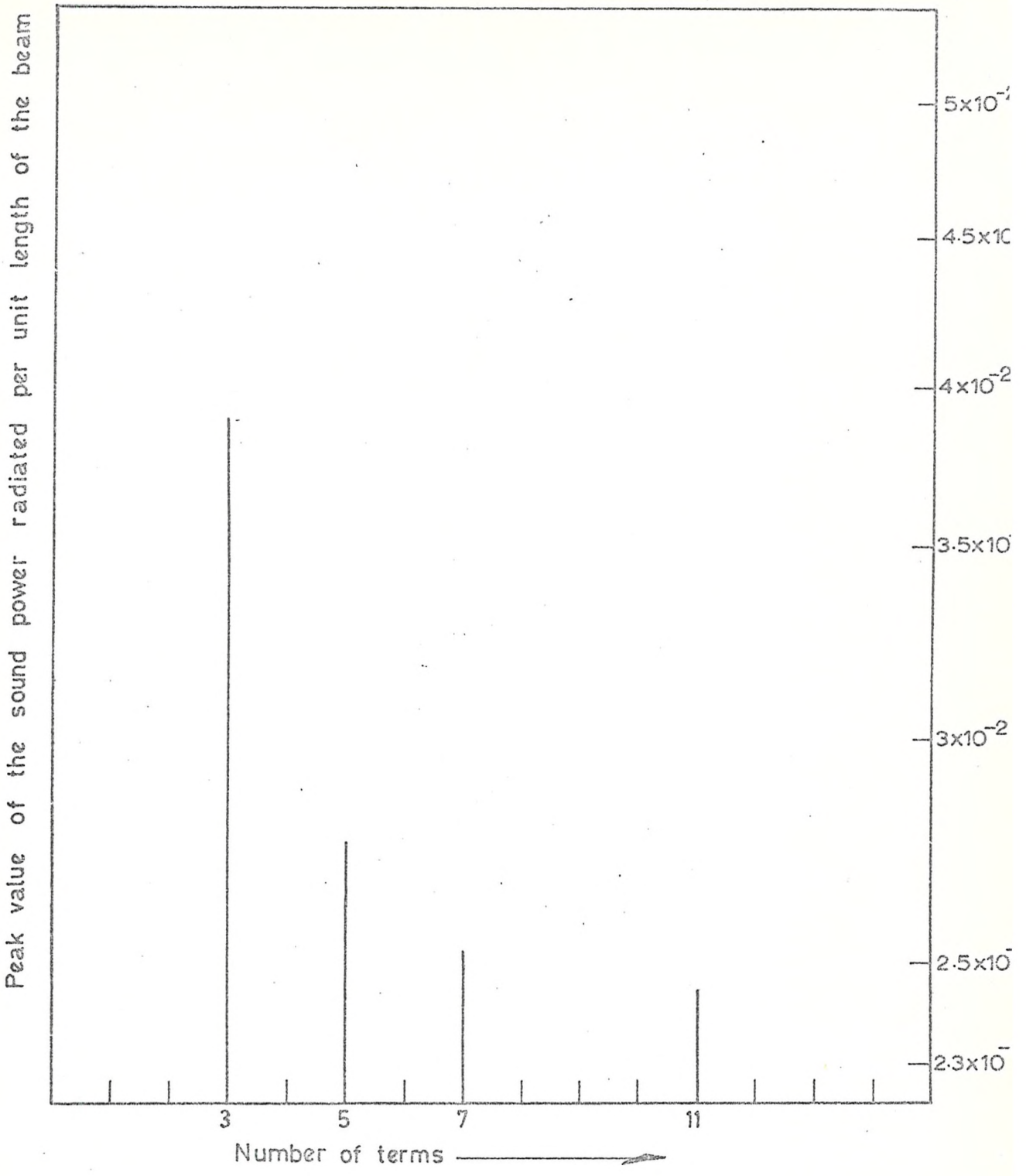

Fig.3·9 Effect of the number of terms on the peak spectral density of the sound power radiated when the beam is excited by boundary layer pressure field. cv = 4·0, boundary layer decay parameter = 0·1, sv = 10·0 .

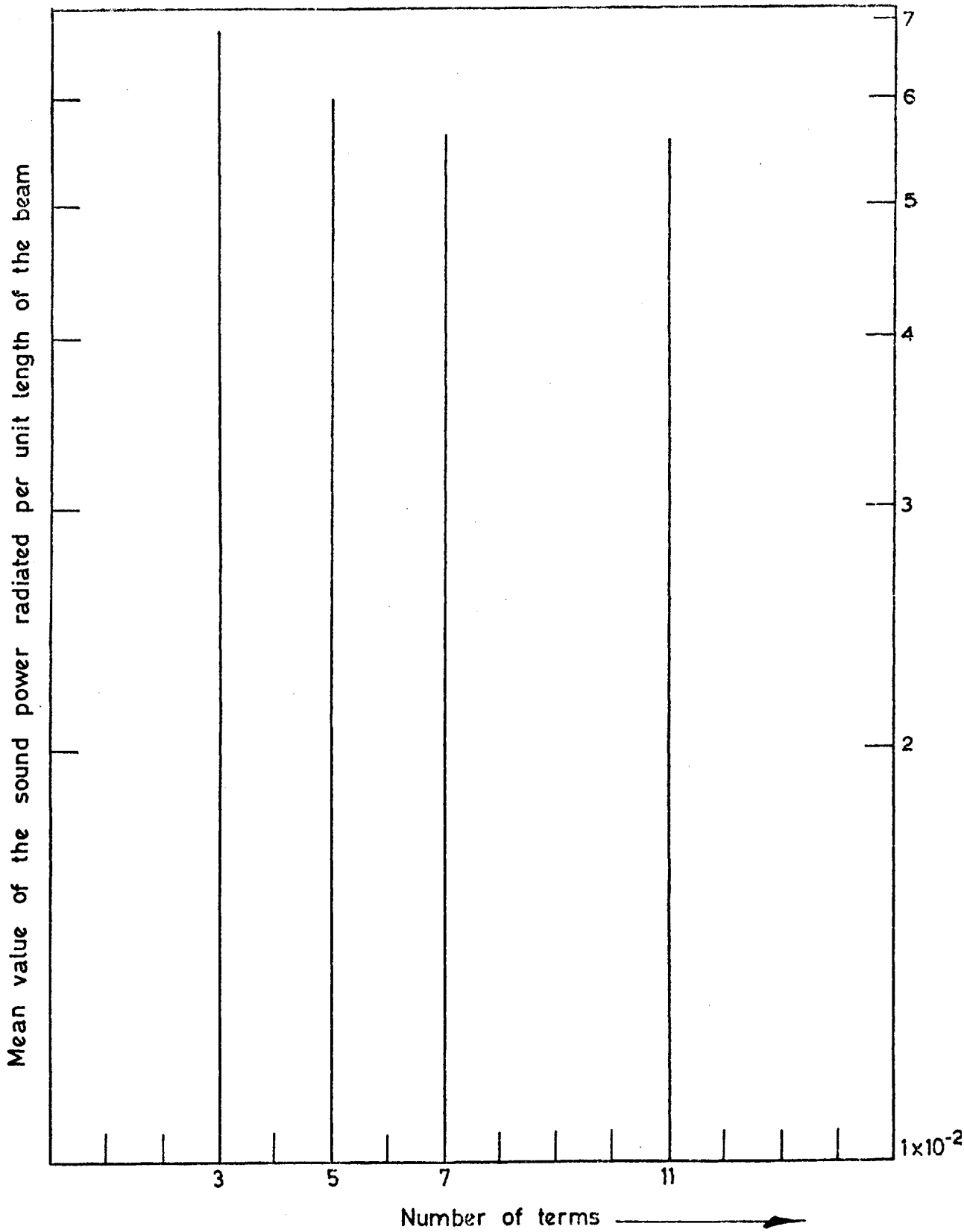

Fig. 3.10 Effect of the number of terms on the mean value of the sound power radiated when the beam is excited by boundary layer pressure field. cv = 4.0, boundary layer decay parameter = 0.1, sv = 10.0.

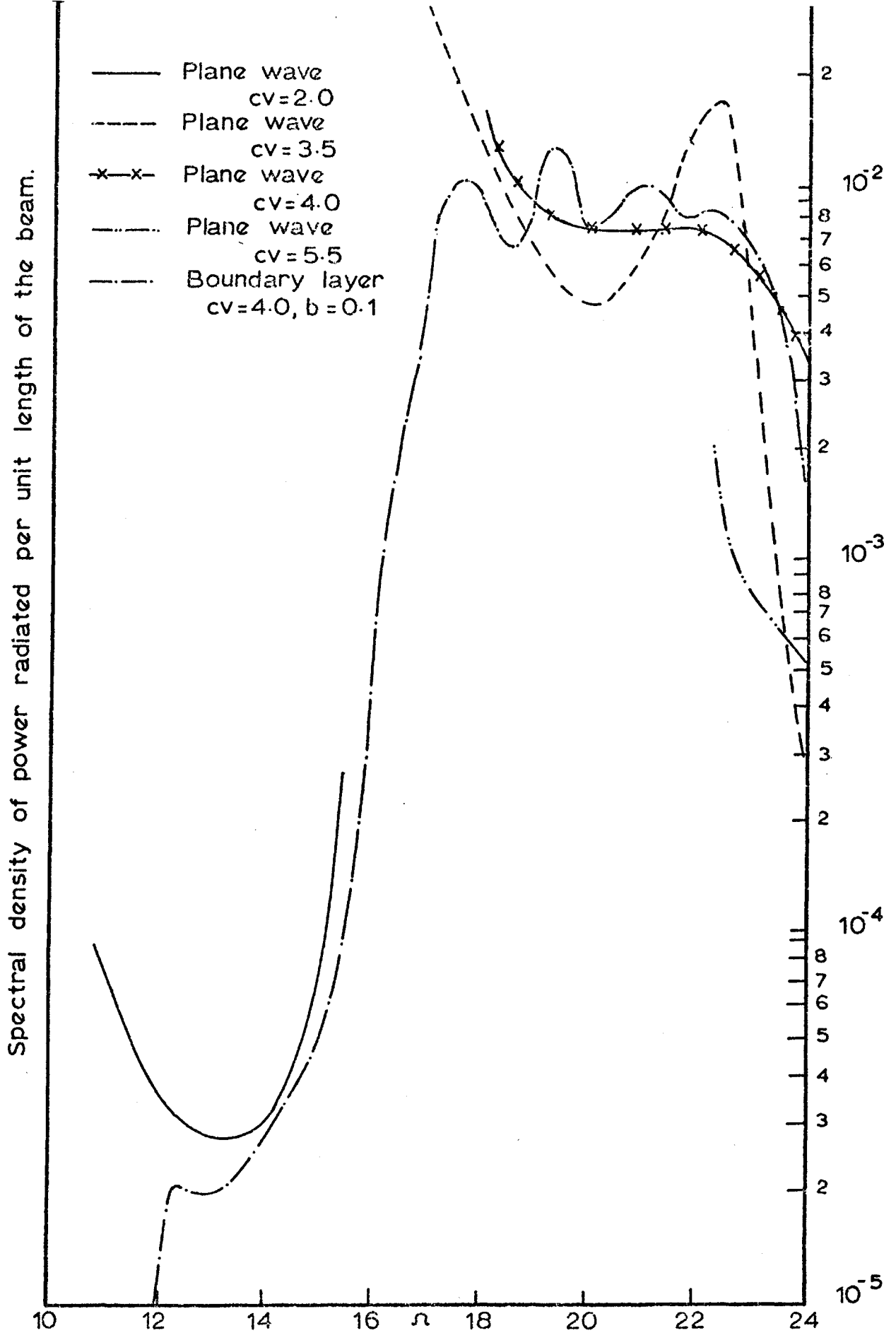

Fig. 3.11 Spectral density of sound power radiated per unit length of the beam for acoustic plane waves and boundary layer pressure field sv=10.0.

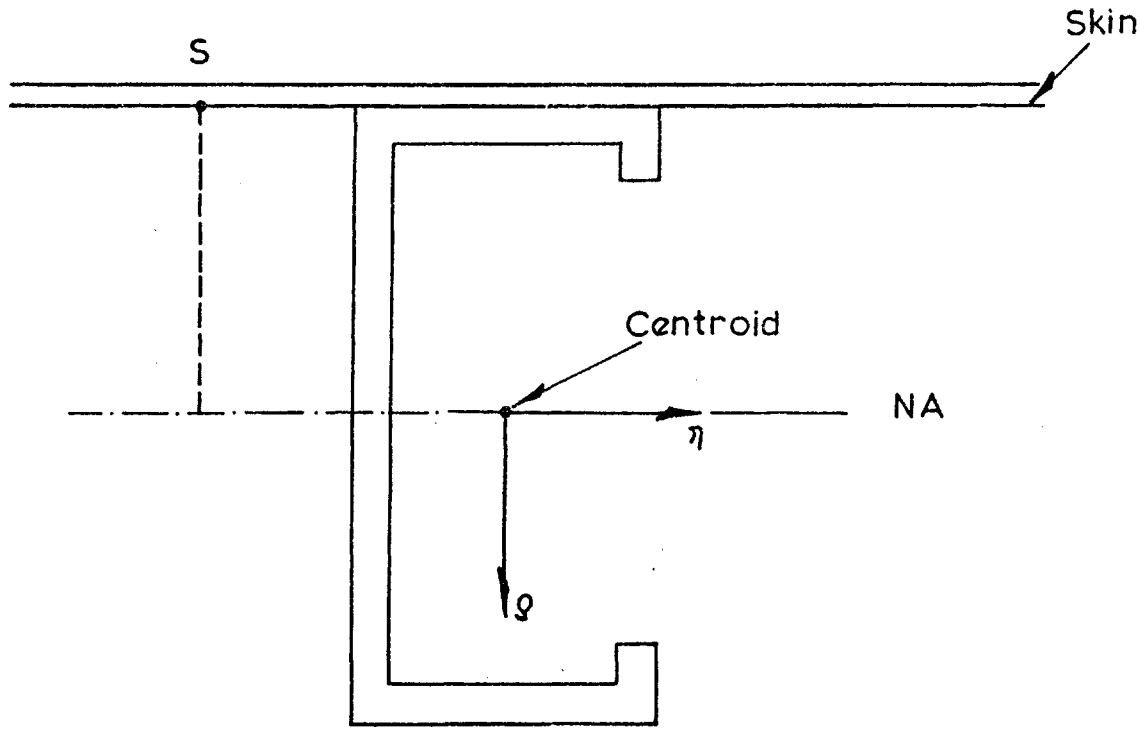

a) Conventional structure.

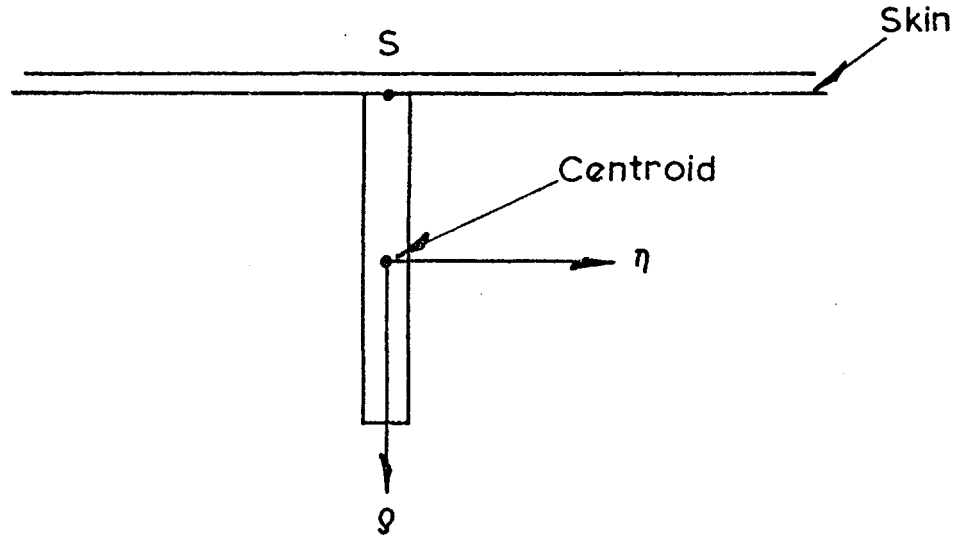

b) Integrally stiffened structure.

Fig. 4.1 Correspondence of the stringer geometry in the case of two types of stiffeners.

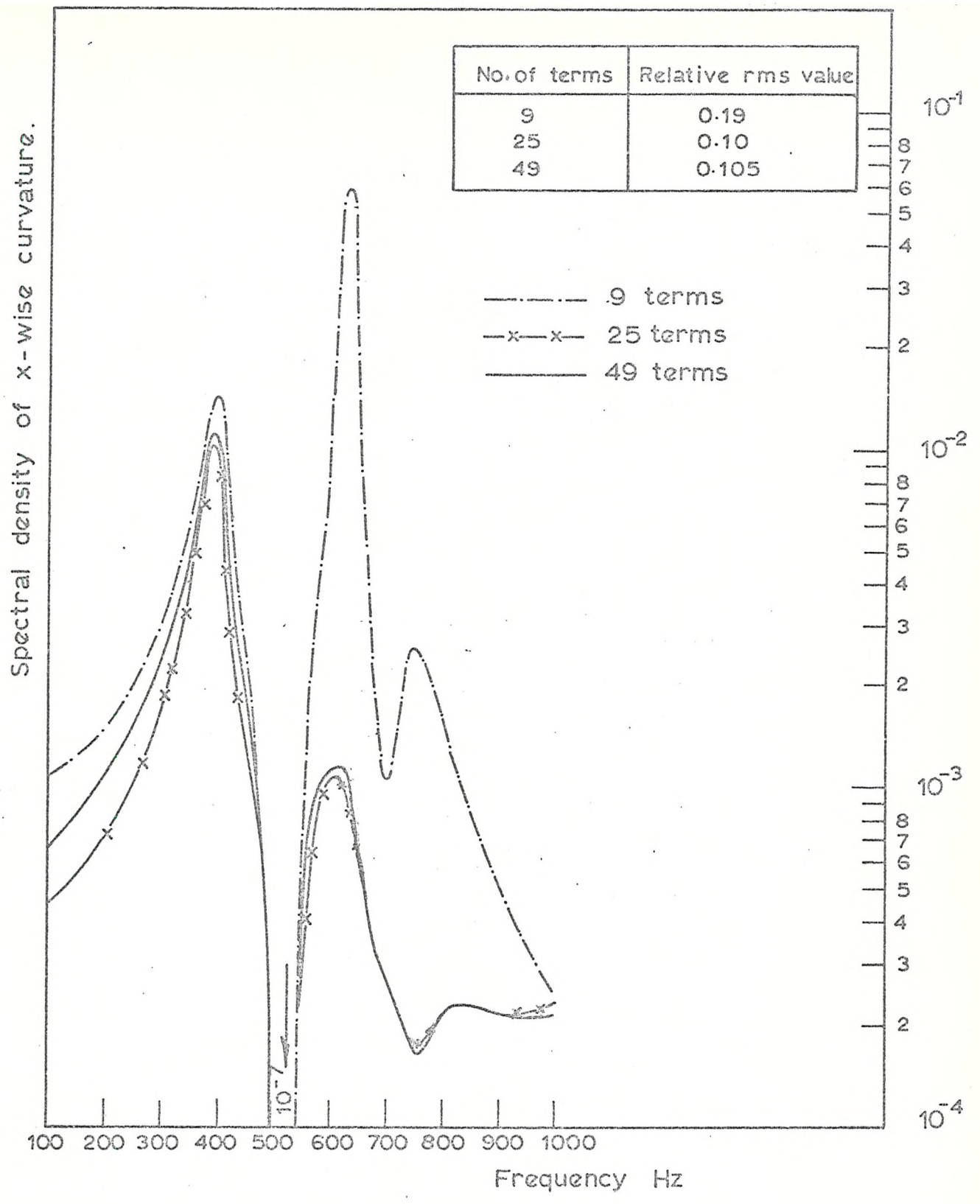

Fig. 4.2 Effect of the number of terms on curvature. Structure A. $\eta = 0.15$. Trace velocity = 1.5 times the velocity of sound. Convection parallel to x-axis.

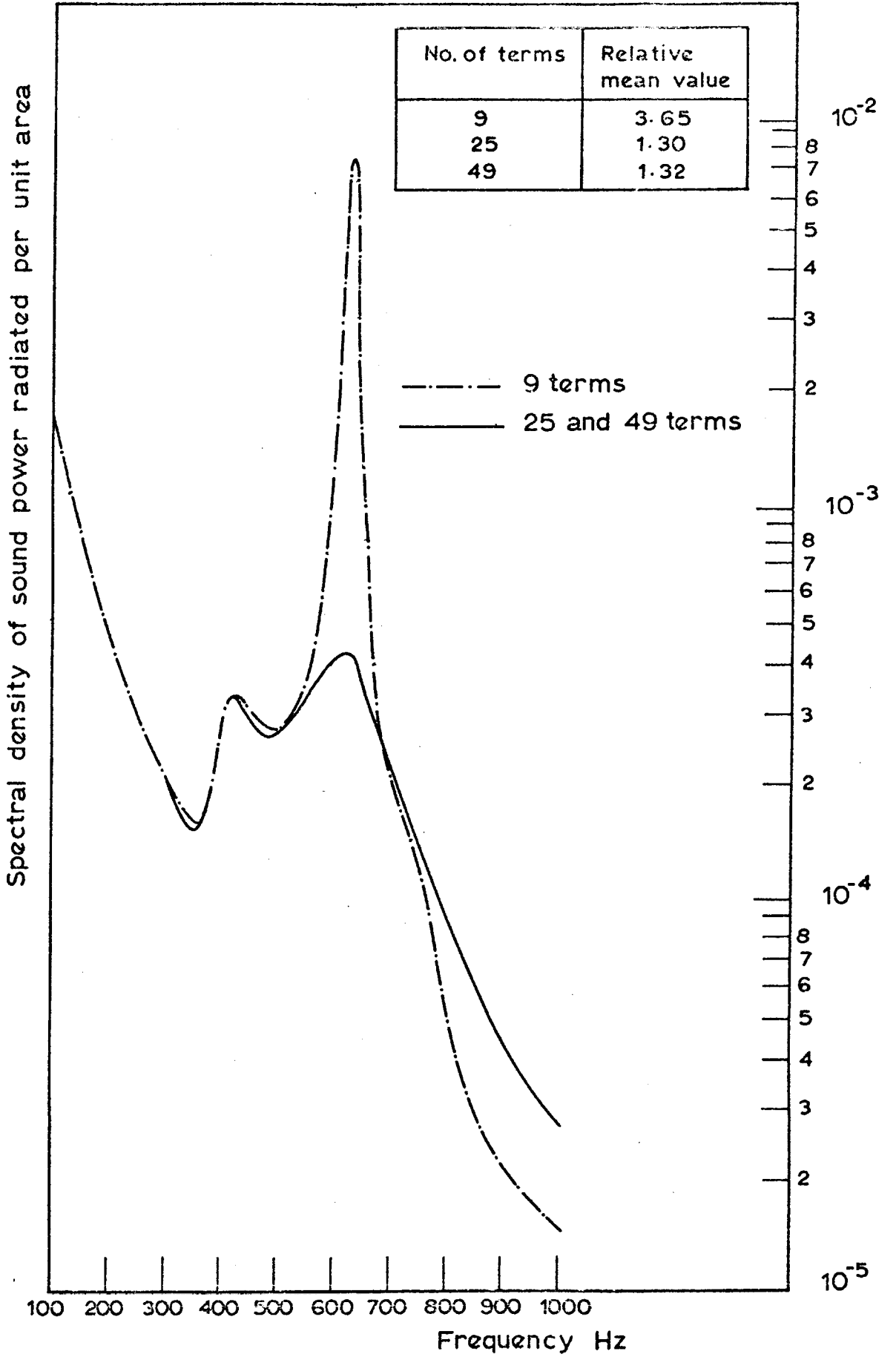

Fig. 4.3 Effect of the number of terms on sound power structure A, η =0·15. Trace velocity = 1·5 times the velocity of sound. convection parallel to x-axis.

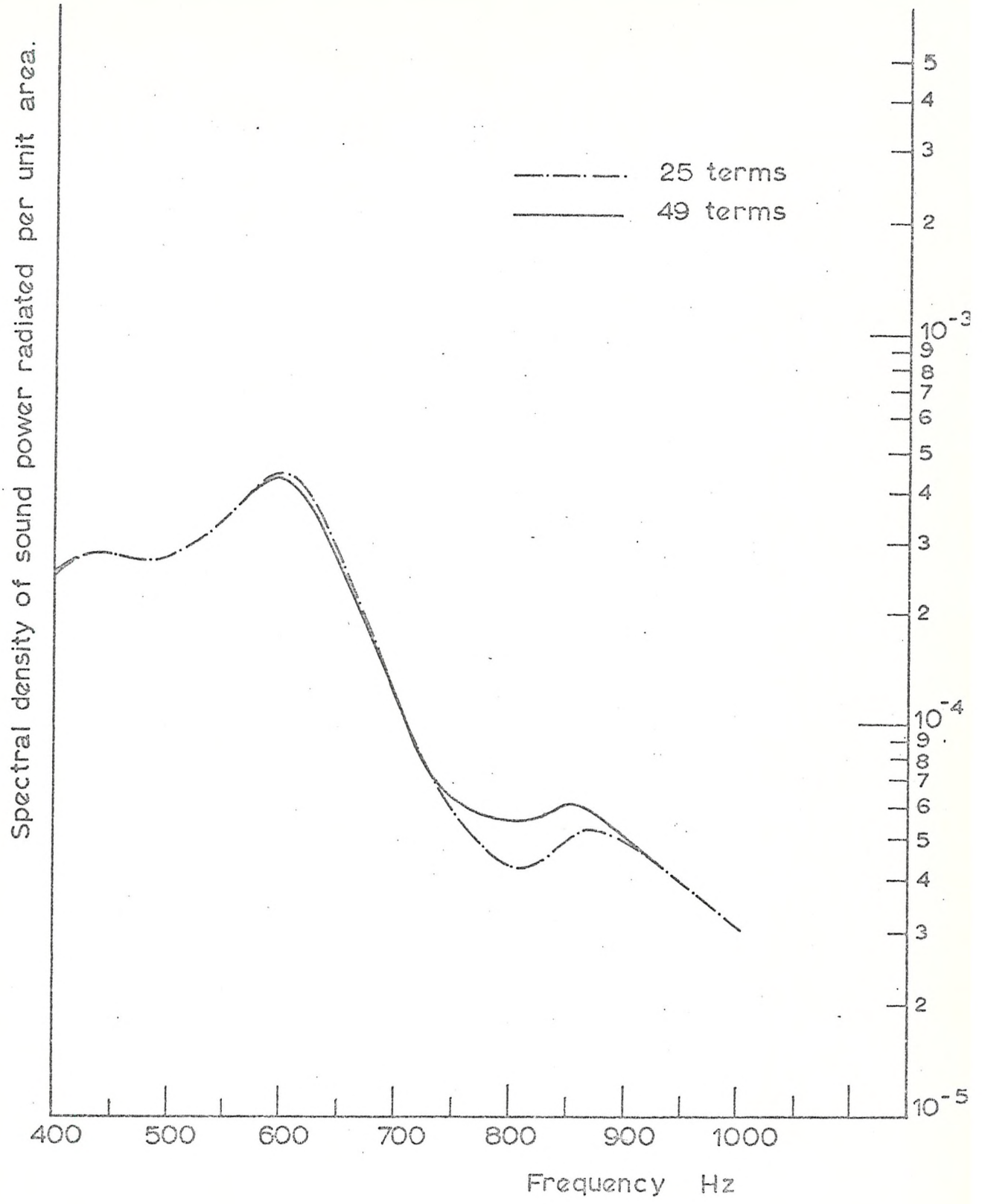

Fig. 4.4 Effect of the number of terms on sound radiation. Structure B, $\eta = 0.25$, $C_t = 1.5C$.

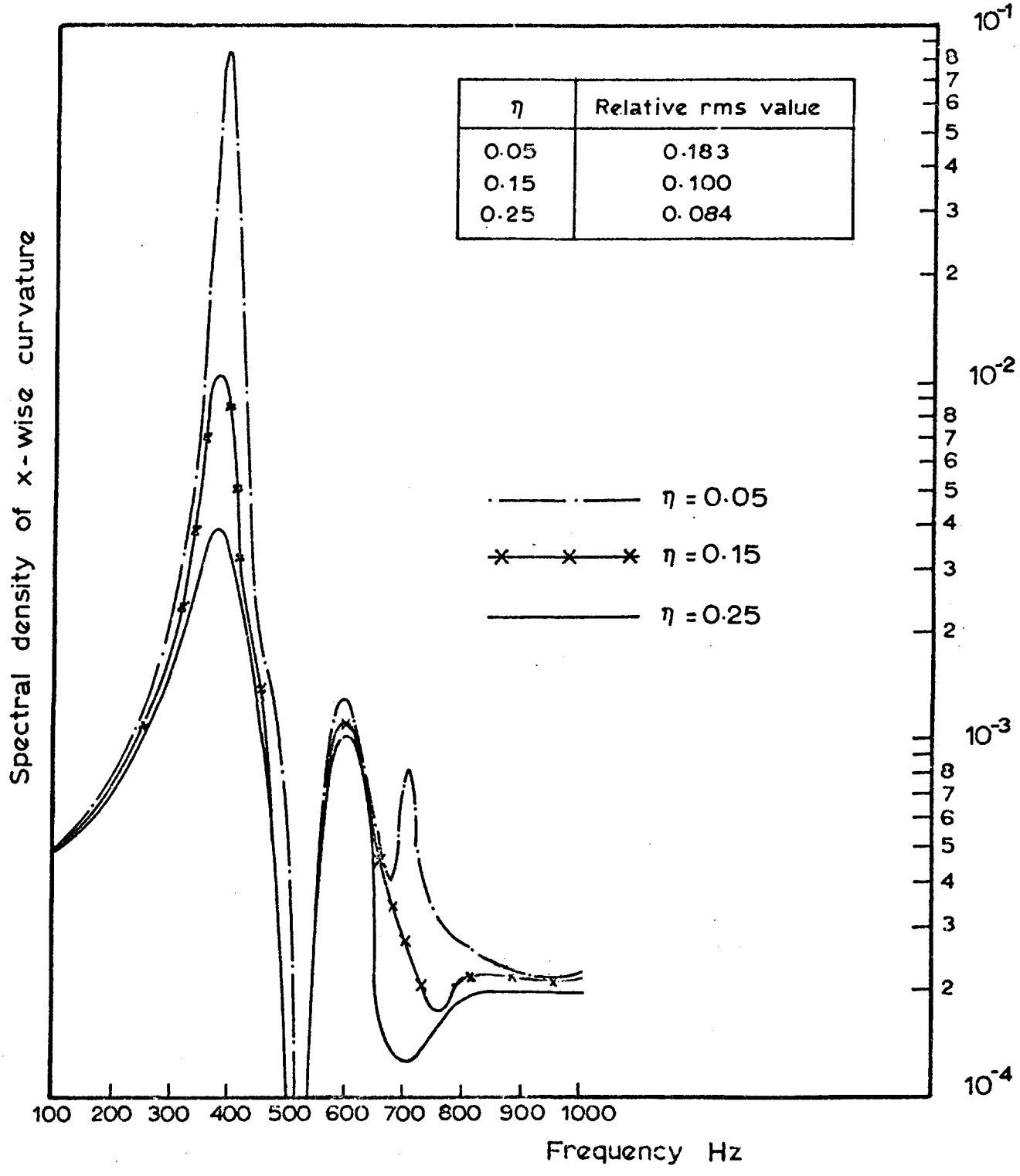

Fig. 4.5 Influence of damping on the curvature. Structure A. Trace velocity = 1.5 times the velocity of sound. Convection parallel to x-axis. Number of terms = 25.

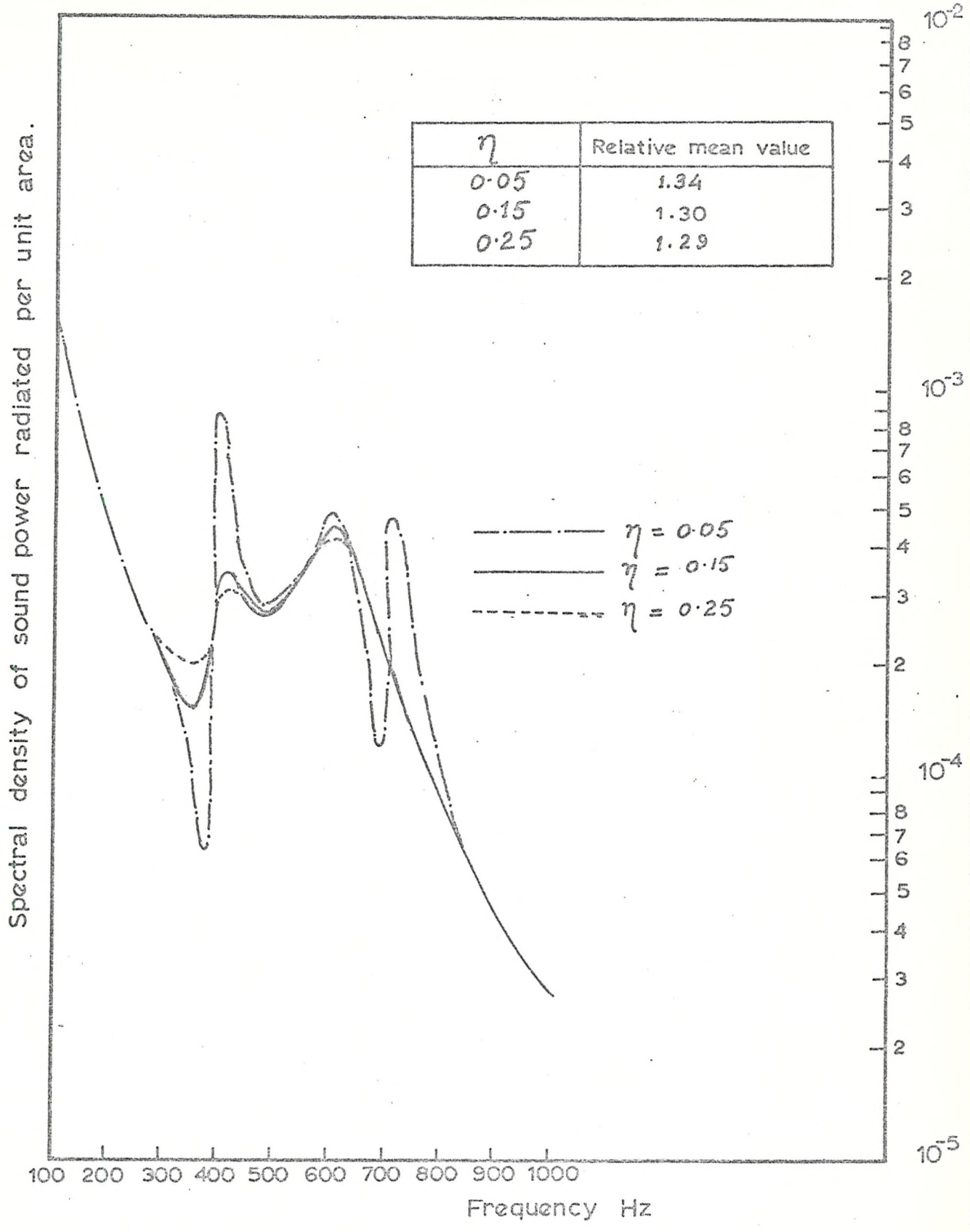

Fig. 4.6 Effect of the damping in structure on sound power. Structure A . Trace velocity = 1.5 times the velocity of sound. Convection parallel to x-axis.

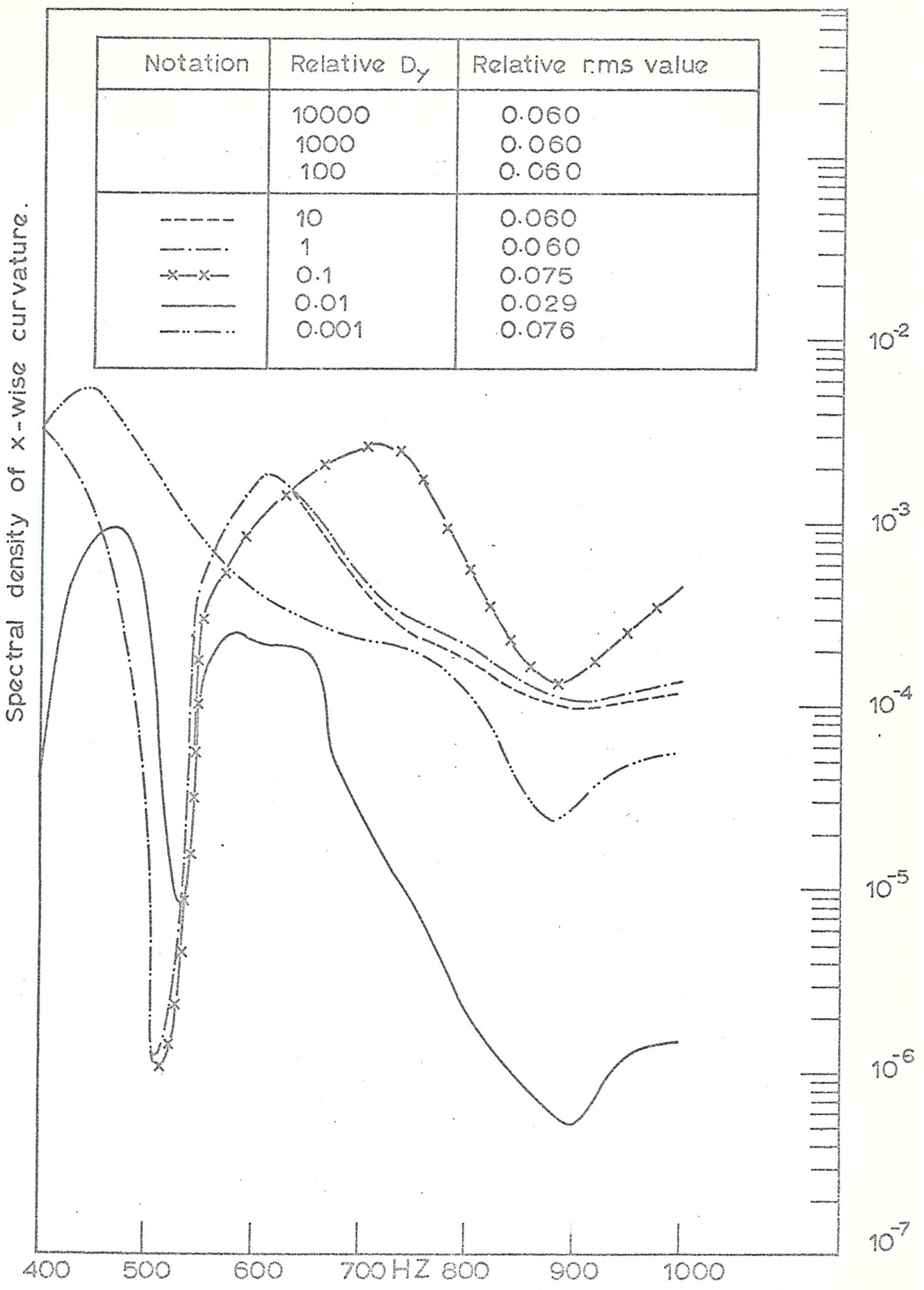

Fig. 4.7 Effect of variation of transverse stiffness of y-wise stiffness on curvature. Structure B. $\eta = 0.25$. Number of terms included = 25. Trace velocity = 1.5 times the velocity of sound. Convection in the direction of x-axis.

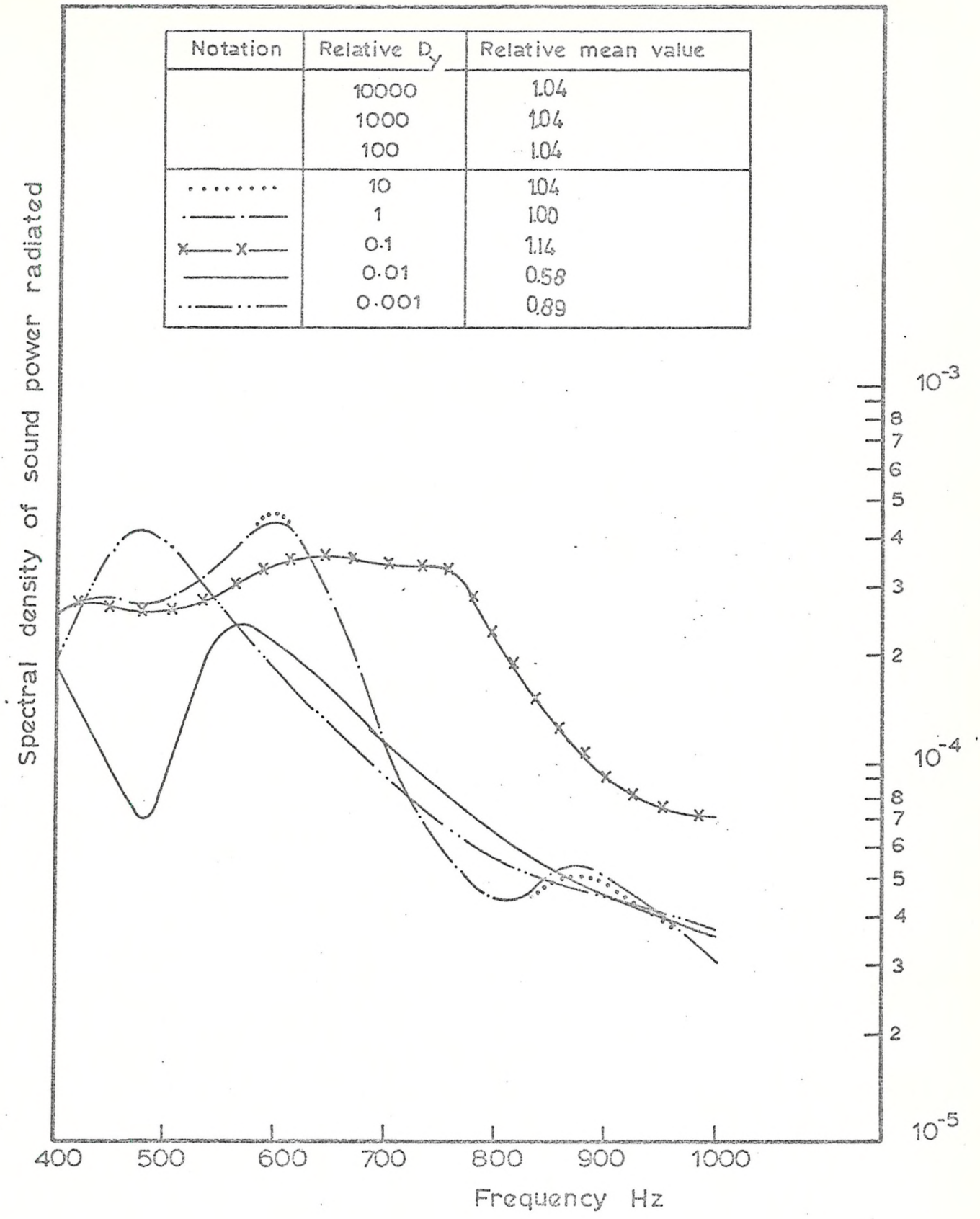

Fig. 4.8 Effect of variation of transverse stiffness of y-wise stiffeners on sound power. Structure B $\eta = 0.25$. Number of terms included = 25. Trace velocity = 1.5 times the velocity of sound. Convection in the direction of x-axis.

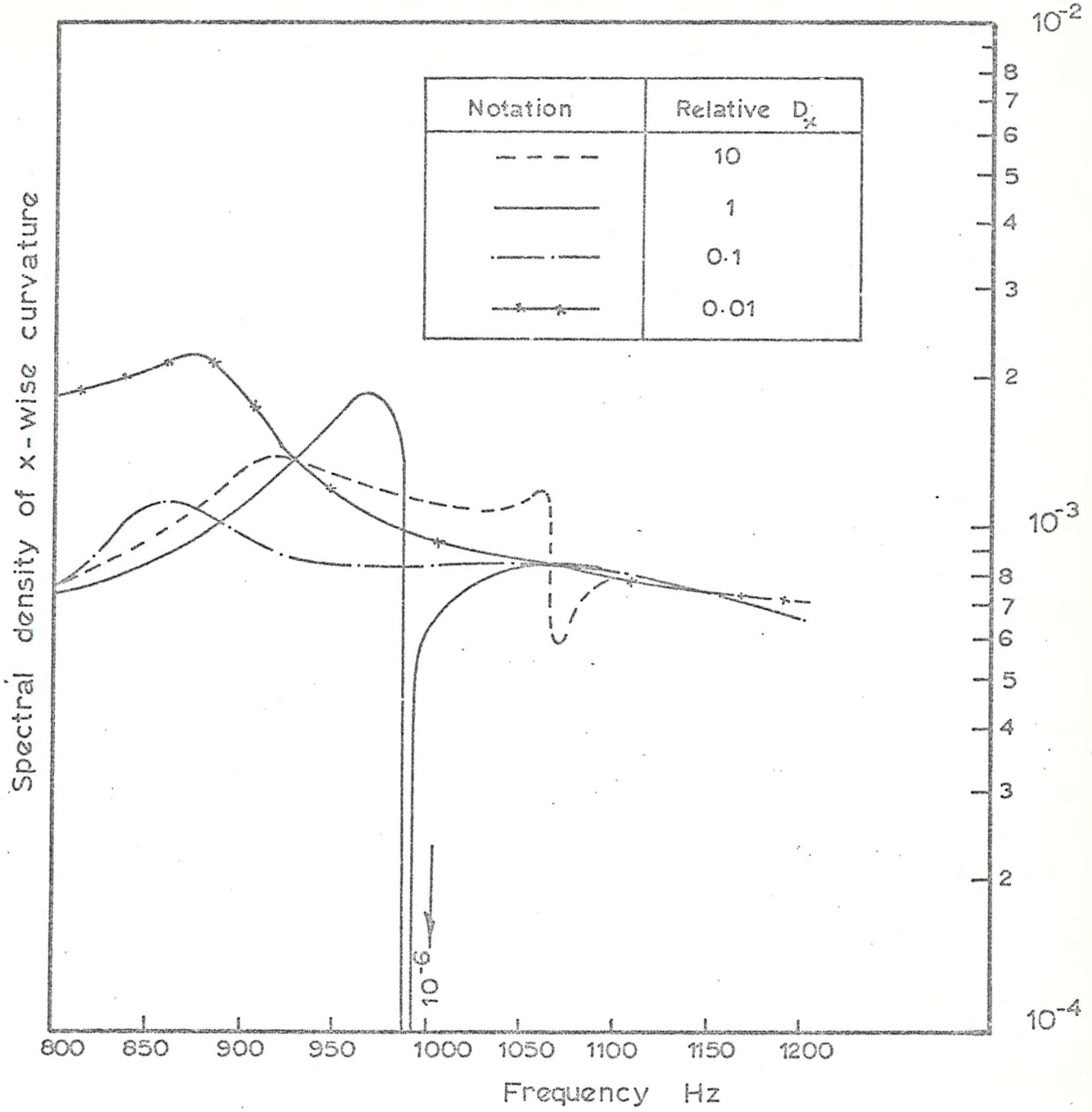

Fig. 4.9 Effect of transverse stiffness of X-wise stiffners on the curvature at midspan. Structure B. $\eta = 0.25$ Trace velocity = 0·28 times the velocity of sound. Direction of convection 45° to x-axis.

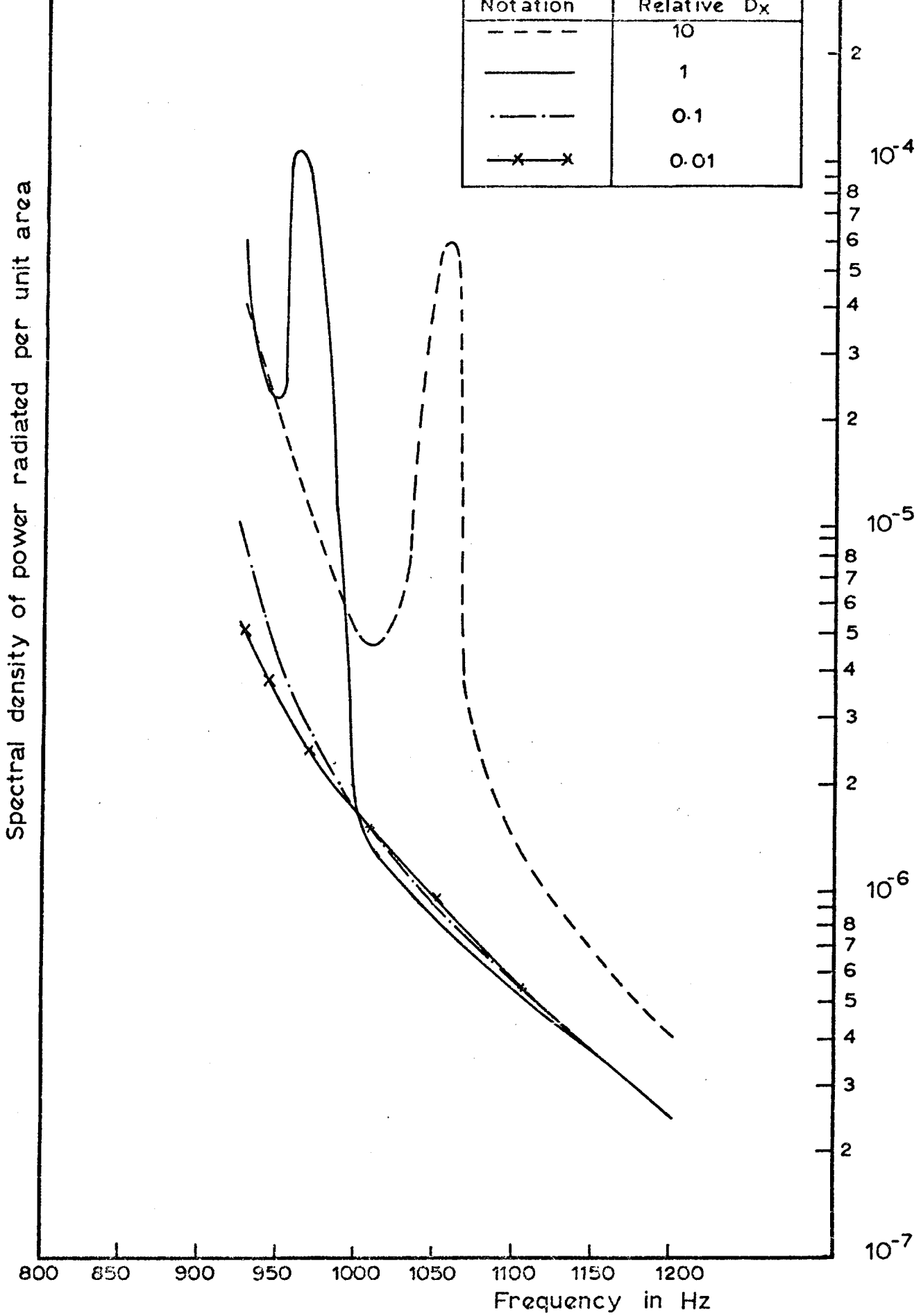

Fig. 4·10 Effect of transverse stiffness of x-wise stiffners on the sound power radiated. Structure B, $\bar{\eta} = 0.25$. Direction of convection 45° to x-axis. Trace velocity = 0·28 times the velocity of sound. No. of terms included = 25.

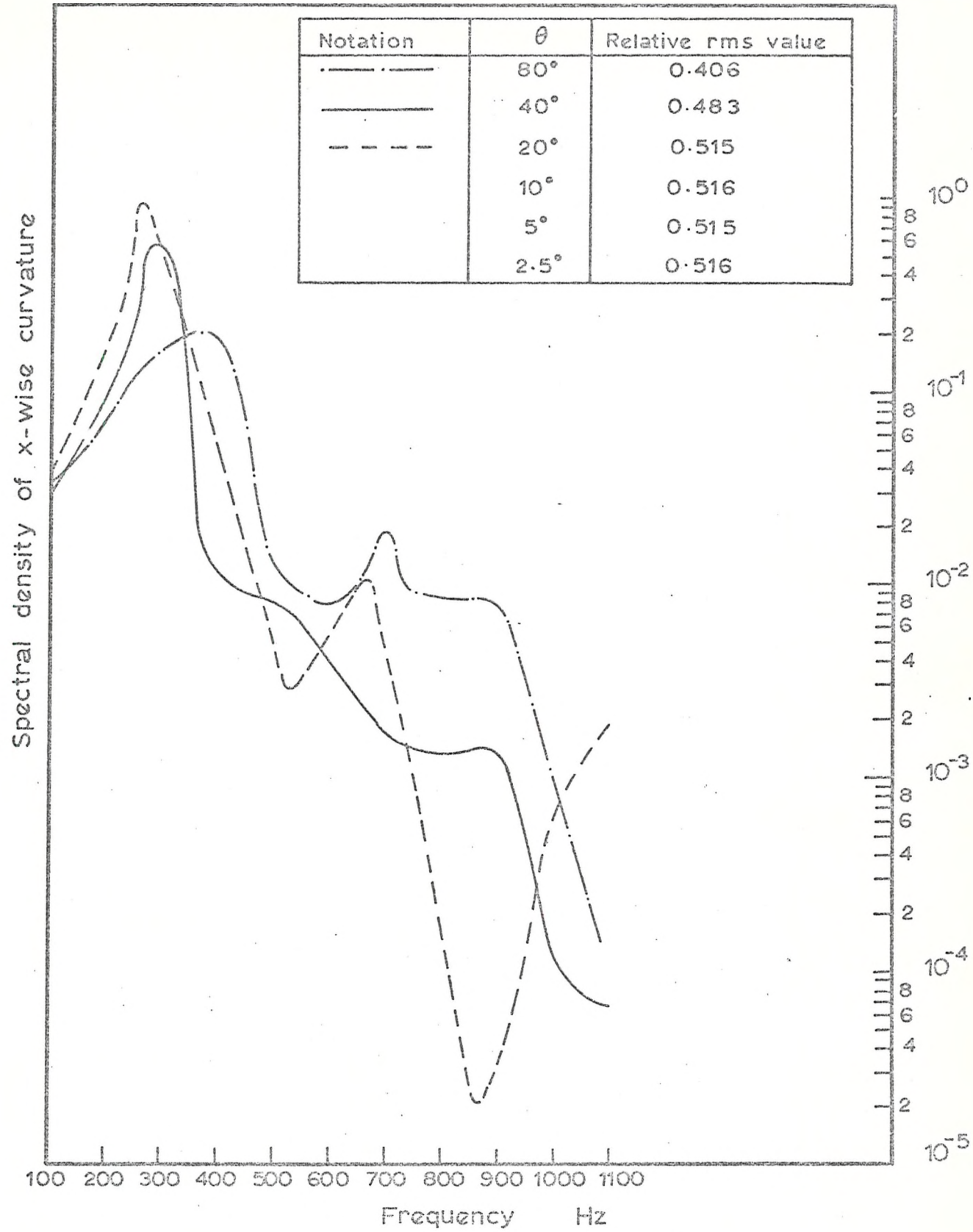

Fig. 4.11 Effect of the angle of convection on curvature. Stucture B η = 0·25. Trace velocity = 0·28 times the velocity of sound. Number of terms included = 25.

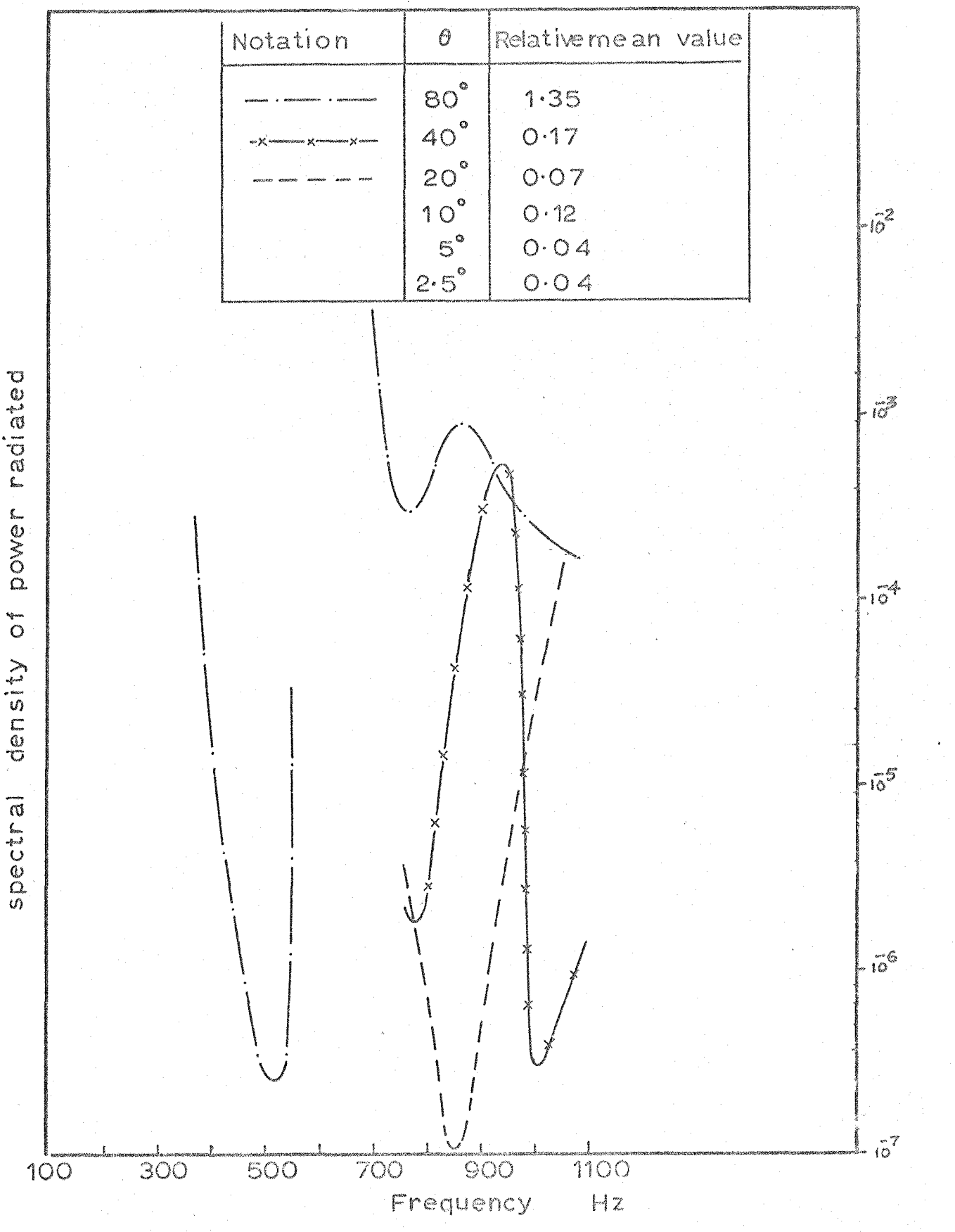

Fig 4·12 Influence of angle of inclination on sound power. Structure B. $\eta = 0{\cdot}25$. convection velocity = 0·28 times the velocity of sound. No. of terms included 25.

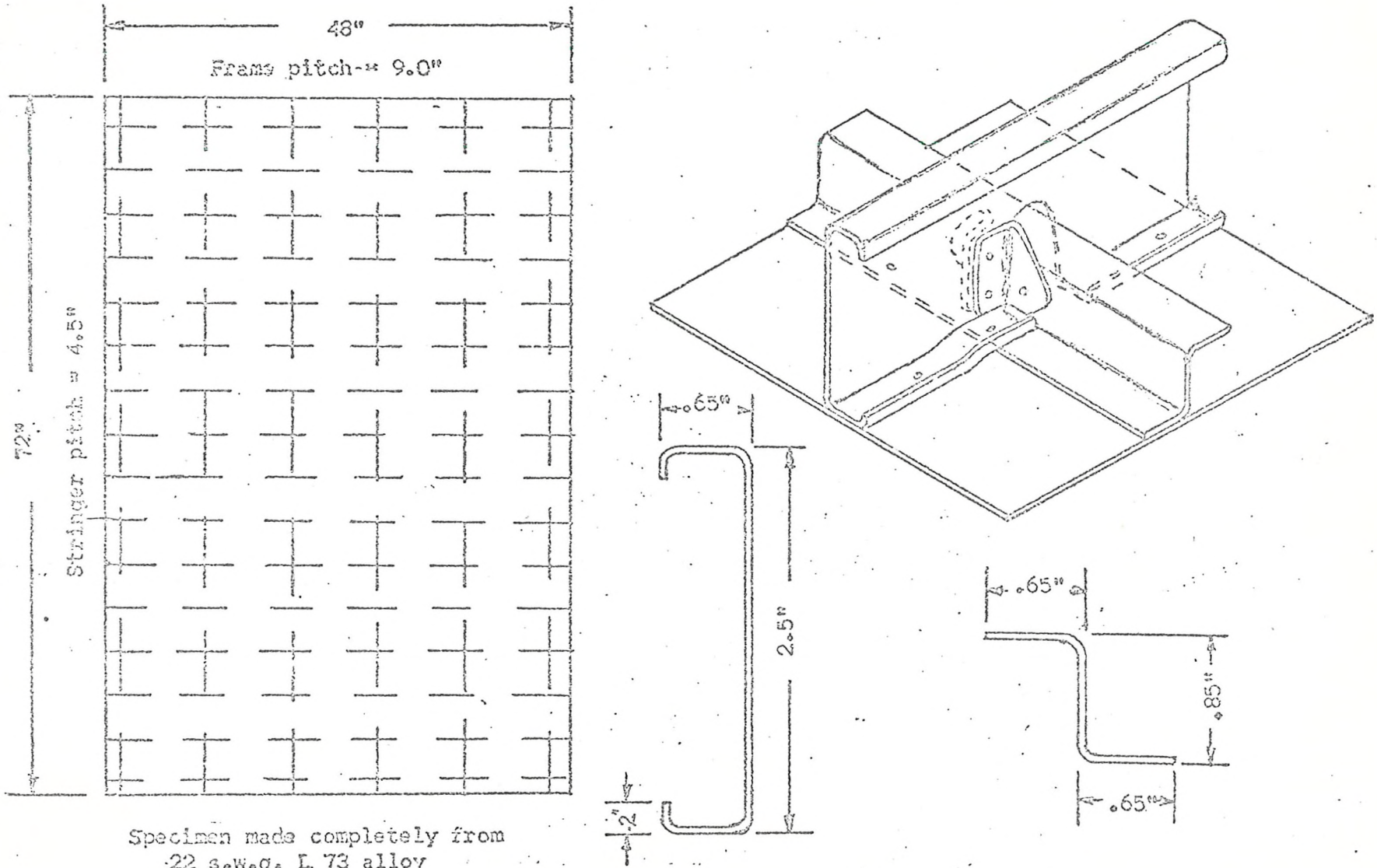

Details of panel construction

FIG. 5.1

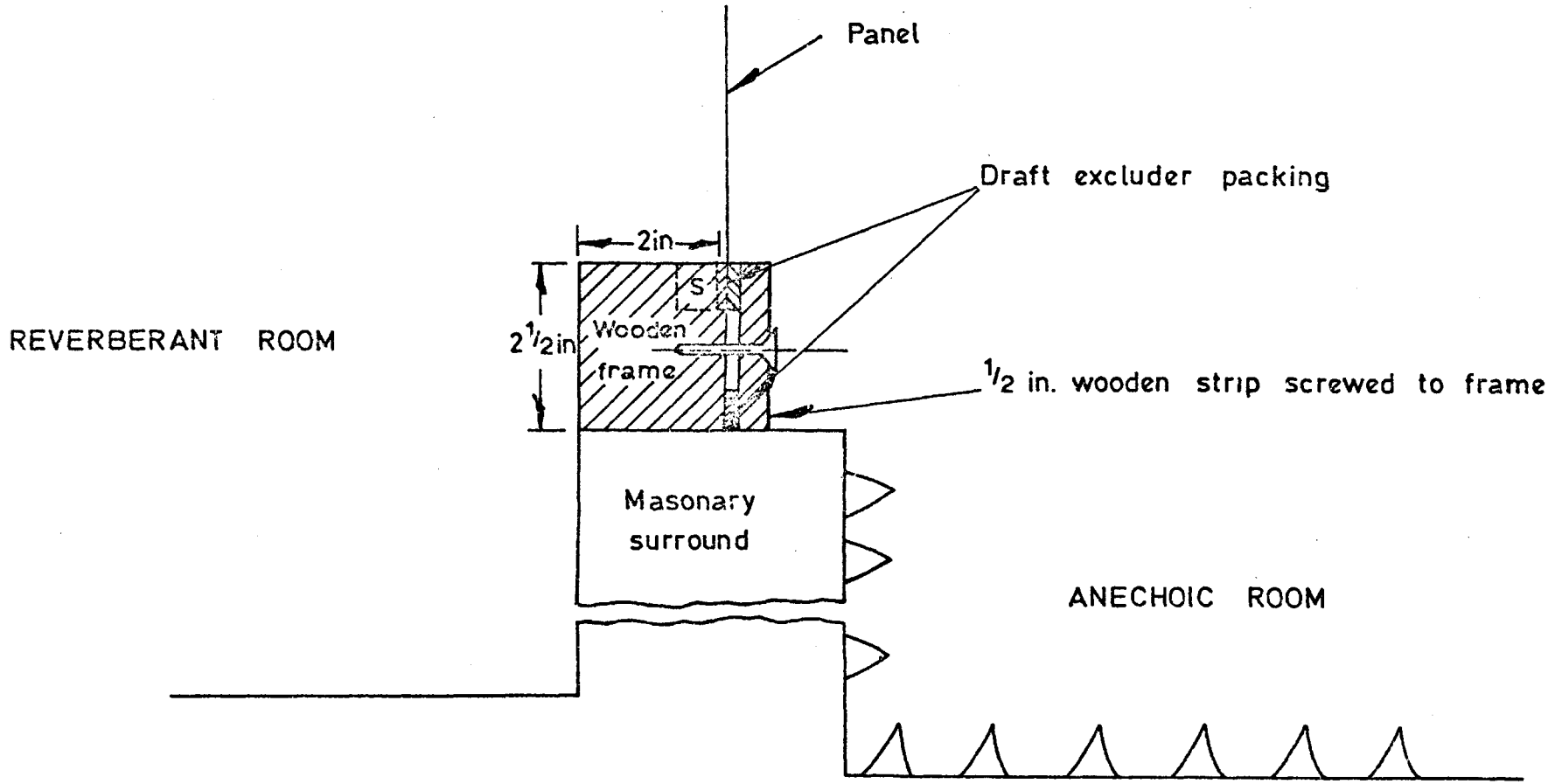

Fig. 5.2 Mounting arrangement for the panel . S indicates space for stiffners which look into the reverberant room.

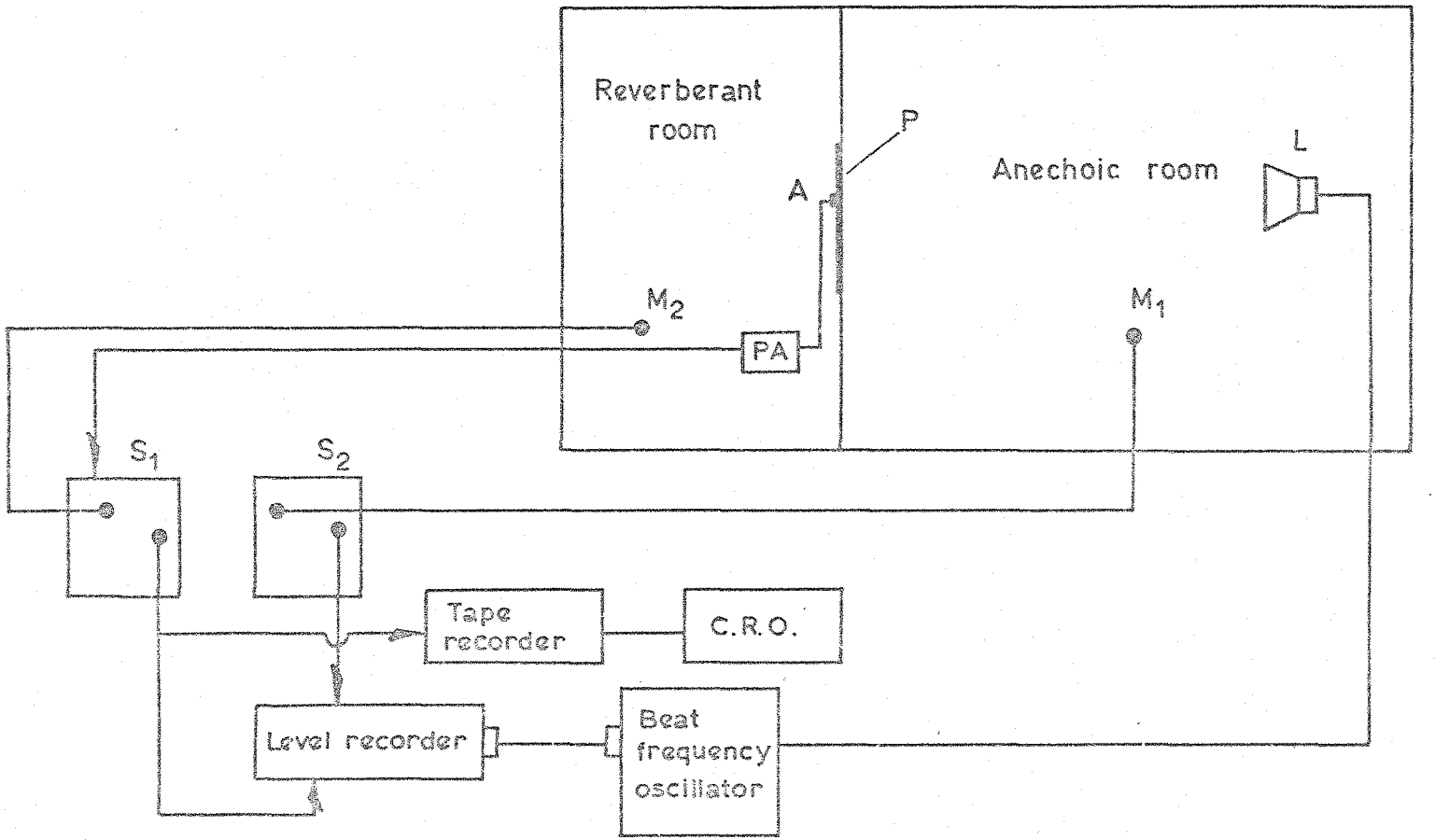

L - Loudspeaker
S_1, S_2 - Spectrometers
A - Accelerometer
M_1, M_2 - Microphones
P - The panel
PA - Pre-amplifier

Fig. 5.3 The general test arrangement.

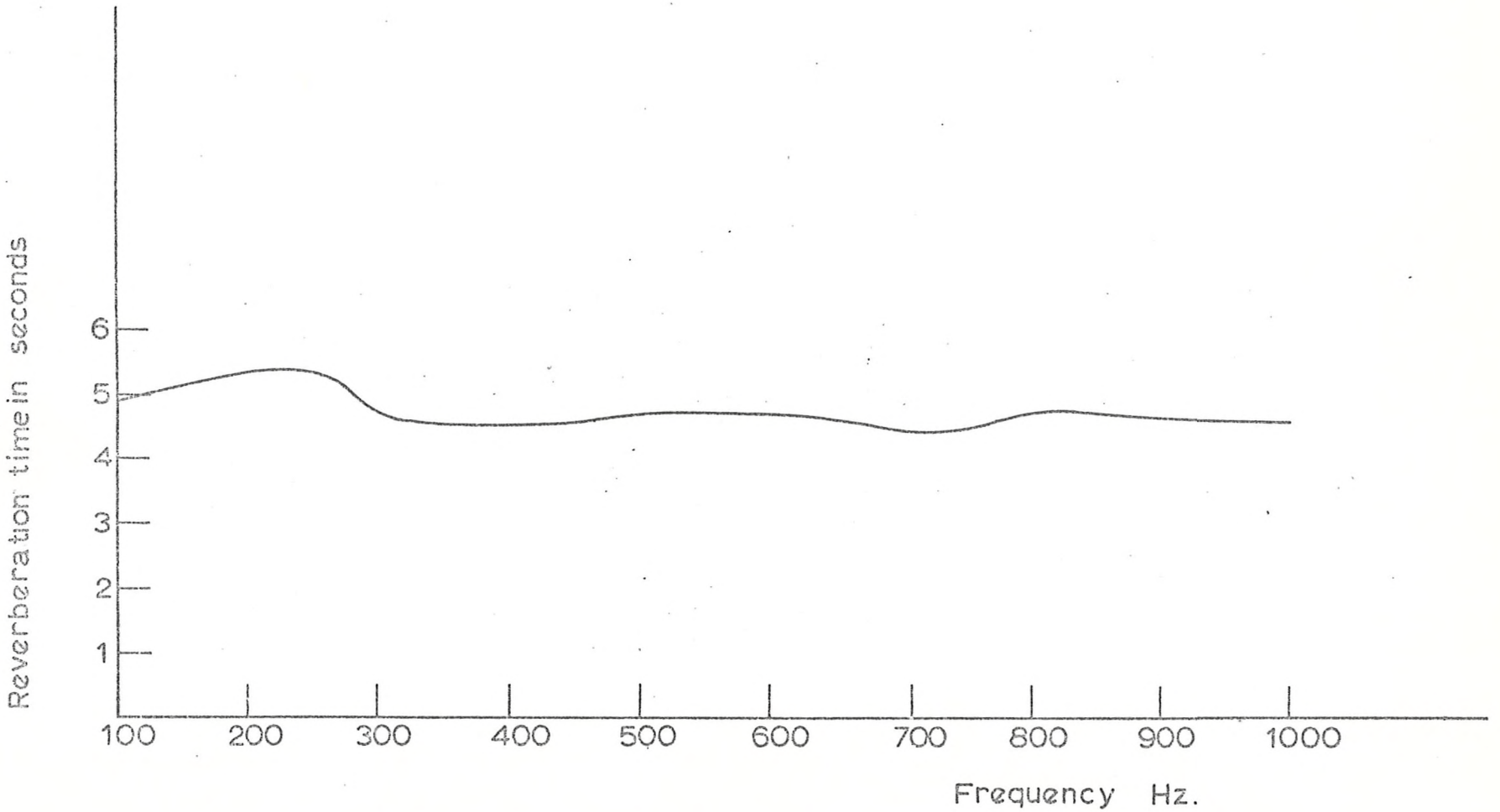

Fig. 5·4 Reverberation time of the small reverberant room.

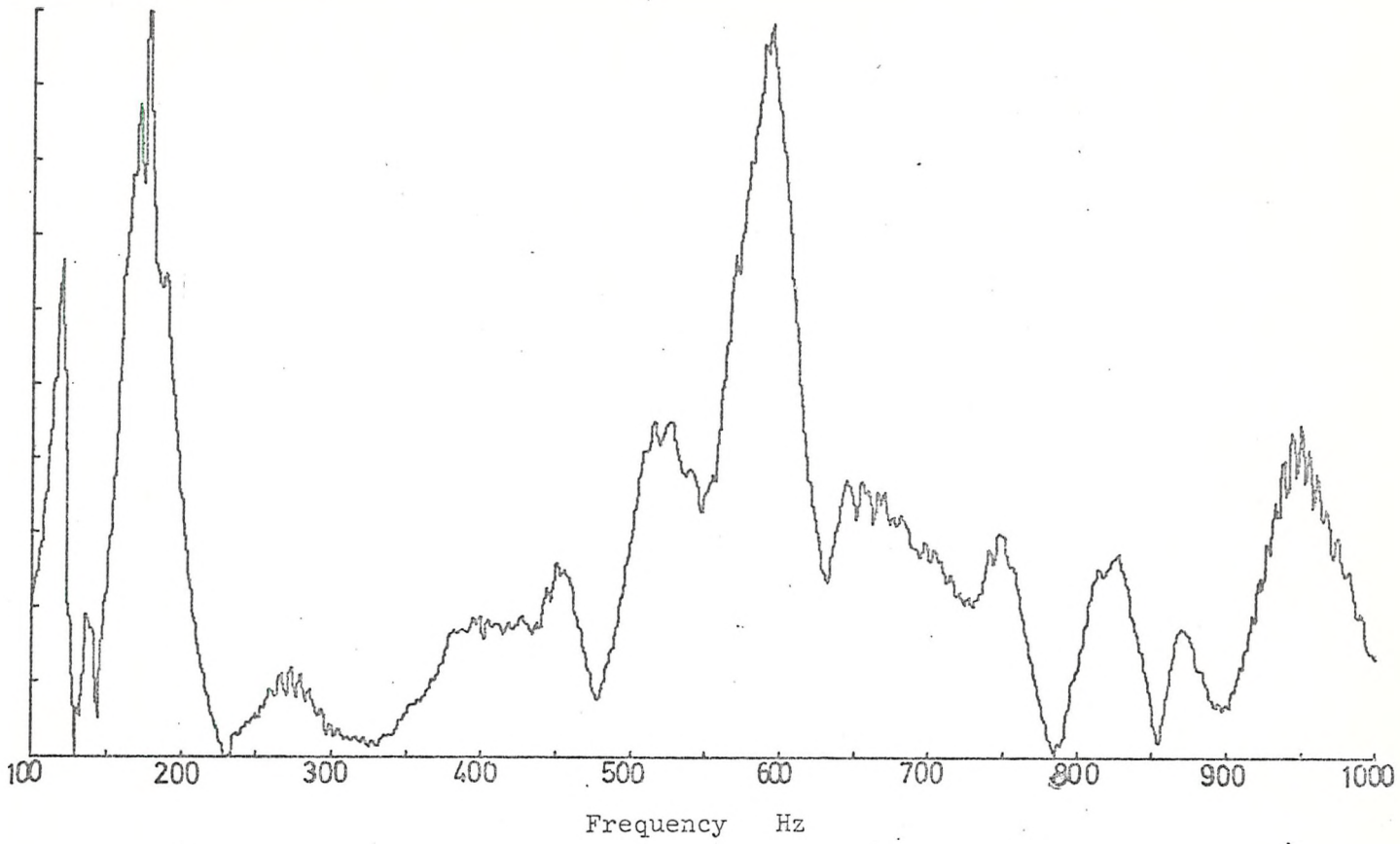

FIG. 5.5 Modulus spectrum of the response of the panel to 0.5 second swept sine wave excitation. Accelerometer was on the skin.

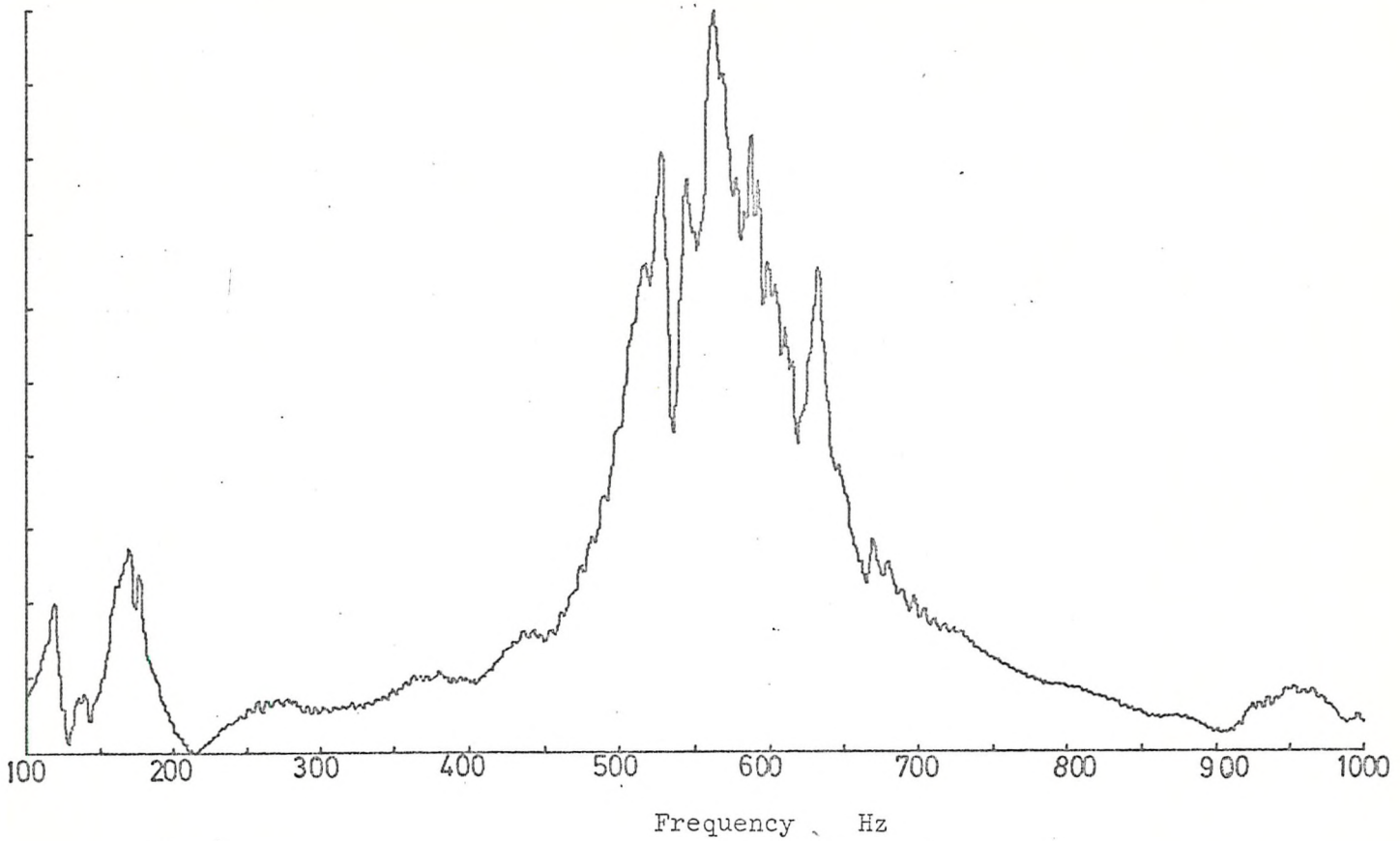

FIG. 5.6 Modulus spectrum of the response of the panel to 0.5 second swept sine wave excitation. Accelerometer was on the stringer.

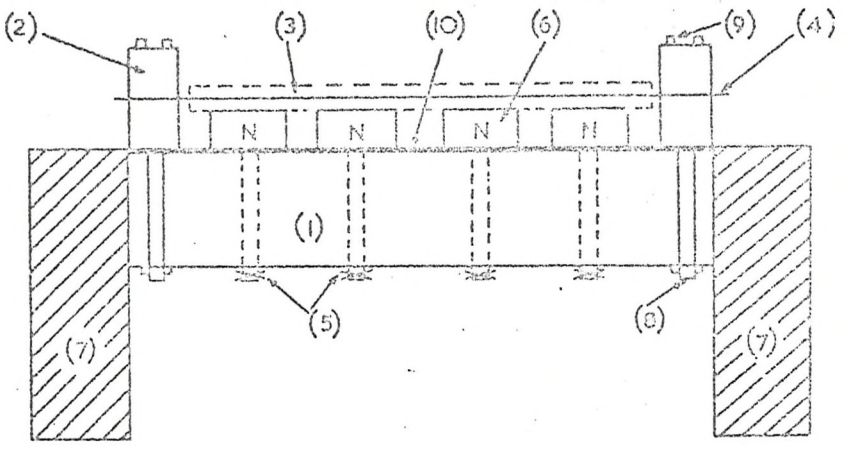

(1) - Massive base plate.

(2) - brass supports.

(3) - mild steel pole piece.

(4) - The damped beam specimen.

(5) - wing nuts.

(6) - permanent steel magnets.

(7) - wooden supports for base plate.

(8) - 2 B.A. screw threaded bolts.

(9) - 2 B.A. allen screws.

(10) - Paxolin insulation.

Figure 5.7 The apparatus used for the measurement of damping.

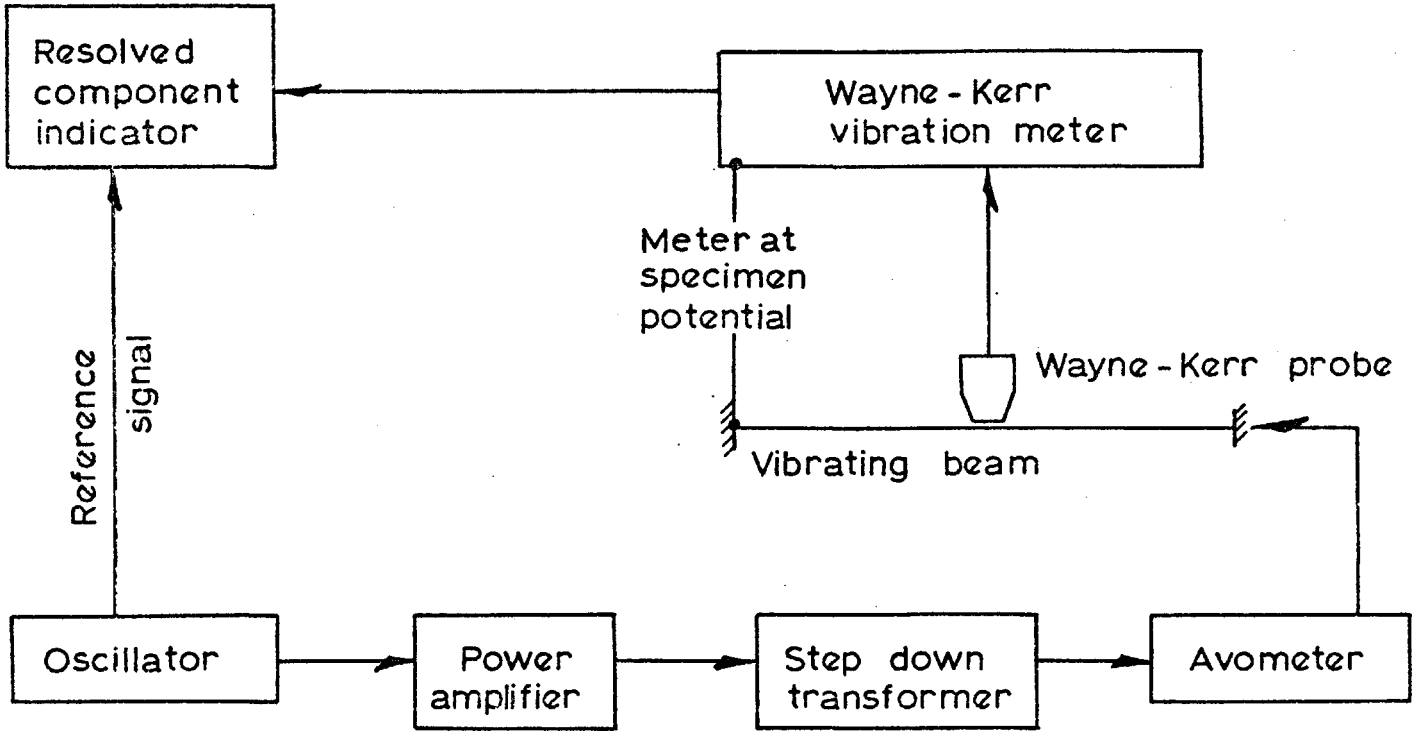

Fig. 5.8 Block diagram for the measurement of beam damping.

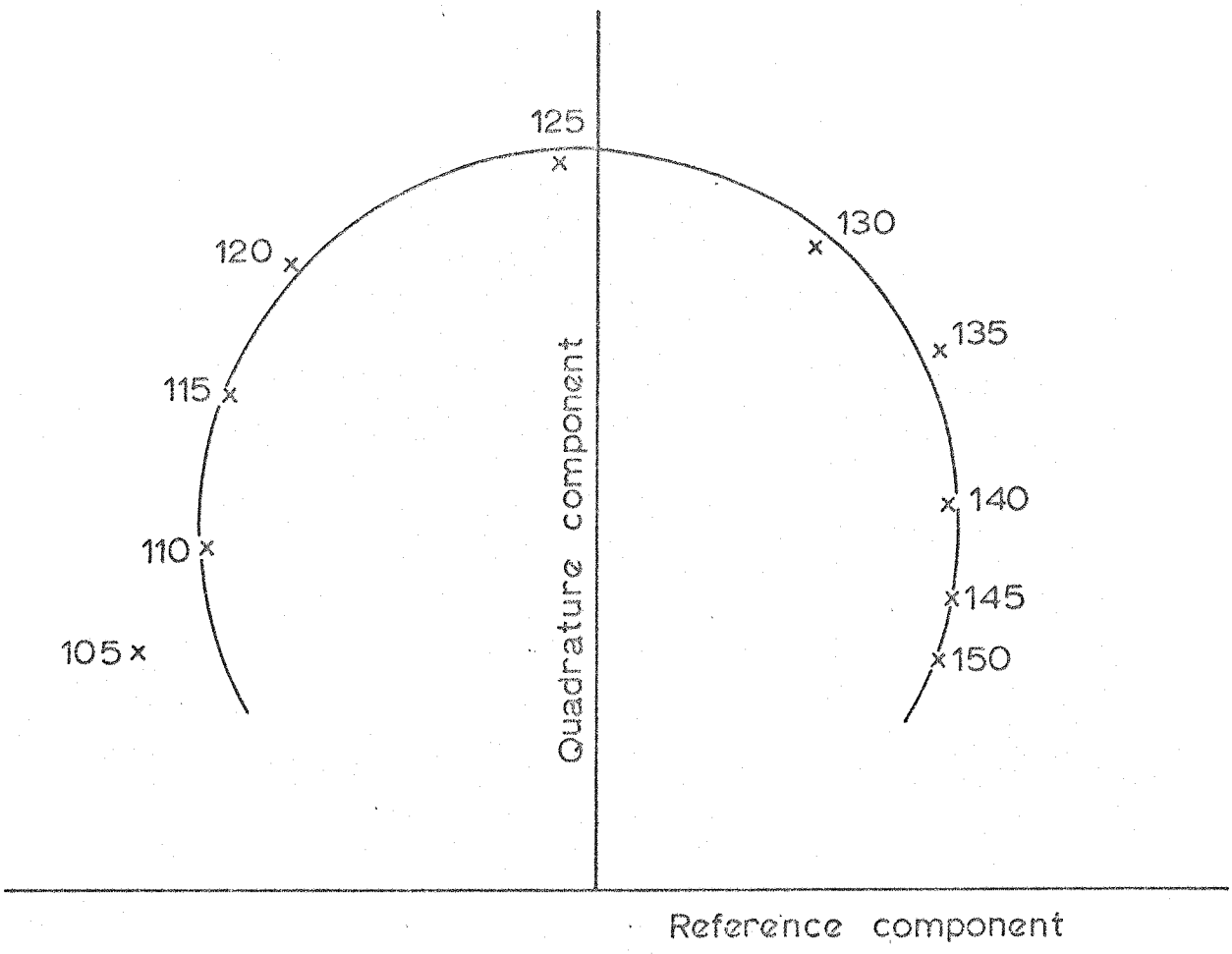

Fundamental mode $\omega_n = 125.5$ Hz

$\eta = 0.25$

Fig. 5.9 Vector plot obtained by measured values of vibration.

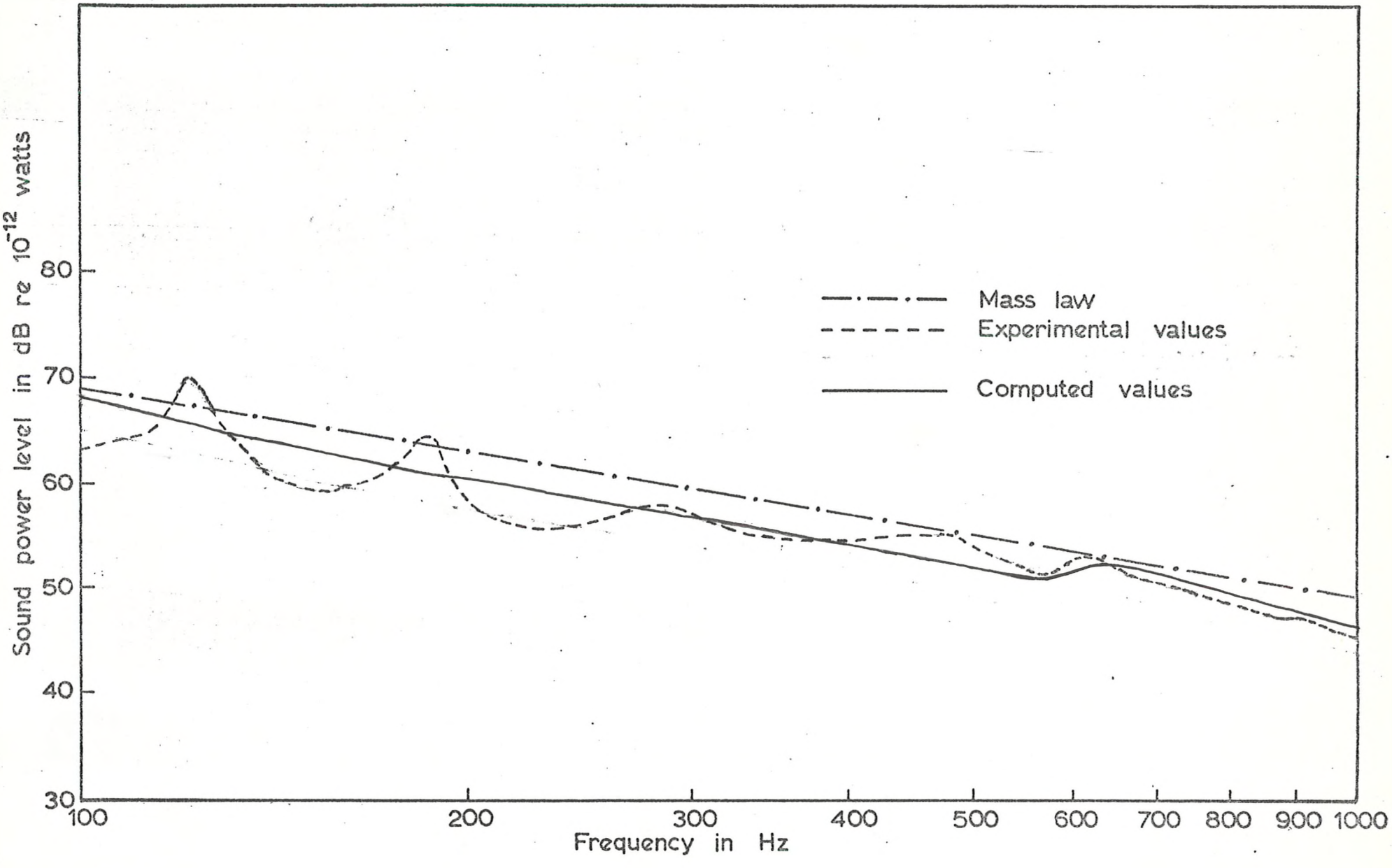

Fig 5.10 Values of sound power radiated . Angle of incidence = $SIN^{-1}1/3$

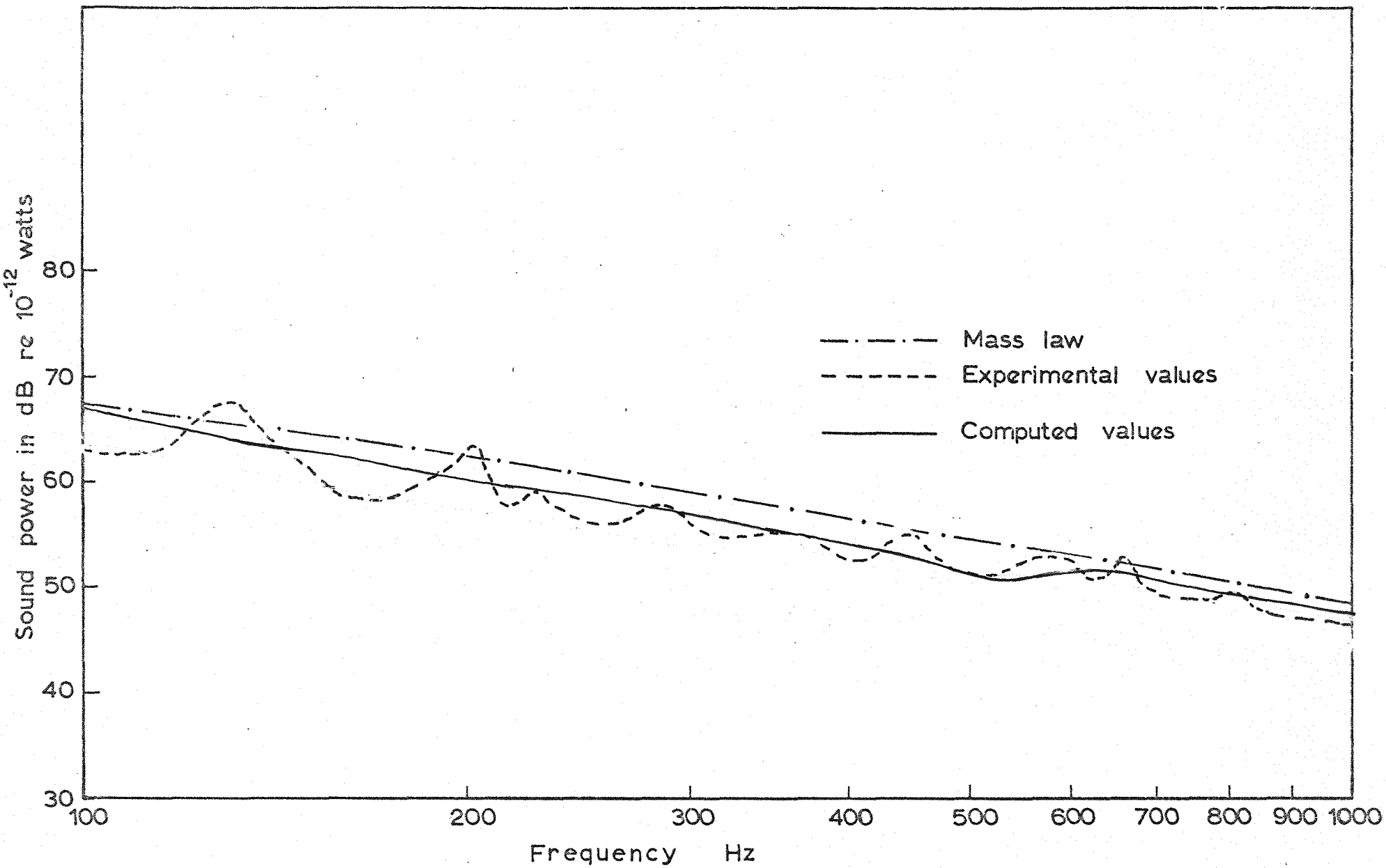

Fig 5.11 Values of sound power radiated. Normal incidence

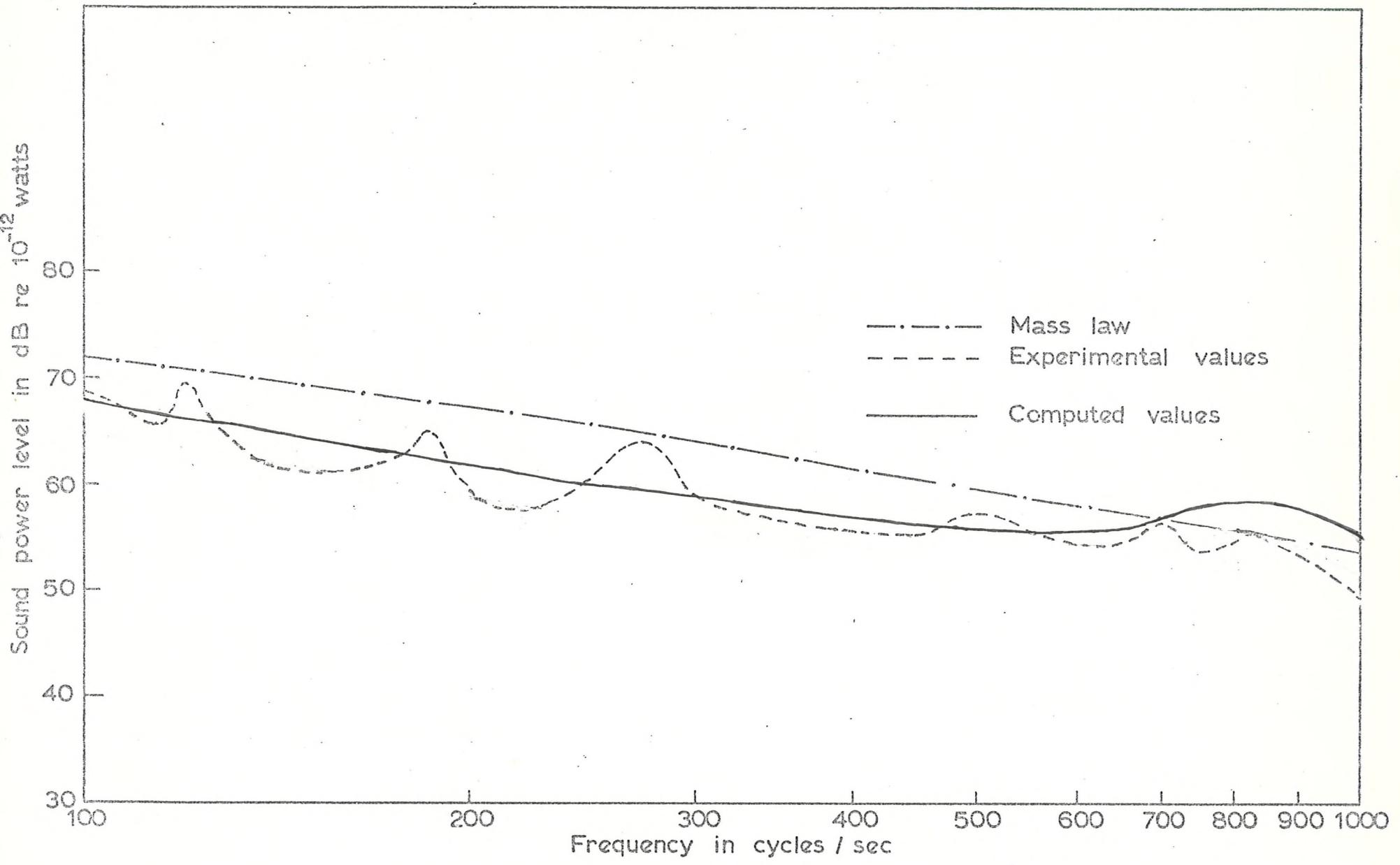

Fig 5.12 Values of sound power radiated. Angle of incidence = $SIN^{-1}\frac{2}{3}$

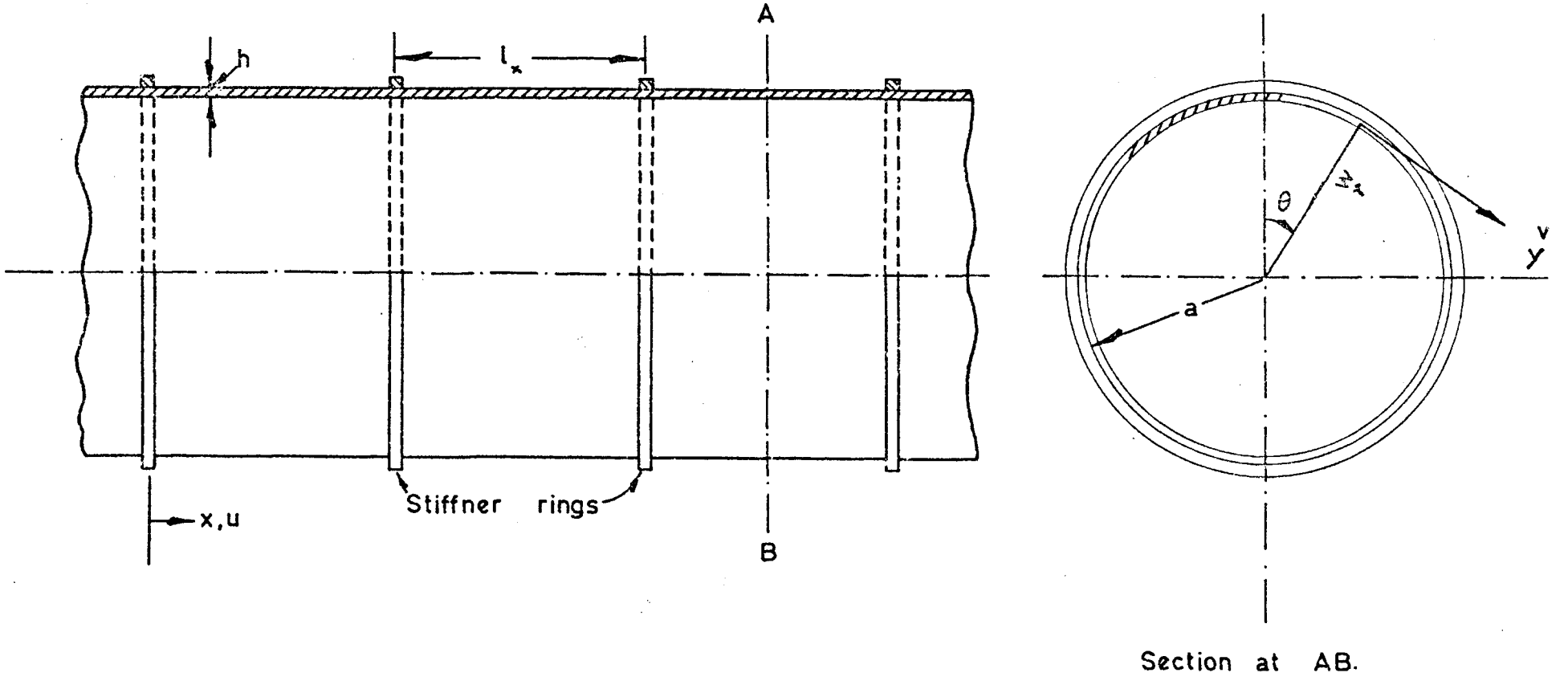

Fig.6.1 A part of an infinitely long ring stiffened cylinder with the co-ordinate system used.

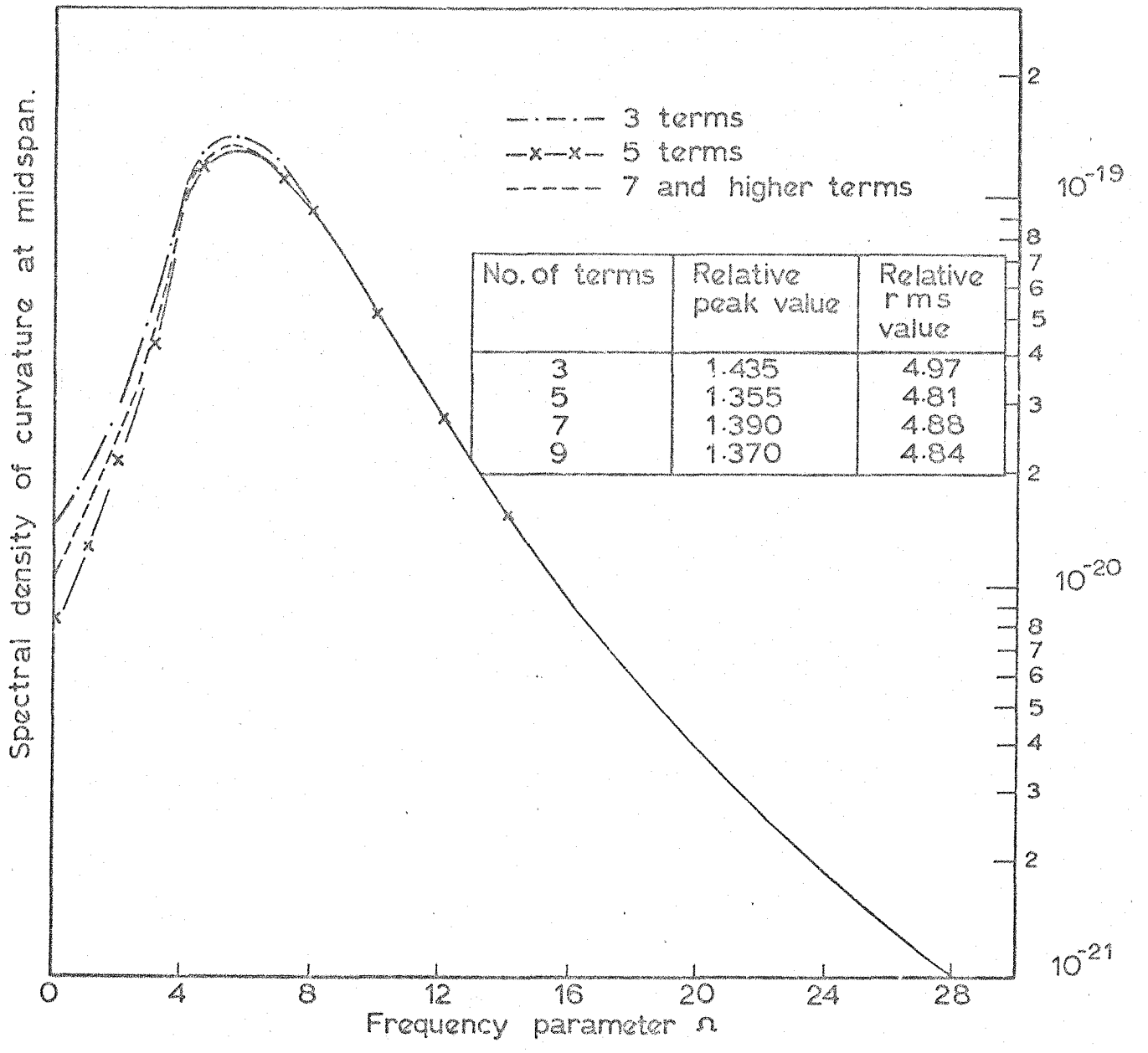

Fig 6.2 Influence of the number of terms on the curvature. CV=80.0, η=0.25, n=1

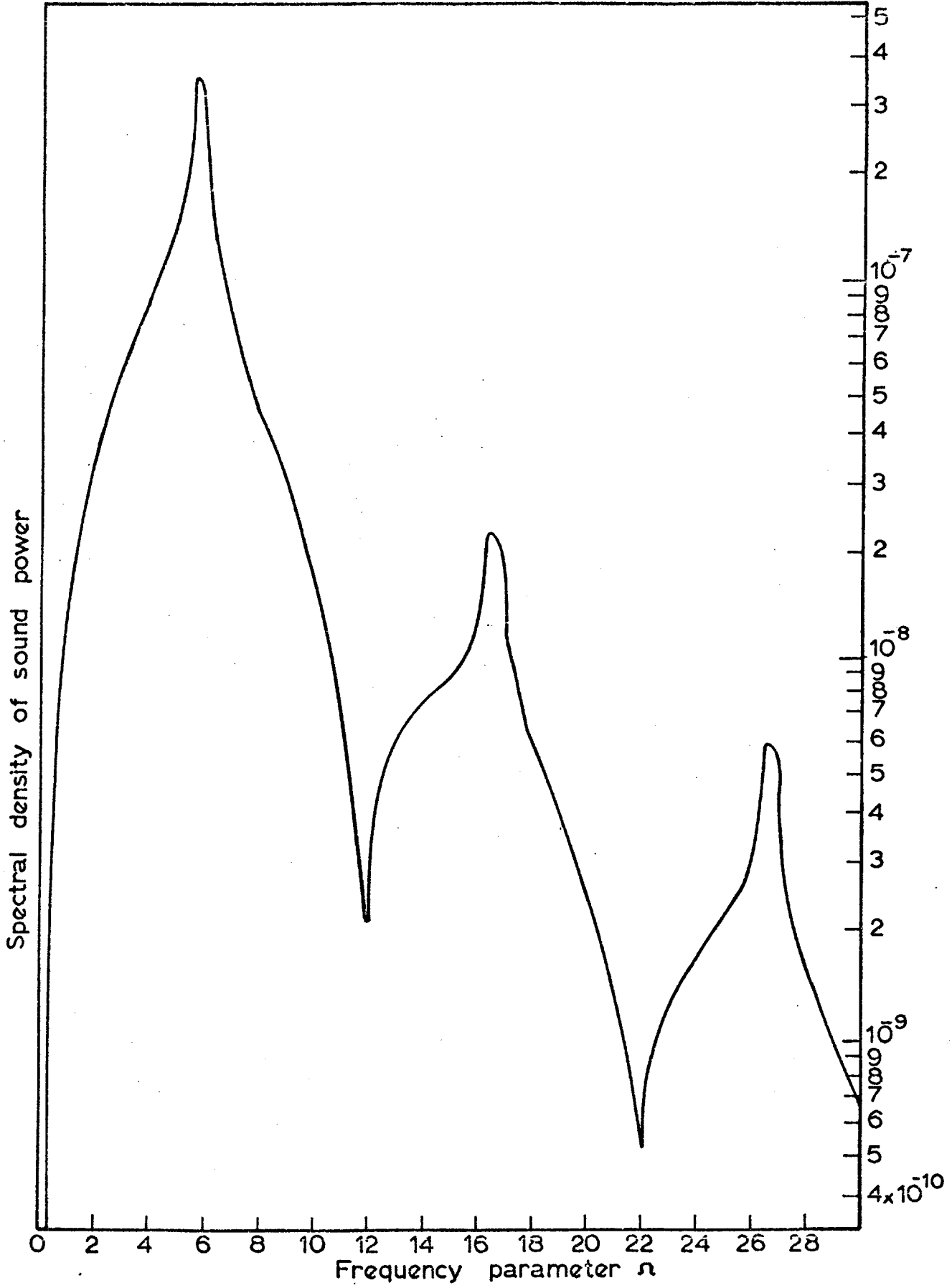

Fig 6.3 The spectral density of reactive sound power at different frequencies . C V = 80.0 η=0.25 n=1

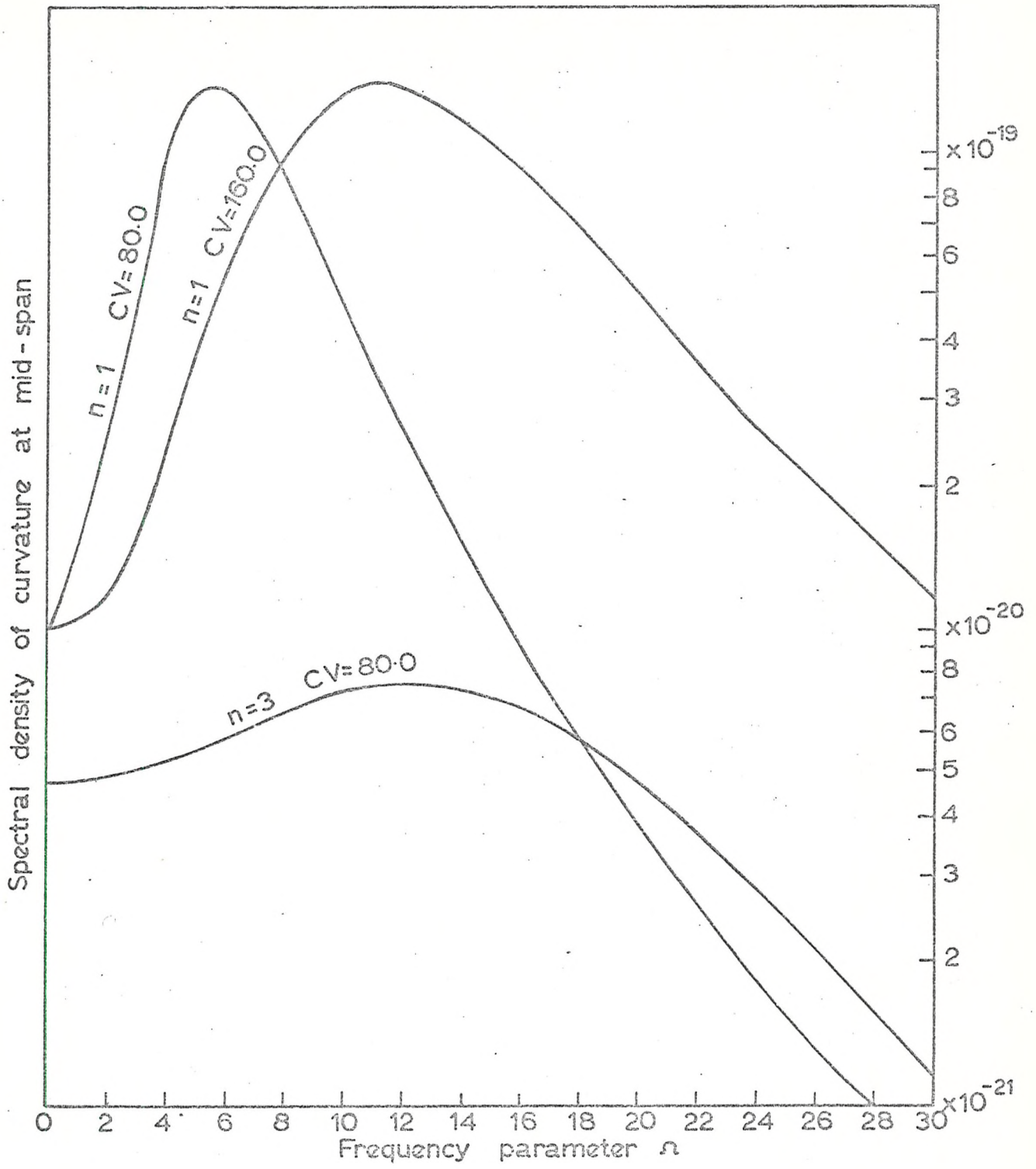

Fig 6.4 Spectral density of curvature at midspan, $\eta = 0.25$

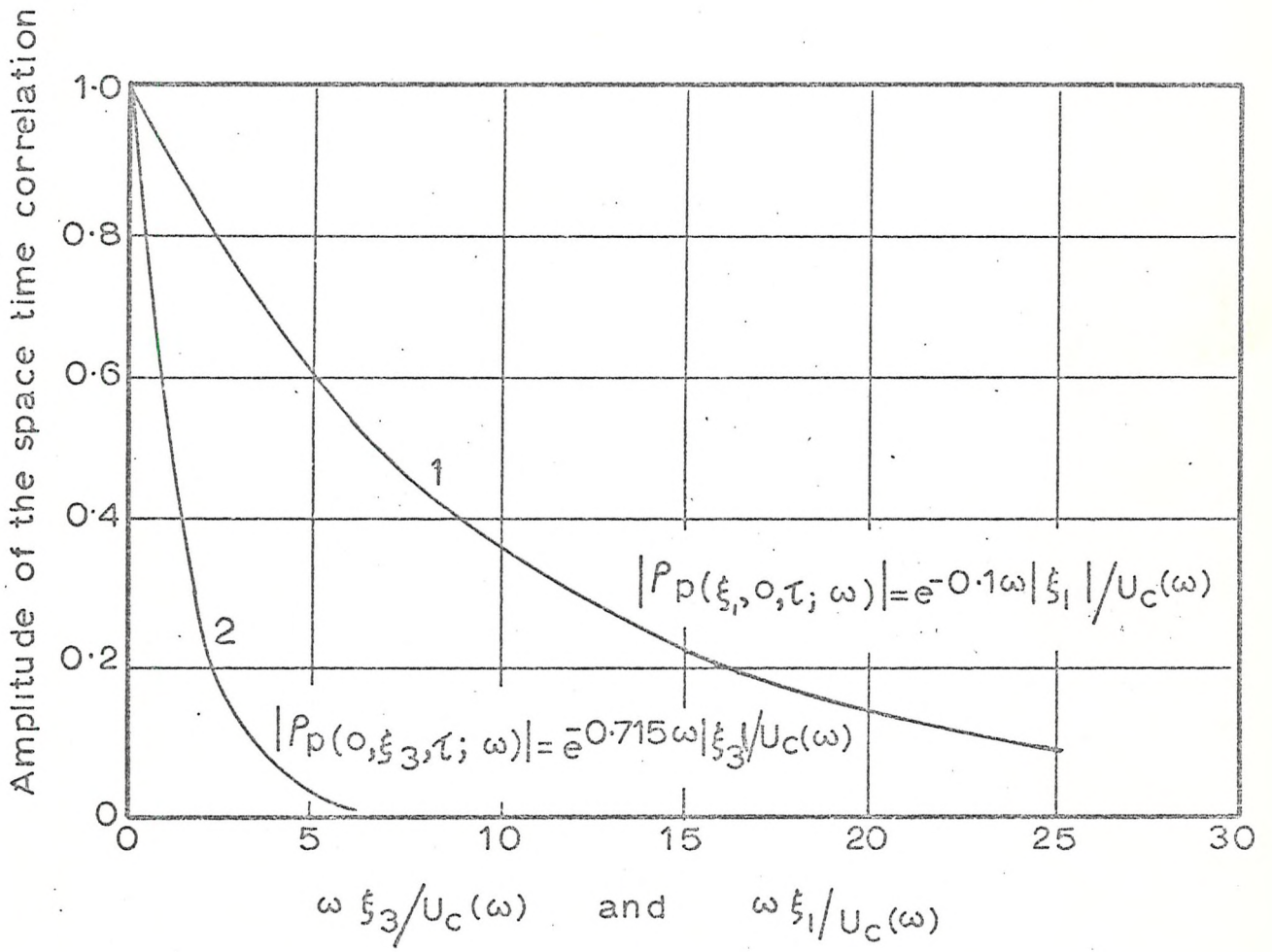

Fig A·1 Amplitudes of narrow band space time correlations of the pressure field. Curve 1 represents the longitudinal correlation and curve 2 the lateral correlation From Bull [54]

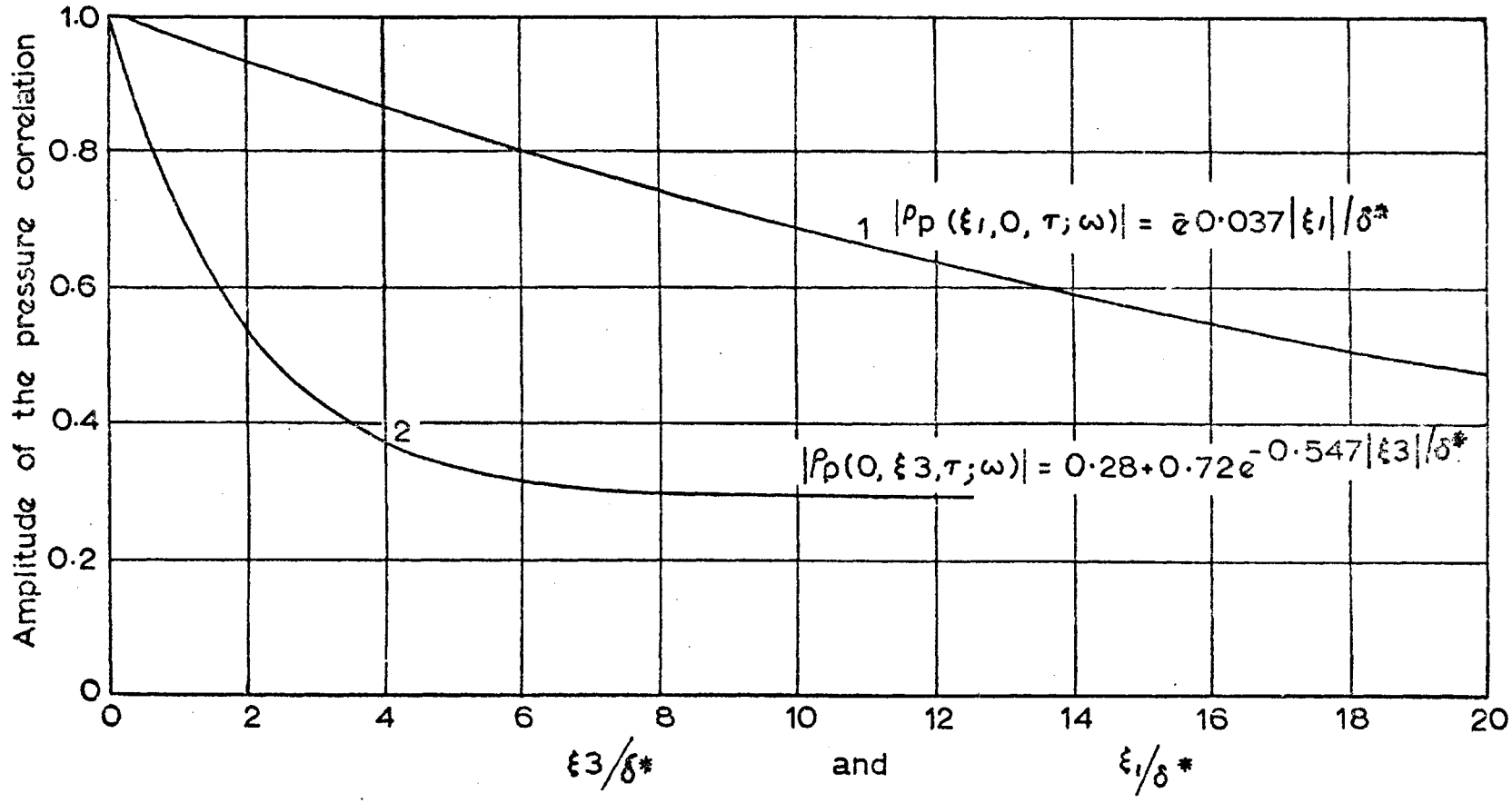

Fig A.2. Low frequency value of narrow band pressure correlation amplitudes Curve 1 represents the longitudinal correlation and curve 2 the lateral correlation From Bull [54]

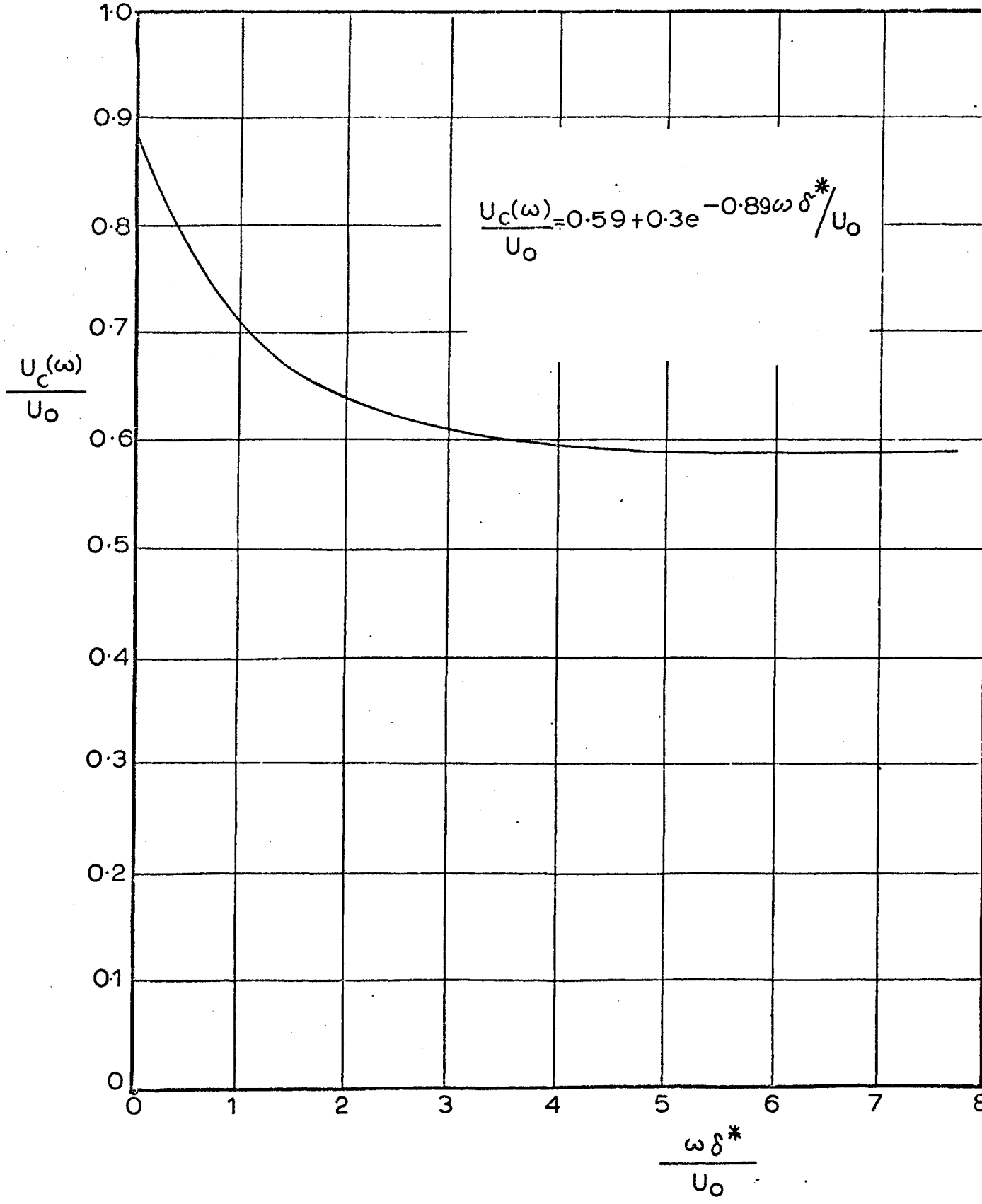

Fig A·3 Convection velocities derived from narrow band longitudinal space-time correlations of the pressure field. From Bull [54]

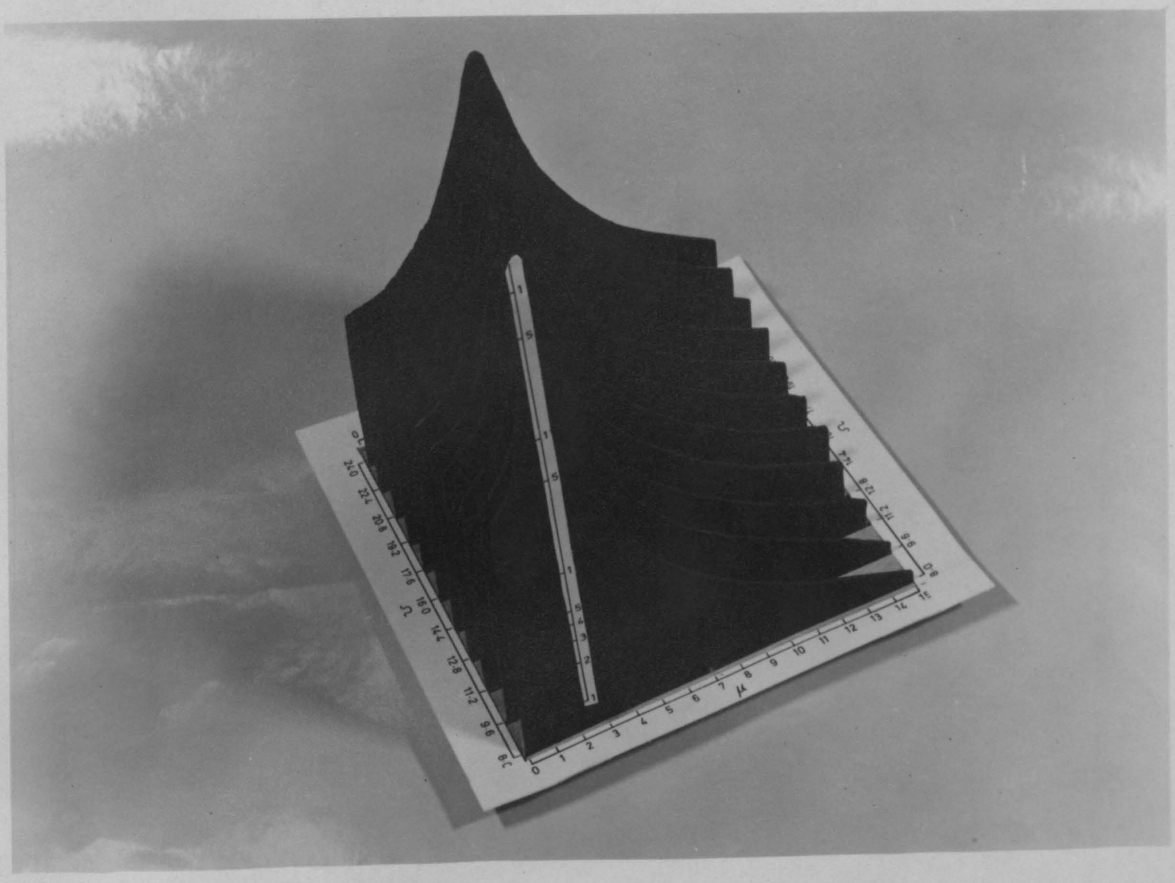

Figure A.4 (see above and below) The wave number frequency spectrum

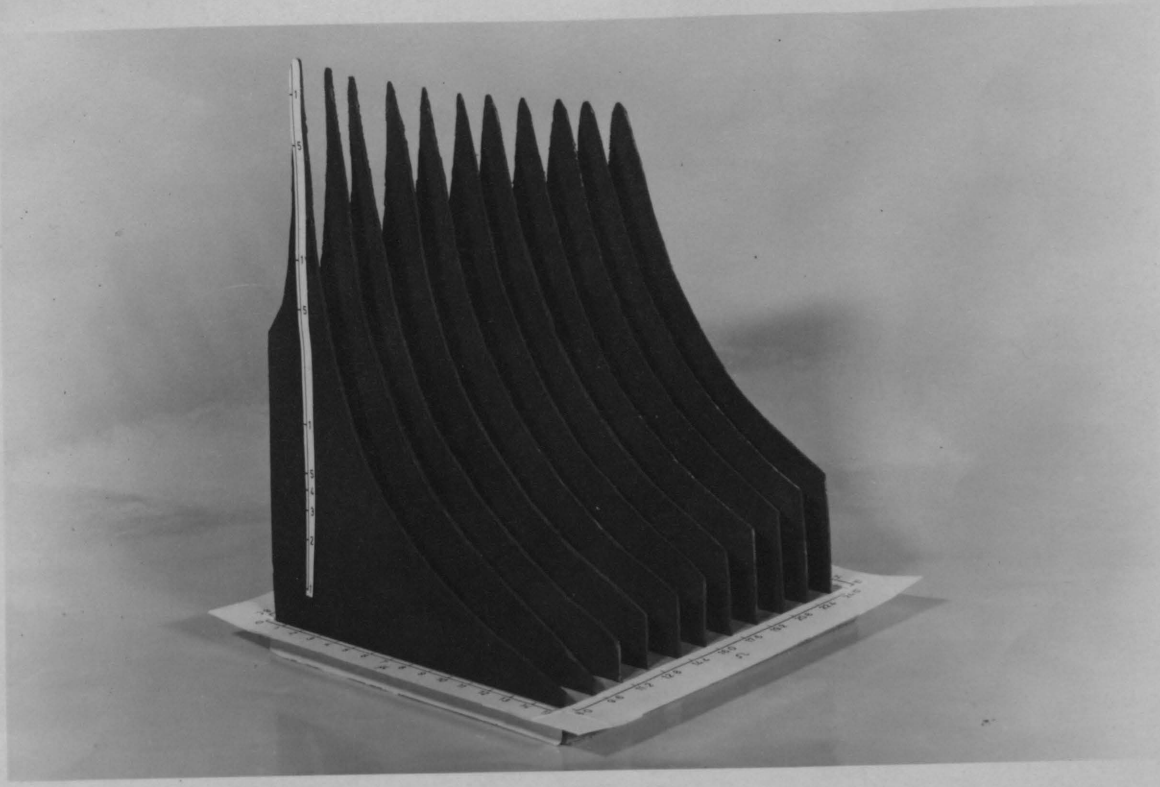

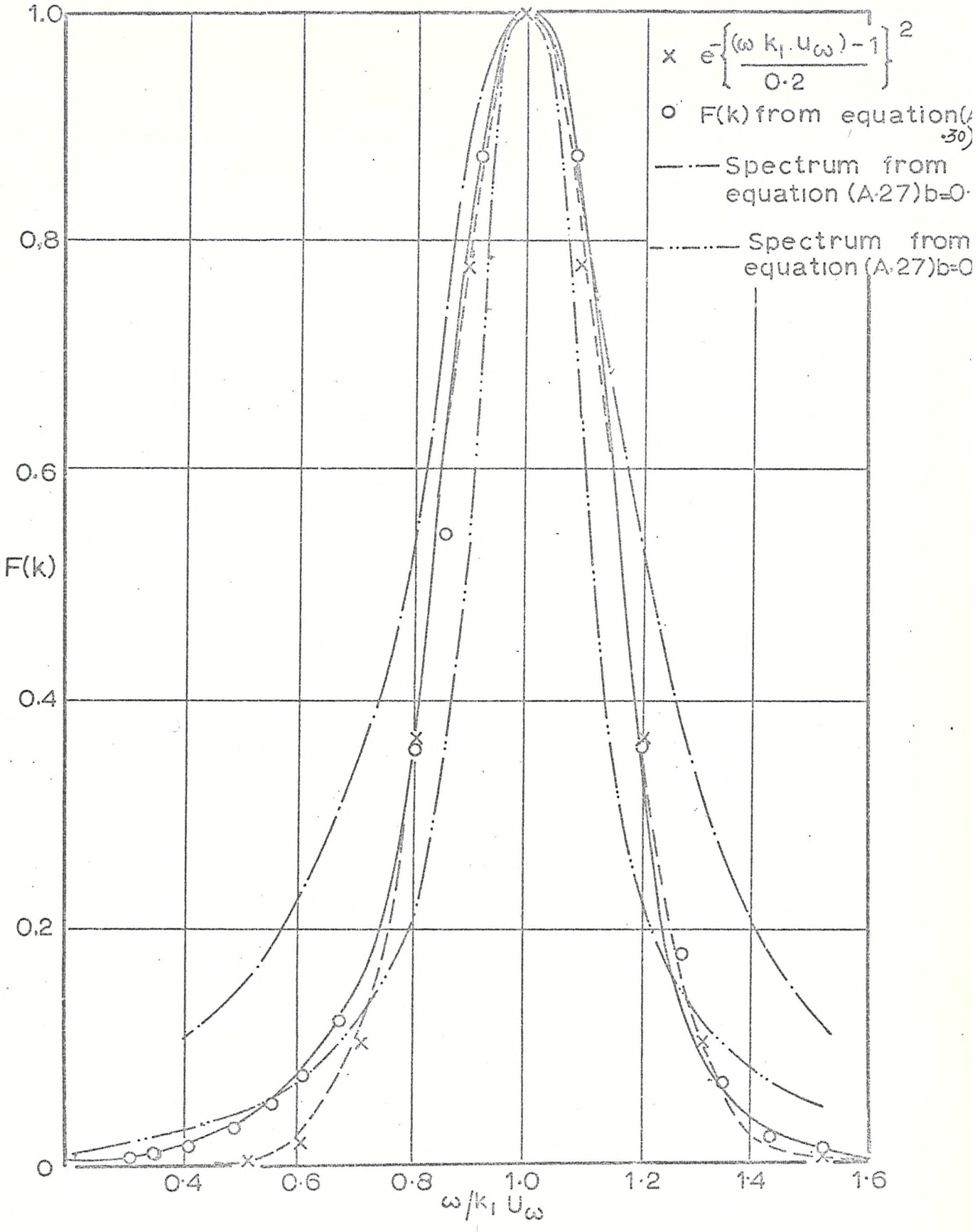

Fig A·5 The wave length spectrum of boundary layer field at constant frequency ω.

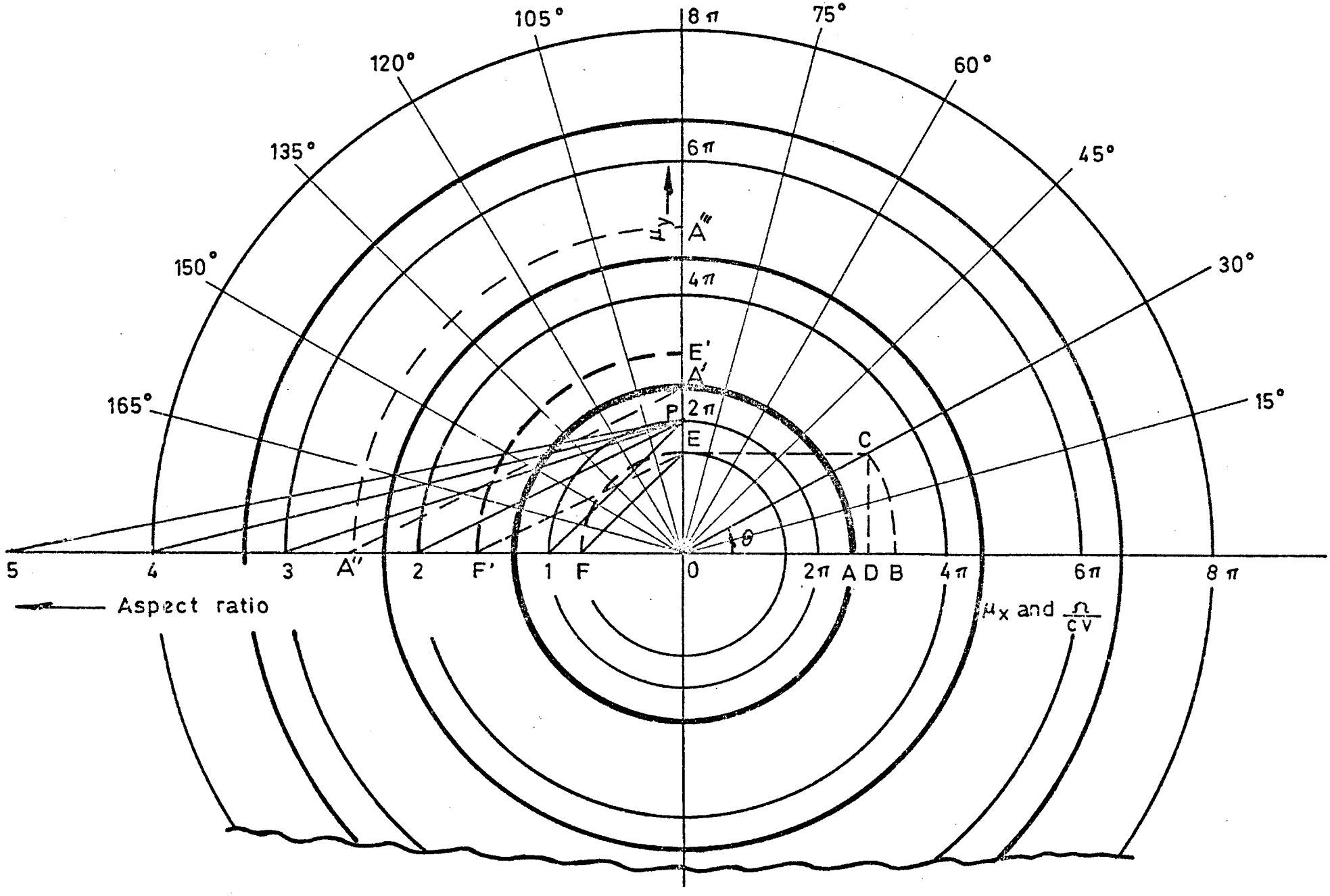

Fig.E.1 Diagram to locate the radiating harmonic in case of orthogonally stiffened plate.

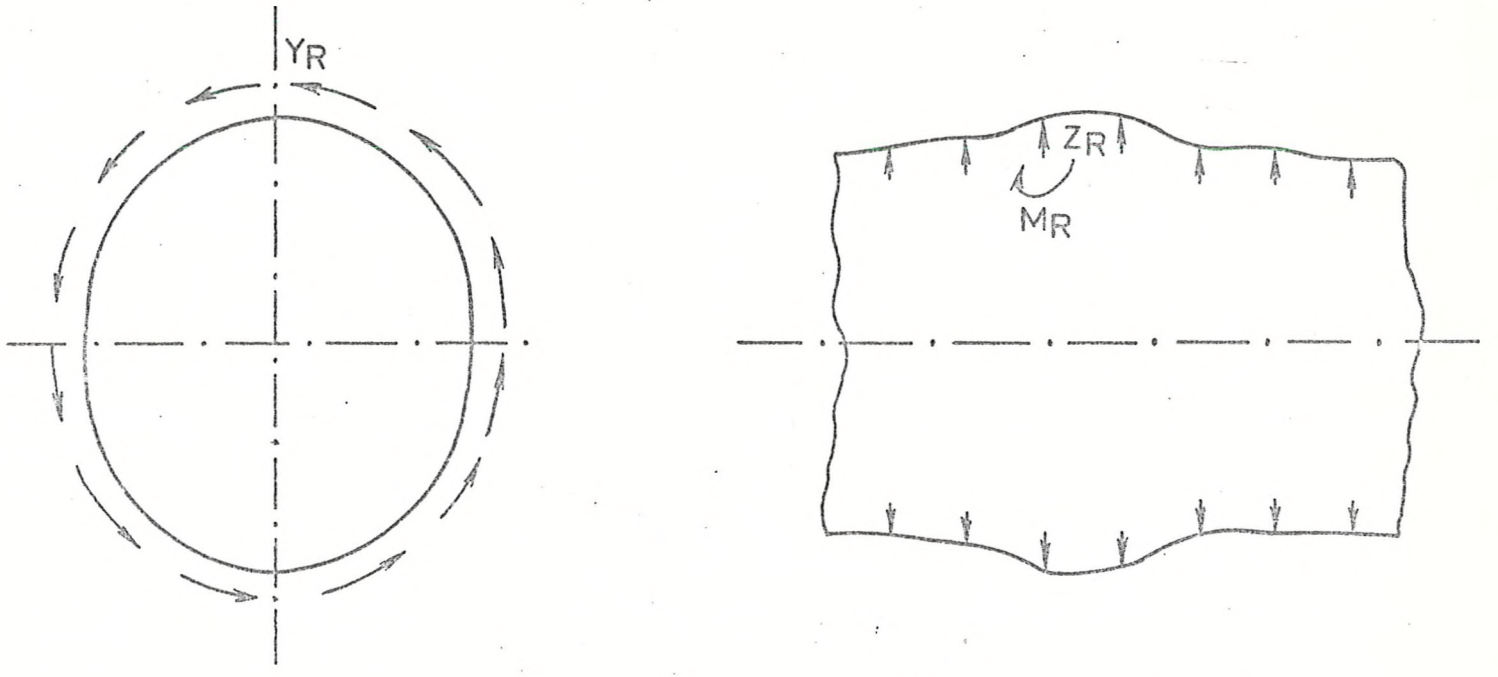

Fig H.1 Vibrating shell with interaction forces Y_R, Z_R and interaction moments M_R